

**DEVELOPMENT AND EVALUATION OF POLYMER BASED  
PHASE CHANGE MATERIALS (PCMs) FOR THERMAL  
ENERGY STORAGE APPLICATIONS**

*A Thesis submitted in the partial fulfillment of the requirements for the award of the degree*

*of*

**DOCTOR OF PHILOSOPHY**

*Submitted By*

**SURYA TANWAR**

**(Reg. No. 2K17/Ph.D./AC/03)**

*Under the supervision of*

**DR. RAMINDER KAUR**

**(Faculty of Polymer Science and Chemical Technology)**



**DEPARTMENT OF APPLIED CHEMISTRY**

**DELHI TECHNOLOGICAL UNIVERSITY**

**SHAHBAD DAULATPUR, BAWANA ROAD, DELHI - 110042 (INDIA)**

**APRIL 2023**

**© DELHI TECHNOLOGICAL UNIVERSITY- 2023  
ALL RIGHTS RESERVED**

# DELHI TECHNOLOGICAL UNIVERSITY

(Formerly Delhi College of Engineering)

Shahbad Daultapur, Bawana Road, Delhi – 110042, India



## DECLARATION

This is to certify that the work presented in this thesis entitled “**Development and Evaluation of Polymer Based Phase Change Materials (PCMs) for Thermal Energy Storage Applications**” is an original work carried out by me for the degree of **Doctor of Philosophy** under the supervision of **Dr. Raminder Kaur**, Faculty of Polymer Science & Chemical Technology, Department of Applied Chemistry, Delhi Technological University, Delhi. This thesis has been prepared in conformity with the rules and regulations of the Delhi Technological University, Delhi. The research work reported and results presented in the thesis have neither partially nor fully submitted to any other university nor institute for the award of any other degree or diploma.

Place: Delhi

(Surya Tanwar)

Date:

(Roll No.: 2k17/Ph.D./AC/03)

Research Scholar

Department of Applied Chemistry

Delhi Technological University,

Delhi-110042

# DELHI TECHNOLOGICAL UNIVERSITY

(Formerly Delhi College of Engineering)

Shahbad Daultpur, Bawana Road, Delhi – 110042, India



## CERTIFICATE

This is to certify that the work appended in the thesis entitled “**Development and Evaluation of Polymer Based Phase Change Materials (PCMs) for Thermal Energy Storage Applications**” by **Mr. Surya Tanwar (Roll No.: 2K17/PhD/AC/03)** in the partial fulfillment of the requirements for the award of degree of **Doctor of Philosophy**, is an authentic record of student’s own work carried by him under the supervision of **Dr. Raminder Kaur**, Assistant Professor, Department of Applied Chemistry, Delhi Technological University, Delhi. This is also certified that this work has not been submitted to any other institute or university for the award of any other diploma or degree.

**DR. RAMINDER KAUR**

Faculty of Polymer Science & Chemical Technology  
Department of Applied Chemistry,  
Delhi Technological University

**PROF. ANIL KUMAR**

HOD, Department of Applied Chemistry  
Delhi Technological University  
Delhi-110042

## ACKNOWLEDGEMENTS

---

*“Research is to see what everybody else has seen and to think what nobody else has thought”.*

Research is an enthralling journey where a person goes out carrying a baton of hope, ambition and passion in a quest of “Re-search” the unexplored hidden treasure of knowledge through a set of binoculars of curiosity and bring out new possible definitions of the existing facts know to the scientific world for the best interest and welfare to society and environment. Successful accomplishment of any research project is not only dependent upon the hard work of the scholar only but also requires the mutual understanding, efforts, support of numerous people and institutions during this entire time period. Foremost, I would like to express my immeasurable gratitude to my supervisor **Dr. Raminder Kaur**, Faculty of Polymer Science & Chemical Technology, Department of Applied Chemistry, Delhi Technological University for guiding me identifying and evaluating the research problem. I will be always thankful to her for constant support and fostering a healthy work environment and providing full degree of entropy with which the research work can be carried out with multi-dimensional thought process in a smooth and forward direction. She played a catalytic role in achieving the goals of the carried research work. I am sincerely grateful for her constant counsel and positive motivation which enabled productivity. I heartily want to thank **Prof. Jai Prakash Saini**, Hon’ble Vice-Chancellor, Delhi Technological University for his kind permission and **Prof. Anil Kumar**, Head, Department of Applied Chemistry, DTU, **Prof. D. Kumar**, Chairperson DRC, Department of Applied Chemistry, DTU for providing me the necessary facilities to carry out this research work.

I duly want to acknowledge and thank all technical and non-technical staff members of the department for their endless help and resource management whenever required the most of the time in crisis situations that accounted for smooth journey of my degree. I would especially like to thank *Mr. Ankesh Kumar, Mr. Jawed Alam* and *Mr. Sachin Kumar* for their constant support.

Also, it is very crucial and essential to be a part of positive work environment that further fuel up the performance to successfully complete your task. I feel fortunate to have certain fellow lab members who were also there to help me out and offered generous support throughout the course of Ph.D. program. For this I would recall to thank my seniors *Dr. Anuja Agrawal, Dr. Monika Duhan, Dr. Neelam Yadav, Dr. Lokesh Kumar* and dearest juniors *Ms. Pooja Singh, Ms. Gunjan Varshney, Ms. Sarla Yadav*.

I do cherish to have the presence of group of musketeers along my side throughout this journey who motivated and let me smoothen and cheer up during my ups and downs in this journey and I owe them genuine gratitude to all namely, *Dr. Reetu Yadav, Dr. Himansh Goel, Dr. Radhika Batra, Ms. Radha Sachan, Dr. Atul Varshney, Dr. Babita Veer, Ms. Deeksha* for their help and keeping the moral high throughout Ph.D. tenure.

Furthermore, I am indebted to *my parents* and my family for their endless encouragement, moral support and guidance throughout my whole life. Finally, I am thankful to all who have helped me directly or indirectly in completion of this research. Above all, I owe to *Almighty God* for granting me wisdom, health and strength to accept and overcome the challenges of the life.

Date:

*(Surya Tanwar)*

## ABSTRACT

---

Energy and environment conservation are the two major issues that the human beings are facing nowadays. Rapid industrial developments and population boom in the past few centuries have resulted in an enormous increase in energy demand. We are preeminently surviving on the mercy of fossil fuels that on average, account for almost 80% of the total energy production. However, the burning of fossil fuels brought the largest environmental issue ever, which is climate change caused by CO<sub>2</sub> emissions. According to the report of BP statistical review 2020, primary global energy requirements are derived from the consumption of energy resources in an increasing order as: Oil > Coal > Natural Gas > Hydroelectric > Nuclear etc. On contrary, Indian energy consumption is mainly driven by coal as fuel source which is followed by oil. Also, our home turf is expected to witness the highest energy consumption growth rate of 129 % among major economies across the world by 2035.

Among various forms of energies being considered, thermal energy is also an important concern topic of interest and therefore it necessitates the need of an effective energy storage and conservation systems to store the energy whenever it is available, which can be utilized especially over viewing the diverse climatic conditions and population blast existing in the Indian subcontinent. Developing Thermal Energy Storage (TES) systems by effective utilization of Phase Change Materials (PCMs) has proved to be the key technology in energy systems for conserving energy and increasing energy efficiency. Various studies have been carried out for tailoring out new PCMs with prime attention towards inorganic PCMs or organic ones especially paraffins-fossil fuel product.

Renewable initiative can be a game changer in field of energy science because the demand for energy is constantly increasing as some of the possible sources like fossil fuels, coal and nuclear are decreasing. In this research work, efforts have been made in the direction for the development of new PCMs derived from non-paraffin origin compounds belonging to organic genre of PCMs family mainly composed of renewable resource material; fatty acids (caprylic acid, undecylenic acid, capric acid) and polyethylene glycols (PEG600, PEG1500, PEG20000) in combination of polymeric materials to successfully manufacture latent heat thermal energy storage products in the form of encapsulated (micro and nano dimensions) and form-stable configurations. Furthermore, lab-synthesized metal oxide nanoparticles have been incorporated to PEG based PCMs in order to optimize their characteristics; and subsequent effect of the presence of nano-size filler on the latent heat storage characteristics, resistance towards thermal and ultraviolet exposure and flame-retardant properties has been studied.

Fourier Transform Infrared (FTIR) analysis confirmed the successful confinement of the fatty acids inside the polymers used for encapsulation as a core-sheath assembly in the resultant micro- and nanoencapsulated PCMs. Morphological studies suggested that the PCM microcapsules and nanofibrous PCMs were formed successfully with average diameter found to be 4  $\mu\text{m}$  and 56.4 nm respectively. Differential Scanning Calorimetry (DSC) data vouched the capability of the both prepared encapsulated PCMs as efficient latent heat thermal energy storage (LHTES) material systems with latent heats of fusion values deduced as 98.7 J/g and 55.68 J/g respectively for the microencapsulated and the nanoencapsulated PCMs. They also possessed favourable thermal energy storage/release potential and thermal cycling stability.

Form-stable PCMs, prepared as thin nanocomposite films derived from PEG1500 and PEG600 as active latent heat storage components supported by hydrophilic polymer matrix duly



reinforced with titanium dioxide nanoparticles (NTO) have fabricated through solvent casting method. It was observed that the latent heat density tends to increase with increased concentration of PEGs in the PVA matrix. The incorporation of metal oxide nanoparticles lead to notable enhancement in the phase change properties, thermal stability, ultraviolet irradiation resistance and flame retardant characteristics of the resultant nanocomposite PCMs. It was concluded that the shifting of phase change temperatures, along with surge in latent heat values and control over degree of supercooling were found to vary linearly with the increasing dosage of the added nanoparticles.

Thermogravimetric analysis (TGA) also suggested the improvement in thermal stabilities of PEG based form-stable PCMs at higher temperatures, after the introduction of the nanoparticles in proportional loadings. The presence of nanoparticles also altered the latent heat energy storage and release characteristics within the prepared PCMs. The presence of metal oxide nanoparticles in the formulated nanocomposite films resulted in efficient ameliorating of the UV resistance and flame-retardant nature of the produced PEG based form-stable PCMs.

In addition, the polyurethane (PU) based PCMs have been prepared containing capric acid as working PCM confined into the macromolecular framework of PU matrix. They undergo melting and crystallization transitions at 28.8 °C and 26.1 °C with accompanying latent heat capacities of 30.7 J/g and 31.9 J/g, respectively. The obtained PCMs also found to exhibit decent thermal reliability behaviour post 100 thermal cycles experience. The incorporation of fatty acid has resulted into significant change in the topographical arrangement of formed polyurethane based PCMs.

## TABLE OF CONTENTS

---

<b>Contents</b>	<b>Page no.</b>
Declaration	
Certificate	
Acknowledgements	I
Abstract	III
Table of Content	VI
List of Figures	XIV
List of Tables	XIX
List of Abbreviations	XXII
<b>CHAPTER 1:</b>	
<b>INTRODUCTION AND LITERATURE REVIEW</b>	<b>1-53</b>
1.1 Thermal Energy Storage (TES)	2
1.1.1 Phase Change Materials (PCMs)	5
1.1.2 Phase Change Phenomenon	5
1.1.3 Selection Criteria of Phase Change Materials (PCMs) for TES Applications	7
1.2 Classification of Phase Change Materials	9
1.2.1 Based on Temperature	10
1.2.2 Based on Phase Transitions	11
1.2.3 Based on Chemical Nature	11

<b>Contents</b>	<b>Page No.</b>
1.3 Methods for PCM Protection & Storage	24
1.3.1 Encapsulation Method	24
1.3.1.1 In-situ Polymerization	26
1.3.1.2 Interfacial Condensation Polymerization	27
1.3.1.3 Suspension Polymerization	28
1.3.1.4 Emulsion Polymerization	30
1.3.1.5 Coacervation	32
1.3.2 Shape-Stabilized Method	33
1.4 Applications of Phase Change Materials (PCMs)	34
1.4.1 Thermo-regulating Textiles	34
1.4.2 Energy-saving Buildings	36
1.4.3 Temperature-regulating Coatings	38
1.4.4 Phase Change Slurries	39
1.4.5 Electronics	41
1.4.6 Food Packaging	42
1.5 Significant Findings from Literature	43
1.6 Research Gap	50
1.7 Research Objectives	51
1.8 Overview of the thesis	52
 <b>CHAPTER 2:</b>	
<b>MATERIALS AND METHODS</b>	<b>54-75</b>

<b>Contents</b>	<b>Page No.</b>
2.1 Raw Materials/Chemicals	54
2.1.1 Specification and Sources of Raw Materials/Chemicals	55
2.2 Research Methodology	57
2.2.1 Synthesis of Microencapsulated PCMs	57
2.2.2 Synthesis of Nanoencapsulated PCMs	59
2.2.3 Synthesis of Metal Oxide Nanoparticles by Sol-Gel Approach	60
2.2.4 Preparation of Metal Oxide Nanoparticles filled PEG1500 based Form- Stable PCMs	61
2.2.5 Preparation of Metal Oxide Nanoparticles filled PEG600 based Form- Stable PCMs	62
2.2.6 Development of Fatty Acid incorporated Polyurethane Based PCMs	63
2.2.7 Characterization of Synthesized Polymer Based Phase Change Materials (PCMs)	64
2.2.7.1 Fourier Transform Infrared Spectroscopy (FTIR)	64
2.2.7.2 Differential Scanning Calorimetry Analysis (DSC)	65
2.2.7.3 Thermogravimetric Analysis (TGA)	66
2.2.7.4 Thermal Energy Storage/Release Ability Test (T-History)	67
2.2.7.5 Thermal Reliability Test	68
2.2.7.6 Field-Emission Scanning Electron Microscopy (FE-SEM)	69
2.2.7.7 High-Resolution Transmission Electron Microscopy (HR-TEM)	69
2.2.7.8 Dynamic Light Scattering (DLS)	70

<b>Contents</b>	<b>Page no.</b>
2.2.7.9 X-Ray Diffraction (XRD) Analysis	71
2.2.7.10 Brunauett–Emmett–Teller (BET) Analysis	71
2.2.7.11 UV-Visible Analysis	72
2.2.7.12 Flame-Retardancy Characteristics	73
2.2.7.13 Electrical Conductivity Measurement	73
2.2.7.14 Form-Stability Test (Leakage Test)	74
<b>CHAPTER 3:</b>	
<b>SYNTHESIS OF MICROENCAPSULATED PCMs</b>	<b>76-91</b>
3.1 Introduction	76
3.2 Results and Discussion	79
3.2.1 Fourier Transform Infrared (FTIR) Spectroscopy	79
3.2.2 Morphology of Microencapsulated PCMs	81
3.2.3 Thermal Performance of Microencapsulated PCMs	83
3.2.4 Thermal Stability of Microencapsulated PCMs	86
3.2.5 Thermal Energy Storage/Release Ability of Microencapsulated PCMs	88
3.2.6 Thermal reliability of Microencapsulated PCMs	89
3.3 Significant Findings	90
<b>CHAPTER 4:</b>	
<b>SYNTHESIS OF NANOENCAPSULATED PCMs</b>	<b>92-106</b>
4.1 Introduction	92
4.2 Results and Discussion	96

<b>Contents</b>	<b>Page No.</b>
4.2.1 Fourier Transform Infrared (FTIR) Spectroscopy	96
4.2.2 Morphology of Nanoencapsulated PCMs	97
4.2.3 Thermal Performance of Nanoencapsulated PCMs	99
4.2.4 Thermal Stability of Nanoencapsulated PCMs	102
4.2.5 Thermal Energy Storage/Release Ability of Nanoencapsulated PCMs	103
4.2.6 Thermal reliability of Nanoencapsulated PCMs	104
4.3 Significant Findings	105

## **CHAPTER 5:**

### **PROPERTY EVALUATION OF SYNTHESIZED TITANIUM DIOXIDE 107-119**

#### **NANOPARTICLES**

5.1 Introduction	107
5.2 Results and Discussion	112
5.2.1 Morphology of Nano-TiO <sub>2</sub> (NTO)	112
5.2.2 X-Ray Diffraction (XRD) study of Nano-TiO <sub>2</sub> (NTO)	113
5.2.3 Fourier Transform Infrared (FTIR) Spectroscopy of Nano-TiO <sub>2</sub> (NTO)	114
5.2.4 Thermal Stability of Nano-TiO <sub>2</sub> (NTO)	115
5.2.5 Brunauer-Emmett-Teller (BET) Studies of Nano-TiO <sub>2</sub> (NTO)	116
5.2.6 Energy -Dispersive X-ray (EDX) Spectra of Nano-TiO <sub>2</sub> (NTO)	117
5.3 Significant Findings	118

<b>Contents</b>	<b>Page No.</b>
<b>CHAPTER 6:</b>	
<b>FABRICATION OF PEG1500 BASED FORM-STABLE PCMs</b>	<b>120-143</b>
6.1 Introduction	120
6.2 Results and Discussion	123
6.2.1 Form-Stability of PEG1500/PVA Blends	123
6.2.2 Fourier transform infrared (FTIR) spectroscopy of PEG1500/PVA Blends and NTO/PEG1500/PVA form-stable PCMs Nanocomposites	124
6.2.3 Phase Change Characteristics of PEG1500/PVA Blends and NTO/PEG1500 /PVA Form-Stable PCM Nanocomposites	127
6.2.4 Thermal stability of PVA/PEG1500 blends and NTO/PEG1500/PVA Form- Stable PCM Nanocomposites	132
6.2.5 Thermal energy storage performance of NTO/PEG1500/PVA Form-Stable PCM Nanocomposites	134
6.2.6 Thermal reliability performance of NTO/PEG1500/PVA Form-Stable PCM Nanocomposites	136
6.2.7 Structural characterization of NTO/PEG1500/PVA Form-Stable PCMs	137
6.2.8 UV-blocking characteristics of NTO/PEG1500/PVA Form-Stable PCMs	139
6.2.9 Flammability Characteristics of NTO/PEG1500/PVA PCM Nanocomposites	140
6.3 Significant Findings	142

<b>Contents</b>	<b>Page No.</b>
 <b>CHAPTER 7:</b>	
<b>DEVELOPMENT OF PEG600 BASED FORM-STABLE PCMs</b>	<b>144-160</b>
7.1 Introduction	144
7.2 Results and Discussion	147
7.2.1 Form-Stability of PEG600/PVA Blends	147
7.2.2 Fourier Transform Infrared (FTIR) Spectroscopy of PEG600/PVA Blends and NTO/PEG600/PVA form-stable PCMs Nanocomposites	147
7.2.3 Phase Change Characteristics of PEG600/PVA Blends and NTO/PEG600 /PVA Form-Stable PCM Nanocomposites	149
7.2.4 Thermal stability of PVA/PEG600 blends and NTO/PEG600/PVA Form- Stable PCM Nanocomposites	153
7.2.5 Thermal reliability performance of NTO/PEG600/PVA Form-Stable PCM Nanocomposites	154
7.2.6 Structural characterization of NTO/PEG600/PVA Form-Stable PCMs	155
7.2.7 UV-blocking characteristics of NTO/PEG600/PVA Form-Stable PCMs	157
7.2.8 Flammability Characteristics of NTO/PEG600/PVA PCM Nanocomposites	158
7.3 Significant Findings	160
 <b>CHAPTER 8:</b>	
<b>DEVELOPMENT OF PU BASED PCMs (PUPCMs)</b>	<b>161-172</b>
8.1 Introduction	161
8.2 Results and Discussion	165



<b>Contents</b>	<b>Page No.</b>
8.2.1 Fourier Transform Infrared (FTIR) Spectroscopy of PUPCMs	165
8.2.2 Thermal Energy Storage Characteristics of PUPCMs	167
8.2.3 Thermal Stability of PUPCMs	168
8.2.4 Structural characterization of PUPCMs	169
8.2.5 Thermal reliability performance of PUPCMs	170
8.3 Significant Findings	171
<b>CHAPTER 9:</b>	
<b>CONCLUSIONS AND FUTURE PROSPECTS</b>	<b>173-176</b>
9.1 Conclusions	173
9.2 Future Prospects	176
<b>REFERENCES</b>	<b>177</b>
<b>LIST OF PUBLICATIONS</b>	<b>210</b>
<b>BRIEF BIO-DATA OF THE AUTHOR</b>	<b>212</b>

## LIST OF FIGURES

---

<b>Figure No.</b>	<b>Title</b>	<b>Page No.</b>
1.1	Types of Thermal Energy Storage (TES) Methods	3
1.2	Mechanism of Phase Change Process	6
1.3	Classification of Phase Change Materials (PCMs)	10
1.4	Strategic Advantages of Polymers for PCM Storage	26
1.5	Schematic Representation of Interfacial Polymerization	28
1.6	Schematic Representation of Suspension Polymerization	29
1.7	Schematic Representation of Early Stages of Emulsion Polymerization	31
2.1	Experimental Procedure for the synthesis of Micro-PCMs	58
2.2	Experimental Procedure for the synthesis of Nano-PCMs	60
2.3	Synthesis of Titanium Dioxide Nanoparticles via Sol-Gel Route	61
2.4	Schematic representation of the experimental procedure to obtain form-stable NTO/PEG1500/PVA nanocomposites	62
2.5	Experimental methodology adopted to obtain form-stable NTO/PEG600/PVA nanocomposites	63
2.6	Experimental methodology adopted for the preparation of Polyurethane based Form-Stable PCMs	64
2.7	FTIR (Spectrum Two, Perkin Elmer)	65
2.8	Differential Scanning Calorimeter (DSC 8000, Perkin Elmer) used to determine phase change characteristics	66

2.9	Thermogravimetric Analyzer (Perkin Elmer 4000)	67
2.10	Schematic representation of the experimental set-up for T-History Test	68
2.11	Field-Emission Scanning Electron Microscope	69
2.12	High-Resolution Transmission Electron Microscope	70
2.13	Malvern Zetasizer Nano ZS	70
2.14	X-Ray Diffractometer	71
2.15	Brunauett-Emmett-Teller (BET) Tester (Microtrac BEL)	72
2.16	UV-Vis Spectrophotometer	72
2.17	Oxygen Index Apparatus (Fire Testing Technology, UK)	73
2.18	Electrical Resistivity Four Point Probe Set-up	74
3.1	FTIR of Caprylic Acid (CpA), Micro-PCMs and PMMA	80
3.2	SEM micrograph of the synthesized Micro-PCMs (A) magnification-5.00 K X (B) magnification-10.00 K X (C) and (D) magnification-20.00 K X	82
3.3	Schematic illustration of Caprylic Acid inside PMMA Microcapsule	82
3.4	Particle Size Distribution Analysis of the Micro-PCMs	83
3.5	DSC Curves for Heating/Cooling Cycles for (a) Pure CpA and (b) Micro PCMs	85
3.6	TGA Curves for CpA, Micro-PCMs and PMMA	87
3.7	Thermal Energy Storage/Release curves for CpA and Micro-PCMs during charging and discharging cycles (T-History)	89
3.8	Thermal Reliability Curves of Micro-PCMs: (a):Heating Cycle; (b) Cooling Cycle	90
4.1	FTIR Spectra of: (a) Undecylenic Acid (UA), (b) PANI NFs and (c) PANI/UA NFs	97
4.2	HR-TEM Micrographs of the Synthesized Raw PANI nanofibres: (a) magnification-500 nm, (b) magnification-200 nm; and PANI/UA NF PCMs: (c) magnification-1 $\mu$ m, (d)	99

magnification-200 nm

4.3	DSC Curves for Heating/Cooling Cycles for (a) Pure UA and (b) PANI/UA-NF PCMs	100
4.4	TGA Cures for the UA, Nanoencapsulated PCMs and PANI	103
4.5	Thermal Energy Storage/Release curves for UA and Nanoencapsulated PCMs during charging and discharging cycles (T-History)	104
4.6	Thermal Reliability Curves of Nanoencapsulated PCMs: (a) Heating Cycle; (b) Cooling Cycle	105
5.1	High-Resolution Transmission Electron Microscope (HR-TEM) and Selected Area Electron Diffraction (SAED) images of the synthesized NTO	113
5.2	X-Ray Diffraction (XRD) pattern of NTO particles	114
5.3	FTIR Spectra of Nano-Titanium Dioxide (NTO) derived by Sol-Gel Approach	115
5.4	TGA cure of NTO particles	116
5.5	Nitrogen adsorption isotherm of prepared titanium dioxide nanoparticles with pore volume distribution (inset)	117
5.6	EDX Spectra of synthesized NTO particles	118
6.1	Leakage rates observed for various prepared blend compositions based on (a) measuring the mass loss percentage on weight basis; (b) measuring the diameter of seepage area	124
6.2	FTIR spectra for (a) PVA; (b) PVA; (c) PEG1500/PVA blends with different PEG concentrations; (d) NTO/PEG1500/PVA nanocomposites at different NTO loadings	126
6.3	Phase change characteristics for (a) PEG1500 and its associated blends; (b) form-stable PCMs	129
6.4	Effect of Nanoparticles concentrations on (a) Latent Heat Enthalpy of Fusion; (b) Degree of Supercooling	131
6.5	TGA Cures for (a) PEG1500/PVA blends with different PEG concentrations; (b) NTO/PEG1500/PVA nanocomposites at different NTO loadings	133

6.6	Thermal Energy Storage Curves for bulk PEG1500 and Form-Stable PCMs (T-History)	136
6.7	Thermal Reliability Curves of form-stable PCMs (a) Heating Cycle; (b) Cooling Cycle	137
6.8	FE-SEM Micrographs of the prepared Form-Stable PCMs (a) magnification-7.6 mm X 70.0 K X PCMs; (b) magnification-7.6 mm X 25.0 K X PCMs; (c) magnification-7.6 mm X 5.0 K X and PCMs and (d) magnification-7.6 mm X 1.50K X	138
6.9	UV-vis transmittance spectra of NTO/PEG1500/PVA with varying loading of titanium dioxide nanoparticles	140
7.1	Features of PEGs	145
7.2	FTIR spectra for (a) PVA; (b) PEG600; (c) PEG600/PVA Blend (50 wt. % PCM) concentration and (d) NTO/PVA/PEG600 composites with varying NTO concentrations	149
7.3	Phase change properties of PEG 600 and metal oxide filled composites (a) Heating Cycle and (b) Cooling Cycle	151
7.4	Effect on Latent Heat Enthalpy of Fusion of PEG600 based form-stable PCMs as a function of nanoparticles loading	152
7.5	TGA Cures for (a) PEG600, PVA, PVA with 50 wt. % PEG concentration; (b) NTO/PEG600/PVA composites at different NTO concentrations	154
7.6	Data for Thermal Reliability of form-stable PCMs; (a) Heating Cycle; (b) Cooling Cycle	155
7.7	FE-SEM Micrograph of the prepared NTO/PEG600/PVA nanocomposites PCMs at magnification-7.6 mm X 3.50K X	156
7.8	UV-vis transmittance spectra of NTO/PEG600/PVA PCMs with varying loading of titanium dioxide nanoparticles	158
7.9	Flammability characteristics of NTO/PEG600/PVA nanocomposite PCMs	159
8.1	FTIR of Capric Acid (CA), Raw PU and PUPCMs	166

8.2	DSC Curves for Heating/Cooling Cycles for (a) Pure CA and (b) PUPCMs	167
8.3	TGA Cures for the Capric Acid (CA), PUPCMs and Raw PU	169
8.4	SEM Micrographs of the Synthesized: (1) Raw PU- (a) magnification-2000 X ;(b) magnification-1000 X; (c) magnification-500 X and (2) PUPCMs-(d) magnification-2000 X ;(e) magnification-1000 X; (f) magnification-500 X	170
8.5	Data for Thermal Reliability of PUPCMs; (a) Heating Cycle; (b) Cooling Cycle	171

## LIST OF TABLES

---

<b>Table No.</b>	<b>Title</b>	<b>Page No.</b>
1.1	Basic Requirements of PCMs for TES Applications	9
1.2	Comparison of different types of PCMs based on physical phase transformations	11
1.3	Phase Change Temperatures and Latent Heat of Fusions of Salt Hydrates	12
1.4	Phase Change Temperatures and Latent Heat of Fusions of Paraffins	15
1.5	Phase Change Temperatures and Latent Heat of Fusions of Fatty Acids	16
1.6	Phase Change Temperatures and Latent Heat of Fusions of Fatty Acid Derivatives	17
1.7	Phase Change Temperatures and Latent Heat of Fusions of some Organic PCMs	17
1.8	Phase Change Temperatures and Latent Heat of Fusions of Inorganic Eutectics	18
1.9	Phase Change Temperatures and Latent Heat of Fusions of Fatty Acid Eutectics	19
1.10	Phase Change Temperatures and Latent Heat of Fusions of Different Molecular Weights of PEGs	21
1.11	Phase Change Temperatures and Latent Heat of Fusion of Polyalcohols	22
1.12	Phase Change Temperatures and Latent Heat of Fusions of Metal PCMs	23
1.13	Representation of individual traits of various PCMs	23
2.1	Specification and Sources of Raw Materials/Chemicals	55
2.2	Leakage Criteria considered for as prepared PEG/PVA Blends	75
3.1	DSC Data of Pure PCM and Micro-PCMs Representing Their Phase Change Characteristics	85
3.2	Comparison of some microencapsulated PCMs from literature and synthesized microencapsulated PCM	86

3.3	Thermal Stabilities of the Caprylic Acid (CpA), Micro-PCMs and PMMA	88
3.4	Phase change characteristics of Micro-PCMs post thermal cycling exposure	90
4.1	DSC Data of Pure PCM and Nanoencapsulated PCMs Representing Their Phase Change Characteristics	101
4.2	Comparison of some encapsulated PCMs from literature and synthesized nanoencapsulated PCMs	101
4.3	Thermal Stabilities of the Undecylenic Acid UA, PANI/UA-NFs PCMs and PANI	103
4.4	Phase change characteristics of Nanoencapsulated PCMs post thermal cycling exposure	105
5.1	BET Characteristics of as synthesized NTO particles	117
6.1	DSC Data of Pure PCM and PEG Blends Representing Their Phase Change Characteristics	129
6.2	DSC Data of NTO/PEG1500/PVA form-stable PCMs Representing Their Phase Change Characteristics	130
6.3	Comparison of some form-stable PCMs from literature and prepared form-stable PCMs	131
6.4	Thermal Stabilities of (a) PEG1500/PVA blends with different PEG concentrations; (b) NTO/PEG1500/PVA nanocomposites PCMs at different NTO loadings	134
6.5	Phase change characteristics of 1% NTO/PEG1500/PVA Nanocomposite PCMs post thermal cycling exposure	137
6.6	Flammability characteristics of NTO/PEG1500/PVA form-stable PCMs	142
7.1	DSC Data of NTO/PEG600/PVA form-stable PCMs	151
7.2	Comparison of some form-stable PCMs from literature and prepared form-stable PCMs	152
7.3	Thermal Stabilities of NTO/PEG600/PVA nanocomposites PCMs	154
7.4	Phase change property of 1% NTO/PEG600/PVA PCMs post thermal cycling experience	155
8.1	DSC Data of Pure PCM and PUPCMs Representing Their Phase Change Characteristics	168



8.2	Thermal Stabilities of the Capric Acid (CA), PUPCMs and PU	169
8.3	Phase change property of PUPCMs post thermal cycling experience	171

## LIST OF ABBREVIATIONS

---

<b>Symbol</b>	<b>Notations</b>
AA	Acrylic Acid
AMPL	2-Amino-2-Methyl-1, 3-Propanediol
BA	n-Butyl Acrylate
BDDA	1,4-Butylene Glycol Diacrylate
BDO	1,4-butanediol
BET	Brunauett–Emmett–Teller
BJH	Barrett-Joyner-Halenda
BMA	n-Butyl Methacrylate
BPO	Benzoyl Peroxide
CA	Capric Acid
CpA	Caprylic Acid
CHTES	Thermo-chemical Energy Storage Systems
CNTs	Carbon Nanotubes
DLS	Dynamic Light Scattering
Dot	n-Dotriacontane
DSC	Differential Scanning Calorimetry
DVB	Divinyl Benzene
EDX	Energy Dispersive X-ray
EG	Expanded Graphite
EGDMA	Ethylene Glycol Dimethacrylate

EP	Expanded Perlite
EPCMs	Encapsulated Phase Change Materials
EPDM	Ethylene Propylene Diene Monomer
$E_R$	Encapsulation Ratio
EVA	Ethylene-Vinyl Acetate
EVM	Expanded Vermiculite
FE-SEM	Field-Emission Scanning Electron Microscopy
FR	Flame Retardant
FTIR	Fourier Transform Infrared
GF	Glass-Fibers
GNPs	Graphene Nanoplatelets
$\Delta H_c$	Latent Heat of Crystallization
$\Delta H_m$	Latent Heat of Fusion
HDI	Hexamethylene Diisocyanate or 1,6-Hexamethylene Diisocyanate
HDPE	High-Density Polyethylene
HEMA	Hydroxy Ethyl Methyl Acrylate
HLB	Hydrophile-Lipophile Balance
HNT	Halloysite Nanotubes
HR-TEM	High-Resolution Transmission Electron Microscopy
H-PW	High-Temperature Paraffin Wax, Melting Temperature: 56-58 °C
HSA	Hydroxy Stearic Acid
IPDI	Isophorone Diisocyanate
LA	Lauric Acid

LDPE	Low-Density Polyethylene
LHTES	Latent Heat Thermal Energy Storage Systems
LFTF	Latent Functionally Thermal Fluid
LLDPE	Linear-Low Density Polyethylene
LOI	Limiting Oxygen Index
L-PW	Low-Temperature Paraffin Wax, Melting Temperature: 18-23 °C
MA	Myristic Acid
MAA	Methacrylic Acid
MDI	4,4-Diphenylmethane Diisocyanate
MF	Melamine-Formaldehyde
MMA	Methyl Methacrylate
MPEG	Methoxy Polyethylene Glycol
MUF	Melamine-Urea-Formaldehyde
MWCNTs	Multi-Walled Carbon Nanotubes
NEPCM	Nanoencapsulated Phase Change Material
NPG	Neopentylglycol
NTO	Nano-TiO <sub>2</sub> or Titanium Dioxide Nanoparticles
OA-MNs	Oleic Acid-Coated Magnetic Nanoparticles
PA	Palmitic Acid
PAN	Polyacrylonitrile
PANI	Polyaniline
PASS	Sodium Polyacrylate
PC	Polycarbonate

PCL	Polycaprolactone
PCMs	Phase Change Materials
PDI	Particle Distribution Index
PEGs	Polyethylene Glycols
PEMA	Poly-(Ethyl Methacrylate)
PERT	Pentaerythritol
PET	Polyethylene Terephthalate
PG	Pentaglycerine
PMDI	Polymeric-4,4-Diphenylmethane Diisocyanate
PMIA	Poly-(Meta-Phenylene Isophthalamide)
PMMA	Poly-(Methyl Methacrylate)
PoA	Polyamide
PP	Polypropylene
PS	Polystyrene
PSD	Particle Size Distribution
PScEA	Poly-(Styrene-co-Ethyl Acrylate)
PU	Polyurethane
PUF	Poly-(Urea-Formaldehyde)
PUPCMs	Polyurethane based PCMs
PVA	Polyvinyl Alcohol
PVAc	Polyvinyl Acetate
PVC	Polyvinyl Chloride
PV/T	Photovoltaic/Thermal

PWO	Lead Tungstate
SA	Stearic Acid
SAED	Selected Area Electron Diffraction
SAL	Stearyl Alcohol
SBS	Styrene-Butadiene-Styrene
SEBS	Styrene-block-(Ethylene-co-Butylene)-block-Styrene
SEM	Scanning Electron Microscopy
SHTES	Sensible Heat Thermal Energy Storage
SiO <sub>2</sub>	Silica or Silicon Dioxide
SIS	Styrene-Isoprene-Styrene
SLS	Sodium Lauryl Sulphate
SWCNTs	Single-Walled Carbon Nanotubes
T <sub>10</sub>	10% Weight Loss Temperature
T <sub>50</sub>	50% Weight Loss Temperature
T <sub>80</sub>	80% Weight Loss Temperature
T <sub>Ce</sub>	Offset Crystallization Temperature
T <sub>Co</sub>	Onset Crystallization Temperature
T <sub>Cp</sub>	Peak Crystallization Temperature
T <sub>Me</sub>	Offset Melting Temperature
T <sub>Mo</sub>	Onset Melting Temperature
T <sub>Mp</sub>	Peak Melting Temperature
TEOS	Tetraethoxysilicate
TES	Thermal Energy Storage

TGA	Thermogravimetric Analysis
TiO <sub>2</sub>	Titanium Dioxide
TRIS	Tris-(Hydroxymethyl)-Aminomethane
UA	Undecylenic Acid or (10-Undecenoic Acid)
UF	Urea-Formaldehyde
UV	Ultraviolet
WPCs	Wood Plastic Composites
XRD	X-Ray Diffraction
ZnO	Zinc Oxide

# CHAPTER 1

## INTRODUCTION AND LITERATURE REVIEW

---

With the evolution of human civilization, the necessities of the society change gradually over time, according to the lifestyle of people across the centuries. The development of the society, growth in industrialization, advancements in technology and population boom in the past few centuries are the key driving factors behind an enormous increase in energy demand [1]. Approximately 80% of the world's energy needs are derived from the use of conventional fossil fuels [2]. The quest to fulfilling the energy supply by high dependency on fossil fuels has posed a severe impact on the less availability of fossil fuels in the reservoir of the earth which led to a hike in fuel prices. Also, the burning of fossil fuels accounts for drastic environmental and climatic changes such as the emission of harmful gases, the greenhouse effect, ozone layer depletion, elevation in daily average temperature and environmental pollution, etc. [3].

The post-1970s energy crises along with financial instabilities push countries to develop new energy policies [4]. All over the world, the researchers were compelled to search for the new and renewable energy sources. Few theories were proposed advocating the solar radiations to be one of the most primary sources of energy. The use of solar energy for applications such as water heating, space heating, cooking, and drying sometimes becomes unreliable, as the solar energy is variable and unpredictable. As a result, there exists a mismatch between the availability and utilization time of solar radiations [5]. The need for energy for a wide variety of applications in different forms and stages are time-dependent because of the limitation of available energy sources. This indicates the requirement of novel sources of energy whose applications should be complemented strongly with an efficient energy storage system.



One of the options is to develop energy storage devices, which are as important as developing new sources of energy. The storage of energy in suitable forms, which can conventionally be converted into the required form, is a present-day challenge to the technologists. Energy storage not only reduces the mismatch between the supply and demand but also improves the performance and reliability of energy systems and plays a vital role in energy conservation [6]. Thermal energy storage plays a very important role when energy demand and supply are not equal. Excess energy available in the off-peak time can be stored in thermal energy storage (TES) devices for later use e.g. as, solar energy is available only in sunshine hours, thus, the excess heat may be stored in the daytime, and can be used later in the night hours. Energy storage helps in the saving of expensive fuels and reduces the wastage of energy and capital cost, which leads to a cost-effective system [7]. Thermal energy storage (TES) systems based on phase change materials (PCMs) have been gained more and more attention in the research community in the last 3-4 decades and have become an important aspect of energy management. Phase change materials (PCMs) are called the latent heat storage materials. Thermal energy transfer occurs when a material changes from the solid to a liquid state or vice-versa [8].

### **1.1 Thermal Energy Storage (TES)**

Thermal Energy Storage (TES) is one of the key technologies for increasing efficiency in energy conservation of available sources of heat. Thermal energy storage (TES) is the temporary storage of high or low-temperature energy for later use and can be achieved by the heating process (melting), solidifying process (cooling), or vaporizing a material with the energy in the form of heat, when the process is reversed. TES methods can be classified into three broad categories as mentioned: (1) Sensible Heat Storage; i.e. due to temperature change or change in internal energy of material; (2) Latent Heat Storage, based on the heat capture or release during phase

change of storage material; (3) Thermo-chemical Heat Storage, relying on heat energy derived from the chemical reactions of materials being used for storage purposes [9].

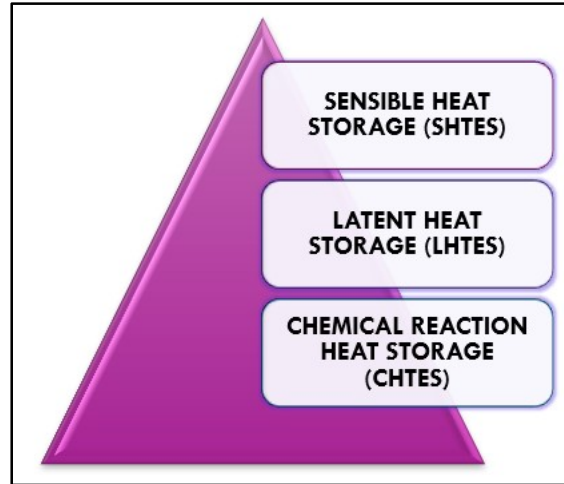


Figure 1.1: Types of Thermal Energy Storage (TES) Methods

### (1) Sensible Heat Thermal Energy Storage Systems

Sensible heat storage (SHTES) involves the storage of thermal energy by increasing or decreasing the temperature of the storage medium (solid or liquid). Energy storage potential depends upon the specific heat of the medium, density of the material, thermal conductivity, and the change in temperature during the initial and final stage, the amount of storage material. No phase change occurs during the energy storage function [1]. The sensible heat stored in any material can be calculated as follows using equation 1:

$$Q = \int_{T_i}^{T_f} mC_p dT = mC_{ap}(T_f - T_i) \quad (1)$$

Where  $Q$  – the quantity of heat stored (J),  $T_i$  – initial temperature ( $^{\circ}\text{C}$ ),  $T_f$  – final temperature ( $^{\circ}\text{C}$ ),  $m$  – the mass of heat storage medium (kg),  $C_p$  – specific heat (J/kg K),  $C_{ap}$  – average specific heat between  $T_i$  and  $T_f$  (J/kg K).

They have low energy density and require a large volume for storage which considerably increases the unit size and therefore preferred for small applications where economics is a major concern. Traditional materials used since ancient times are sand, rocks, concrete, bricks, water, oils, metals, molten salts, etc. Water is considered to be the best SHTES material owing to abundance in nature, high specific heat capacity, and inexpensive.

## **(2) Thermo-chemical Energy Storage Systems (CHTES)**

Thermal energy can also be stored based on the energy absorbed and released during a chemical reaction, by breaking and reforming molecular bonds which is reversible. It is more advantageous compared to sensible and latent heat storage techniques, such as high energy density, ambient temperature storage, and the possibility of heat pumping and long-distance transport. The amount of energy stored is based on the amount of the reacting materials, endothermic heat of reaction, and the extent of conversion [6, 9]. Equation 2 gives the amount of energy stored in a thermo-chemical energy storage system.

$$Q = a_r m \Delta h_r \quad (2)$$

Where Q – the quantity of heat stored (J), m – the mass of heat storage medium (kg),  $\Delta h_r$ - the heat of reaction,  $a_r$ - fraction reacted.

## **(3) Latent Heat Thermal Energy Storage Systems (LHTES)**

In the case of LHTES systems, the thermal energy storage process takes place by absorbing and retrieving the thermal energy in the form of latent heat when a storage material goes under a change in physical state or phase i.e.; from solid to liquid or liquid to gas or vice versa. LHTES systems are the most efficient method of storing thermal energy compared to other heat energy storage methods as they provide higher energy storage density with a shallower and almost

constant temperature range [8]. The energy storage of LHTES systems can be described by given equation 3:

$$Q = \int_{T_i}^{T_m} mC_p dT + ma_m \Delta H_m + \int_{T_m}^{T_f} mC_p dT \quad (3)$$

Where  $a_m$  – fraction melted,  $\Delta H_m$ – the heat of melting per unit mass (J/kg).

Phase Change Materials (PCMs) falls under the category of the LHTES system.

### **1.1.1 Phase Change Materials (PCMs)**

Phase Change Materials (PCMs) belongs to the group of Latent Heat Storage Materials (LHTES). The thermal energy transfer is entrusted on the phase change enthalpy of the material without any temperature change. Thermal energy storage occurs in form of latent heat when storage material shows phase transformations typically solid-liquid, solid-solid, liquid-gas or solid-gas, etc. Energy storage based on PCMs possess certain merits: (a) storing a large quantity of latent heat per unit volume, leading to high energy storage densities (b) phase change at constant temperature, leading to uniform latent heat transfer (c) availability of a broad spectrum of PCMs, with a wide range of operating temperatures which enable to develop products with tunable temperatures as per required application [10].

### **1.1.2 Phase Change Phenomenon**

Latent heat storage with the help of PCMs is one of the most efficient ways of thermal energy management. Every PCM works upon the basic principle of phase transformation when they encounter a temperature swing.

When a solid-liquid PCM is exposed to the heating process its temperature rises constantly. When the temperature of a storage material reaches the melting point, it begins to melt completely and uniformly. As the melting process is endothermic, it absorbs and stores the thermal energy available in its surrounding in the form of latent heat in a liquidity state. And when the cycle is reversed and the temperature falls progressively the storage material temperature decreases continuously. During the cooling process, the PCM liberates the equal amount of stored energy in the surrounding and transforms back into a solidified state. During the entire heat-cool cycle the temperature remains constant during phase change [11].

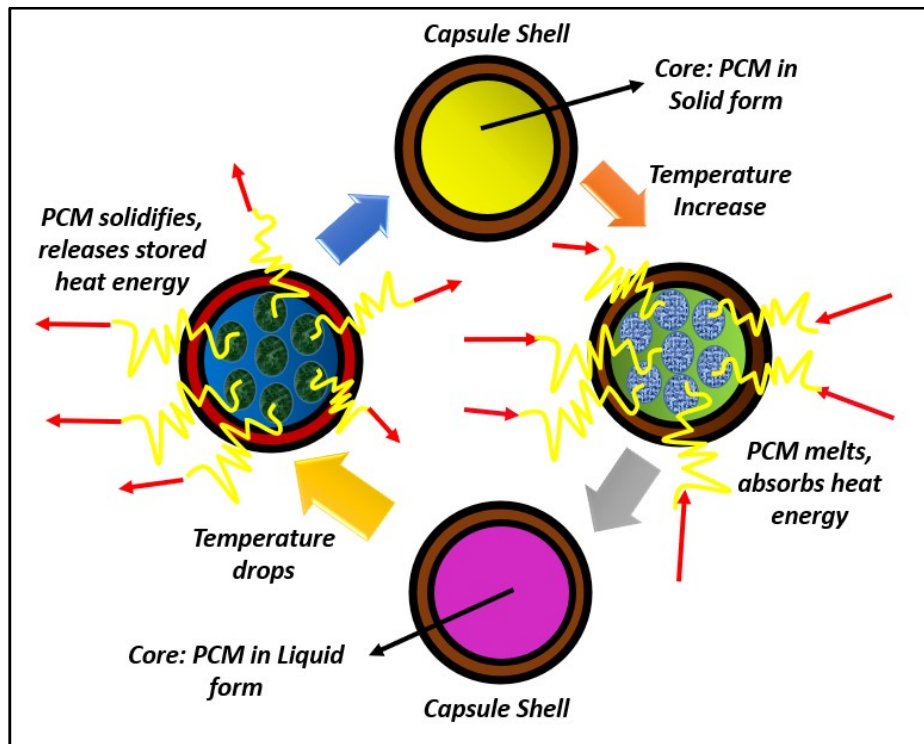


Figure 1.2: Mechanism of Phase Change Process

### 1.1.3 Selection Criteria of Phase Change Materials (PCMs) for TES Applications

According to the available TES related data for the efficient performance of PCMs, to achieve good storage of thermal energy, the PCMs should fulfill basic eligibility in terms of thermo-physical, kinetic, and chemical properties, etc. A potential PCM must have:

- ✓ Phase change temperature lie in the domain of operating temperature of the heating or cooling of the product to achieve optimum performance.
- ✓ High latent heat energy per unit volume to minimize and control the product design and also to store high thermal energy.
- ✓ High thermal conductivity of PCM, that aids in higher heat transfer rates and faster the charging and discharging of the energy storage.
- ✓ Must undergo uniform melting at a constant temperature.
- ✓ Must have a negligible or low supercooling degree (Supercooling is a phenomenon where the temperature of a liquid drops below its solidification temperature without becoming a solid. This alters the working of PCMs while energy storage applications), as supercooling of more than a few degrees will interfere with proper heat extraction from the storage cycle.
- ✓ High Nucleation rates, which promote a faster solidification process and reversible cycles, occur nearly at the same temperature.
- ✓ Small volume change during phase transitions, to solve the complexity of the geometry of the container and helps in in-housing them into various structures.
- ✓ Low vapour pressure that helps to overcome the risk of rupture of encapsulating material due to high-pressure build-up situations.
- ✓ Endure repeatable phase transformation cycles for a long period.

- ✓ High density which facilitates higher energy storage capacity, as the size of storage containers is dependent on the density of PCMs.
- ✓ Chemically stability, as the PCMs are beneficial to operate at the required temperature for long period and reduce the threat for PCMs reaction with materials that are in contact with them improving their operational lifetime.
- ✓ Inert towards the encapsulating matrix to form undesirable products and doesn't leak from the containers.
- ✓ Non-corrosive to avoid deterioration of containers.
- ✓ Non-flammable as they are generally incorporated in building materials and textiles which are close to the public.
- ✓ Not hazardous or poisonous. To be allowed in various applications there must be no poisonous emissions during a fire or if the encapsulation is ruptured during regular use. And, also should not release dangerous emissions to the environment.
- ✓ Easily available and low in cost.

From the information compiled over different studies [12], that the main characteristics required for an ideal PCM for TES applications are summarized in Table 1.1:

**Table 1.1: Basic Requirements of PCMs for TES Applications**

<b>Thermal Properties</b>	<b>Kinetic Properties</b>	<b>Physical Properties</b>	<b>Chemical Properties</b>	<b>Others</b>
Suitable phase-transition temperature (melting point) in desired operating temperatures	Low Supercooling	Favourable phase equilibrium- No Phase Segregation	Chemical stability during phase transformations	Abundant
High Latent Heat of Phase Change	High Nucleation Rate	Small volume change	Complete reversible melting/freezing cycles	Economic
Good Thermal Conductivity in both solid & liquid phases		Low vapor pressure	Compatible with host matrix/encapsulating shell	
Congruent melting pattern		Reproducible Phase Change Cycles	Non-Corrosive	
		High Density	Non-Flammable	
			Non-Toxic	

## 1.2 Classification of Phase Change Materials

Phase Change Materials (PCMs) can be divided into three categories (Figure 1.3): (a) Based on Temperature (b) Based on Phase Change (c) Based on Chemical Nature.



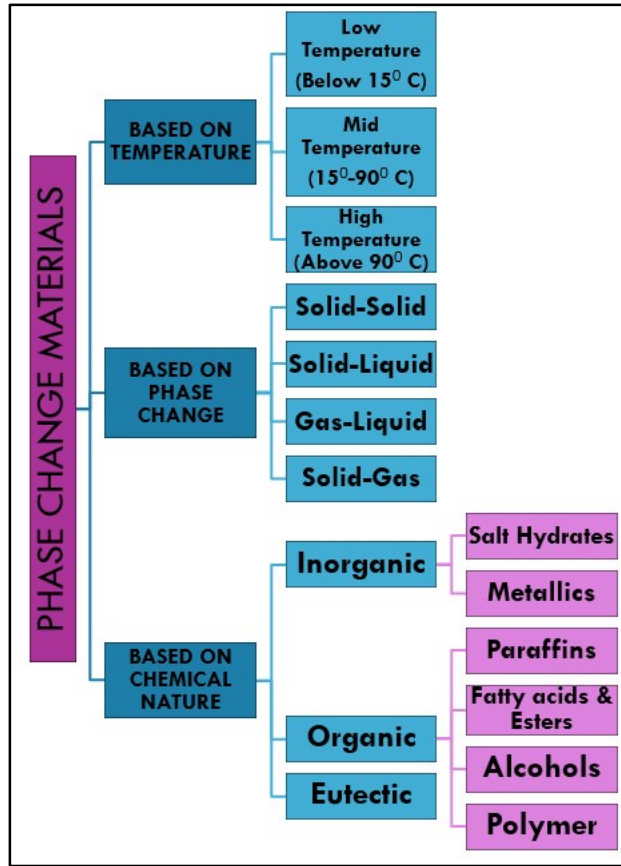


**Figure 1.3: Classification of Phase Change Materials (PCMs)**

### 1.2.1 Based on Temperature

The temperature range governing the phase transformation of PCMs falls within three temperature zones: (i) Low-Temperature PCMs-with phase change temperatures below 15 °C (Fields: Air Conditioning, Cold Storage, Food Industry); (ii) Mid-Temperature PCMs – with phase change temperature 15-90 °C (Fields: Solar Power, Electronics, Smart Textiles, Biomedical Applications, Energy-Efficient Buildings); (iii) High-Temperature PCMs – with phase change temperature beyond 90 °C (Fields: Industrial, Aerospace Applications, Absorptive Refrigeration) [8,13].

### 1.2.2 Based on Phase Transitions

PCMs can also be classified based on their type of physical phase transformations: Solid-Solid; Solid-Liquid; Liquid-Gas; Solid-Gas etc. [14]. The characteristics of each transition are summarized in Table 1.2.

**Table 1.2: Comparison of different types of PCMs based on physical phase transformations**

<b>Solid-Solid PCMs</b>	<b>Solid-Liquid PCMs</b>	<b>Liquid-Gas PCMs</b>	<b>Solid-Gas PCMs</b>
Involves Transformation from Crystalline state to Amorphous state	Involves Transformation from Solid-state to Liquid state	Involves Transformation from Liquid state to Gaseous state	Involves Transformation from Solid-state to Gaseous state
Low Latent Heat Energy compared to solid-liquid PCMs	High Latent Heat Energy compared to solid-solid PCMs	Higher Latent Heat Energies	Higher Latent Heat Energies
Small Volume Change during transitions compared to solid-liquid PCMs	Higher Volume Change during transitions compared to solid-solid PCMs	Higher Volume Change during transitions compared to solid-solid PCMs & solid-liquid PCMs	Higher Volume Change during transitions compared to solid-solid PCMs & solid-liquid PCMs
Need no or lesser encapsulation; Leak-Proof	Requires Encapsulation; Leak-Prone	Requires Large and Bulky Containment; Leak-Prone	Requires Large and Bulky Containment; Leak-Prone
Gives better flexibility in design	Practical & Economically attractive	Impractical and Complex system	Impractical and Complex system

### 1.2.3 Based on Chemical Nature

#### (i) Inorganic PCM

These phase change materials are considered to be the oldest and most widely studied latent heat energy storage entities. These types of PCMs mainly constitute salt hydrates.

## Salt Hydrates

Salt Hydrates are the chemical compounds of inorganic nature comprising of inorganic salts and bounded water molecules typically known as the water of crystallization or water of hydration. From a thermodynamics point of view, the process of dehydration of water from the inorganic salts is considered as the phase transformation for salt hydrates which is equivalent to the melting or freezing of salt crystals. During the melting stage, the salt hydrates disintegrate into anhydrous salt and water or lower hydrates and water. Depending upon their nature the salts hydrates show three different types of melting behavior, (1) Congruent Melting- occurs when anhydrous salt is readily soluble in its water of hydration at melting; (2) Semi-Congruent Melting- occurs when an equilibrium exists between both liquid and solid phases at melting point; (3) Incongruent Melting- occurs when the salt is not soluble in its water of hydration upon melting [8, 15].

**Merits:** High latent energy storage density, sharp melting transitions, high thermal conductivity, low cost, inflammable.

**Demerits:** Although these materials possess good energy storage properties but suffer from supercooling, segregation, corrosion, etc.

Phase change temperatures and latent heat of fusions of salt hydrates is given in Table 1.3.

**Table 1.3: Phase Change Temperatures and Latent Heat of Fusions of Salt Hydrates**

Salt Hydrates	Melting Point (°C)	Latent Heat (kJ/Kg)	References
$K_2HPO_4 \cdot 6H_2O$	14	109	[6]
$FeBr_3 \cdot 6H_2O$	27	105	[15]
$Mn(NO_3)_2 \cdot 6H_2O$	25	148	[6]
$CaCl_2 \cdot 12H_2O$	29.8	174	[6]
$LiNO_3 \cdot 3H_2O$	30	296	[6]
$Na_2CO_3 \cdot 10 H_2O$	32	267	[6]

$\text{Na}_2\text{SO}_4 \cdot 10\text{H}_2\text{O}$	32.4	241	[6]
$\text{CaBr}_2 \cdot 6\text{H}_2\text{O}$	34	138	[6]
$\text{LiBr} \cdot 2\text{H}_2\text{O}$	34	124	[6]
$\text{Zn}(\text{NO}_3)_2 \cdot 6\text{H}_2\text{O}$	36	136	[15]
$\text{FeCl}_3 \cdot 6\text{H}_2\text{O}$	37	223	[6]
$\text{Mn}(\text{NO}_3)_2 \cdot 4\text{H}_2\text{O}$	37	115	[6]
$\text{CuSO}_4 \cdot 7\text{H}_2\text{O}$	40	171	[15]
$\text{KF} \cdot 2\text{H}_2\text{O}$	42	162	[6]
$\text{MgI}_2 \cdot 8\text{H}_2\text{O}$	42	133	[6]
$\text{Zn}(\text{NO}_3)_2 \cdot 4\text{H}_2\text{O}$	45	110	[6]
$\text{Mg}(\text{NO}_3)_3 \cdot 4\text{H}_2\text{O}$	47	142	[6]
$\text{Na}_2\text{SiO}_3 \cdot 5\text{H}_2\text{O}$	48	168	[6]
$\text{Na}_2\text{S}_2\text{O}_3 \cdot 5\text{H}_2\text{O}$	48	210	[6]
$\text{Ca}(\text{NO}_3)_2 \cdot 3\text{H}_2\text{O}$	51	103	[6]
$\text{Zn}(\text{NO}_3)_2 \cdot 2\text{H}_2\text{O}$	55	68	[6]
$\text{FeCl}_3 \cdot 2\text{H}_2\text{O}$	56	90	[6]
$\text{Ni}(\text{NO}_3)_2 \cdot 6\text{H}_2\text{O}$	57	168	[6]
$\text{MnCl}_2 \cdot 4\text{H}_2\text{O}$	58	151	[6]
$\text{CH}_3\text{COONa} \cdot 3\text{H}_2\text{O}$	58	270	[15]
$\text{Fe}(\text{NO}_3)_2 \cdot 6\text{H}_2\text{O}$	60	125	[15]
$\text{NaAl}(\text{SO}_4)_2 \cdot 10\text{H}_2\text{O}$	61	181	[15]
$\text{FeSO}_4 \cdot 7\text{H}_2\text{O}$	64	200	[15]
$\text{Na}_3\text{PO}_4 \cdot 12\text{H}_2\text{O}$	65	168	[15]
$\text{LiCH}_3\text{COO} \cdot 2\text{H}_2\text{O}$	70	150	[6]
$\text{Al}(\text{NO}_3)_3 \cdot 9\text{H}_2\text{O}$	72	155	[6]
$\text{Ba}(\text{OH})_2 \cdot 8\text{H}_2\text{O}$	78	265	[15]
$\text{Mg}(\text{NO}_3)_2 \cdot 6\text{H}_2\text{O}$	89	165	[15]
$\text{KAl}(\text{SO}_4)_2 \cdot 12\text{H}_2\text{O}$	91	184	[15]
$\text{MgCl}_2 \cdot 6\text{H}_2\text{O}$	117	165	[15]

## Phase Separation

This phenomenon arises due to incongruent melting behavior in which the released water of hydration is insufficient to dissolve the solid phase present around which leads to the anhydrous salt get settles down at the bottom of the container due to difference in densities of the separated salt and water. At solidification temperature, the salt will be saturated at the bottom surface and some salt will be unable to reabsorb the water of crystallization. Therefore, the total volume of salt that can undergo phase change has decreased, and the effectiveness of the PCM will be

reduced. To eliminate this problem addition of gelling or thickening agents is found to be well effective [8, 16].

### **Supercooling**

Apart from phase segregation, one more particular issue with salt hydrates related to energy storage performance is supercooling. Poor nucleating properties of salt hydrates lead to a supercooling phenomenon before freezing occurs. During supercooling, the liquid phase of inorganic hydrates does not crystallize (solidify) at respective temperatures, but it reaches to a temperature much below the freezing point before actual solidification takes place. To eliminate this problem the rate of nucleation must be enhanced to do such addition of nucleating agents are found to be well effective [17].

#### **(ii) Organic PCM**

##### **(a) Paraffins**

Paraffin is known to be a by-product of a petroleum refinery. They belong to the family of saturated hydrocarbons or alkanes with common molecular formula-  $C_nH_{2n+2}$ , where n is the number of carbons (C). Depending upon the carbon content, paraffin exists in different physical states: n= 1-4 C atoms the material is gaseous; n= 5-17 C is liquid and n >17 C is solid. It is considered a paraffin wax when the C is in the range of 20-40. The melting temperature of these materials increases with an increase in the number of hydrocarbon chains in the molecules because of the elevated induced dipole attraction between n-alkane chains [1].

**Merits:** These PCM materials exhibit congruent melting behavior, no phase segregation, no supercooling tendency, chemically and thermally stable over a long period of phase change cycles, have a low vapour pressure in the molten state, non-corrosive, etc.

**Demerits:** Paraffins have possessed low thermal conductivity which affects energy storage ability, shows large volume change during the phase transformations. They also undergo slow oxidation when exposed to oxygen. Metallic fillers and matrix structures are used to improve the thermal conductivity, while containers and different geometries of containers are used to overcome the volume change during melting and freezing and to limit the outdoor exposure. Table 1.4 presents an overview of the phase change temperatures and latent heat of fusions of paraffins.

**Table 1.4: Phase Change Temperatures and Latent Heat of Fusions of Paraffins**

Alkanes	Formula	Melting Point (°C)	Latent Heat (kJ/Kg)	References
n-Dodecane	C <sub>12</sub> H <sub>26</sub>	-10	216	[18]
n-Tridecane	C <sub>13</sub> H <sub>28</sub>	-5	160	[18]
n-Tetradecane	C <sub>14</sub> H <sub>30</sub>	5-6	226	[18]
n-Pentadecane	C <sub>15</sub> H <sub>32</sub>	10	207	[15]
n-Hexadecane	C <sub>16</sub> H <sub>34</sub>	18	236	[9]
n-Heptadecane	C <sub>17</sub> H <sub>36</sub>	22	215	[15]
n-Octadecane	C <sub>18</sub> H <sub>38</sub>	28	245	[9]
n-Nonadecane	C <sub>19</sub> H <sub>40</sub>	32	222	[18]
n-Eicosane	C <sub>20</sub> H <sub>42</sub>	36-37	247	[8]
n-Heneicosane	C <sub>21</sub> H <sub>44</sub>	41	215	[15]
n-Docosane	C <sub>22</sub> H <sub>46</sub>	44	249	[6]
n-Tricosane	C <sub>23</sub> H <sub>48</sub>	47	234	[15]
n-Tetracosane	C <sub>24</sub> H <sub>50</sub>	51	255	[15]
n-Pentacosane	C <sub>25</sub> H <sub>52</sub>	54	238	[15]
n-Hexacosane	C <sub>26</sub> H <sub>54</sub>	56	255	[18]
n-Heptacosane	C <sub>27</sub> H <sub>56</sub>	59	236	[15]
n-Octacosane	C <sub>28</sub> H <sub>58</sub>	61	255	[15]
n-Nonacosane	C <sub>29</sub> H <sub>60</sub>	64	240	[15]
n-Triacontane	C <sub>30</sub> H <sub>62</sub>	65	252	[8]
n-Hentriacontane	C <sub>31</sub> H <sub>64</sub>	68	242	[6]
n-Dotriacontane	C <sub>32</sub> H <sub>66</sub>	70	170	[6]
n-Tritriacontane	C <sub>33</sub> H <sub>68</sub>	71	189	[15]
n-Tetratriacontane	C <sub>34</sub> H <sub>70</sub>	75	269	[6]

**(b) Fatty Acids**

These naturally derived products constitute another segment of organic PCMs. They give strong competition to paraffin counterparts, in the organic category. These are the carboxylic acid (COOH) terminally attached to long-chain hydrocarbon with a general formula  $\text{CH}_3(\text{CH}_2)_{2n}\text{COOH}$ . Fatty acids are typically derived from glycerides or phospholipids found in plants and animals and can be saturated or unsaturated [5].

**Merits:** High heat of fusion, no supercooling effect, no segregation, renewable in nature, abundant, compatible with most of the wall materials, biodegradable, non-toxic.

**Demerits:** Less heat storage density than inorganic PCMs, flammable, mildly corrosive, some fatty acids show undesirable odor. Phase change temperatures and latent heat of fusions of the fatty acids and fatty acid derivatives are given in Table 1.5 and Table 1.6 respectively.

**Table 1.5: Phase Change Temperatures and Latent Heat of Fusions of Fatty Acids**

Fatty Acids	Formula	Melting Point (°C)	Latent Heat (kJ/Kg)	References
Butyric Acid	$\text{CH}_3(\text{CH}_2)_2\text{COOH}$	-5	126	[18]
Caproic Acid	$\text{CH}_3(\text{CH}_2)_4\text{COOH}$	-3	131	[18]
Caprylic Acid	$\text{CH}_3(\text{CH}_2)_6\text{COOH}$	16	148	[15]
Undecylenic Acid	$\text{CH}_3(\text{CH}_2)_6\text{COOH}$	23	141	[8]
Capric Acid	$\text{CH}_3(\text{CH}_2)_8\text{COOH}$	32	153	[18]
Lauric Acid	$\text{CH}_3(\text{CH}_2)_{10}\text{COOH}$	44	178	[15]
Myristic Acid	$\text{CH}_3(\text{CH}_2)_{12}\text{COOH}$	54	205	[15]
Margaric Acid	$\text{CH}_3(\text{CH}_2)_{15}\text{COOH}$	60	172	[18]
Palmitic Acid	$\text{CH}_3(\text{CH}_2)_{14}\text{COOH}$	64	212	[18]
Stearic Acid	$\text{CH}_3(\text{CH}_2)_{16}\text{COOH}$	70	203	[15]

**Table 1.6: Phase Change Temperatures and Latent Heat of Fusions of Fatty Acid Derivatives**

<b>Fatty Acid Derivates</b>	<b>Melting Point (°C)</b>	<b>Latent Heat (kJ/Kg)</b>	<b>References</b>
Propyl Palmitate	16-19	186	[9]
Isopropyl Palmitate	11	95-100	[9]
Isopropyl Stearate	14-18	140-142	[9]
Butyl Stearate	19	140-200	[9]
Vinyl Stearate	27-29	122	[9]
Methyl Palmitate	29	205	[15]
Cetyl Alcohol	49	141	[5]
Ethyl Myristate	11	184	[5]
Stearyl Laurate	42	201	[5]
Stearyl Myristate	48	203	[5]
Cetyl Palmitate	51	214-220	[5]
Cetyl Myristate	49.4	220-228	[5]
Cetyl Stearate	54.6	212-216	[5]
Methyl Stearate	29	169	[9]

Some more hydrocarbon chemicals that serve as organic PCM apart from the above-stated compounds are mentioned in Table 1.7 as shown as below:

**Table 1.7: Phase Change Temperatures and Latent Heat of Fusions of some hydrocarbon chemicals that serve as Organic PCMs**

<b>Organic PCM</b>	<b>Melting Point (°C)</b>	<b>Latent Heat (kJ/Kg)</b>	<b>References</b>
Formic Acid	7.8	247	[9]
Glycerin	18	199	[9]
D-Lactic Acid	26	184	[9]
Phenol	41	120	[6]
Caprylone	40	259	[15]
p-Toluidine	43	167	[6]
Cyanamide	44	209	[15]
Camphene	50	238	[6]



Thymol	51.5	115	[6]
Chloroacetic Acid	56	130	[15]
Bees Wax	61.8	177	[15]
Glycolic Acid	63	109	[6]
Acetamide	81	241	[15]
Catechol	104.3	207	[15]
Succinic Anhydride	119	204	[6]
Benzoic Acid	121.7	142.8	[6]
Salicylic Acid	159	199	[15]
Hydroquinone	172.4	258	[15]

**(c) Eutectics**

Eutectics PCMs are the mixture, resulting from the combination of two or more PCMs in a particular weight percent composition ratio. The compounds can be of any combination like organic-organic, inorganic–inorganic, and organic-inorganic. Eutectic PCMs always follow a congruent melt-freeze cycle and tend to form a mixture of the components’ crystals during crystallization. The exhibits phase change at lower temperatures compared to any other composition obtained from the same components. The main advantage of eutectics PCMs is the flexibility with which melting points can be altered by combining different weight percentages of different PCM components [17]. Phase change temperatures and latent heat of fusions of inorganic eutectics is given in Table 1.8 and phase change temperatures and latent heat of fusions of fatty acid eutectics is given in Table 1.9.

**Table 1.8: Phase Change Temperatures and Latent Heat of Fusions of Inorganic Eutectics**

<b>Inorganic Eutectic Mixtures</b>	<b>Melting Point (°C)</b>	<b>Latent Heat (kJ/Kg)</b>	<b>References</b>
31% Na <sub>2</sub> SO <sub>4</sub> +13% NaCl + 16% KCl + 40% H <sub>2</sub> O	4	234	[9]
45% Ca(NO <sub>3</sub> ) <sub>2</sub> .6H <sub>2</sub> O + 55% Zn(NO <sub>3</sub> ) <sub>2</sub> .6H <sub>2</sub> O	25	130	[9]
45-52% LiNO <sub>3</sub> .3H <sub>2</sub> O + 48-	17.2	220	[9]

55% Zn(NO <sub>3</sub> ) <sub>2</sub> .6H <sub>2</sub> O			
47% Ca(NO <sub>3</sub> ) <sub>2</sub> .4H <sub>2</sub> O + 53% Mg(NO <sub>3</sub> ).6H <sub>2</sub> O	30	136	[9]
66.6% CaCl <sub>2</sub> .6H <sub>2</sub> O + 33.3% MgCl <sub>2</sub> .6H <sub>2</sub> O	25	127	[9]
50% CaCl <sub>2</sub> + 50% MgCl <sub>2</sub> . 6H <sub>2</sub> O	25	95	[9]
61.5 % Mg(NO <sub>3</sub> ) <sub>2</sub> .6H <sub>2</sub> O + 38.5% NH <sub>4</sub> NO <sub>3</sub>	52	125.5	[15]
58.7% Mg(NO <sub>3</sub> ) <sub>2</sub> .6H <sub>2</sub> O + 41.3% MgCl <sub>2</sub> .6H <sub>2</sub> O	59	132.2	[15]
53% Mg(NO <sub>3</sub> ) <sub>2</sub> .6H <sub>2</sub> O + 47% Al(NO <sub>3</sub> ).9H <sub>2</sub> O	61	148	[15]
59% Mg(NO <sub>3</sub> ) <sub>2</sub> .6H <sub>2</sub> O + 41% MgBr <sub>2</sub> .6H <sub>2</sub> O	66	168	[6]
66% AlCl <sub>3</sub> + 20% NaCl + 14% KCl	70	209	[15]
25% LiNO <sub>3</sub> + 65% NH <sub>4</sub> NO <sub>3</sub> + 10% NaNO <sub>3</sub>	80.5	113	[15]
66% AlCl <sub>3</sub> + 34% NaCl	93	201	[15]

**Table 1.9: Phase Change Temperatures and Latent Heat of Fusions of Fatty Acid Eutectics**

<b>Fatty Acid Eutectic Mixtures</b>	<b>Melting Point (°C)</b>	<b>Latent Heat (kJ/Kg)</b>	<b>References</b>
65% Capric Acid + 35% Lauric Acid	13	117	[18]
61.5% Capric Acid + 38.5% Lauric Acid	19	132	[9]
26% Myristic Acid + 74% Capric Acid	23	155	[18]
34% Myristic Acid + 66% Capric Acid	24	147.7	[5]
75.2% Capric Acid + 24.8% Palmitic Acid	22.1	153	[9]
87% Capric Acid + 13% Stearic Acid	27	160	[18]
45% Capric Acid + 55% Lauric Acid	17-21	143	[5]
66% Lauric Acid + 34% Palmitic Acid	33-37	169	[18]
63% Lauric Acid + 37%	31-37	170	[18]

Myristic Acid			
76% Lauric Acid + 24% Stearic Acid	37	171	[18]
50% Myristic Acid + 50% Stearic Acid	35-52	189	[18]
66% Myristic Acid + 34% Palmitic Acid	44	181	[18]
65% Palmitic Acid + 35% Stearic Acid	51	179	[18]
70% Capric Acid + 30% Lauric Acid	21.09	123.98	[5]
70% Capric Acid + 30% Stearic Acid	23.4	104.9	[5]
70% Capric Acid + 30% Myristic Acid	21.79	123.62	[5]
70% Capric Acid + 30% Palmitic Acid	27.07	142.61	[5]
89% Capric Acid + 11% Palmitic Acid	28.7	141.4	[5]
60% Lauric Acid + 40% Myristic Acid	28.8	172	[5]
65% Lauric Acid + 35% Palmitic Acid	32.8-37.1	170.2	[5]

**(c) Polyethylene Glycols (PEGs)**

Polyethylene Glycols, also known as Polyethylene oxide, buildup of dimethyl ether chains bearing hydroxyl functionality (-OH) at the terminal end, commonly represented as HO-CH<sub>2</sub>-(CH<sub>2</sub>-O-CH<sub>2</sub>)<sub>n</sub>-CH<sub>2</sub>-OH. They adore the presence of both hydrophilic and hydrophobic moieties in the main chain backbone, allowing them to be dually miscible with aqueous and organic compounds. PEGs are marketed in many grades based on their molecular weights. Both melting temperatures and heat storage enthalpies of PEGs increases with increasing molecular weights. The high crystalline nature of PEGs is mainly responsible for the high latent heat enthalpy of these polymeric materials [5, 8, 18]. These are the only member of the organic PCM family possessing a macromolecular nature forming a class of solid-solid PCMs.

**Merits:** High latent heat of fusion, available in various melting points, highly crystalline, possess good chemical and thermal stability, low vapor pressure, non-flammable, biodegradable, and economically cheap.

**Demerits:** Less heat storage density than inorganic PCMs, show supercooling tendency due to difficulty in crystalline long chains packing during cooling. Table 1.10 presents the phase change temperatures and latent heat of fusions of PEGs with different molecular weights.

**Table 1.10: Phase Change Temperatures and Latent Heat of Fusions of PEGs of Different Molecular Weights**

PEGs	Melting Point (°C)	Latent Heat (kJ/Kg)	References
PEG 400	4.2	117.6	[8]
PEG 600	12.5	129.1	[8]
PEG 1000	40	168.8	[8]
PEG 1500	46.5	176.3	[18]
PEG 2000	51	181.4	[18]
PEG 4000	59.7	189.7	[18]
PEG 6000	64.8	189	[18]
PEG 10000	66	189.6	[18]
PEG 20000	68.7	187.8	[18]

**(d) Poly-alcohols**

Poly-alcohols exhibit a solid-solid phase change nature. At the temperature below phase change, they found to be heterogeneous and when the phase transformation temperatures arrive, they organize themselves into a highly symmetric homogenous face-centred cubic crystal structure, with the ability to take up hydrogen bond energy [18]. These are also known as Plastic Crystals.

**Merits:** High latent heat of fusion, available in various melting points, small volumetric changes, no leakage, no phase segregation. Phase change temperatures and latent heat of fusions of poly-alcohols is given in Table 1.11.

**Table 1.11: Phase Change Temperatures and Latent Heat of Fusions of Poly-alcohols**

Poly-alcohols	Melting Point (°C)	Latent Heat (kJ/Kg)	References
Neopentylglycol (NPG)	42	110-120	[8]
2-amino-2-methyl-1,3-propanediol (AMPL)	80	239	[19]
Pentaglycerine (PG)	82	172.5	[8]
Tris-(hydroxymethyl) aminomethane (TRIS)	132.4-134.5	285.3–295.6	[8]
Pentaerythritol (PERT)	185-187	289-339.5	[8]

**(iii) Metals**

Metallic alloys are suitable for phase change applications and they also found to exhibit low melting points. They display high heat of fusion but they suffer from a drawback of weight constraints. Perhaps on a volumetric basis, they are potential candidates with high energy storage densities. These low melting point metals found to be useful in a laser system, USB flash memory, smart phone cooling, electronics heat sinks, etc. [6, 14]. Phase change temperatures and latent heat of fusions of metal PCMs has been reported in Table 1.12.

**Merits:** High latent heat of fusion per unit volume, low specific heat, high thermal conductivity, low vapor pressure.

**Demerits:** Corrosive, bulky in terms of weight basis.

**Table 1.12: Phase Change Temperatures and Latent Heat of Fusions of Metal PCMs**

<b>Metals</b>	<b>Melting Point (°C)</b>	<b>Latent Heat (kJ/Kg)</b>	<b>References</b>
Gallium	30	80.3	[6]
Bi-Cd-In Eutectic	61	25	[6]
Bi-Pd-In Eutectic	70	29	[6]
Bi-In Eutectic	72	25	[6]

Table 1.13 represents the individual traits of various PCMs.

**Table 1.13: Representation of individual traits of various PCMs**

<b>Classification</b>	<b>Inorganic</b>	<b>Organic</b>	<b>Eutectic</b>
<b>Characteristics</b>	Typical crystalline solids Molten salts, metal or alloy, hydrates	Saturated hydrocarbon Acids/esters, high aliphatic hydrocarbons, alcohols, polymers	Mixture of inorganics or organics or inorganic-organic
<b>Advantages</b>	Higher energy storage density, High thermal conductivity, non-flammable, inexpensive	Good thermal & chemical stability, adjustable transition zone	Sharp melting temperature, no segregation, congruent melting temperature
<b>Disadvantages</b>	Supercooling, phase segregation, corrosive, incongruent melting behavior	Low storage density, low thermal conductivity, flammable	Limited data available on their thermo-physical properties

### **1.3 Methods for PCM Protection and Storage**

To ensure the proper functioning, avoiding undesirable reactivity or exposure to the environment and to from a user-friendly handling perspective, various researchers across the globe have developed different storage strategies for PCMs, such as:

(1) Encapsulation Method

(2) Shape Stabilization

#### **1.3.1 Encapsulation Method**

Encapsulation simply means, housing of material in a container/shell of fixed volume to reach certain objectives [5], like:

- Prevent undesirable exposure of working PCM with an outdoor environment which could alter the performance of the PCM
- Control PCM leakage during phase change.
- Increase in heat transfer
- Accommodate volume change during the transition

The encapsulation method is sub-categorized into (i) Macroencapsulation (ii) Microencapsulation (iii) Nanoencapsulation

Macroencapsulation deals with enclosing PCM in a container of any geometry such as pouches, shells, tubes, thin plates, and spheres, etc. and this enables easy installation of PCM in buildings or acting heat exchangers. The size of macroencapsulated PCM can reach beyond a few centimeters level ranges. Features of macroencapsulated PCM includes good leakage prevention but inferior to microencapsulated ones and volume control, weathering protection, poor heat transfer, the tendency of solidification at the edges, poor thermal conductivity, etc. [16, 17, 20]

Microencapsulation is a process of embedding solid or liquid PCM materials as core inside a thin layer of polymer or inorganic material as a shell to form a capsule having a diameter range of 1-1000  $\mu\text{m}$  [5]. Microencapsulation helps in controlling leakage of PCM, volume change during heat cycles, improving heat transfer surface area, adding physical support to the product, easy handling, mitigation of odor or taste, prevention against degradation, and evaporation, etc. Shell materials of the microcapsules can be based on natural or synthetic inorganic materials or polymers [18, 21].

Nanoencapsulation is a method of encapsulating PCM inside a nano-sized entity with a diameter of less than 1  $\mu\text{m}$  termed as nanocapsules or nanoencapsulated PCM. Nanoencapsulated PCM has gathered much attention as TES materials in the last two decades due to their high surface area to volume ratio, much better than microencapsulated PCM [22]. C.Y Zhao et al. [23] synthesized octadecane containing Nanocapsules encapsulated by Poly-(Ethyl Methacrylate) (PEMA) and Poly-(Methyl Methacrylate) (PMMA) copolymers with a core/shell ratio of 80:20 via miniemulsion method. The nanocapsules of 119 nm capsules showed latent heats of melting and crystallization of 198.5 and 197.1 kJ/kg, respectively. The prepared nanocapsules had a high encapsulation ratio of 89.5%. Fuensanta et al. [24] carried out miniemulsion polymerization to encapsulate paraffin inside styrene-butyl acrylate copolymer shell nanocapsules. The nanoencapsulated paraffin showed a good encapsulation efficiency of nearly 80%. Nanocapsules had a regular spherical shape, uniform structure with a size distribution range of 52-112 nm. Heat energy storage capacities were found to be 5-25 J/g. These nanocapsules exhibited good thermal stability even surpassing 200 heat-cool cycles.



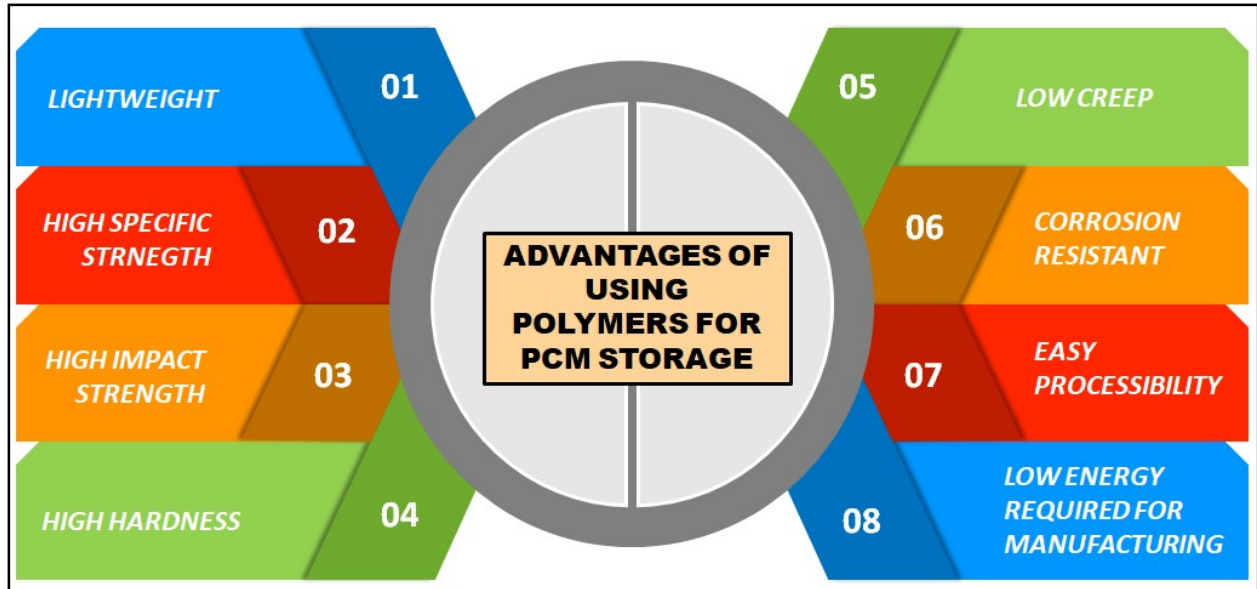


**Figure 1.4: Strategic Advantages of Polymers for PCM Storage**

Different approaches such as Chemical, Physical, Physio-Mechanical have been used by the investigators, to encapsulate PCM resulting into micro/nanoparticles encapsulated PCMs [18]. Among all the foresaid, chemical approaches are most widely used and adopted by many researchers. Different chemical methodologies adopted by the researchers and scientists are as follows:

### **1.3.1.1 In-situ Polymerization**

This technique is the most common and simple chemical synthesis method used for the encapsulation of PCM. The polymerization is carried out in an aqueous continuous phase. A low molecular weight prepolymer is formed at the beginning. The core materials are dispersed along with the monomer or prepolymer into the aqueous medium, thereby reacting chemically, to form a spherical enclosure around the core material. This polymerization technique yields microencapsulated PCM with better wall shielding and thermal diffusion characteristics [25]. F. Salaün et al. [26] manufactured thermo-responsive textile fabric by incorporating melamine-

formaldehyde microcapsules of diameter, ranging from 1-2  $\mu\text{m}$ , containing an n-alkane mixture as thermal energy storage material, produced by in-situ polymerization. These microcapsules had shown good energy storage characteristics, better mechanical and thermal stability. Wang et al. [27] performed an in-situ polymerization technique for the encapsulation of nonadecane by melamine-formaldehyde (MF) polymeric shells, to prepare microencapsulated PCM slurries, to conduct heat storage experiments in a rectangular enclosure by natural convection process. Giro-Paloma et al. [28] employed in-situ polymerization to study the optimum core/shell ratio for Tetracosane/Polystyrene (PS) and PMMA to obtain microencapsulated PCM having better mechanical and thermal properties. The Tetracosane/Polystyrene (PS) microcapsules with effective desirable properties were obtained when the best core/shell ratio reached 1:3.

#### **1.3.1.2 Interfacial Condensation Polymerization**

Interfacial polymerization is a polymerization technique wherein a polymer constituting microcapsule wall is formed at the interface existing between two phases containing the required monomers, participating in the reaction, as shown in Figure 1.5. More specifically, a multi-functional monomer (e.g., diisocyanate) is dissolved in the organic phase, containing core material. Then, the organic component is subsequently dispersed in an aqueous phase, containing emulsifier and protective colloids. After that, a reactive multi-functional comonomer (e.g., amine) is added to the aqueous phase. The monomers from the both organic and aqueous phases diffuse to the interface, where they react chemically in the presence of a catalyst, which in turn leads to the formation of microcapsule shells at the interface, that are insoluble in both phases and accumulates at the surface of the suspended core material droplets, resulting in encapsulation of phase change materials [14, 25]. Polyurea based microencapsulated PCMs are most

commonly obtained from this method. Liang et al. [29] employed the interfacial polymerization technique to achieve polyurea microcapsules containing butyl stearate as a core PCM.

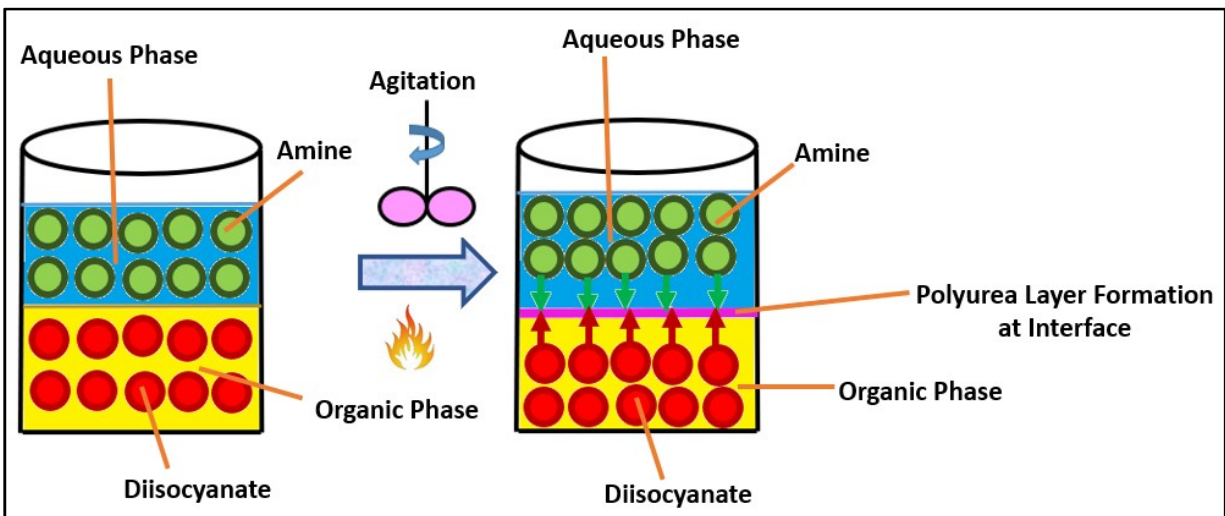


**Figure 1.5: Schematic Representation of Interfacial Polymerization**

### 1.3.1.3 Suspension Polymerization

The suspension polymerization technique is reported more suitable for the PCM encapsulation with water-insoluble polymers, such as, Polymethyl Methacrylate (PMMA), Divinyl Benzene (DVB), Polystyrene (PS), Polyvinyl Chloride (PVC), Polyvinyl Acetate (PVAc), etc. The monomer is suspended in the form of tiny droplets in an appropriate solvent, which is stabilized, and prevented from coalescing by using water-soluble protective colloids, surface-active agents, and stirring [20]. Since each monomer droplet is isolated and independent of other droplets, hence, acts as an individual polymerization nucleus. The continuous aqueous phase, separating the monomer droplets, acts as an efficient heat transfer medium and controls the exothermicity of the reaction. As the entire bulk of the monomer is divided into innumerable tiny droplets, the control on the kinetic chain length of the polymer formed is also very good, which in turn leads to a fairly narrow molecular weight distribution of the product, as shown in Figure 1.6. Silva et

al. [30] produced Polystyrene (PS) microcapsules incorporated with paraffin wax via suspension polymerization, for textile applications. The fabric containing 35 wt. % microcapsules showed an energy storage capacity of 7.6 J/g, high durability, and adequate stability after washing, rub fastness, and ironing treatments. Qiu et al. [31] focused on the energy-saving smart building applications, carried out the copolymerization of n-Butyl Methacrylate (BMA) with n-Butyl Acrylate (BA), Methacrylic Acid (MAA), and Acrylic Acid (AA) to achieve microencapsulation of n-octadecane, using suspension polymerization. Microencapsulated PCMs with BMA based copolymer shells; mainly Poly-(BMA-co-MAA) showed the highest heat of fusion and heat of crystallization of 144.3 J/g and 152.9 J/g respectively. These microcapsules when incorporated in the gypsum board, showed good thermal regulation properties and cycling stabilities up to 1000 thermal cycles.

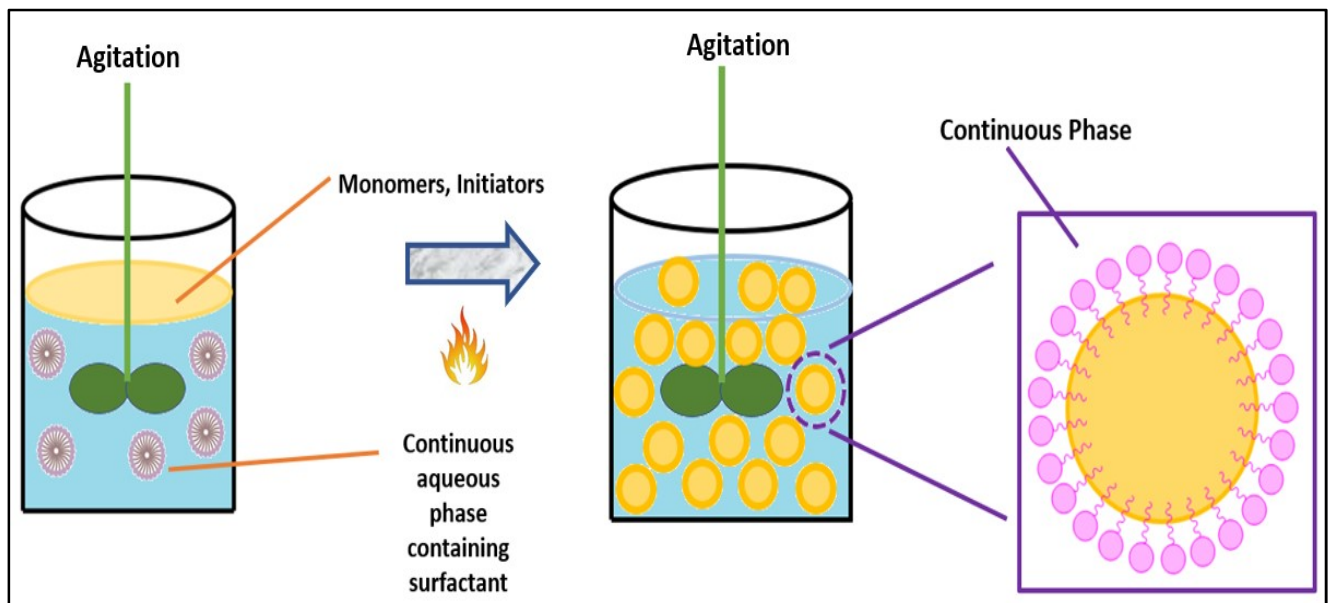


**Figure 1.6: Schematic Representation of Suspension Polymerization**

#### **1.3.1.4 Emulsion Polymerization**

Analogous to suspension polymerization, the emulsion polymerization also involves monomer dispersion in the aqueous phase, not in the form of individual droplets, but as an emulsion. The emulsion is stabilized by using emulsifying agents and protective colloids. Emulsifying agents lower the surface tension at the monomer-water interface which eases the emulsification of monomer in water [20]. A unique attribute of emulsion polymerization is the micelle formation, which presents the site of polymerization. Polymerization is initiated by a free radical thermal initiator. The monomer droplets act as a reservoir from where the monomer diffuses into micelles. Monomer radical chains in the reaction mixture reach toward a monomer droplet-emulsifier micelle domains, and proceeds propagation by attaching to the micelle structure as shown in Figure 1.7. At the final stage, polymer microcapsules in the form of fine powder, uniformly dispersed in the aqueous phase, are isolated and thoroughly washed [14]. Typical polymers suitably synthesized from this technique are PVC, PS, PMMA, or other acrylates, etc.

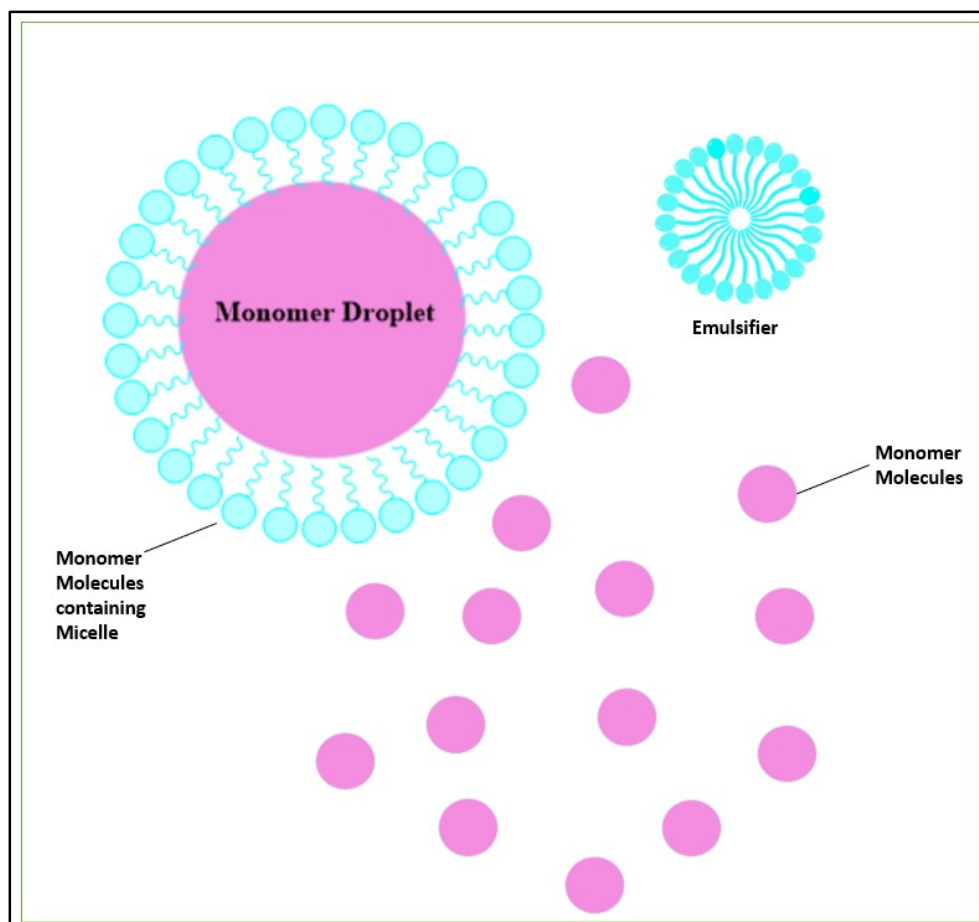


**Figure 1.7: Schematic Representation of Early Stages of Emulsion Polymerization**

Alkan et al. [32] adopted an emulsion technique for the microencapsulation of n-eicosane by Polymethylmethacrylate (PMMA), yielding microcapsules of an average diameter of  $0.70 \mu\text{m}$  with latent heat enthalpies of 84.2 and  $-87.5 \text{ J/g}$ , respectively. Song et al. [33] synthesized PMMA-Silica ( $\text{SiO}_2$ ) hybrid shell microcapsules containing n-octadecane, utilizing UV irradiation-initiated emulsion polymerization. The encapsulation efficiency of PMMA- $\text{SiO}_2$  capsules was turned out to be 62.55%, with storage density around  $122.31 \text{ J/g}$ , when the n-octadecane/MMA feed ratio reached 1.5/1.5. Tang et al. [34] also prepared Polymethylmethacrylate (PMMA) microcapsules containing paraffin by applying UV irradiation for 30 minutes, under constant agitation, during the emulsion polymerization process. The

obtained microcapsules had shown the phase change temperatures ranging from 24-33 °C, having a core content of approximately 61.2 wt. %, with latent energy measured as 101 J/g.

### **1.3.1.5 Coacervation**

This process is also commonly known as the phase separation method. This technique is suitably applied for the encapsulation of PCM with shell wall materials of organic origin, such as, gum-arabic, agar-agar, gelatin, chitosan, silk, etc. [20]. The coacervation method is classified into two types: simple and complex coacervation. The main difference between the both is that, in the former process, a low molecular desolvation solvent is added, which interacts with dissolved polymer and performs phase separation, but in the latter one, deals with the reaction between oppositely charged reactants (polymers) [25]. Typical complex coacervation process comprises of three steps: firstly, the shell material, which intends to be coated, is poured into water to form a phase coacervation, and afterward, the core material is dropped to the above solution to form O/W emulsion. The second step involves the addition of a colloid solution, bearing an opposite electric charge, to the emulsion, with simultaneously maintaining the pH of the mixture. In the final step, the mixture is separated and cooled down to revive the microcapsules end product [14]. Santos et al. [35] used this process for the microencapsulation of xylitol by gum-arabica polymers. Hawalder et al. [36] utilized a complex coacervation technique using gum-arabica and gelatin shell wall materials to cover paraffin wax core yielding PCM microcapsules with a smooth surface and well-defined spherical geometries along with high heat absorption ability up to 239.78 Kj/Kg. Özonur et al. [37] also applied this technique for encapsulation of coco fatty acid mixtures with a variety of amino-plastics polymeric shells and observed that gum-arabic and gelatin combination was potentially very suitable shell wall material obtained by complex coacervation, for fatty acids confinement.

### 1.3.2 Shape-Stabilized Method

These are another class of TES system material in which the PCM is dispersed in a supporting matrix to produce dimensionally form-stable composites. These materials possess certain attractive features such as large heat densities, good thermal conductivity, providing shape stability and leak proofing during the phase change, and thus, eliminating the need for any container for encapsulation, and offer durability over long thermal cycling [16,18]. Feng et al. [38] investigated the shape-stable behavior by rheological analysis of paraffin dispersed in Styrene-b-(Ethylene-co-Butylene)-b-Styrene triblock copolymer (SEBS) supporting matrix. The amount of paraffin PCM successfully retained by the SEBS matrix was determined as 90 wt.%, without leakage above the paraffin melting point, indicating excellent heat storage potential. Yang et al. [39] studied the form stability and mechanical properties of developed PCM, where paraffin melt-blended polymer alloys including High-Density Polyethylene (HDPE) and various elastomeric materials, as Ethylene Propylene Diene Monomer (EPDM), Styrene-Butadiene-Styrene (SBS), Styrene-Isoprene-Styrene (SIS). These alloys possessed heat energy of 80-100 J/g and showed 8-10% weight loss post 100 thermal cycles. Cross-linking of polymer matrices could improve tensile strength without compromising the cyclic stability. Luyt et al. [40] put their efforts to enhance the thermal conductivity of Paraffin/Low-Density Polyethylene (LDPE) shape-stabilized composites by incorporating two types of graphite namely, expandable graphite and natural graphite flakes processed by the twin-screw extruder. It was observed that expanded graphite improved the thermal conductivity by more than 200% at loading of 10 wt. % against a 60% increase of conductivity when graphite flakes are used at the same loading. Besides, the presence of graphite increased the heat transfer rate to PCM irrespective of any form of used filler.



## 1.4 Applications of Phase Change Materials (PCMs)

### 1.4.1 Thermo-regulating Textiles

Thermo-responsive textile monofilaments containing 12 % of PCM microcapsules made up of octadecane as core and melamine-formaldehyde (MF) as shell wall materials were successfully extruded. Polypropylene (PP) fibres containing 12 % of microencapsulated PCM capsules exhibited maximum latent heat energy storage of 9.2 J/g. Statistical models were also developed which can predict the latent heat, modulus and tenacity of any microencapsulated PCM incorporated inside PP fibers. The obtained fibres supported good response values of 98.69 %, 93.60 % and 83.56 % for latent heat, modulus, and tenacity, respectively [41].

Cai et al. [42] studied the influence of 10 wt. % of Expanded Graphite (EG) on structural and thermal properties of Nylon-6 electrospun nanofibrous mats, consisting of fatty acids eutectic mixtures of Capric Acid (CA). These polyamide nanofibres composite was made as a phase change material by soaking them for 10 hours until saturated absorption into an ultrasonically melt-blended solution of three fatty acid eutectics of Capric Acid (CA)-Lauric Acid (LA), Capric Acid (CA)-Palmitic Acid (PA) and Capric Acid (CA)-Stearic Acid (SA) by the fabricated nanofibrous mats. SEM images indicated that Nylon-6/EG nanofibres become more uniform and straight upon EG addition; also, the average diameter of Nylon-6/EG was lower than that of pure Nylon-6. A decrease in the fiber diameters is due to increased conductivity of the spin dope upon the addition of EG. Morphologies of CA-LA/Nylon-6/EG, CA-PA/Nylon-6/EG, CA-SA/Nylon-6/EG, and CA/PA6/EG indicated all nanofibrous mats became bulkier following physical absorption of fatty acid eutectics. It was interesting observed that the added EG itself acts as a supporting matrix to the absorbed fatty acid. The characteristic large specific surface area and porous structure of EG enhanced the porosity of nanofibres which further resulted in the high

absorption capacity of the Nylon-6 nanofibrous composite mats. The absorption capacities of EG/Nylon-6/CA-LA, EG/Nylon-6/CA-PA, and EG/Nylon-6/CA-SA were determined as 90.7 %, 90.0 %, 90.2 % and 90.0 %, respectively.

Wei et al. [43] investigated the effect of the addition of Silica Nanoparticles (Nano-SiO<sub>2</sub>) on the morphological, heat storage, thermal stability, and combustion characteristics of electrospun Lauric Acid (LA) containing Polyethylene Terephthalate (PET) composite fibers. SEM images showed that the Nano-SiO<sub>2</sub> addition altered the morphologies of the LA/PET fibers. SiO<sub>2</sub>/LA/PET fibers had smooth surface texture and low average diameters as compared to composite fibers without Nano-SiO<sub>2</sub>. DSC analysis indicated the heat storage enthalpy values initially increases with increasing Nano-SiO<sub>2</sub>, and then decreases with the further nanoparticles loading, suggesting that, the concentration of Nano-SiO<sub>2</sub> in the composite fibers might have influenced the LA crystallization process with no visible effect on phase change temperatures. Initial combustion temperatures of SiO<sub>2</sub>/LA/PET composite fibers had shifted to higher temperatures, when Nano-SiO<sub>2</sub> was added, and the heat release rate for electrospun composite fibers showed decreasing trends with increasing Nano-SiO<sub>2</sub> concentration.

Weng et al. [44] fabricated ultrafine poly-(meta-phenylene isophthalamide) (PMIA) fibers by electrospinning containing a eutectic binary mixture of lauric–myristic acid (LA-MA) in the molar ratio: 69/31, and investigated the effects of fatty acid content and applied voltage during the processing stage on fibre morphology. Morphological studies revealed that the raw ultrafine fibers prepared at 14 kV had an average fibres diameter of 335 nm with severe conglutination effects. On the addition of fatty acid eutectics at low concentration in the PMIA spinning solution (0.5/1), the average diameter of fibres was increased to 377 nm. When the fatty acid eutectics/PMIA concentration ratio reaches 1/1, a significant reduction in fibre diameter to 210

nm was observed. Further increasing the eutectics concentration in the polymer solution resulted in a gradual increase in average fibre diameter, which is attributed to the increased concentration and viscosity of spinning solutions. Fatty acid eutectic concentration affected the flying fibre jets coverage angles during spinning under a given applied voltage of 14 kV.

Cieslak et al. [45] interestingly studied the effects of different heating/cooling cycle rates (1, 5, 10, 15 °C/min) on thermal energy storage and retrieval properties of Polyester based knitted and woven fabrics impregnated with polymer pastes containing 40 wt.% of two microencapsulated PCMs and its equilibrium mixtures with phase change temperatures of 18 and 28 °C respectively. It was observed that, an increase in heating/cooling rates led to an increase in melting temperatures and a decrease in crystallization temperatures. However, the phase change enthalpy values remained unchanged with varying heating/cooling rates. The difference in energy storage findings was aroused due to structural differences in textile fabrics. The woven fabric structure was tighter and the paste did not penetrate the spaces whereas in the case of knitted fabric; the paste filled the numerous spaces in the material structure.

#### **1.4.2 Energy saving Buildings**

Ramakrishnan et al. [46] developed for PCM energy storage building applications by impregnating paraffin into silicone coating porous expanded perlite by vacuum impregnation and integrating with concrete. The coated porous material containing 50 % by weight of PCM showed no leakage as compared to uncoated perlite. The introduction of porous PCM into concrete remarkably increase the thermal inertia as well as and thermal energy storage property with good thermal cycling stability.

Chen et al. [47] prepared cementitious composites, with significant thermal reliability, incorporated with flaky graphite-doped microencapsulated PCM comprising of hybrid polymer-

inorganic shells in varying loading (10-30 %) having phase change temperature of 30.58 °C and associated heat of fusion equal to 135.8 J/g. SEM analysis suggested that good distribution and interfacial bonding for microencapsulated PCM was observed, throughout the cement. The presence of PCM microcapsules in cement composite in the increasing concentrations led to decrease in both compressive and flexural strengths of the composites, as with 30 % graphite doped PCM found to be reduction in 34.9 % of the flexural strength and 58.4 % of the compressive strength owing to increase porosity of cement composites.

Gypsum composites were fabricated containing three different types of paraffin based microencapsulated PCM to obtain thermo-regulating building material and estimated for such as inherent properties such as heat capacity, thermal stability, thermal conductivity, porosity, density and compressive strength etc. [48]. The findings inferred that with increasing the microcapsules concentration in gypsum caused reduction in the density and compressive strength but enhanced the heat capacity and accumulated heat power of the composites.

A series of microencapsulated PCM consisting of the n-octadecane as core material and melamine–formaldehyde (MF) resin as shell wall material made by in-situ polymerization were prepared and added into gypsum boards in different weight fractions. Boards prepared with 60 % microencapsulated PCM showed phase change temperature in the range of 22–27 °C for about 1735 seconds, indicating thermal regulating property. In addition, gypsum boards offered excellent thermal cycling stability [49].

In a recent study, phase change material composites was developed by using the Eutectic PCMs mixture of capric acid (CA) and lauric acid (LA) as the active PCM and waste fly ash as a supporting material [50]. The performance of these PCM composite were evaluated through simulation, by taking Guangdong as a reference city, with desirable temperature around 25 °C.

The required temperature properties were achieved by using a mass ratio of CA/LA of 4:6. The optimum FA/PCMs composite has a latent heat of 45.38 J/g and has good thermal reliabilities. The results proved that the preparation of such PCM is an efficient way for the reuse of solid waste FA by subjecting the inorganic material for good contribution to the development of energy saving building [50].

### **1.4.3 Temperature-regulating Coatings**

Form-stable PCM composite coatings consisting paraffin as heat storage component and High-Density Polyethylene (HDPE) acting as the supporting material were reported to offers structural stability and leakage protection during phase change [51]. Afterwards, the prepared composites were crushed into fine powder to act as the functional filler for the phase-change coatings, by adding the pulverized HDPE to the polyurethane coating system, which is further applied to Al alloys substrates. SEM micrographs showed the paraffin is dispersed uniformly in the polymer chains of HDPE. DSC analysis reported melting transitions and associated latent heat capacity found to be 49.6 °C and 150.8 kJ/kg, respectively. These thermo-regulating coatings with 30 % and 40 % HDPE PCM powders showed good shock resistance and adhesion strength. Also, coatings with 40 % paraffin-based composites applied on metal substrate were able to control the surface temperature in a better way against uncoated substrate.

Two different kinds of coatings were developed for reducing based on hydrophilic paint composed of acrylic emulsion resin as well as hydrophobic paint composed of urethane resin with the ability to control peak temperature by the introduction of microencapsulated PCM comprising of RT31 (Rubitherm Corporation) as the core material and melamine-formaldehyde (MF) as the shell material. Morphological results provide insight about the good dispersion of PCM microcapsules in the hydrophilic paint, indicating good compatibility of the

microencapsulated PCM with hydrophilic paints than hydrophobic paints. Both DSC and TGA data confirmed that the hydrophilic coating system exhibited better latent heat capacity and thermal stability compared to hydrophobic coating, implying that the hydrophilic coating system had high energy efficiency [52].

#### **1.4.4 Phase Change Slurries**

Zhang et al. [53] used Graphite nanoparticles as a nucleating agent, which were dispersed into a phase change emulsion containing 30 wt. % of OP10E as PCM and a mixture of Tween-80 and Span-80 as the emulsifier, with an objective of eliminating its supercooling, and improving the thermal conductivity of the formed latent heat slurry. They also investigated the effect of the Hydrophile-Lipophile Balance (HLB) value and concentration of the emulsifier on the properties of emulsions. It was observed with HLB value has more predominant effect on the size distribution and dispersion stability of the obtained emulsions, as compared with the concentration of the emulsifier. It is shown that the emulsion with the smallest average droplet diameter and the highest dispersion stability can be prepared using the emulsifier with a HLB value of 8.9 at a loading of 5 wt. %. The thermal conductivity of the emulsion containing 2 wt. % graphite is  $0.578 \text{ W m}^{-1} \text{ K}^{-1}$ , achieving an enhancement by 88.9 % as compared to the one without graphite. The viscosity of the emulsion containing 2 wt. % graphite is lower than 11.5 mPa s, meeting the transportability requirements for pumping in practical applications. No distinct changes in these properties have been observed for the emulsion after being stored for 30 days or being experienced 300 heating-cooling cycles test, implying its good dispersion stability and thermal reliability. The supercooling of the emulsion can be completely eliminated by the addition of the nano-graphite into it at a loading of more than 2 wt. %.

Zhao et al. [54] studied the thermal and rheological properties of the slurries containing microencapsulated PCM, composed of PMMA shell wall filled with paraffin as an active PCM, along with multi-walled carbon nanotubes (MWCNTs). The addition of nanotubes successfully enhanced the thermal conductivity of heat transfer fluid in a non-linearly manner, with increasing nanotubes content and an optimal thermal performance with maximum 8 % increase in thermal conductivity and stability was achieved in suspension having 10 % microencapsulated PCM and 1 % MWCNTs. From rheological aspect, the resultant fluids displayed shear thinning behaviour at the lower shear rate and Newtonian behaviour at the higher shear rate.

PCMs can also be utilized in the field of photovoltaics to cool photovoltaic modules in which a portion of absorbed solar energy is transformed into electrical energy, and the remaining part is transformed into thermal energy by the means of a photovoltaic/thermal (PV/T) collector. An effort was made by researchers to optimize the performance of a photovoltaic/thermal collector using microencapsulated phase change slurry in varying concentrations (5-20 %) where they noted the effect of working parameters on the output of PV/T collector. The concentrations and mass flow rate of microencapsulated slurry, as well as channel height on collector were also taken into consideration during the investigated. It was concluded that, at flow rate of 0.005 kg/s and the channel height = 0.010 m, PV/T collector delivered the best net efficiency having microencapsulated PCM slurry with mass fraction of 20 % [55].

Microencapsulated PCM composed of graphene oxide supported urea-formaldehyde (UF) resin capsules, filled with paraffin wax with phase change temperature of 30.83 °C with associated heat of fusion equal to 90.23 J/g was developed via in-situ polymerization technique, which is further mixed with cement to form cement slurry to control the heat evolution and prevent or delay the undesirable speed of hydration reaction in the cement, in addition to reducing the

contents of C-S-H and  $\text{Ca(OH)}_2$ . The thermal conductivity values found to be varied linearly with increasing order of graphene oxide concentrations where at 0.30 % graphene oxide content, a hike of 53.84 % in the thermal conductivity value was observed. This evaluated cement slurry can be resourceful in meeting the requirements of marine sector [56].

Guo et al. [57] focused on the synthesis of PCM slurry based direct absorption solar collector with duly behaviour of good heat storage properties as well as the photo-thermal conversion, by dispersing the spherical PCM microcapsules of 4  $\mu\text{m}$  in diameter made up of melamine-formaldehyde (MF) resin and octadecane containing oleic acid-coated magnetic nanoparticles (OA-MNs) as the shell and core, respectively into MWCNTs- $\text{H}_2\text{O}$  nano-fluids. The prepared super paramagnetic microencapsulated PCM particles had encapsulation efficiency of 63.51% corresponding to phase change enthalpy of 145 J/g. The oleic acid modified magnetic nanoparticles found to have boosted the thermal conductivity of the PCM microcapsules and therefore, the resultant the slurry consisting of 0.01 wt. % MWCNTs and 15 wt. % PCMs had the optimal photo-thermal conversion properties and thermal storage capacity.

#### **1.4.5 Electronics**

Yang et al. [58] fabricated novel thermo-regulated gamma radiation shielding composite material by developing microcapsules based lead tungstate (PWO) encapsulated paraffin as functional fillers, which were further incorporated to silicone rubber matrix, using tetraethyl orthosilicate (TEOS) as a vulcanizing agent. The prepared composites exhibited maximum latent heat that can reach 52.72 J/g, along with favourable mass attenuation coefficient for gamma irradiation value of  $1.96 \text{ cm}^2 \text{ g}^{-1}$  at energy of 105.3 KeV approximately, which is in fact, equal to rise of 133.33 % against neat rubber. The manufactured material is found to be suitable for application in comfort wearable personal protection in nuclear energy engineering.



Gao et al. [59] prepared form-stable PCMs to be useful in electronic thermal management based on Wood's Alloy as latent heat storage component at different weight fractions (70 %, 80 %, 90 %), with principal compositions of 50 % Bismuth (Bi)/25 % Lead (Pb)/13 % Tin (Sn)/12 % Cadmium (Cd), having melting temperature of 73 °C and Expanded Graphite (EG) serving dual role of thermal promoter as well as supporting matrix. The formed composite PCMs have found to undergo phase change at around 70.5 °C. The thermal conductivity values of the prepared composites were found to follow a non-linear relationship with respect to the concentration of Wood's alloy inside EG network measured as 28.1 (90 %), 37.6 (80 %) and 48.7 Wm<sup>-1</sup> K<sup>-1</sup> respectively; though, all the obtained values were relatively higher than the conductivity of raw Wood's alloy (23 Wm<sup>-1</sup> K<sup>-1</sup>).

#### **1.4.6 Food Packaging**

Lagarón et al. [60] investigated the encapsulation of dodecane into the domains of zein biopolymer to obtain microstructures and nanostructures through electrospinning technique for food packaging. Thermal and chemical analysis results confirmed the proper encapsulation of the PCM within the zein electrospun structures. The coaxial electrospinning configuration allows better encapsulation efficiencies and PCM product in which storage around 25 J/g was obtained. Heat management materials were developed for cold storage using Rubitherm RT5, a technical grade paraffin wax with melting temperature of 5 °C trapped inside two different polymer matrices including polystyrene (PS) and polycaprolactone (PCL), through electrohydrodynamic processing in order to first produce fibrous electrospun mats, which later on pressed using a hot-plate hydraulic press at 63 °C for 90 seconds, to obtain final article in the form of solid slabs. Morphological results confirmed that the slab fibres diameter made from PCL/RT5 dope solution were found to be ranging from 0.55 to 11.91 mm, whereas in case of PS/PCM slabs consisted of

fibre diameters varying from 1.96-19.77 mm along with many beaded areas within the fibrous mats. It was further observed that the optimum thermal heat storage performance was achieved for PCL/PCM slabs at 4 °C storage temperature having maximum encapsulation efficiency of 98.6 % with core content of 44 % [61].

In cold chain transportation, desirable constant temperature in the range of -5 °C to 8 °C is required in order to maintain the quality of fruits, vegetables, and other agricultural products. For the same purpose a cryogenic transport box was fabricated containing sodium polyacrylate (PASS), multi-walled carbon nanotubes (MWCNTs) and water housed in a polyethylene cold storage plate, which was then placed in a vacuum insulation box and yoghurt was used as the test sample. The prepared material showed a phase change temperature of -0.037 °C with corresponding latent heat capacity of 335.4 J/g. The thermal conductivity of 1 % sodium polyacrylate and water after incorporation of 0.1 % MWCNT got increased from 0.757 Wm<sup>-1</sup> K<sup>-1</sup> to 0.9021 Wm<sup>-1</sup> K<sup>-1</sup>. The pH value of the yoghurt was 4.0, which is still within an acceptable consumption range. This cold storage material exhibited the best cooling retention property and allows an effective cold preservation time up to 87 hours [62].

### **1.5 Significant Findings from Literature**

Su et al. [63] produced microencapsulated PCMs following free-radical polymerization route where they opted for n-octadecane as a core latent heat storage material and PMMA as shell component which exhibited a phase change at 22.68 °C and energy storage density 170 kJ/kg with thermal stability behaviour above 160 °C. Yao et al. [64] synthesized PCM microcapsules containing binary cores (paraffin + butyl stearate) encapsulated with acrylic shell copolymerized with styrene and with divinylbenzene in the presence of different acrylate based cross-linking agents namely ethylene glycol dimethacrylate (EGDMA) and 1,4-butylene glycol diacrylate

(BDDA) in order to improve the thermal stability of the resultant microcapsules via suspension polymerization technique. The obtained PCM microcapsules displayed spherical geometries with encapsulated binary core content ratio ranging from 48-68 %. They also showed exceptional thermal resistance and thermal cycling stability.

Fang et al. [65] prepared and evaluated the properties nanoencapsulated PCMs through miniemulsion polymerization technique using n-octadecane as core and polystyrene shell. The measured size and latent heat of spherical nanocapsules were found to be ranging from 100-123 nm and 124.4 kJ/Kg, respectively. Wang et al. [66] prepared and determined the properties of microencapsulated PCM based on stearic acid (SA) encapsulated by polycarbonate (PC) shell, where they had observed that the successful encapsulation ratio achieved by the prepared microcapsules, having average diameter of 0.50  $\mu\text{m}$  was found to be 52%. The developed microencapsulated PCM, with good thermal reliability behaviour showed phase transitions at 60  $^{\circ}\text{C}$  (melting) and 51.2  $^{\circ}\text{C}$  (crystallization) along corresponding latent heat values as 91.4 J/g and 96.8 J/g, respectively. Arabi et al. [67] employed suspension polymerization technique to produce series of microencapsulated PCM with n-hexadecane as core and binary shell wall of poly-(butyl acrylate-co-methyl methacrylate) [Poly-(BA-co-MMA)]. The effect of comonomers ratio on the encapsulation efficiency and thermal performance of the microcapsules, as well as the variations in the morphologies of microcapsules were observed, depending upon difference in polarity of the system.

Srinivasaraonaik et al. [68] utilized in-situ polymerization technique to obtain microencapsulated PCM consisting of core material having fatty acid eutectic mixture- 75% stearic acid (SA) + 25% capric acid (CA) and melamine-formaldehyde (MF) resin forming the shell material. They found out that, a balanced pH (3.2) and stirring rates (1500 rpm) controlled the microstructures of the

obtained microencapsulated PCM, having spherical configurations, with smooth surface morphology and particle size of 10.41  $\mu\text{m}$ . The melting point and latent heat of fusion of the produced microcapsules were found to be 34.5  $^{\circ}\text{C}$  and 103.9 kJ/kg, respectively. The obtained microencapsulated PCM also showed better thermal stability, offered by outer MF resin protective layer, as compared to raw PCM with high encapsulation efficiency of 85.3 %. Konuklu et al. [69] used in-situ polymerization technique for microencapsulation of pentadecane with poly-(melamine-urea-formaldehyde) (MUF). The prepared PCM exhibited encapsulation ratio of 48% with phase change temperature ranging 8.7  $^{\circ}\text{C}$  and 8.1  $^{\circ}\text{C}$ , as well as heat enthalpy values of 84.5 and  $-88.2$  kJ/kg respectively, as indicated by DSC results.

Yu et al. [70] estimated the thermal energy storage properties of microencapsulated PCM based on n-octadecane and Polymethylmethacrylate (PMMA)/Titanium Dioxide ( $\text{TiO}_2$ ) containing hybrid shell (PMMA +  $\text{TiO}_2$ ), prepared by emulsion polymerization technique. The purpose of incorporation of the metal oxide particles to PCM emulsion was to provide improved stability and thermal conductivity. At 1:1 MMA/n-octadecane ratio, the resultant microcapsules showed a latent heat density of 179.9 J/g, along with encapsulation efficiency of the prepared microcapsules reaching close to 67.2 %. Tang et al. [71] produced microencapsulated PCM by covering n-octadecane into copolymer shells as poly-(n-butyl methacrylate-co-methacrylic acid) through emulsion polymerization technique. The particle size distribution of the obtained PCM ranged from 6-74  $\mu\text{m}$ . The phase change enthalpies of melting and crystallization of binary acrylic shells were measured to be 130.3 J/g and 125.8 J/g respectively, along with encapsulation ratio of 56.9 %. When combined with gypsum board, these microcapsules showed good temperature-regulated property.

Tang et al. [72] have chosen silicon nitride in varying dosages (1-10 %) to boost the thermal energy storage performance of microencapsulated PCM composed of n-octadecane core surrounded by PMMA shells. The microcapsules with highest loading of silicon nitride (10 %) containing active PCM core content of 66.4 % showed values of latent heats of fusion and crystallization as deduced as 121.11 J/g and 122.01 J/g respectively. From mechanical view point also silicon nitride particles led to four-fold increase in the mechanical properties of the microcapsules with potential of withstanding the loading force up to 16.24 mN.

Alkan et al. [73] encapsulated Palmitic Acid (PA) and Capric Acid (CA) eutectic mixtures with three different core/shell mass ratios: 1/1, 1/2, 1/3 inside Polystyrene (PS) shells for building heating cooling applications. Thermal energy storage parameters such as phase-change temperatures and latent heat storage enthalpies were estimated between 13.5-17.9 °C and 45-77.3 J/g, respectively. The encapsulation ratio of PS microcapsules with core/shell mass ratio (1/1) was calculated as 47.3 %. PS microcapsules containing different CA-PA eutectic mass ratio also showed good thermal stability and reliability post 5000 accelerated thermal cycles. Yang et al. [74] demonstrated a new method for suppression of the supercooling phenomenon of melamine–formaldehyde (MF) resin encapsulated octadecane, by controlling the composition and synthesis parameters including melamine to formaldehyde monomers ratio, pH of pre-polymer and emulsion while maintaining the latent heat storage ability of the PCM microcapsules.

Fang et al. [75] employed casting method to produced form-stable PCM comprising of PEG4000 as latent heat storage component and epoxy resin as supporting matrix offering the structural stability to captured PCM as well as to prevent leakage during phase transition of the PCM. FTIR results indicated that no chemical modification or reaction was occurred during the

composite fabrication, but there is possible physical cross-linking existed between PEG PCM and the epoxy resin matrix.

Sun et al. [76] studied the combined effects of the addition of both microencapsulated PCM as temperature-regulating and TiO<sub>2</sub> nanoparticles as an ultraviolet (UV) blocking additive to a thin Polyvinyl Chloride (PVC) film for the solar energy storage applications. The spherical PCM microcapsules of 2-15 μm size range were composed of octadecane as core, well-encapsulated inside melamine-formaldehyde resin as a protective shell, synthesized by in-situ polymerization technique. The amount for both PCM microcapsules and TiO<sub>2</sub> nanoparticles in the PVC matrix film was varied according to a weight fraction of 3 wt. %, 6 wt. % and 9 wt. %. Morphological data inferred that the 6 wt. % PCM microcapsules were homogeneously dispersed and strongly bounded in the polymer matrix, indicating this particular concentration of microcapsules as an optimum loading for the preparation of thermal regulatory PVC films. Also, the addition of TiO<sub>2</sub> nanoparticles of diameters around 100 nm into the PVC matrix, influenced the morphology of the prepared films, where it was observed that the loading of 6 wt. % of the nanoparticles lead to smooth and flat surface appearances of the films, in which these nanoparticles were uniformly dispersed and formed an interconnected network inside films. DSC analysis suggested that PVC films with 6 wt. % octadecane microcapsules showed good heat energy storage density of 8.77 J/g. Further incorporation of 6 wt. % TiO<sub>2</sub> nanoparticles to this particular composition of PCM containing films experienced enhanced phase change temperatures and heat storage energy to 9.226 J/g as compared to other samples, indicating the improved heat response rate due to the presence of TiO<sub>2</sub> nanoparticles, homogeneously dispersed in the PVC matrix phase, leading to the formation of a heat transport layer which transmits heat to melamine-formaldehyde microcapsules. Temperature-regulating films 6 wt. % micro-PCMs and 6 wt. % TiO<sub>2</sub>

nanoparticles displayed excellent thermal reliability where they withstand 100 thermal cycles with very minute variation phase change temperature and enthalpies. The prepared temperature-regulating PVC film performed excellently in maintaining the surrounding temperature. The temperature of a space enclosed by the thin composite films incorporating PCM microcapsules and nano-TiO<sub>2</sub> maintains a temperature in the range 25–28 °C for 3298 s. UV spectra of films fabricated with 6 wt. % micro-PCMs and various amounts of nanoparticles showed a decrease in the UV transmittance with increasing the TiO<sub>2</sub> nanoparticles loading in the films.

Khatibi et al. [77] investigated the effect of incorporation of Eicosane filled melamine-formaldehyde microcapsules into Glass-Fibers (GF) reinforced Epoxy resin on thermo-physical properties of FRP composites. The heat enthalpies varied linearly with a weight fraction of added PCM microcapsules. Also, the coefficient of thermal expansion was increased with increasing microcapsules fraction. Thermal conductivities of produced composites also showed decreasing trends with increasing microencapsulated PCMs owing to the low thermal conductivity of capsules shell layer. The addition of microencapsulated paraffin to the epoxy reinforced composites at higher weight fraction showed a decrement in thermal stabilities of the prepared composite due to lack of interfacial adhesion between fibrous filler and the matrix. Shi et al. [78] synthesized a series of Polyvinyl Alcohol (PVA)-g-octadecanol copolymers with the degree of grafting ratios ranging from 83 to 503%. Thermal data presented that PVA-g-octadecanol exhibited low heat storage density as compared to pure PCM which is attributed to restricted mobility of the grafted C18 alkyl side chains between PVA backbones, as well as decreased order of crystal packing of -CH<sub>2</sub> side groups, leads to lower heat storage density. However, the storage density values exhibit an increasing tendency with the apparent grafting ratio when it increases from 40 to 63 J/g when the apparent grafting ratio varies from 283 to 503%.

McNally et al. [79] produced two different sets of High-Density Polyethylene (HDPE) shape-stabilized phase change materials using twin-screw extruder having low paraffin wax (L-PW,  $T_m$ : 18-23 °C) and high paraffin wax (H-PW,  $T_m$ : 56-58 °C) melting point paraffin waxes as the thermal energy storage component. DSC indicated the latent heat enthalpy of PCMs with H-PW decreases with increasing H-PW concentration to a higher range, due to co-crystallization between H-PW and HDPE. Thermo-mechanical analysis results depicted the plasticizing of both waxes on HDPE polymer and mechanical properties (dynamic stress, moduli, tensile & flexural strength) were higher for H-PW/HDPE samples than L-PW/HDPE samples, at ambient conditions. Sobolciak et al. [80] studied the influence of Expanded Graphite (EG) on Linear-Low Density Polyethylene (LLDPE) based form-stable PCM containing paraffin wax as active PCM. It was found that the addition of EG improved the wax leakage from the LLDPE matrix and the degree of leakage decreases with increasing EG contents. Presence of EG also induced prolong photo-oxidation stability to the final article.

Fernández et al. [81] observed that the use of inorganic filler such as  $Mg(OH)_2$  in the polypropylene (PP) matrix surrounding paraffin wax increases the Hardness (H), Elastic modulus (E) and Loss modulus ( $E_{loss}$ ). Besides, the paraffin waxes added as PCM, it also acts as a plasticizer, and deterioration the mechanical properties of shape stabilized PCM material was recorded. Krupa et al. [82] fabricated form-stable PCM by incorporating microencapsulated PCM having spherical capsules of average diameter of 15  $\mu m$  made up of paraffin wax as core content of 43 % and Melamine-Formaldehyde (MF) resin as shell wall material dispersed inside high-density polyethylene (HDPE) supporting matrix. It was summarized that the PCM microcapsules acted as plasticizer resulting in decrease in phase change temperature of HDPE, where 60 wt. % microcapsules concentration reduced melting and crystallization temperatures by



10 °C. Complex viscosity, storage and loss moduli also found to decrease with increasing content of PCM microcapsules in the HDPE matrix.

## **1.6 Research Gaps**

From in-depth literature survey, it was observed that a high volume of research studies has been conducted, which is mainly oriented towards the development of PCMs products based on inorganic PCMs (mainly salt hydrates) owing to their high latent energy storage density, sharp melting transitions, high thermal conductivity etc. However, these are associated with some serious limitations, such as, incongruent melting behavior of some salt hydrates, phase segregation, supercooling, segregation, corrosion etc. In order to resolve such drawbacks, certain additives, such as, nucleating agents, thickening agents etc., are reported to be incorporated in the salt hydrates PCMs formulations, which further aided in the cost of the product. As per the available literature on organic PCMs, most of the PCMs products (encapsulated or form-stable) developed are based on technical grade paraffins, which are obtained from petrochemical resources, which are non-renewable and more costly compared to other PCMs of organic nature (including fatty acids, sugar alcohols, PEGs, low molecular weight organic solid/liquids etc.). Moreover, in the majority of the previously published articles, the encapsulated phase change materials are made up of shell wall materials of either inorganic nature ( $\text{SiO}_2$ ,  $\text{TiO}_2$  and others) or organic backbone such as carbon based material (expanded graphite) or amino-plastic polymers (urea-formaldehyde, melamine-formaldehyde), which are thermoset in nature and cannot be recyclable post use, thus, leading to plastic littering and pollution; and sometimes may become inappropriate due to the leakage of residual formaldehyde post polymerization, posing serious environmental and health problem. From this intensive literature review related to phase

change materials for thermal energy storage applications, the research gaps observed can be summed up as follows:

- Explorations of Organic PCMs as a LHTES material as a counterpart of Inorganic PCMs.
- New product development based on renewable resources: Reducing the reliance on fossil fuels.
- Indistinct of Polymers in the field of TES applications.
- Need to address the residual formaldehyde issue in case of MF capsules during manufacturing.

### 1.7 Research Objectives

The aim of this research work was **to Develop and Evaluate Polymer Based Phase Change Materials (PCMs) for Thermal Energy Storage Applications**. The developed PCMs were characterized for their phase change characteristics, resistant towards ultraviolet exposure and flame retardant property to explore their application in practical fields. The detailed objectives of the present study are summarized as below:

- Synthesis and Evaluation of Microencapsulated PCMs (Micro-PCMs) as LHTES materials.
- Synthesis and Evaluation of Nanoencapsulated PCMs (Nano-PCMs) as LHTES materials.
- Development and Study of Polymeric Form-stable PCMs.
- Study of the influence of incorporation of metal oxide nanoparticles to the prepared PCMs for phase change attributes, thermal, ultraviolet resistance and flame-retardant properties.

## 1.8 Overview of the Thesis

The objective of this thesis is the development and evaluation of polymer-based phase materials for thermal energy storage applications. The whole thesis is organized in **NINE** chapters. **Chapter 1** of the thesis presents the overview of polymer-based phase change materials, followed by the research work conducted by different researchers to develop different types of PCMs. Gaps in available literature and latest trend in the field are also been highlighted in this chapter. Based upon the literature survey, the objectives of the study have been clearly defined. **Chapter 2** deals with the experimental part which includes the materials and methods employed to develop the polymer supported phase change materials. Various characterization techniques used to analyze the phase change and thermal properties along with resistance towards ultraviolet exposure and flame retardant properties of the synthesized polymer based PCMs have also been discussed in this chapter. **Chapter 3** deals with the development and investigation of microencapsulated caprylic acid-based phase change materials made by suspension polymerization technique. **Chapter 4** represents the synthesis and property evaluation of nanoencapsulated PCMs based on fatty acid (undecylenic acid) filled polyaniline nanofibres. **Chapter 5** highlights the fabrication and determination of individual characteristics of metal oxide nanoparticles (titanium dioxide) which are further added to the polymer matrix for the development of form-stable PCMs. **Chapter 6** investigates the preparation of series of form-stable PCMs containing PEG 1500 as an active latent heat storage component in different weight fractions inside the PVA matrix, along with simultaneous incorporation of titanium dioxide nanoparticles to hydrophilic polymer matrix and their subsequent effect on the form-stable PCMs properties. **Chapter 7** includes the studies on the addition of titanium dioxide nanoparticles to PEG 600 based PCMs and corresponding effect on the phase change parameters, resistance

towards ultraviolet exposure and flame-retardant properties of the final PCMs films have been analyzed. **Chapter 8** is focused towards on the preparation and characterization of capric acid filled polyurethane-based form-stable PCMs. In the last chapter i.e. **Chapter 9** of the thesis, the overall conclusions of the results obtained in the entire study are reported. In addition, some recommendations are made for the future studies to guide researchers, who want to pursue the similar kind of work on PCMs or wish to elaborate the studies to next possible level, followed by the section **References**.

## CHAPTER 2

### MATERIALS AND METHODS

---

#### 2.1 Raw Materials/Chemicals

The raw materials/chemicals which were used for the development of polymer based phase change materials (PCMs) are listed below:

1. Caprylic Acid (CpA)
2. Capric Acid (CA)
3. Undecylenic Acid (UA)
4. Polyethylene Glycol (PEG600)
5. Polyethylene Glycol (PEG1500)
6. Polyethylene Glycol (PEG20000)
7. Polyvinyl Alcohol (PVA) (Hot)
8. Methyl Methacrylate (MMA)
9. Benzoyl Peroxide (BPO)
10. Sodium Lauryl Sulphate (SLS)
11. Titanium (IV) Isopropoxide
12. Concentrated Nitric Acid
13. Sodium Hydroxide
14. Isopropyl Alcohol
15. Aniline
16. Toluene
17. Ammonium Persulphate

18. Hydrochloric Acid (HCl)

19. Ethanol

20. Polymeric-Diphenylmethane diisocyanate (PMDI)

### 2.1.1 Specification, Sources and Purity of Raw Materials/Chemicals

As the accuracy of results depends not only on the accuracy of the instrument used or the experiment performed, but also on the purity of the raw material used. Specification, sources and purity of the raw materials and chemicals used to prepare polymer based PCMs and their characterization is given in Table 2.1.

**Table 2.1: Specification, Sources and Purity of Raw Materials/Chemicals**

S.No.	Chemicals/Raw Materials	Sources	Grade Specifications	Purity Specifications
1.	Caprylic Acid	Loba Chemie , Mumbai	Analytical Reagent Grade	≥99%
2.	Capric Acid	Loba Chemie , Mumbai	Analytical Reagent Grade	≥98%
3.	Undecylenic Acid	Avra Synthesis Pvt. Ltd., Hyderabad	Analytical Reagent Grade	≥98%
4.	Polyethylene Glycol (PEG600)	Loba Chemie , Mumbai	Synthesis Grade	M.W. 570-630
5.	Polyethylene Glycol (PEG1500)	Loba Chemie , Mumbai	Synthesis Grade	M.W. 1400-1600
6.	Polyethylene Glycol (PEG20000)	Otto Chemie Pvt. Ltd., Mumbai	Synthesis Grade	M.W. 20000
7.	Polyvinyl Alcohol (PVA) (Hot)	Central Drug House (P) Ltd, Delhi	Synthesis Grade	M.W. 13,000- 23000
8.	Methyl Methacrylate (MMA)	Loba Chemie , Mumbai	Synthesis Grade	≥99%

9.	Benzoyl Peroxide (BPO)	Loba Chemie , Mumbai	Synthesis Grade	≥98%
10.	Sodium Lauryl Sulphate (SLS)	Sisco Research Laboratories (P) Ltd.	Analytical Reagent Grade	≥98%
11.	Titanium (IV) Isopropoxide	Avra Synthesis Pvt. Ltd., Hyderabad	Analytical Reagent Grade	≥98%
12.	Concentrated Nitric Acid	Thermo Fischer Scientific India Pvt. Ltd, Mumbai	Analytical Reagent Grade	≥98%
13.	Sodium Hydroxide	Thermo Fischer Scientific India Pvt. Ltd, Mumbai	Analytical Reagent Grade	≥98%
14.	Isopropyl Alcohol	Loba Chemie , Mumbai	Analytical Reagent Grade	≥99.5%
15.	Aniline	Loba Chemie , Mumbai	Analytical Reagent Grade	≥99.5%
16.	Toluene	Loba Chemie , Mumbai	Analytical Reagent Grade	≥99.5%
17.	Ammonium Persulphate	Loba Chemie , Mumbai	Analytical Reagent Grade	≥98%
18.	Hydrochloric Acid	Loba Chemie , Mumbai	Analytical Reagent Grade	37%
19.	Ethanol	Chang Yu Hi- Tech Chemicals, China	Analytical Reagent Grade	≥99%
20.	Polymeric-Diphenylmethane diisocyanate (PMDI)	Krishna Enterprises, Delhi	30-32 wt.% NCO	≥99%

## 2.2 RESEARCH METHODOLOGY

The methodology employed to achieve the objectives of the research is divided onto the following sections:

- ✓ Synthesis of microencapsulated PCMs using suspension polymerization technique.
- ✓ Synthesis of nanoencapsulated PCMs using interfacial polymerization technique.
- ✓ Synthesis of metal oxide nanoparticles by sol-gel approach.
- ✓ Preparation of metal oxide nanoparticles filled PEG1500 based form-stable PCMs.
- ✓ Preparation of metal oxide nanoparticles filled PEG600 based form-stable PCMs.
- ✓ Development of fatty acid incorporated polyurethane form-stable PCMs.
- ✓ Characterization of developed polymer based microencapsulated and nanoencapsulated PCMs in terms of thermal energy storage parameters such as phase change attributes, thermal stability, thermal cycling, energy storage potential etc.
- ✓ Characterization of form-stable PCMs to study of the influence of incorporation of metal oxide nanoparticles to the prepared PCMs, for phase change attributes, thermal, ultraviolet resistance and flame-retardant properties.

### 2.2.1 *Synthesis of Microencapsulated PCMs using Suspension Polymerization Technique*

Micro-PCMs capsules were obtained by the suspension polymerization technique. The detailed procedure employed is as follows: Firstly, both water and oil phases were formed separately. The water phase was formed by adding 1.5 g of SLS and 0.5 g of PVA to 80 mL of deionized water, under constant stirring. The oil phase was prepared by adding monomer and PCM in 1:1 ratio. The mass ratio of MMA: CpA was chosen as 1:1 to achieve a high encapsulation ratio and high latent heat enthalpy and also to check the effectiveness of the encapsulation process by PMMA shell wall for the encapsulated fatty acid PCM. A uniform and stable oil-in-water emulsion



(O/W) was obtained, by slow addition of oil phase into the continuous aqueous phase, with vigorous agitation at 5000 rpm. Then, this emulsion was transferred to a 250 mL three-neck round bottom flask to proceed with the polymerization reaction, by adding 0.3 g of benzoyl peroxide free radical initiator, under an inert nitrogen blanket, at 85 °C for 8 hours. After 8 hours, the obtained microcapsules were centrifuged and dried in a hot air oven for 24 hours at 70 °C. The yield of the polymer microcapsules obtained was about 83.2%. A schematic representation of the adopted experimental procedure for the synthesis of Micro-PCMs is shown in Figure 2.1.

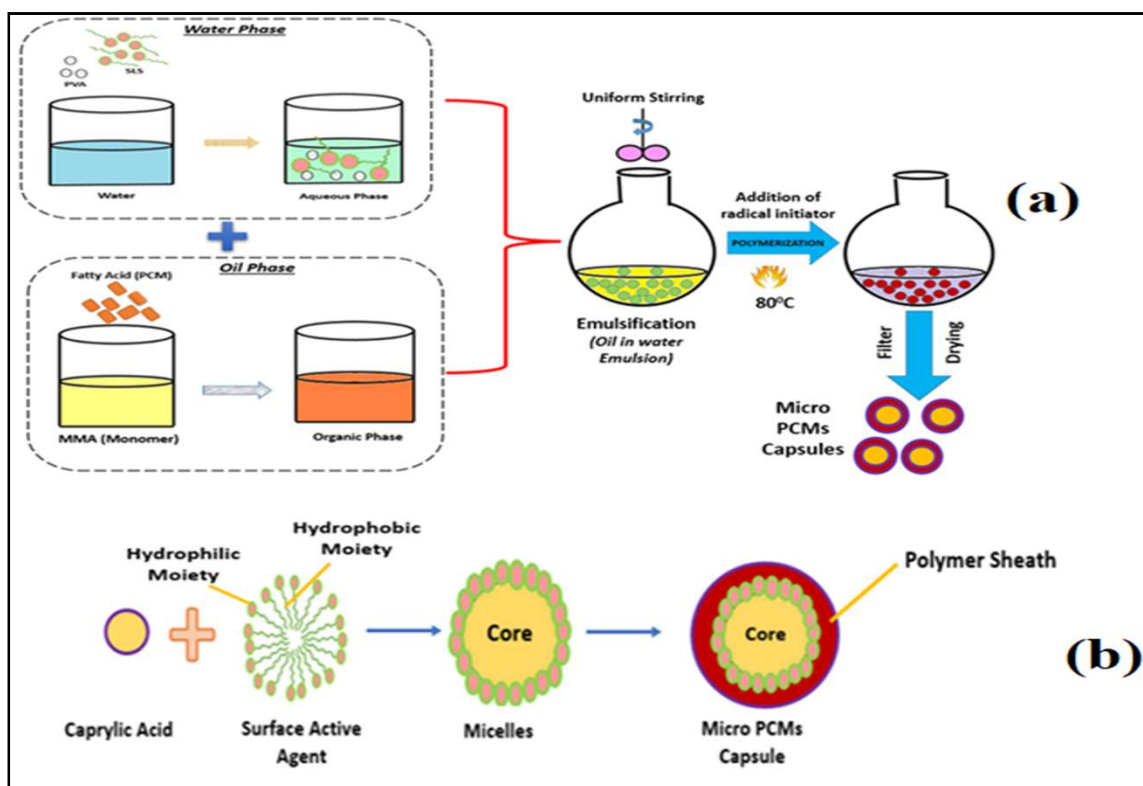


**Figure 2.1: Experimental procedure for the synthesis Micro-PCMs**

### ***2.2.2 Synthesis of Nanoencapsulated PCMs using Interfacial Polymerization Technique***

It is a simple polymerization reaction, carried out without subjecting heat energy to melt the PCM or dropping the temperature below 5 °C to support the successful synthesis of polyaniline (PANI) nanofibres. In brief, the required amount of monomer (aniline) and core PCM fatty acid were dissolved in the toluene (organic solvent) in a beaker under stirring to prepare the organic phase. A free-radical initiator was dissolved in a 1M HCl aqueous solution in another beaker to form aqueous phase. The ratio of aniline and initiator is kept 1:1. The initiator solution was then added dropwise manner to the organic phase within a specific period of time. The reaction mixture was further stirred at 1500 rpm, for 6 hours. After mixing of these two solutions (phases), PANI nanofibres encapsulating fatty acid PCM were formed at the interface of this biphasic system under constant agitation. The reaction mixture was kept unperturbed for next 24 hours, then was filtered and washed with distilled water multiple times. The synthesized nano-encapsulated PCM is the salt form of the polyaniline, with fibrillar morphology containing undecylenic acid as TES component within the resultant nanofibrous structures. The obtained compound was dried in oven at 50 °C for 24 hours. A schematic representation of the adopted experimental procedure for the synthesis of Nano-PCMs is shown in Figure 2.2.

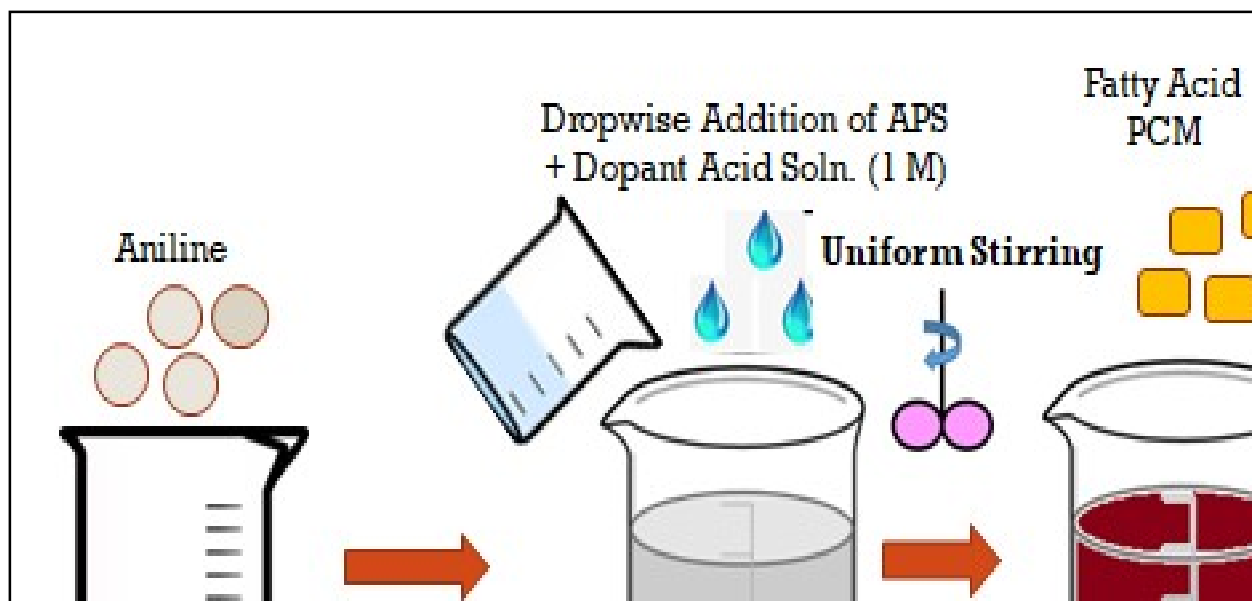


**Figure 2.2: Experimental procedure for the synthesis of Nano-PCMs**

### **2.2.3. Synthesis of Metal Oxide Nanoparticles by Sol-Gel Approach**

The Nano-TiO<sub>2</sub> (NTO) particles were synthesized by Sol-Gel Approach as follows: Titanium (IV) Isopropoxide precursor was dropwise added to Isopropyl Alcohol in a beaker under constant stirring for 30 minutes. The hydrolysis step was carried out by slow addition of Milli-Q water in a molar ratio (Ti:H<sub>2</sub>O = 1:4) to the above reaction mixture, with constant stirring for 2 hours. Afterwards, a few drops of nitric acid were added to maintain the pH range (pH: 2–4) and arrest the extent of the hydrolysis process of titanate solution. The reaction mixture was constantly stirred for another 1 hour to allow the formation of sols. Then, the above mixture was naturally aged for 24 hours to allow gel formation. The obtained gels were filtered, water-washed and finally oven-dried to evaporate water and other organic impurities at 60 °C for 48 hours. The resultant product was calcinated at 500 °C for 5 hours to achieve Titanium Dioxide Nanoparticles (NTO). The scheme for the adopted experimental procedure for the synthesis of Titanium Dioxide Nanoparticles is represented in Figure 2.3.

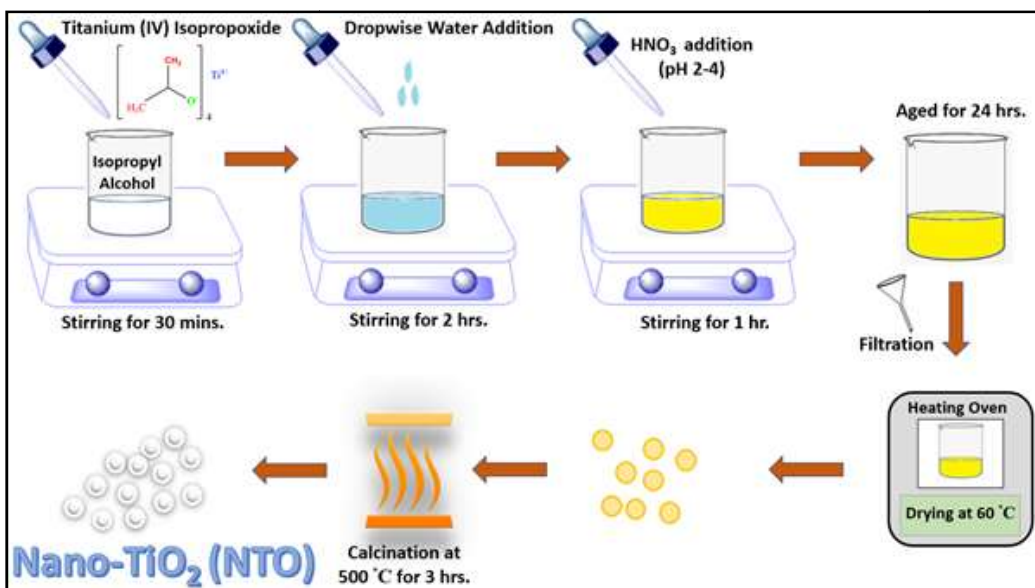


**Figure 2.3: Synthesis of Titanium Dioxide Nanoparticles via Sol-Gel Route**

#### **2.2.4 Preparation of Metal Oxide Nanoparticles filled PEG1500 based Form-Stable PCMs.**

Firstly, to ensure form-stable PCMs with high PCM content, the optimum concentration of PEG 1500 which the PVA matrix can be capable of arresting the PCM into its macromolecular domain without any seepage has to be determined. For this purpose, initially, PEG in different weight fractions (20 wt.%, 30 wt.%, 40 wt.%, 50 wt.%, 60 wt.%, 70 wt.%, 80 wt.%) is added to the PVA matrix to form PVA/PEG blended films by the solvent-casting method. 5 % (w/v) of PVA aqueous solution was made by dissolving the desired amount of PVA powder in Milli-Q water under constant agitation (RPM: 1500) at 75 °C until a clear solution is obtained. To this solution, the PEGs in their respective weight fractions were added and further stirred for 5 hours at 75 °C. After 5 hours, the hot polymer solution was casted into the polypropylene petri-dish and left undisturbed for a few minutes for the removal of bubbles, and then subjected to drying in a hot-air oven at 30 °C for 24 hours. The resultant film was peeled from the petri-dish and strongly pressed between the folds of filter paper, under load to squeeze out unreacted PEG present on the surface. To obtain nanocomposite films, a similar methodology was adopted as

explained above, where the films were produced by adding the prepared Nano-TiO<sub>2</sub> (NTO) in different weight fractions (0.25 wt.%, 0.50 wt.%, 0.75 wt.%, 1 wt.%) to the optimized PVA-PEG blend concentration, (which was deduced accordingly by leakage tests). A schematic representation of the adopted experimental procedure for the synthesis of PVA/PEG/NTO Nanocomposite Form-Stable Composite PCMs is shown in Figure 2.4.

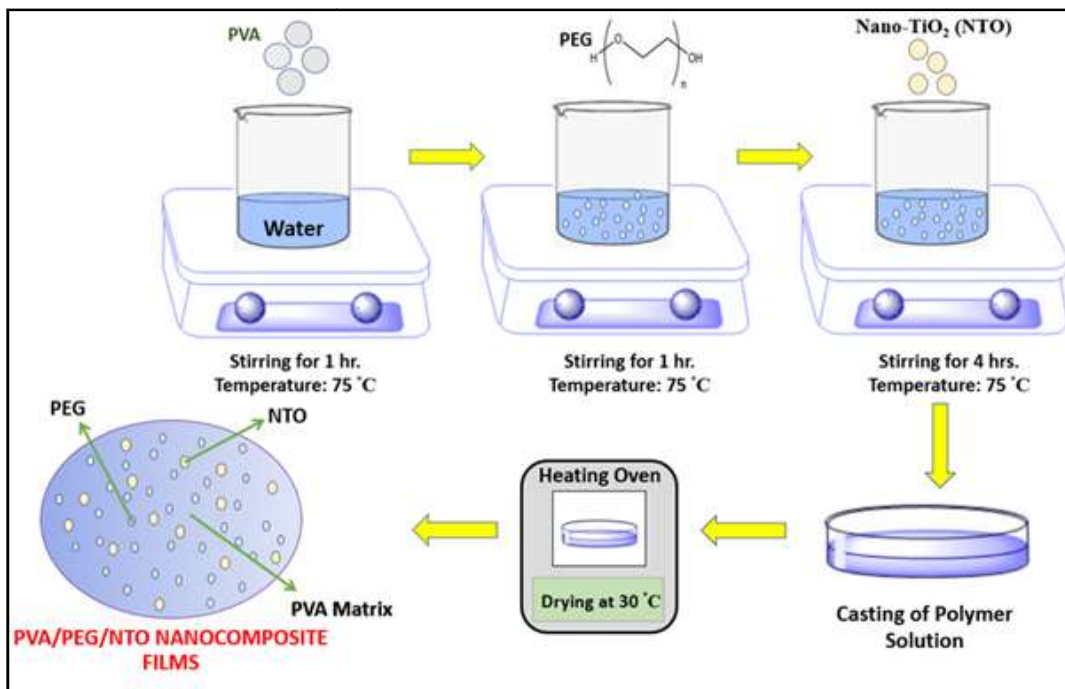


**Figure 2.4: Schematic representation of the experimental procedure to obtain form-stable NTO/PEG1500/PVA nanocomposites**

### 2.2.5 Preparation of Metal Oxide Nanoparticles filled PEG600 Based Form-Stable PCMs

To obtain metal oxide-filled PCMs, solvent-casting method has been employed. 5% (w/v) homogeneous PVA solution was prepared in Milli-Q water with constant stirring at 1500 RPM, at 75 °C. Then, PEG 600 in a proportional ratio (1:1) was mixed and the solution is left undisturbed under stirring for 1 hour. The composite films were formed by adding the synthesized Titanium Dioxide Nanoparticles (NTO) in discrete concentrations (0.25 wt. %, 0.50

wt. %, 0.75 wt. %, 1 wt. %) to the above solution, under constant stirring. Following 5 hours interval, the hot polymer solution was poured into the polypropylene petri dish, and then kept in hot-air oven for drying at 30 °C, for 24 hours. The dried composite films were then removed carefully from the petri-dish. The methodology followed for the fabrication of the Nanocomposite Form-Stable Composite PCMs is represented in Figure 2.5.

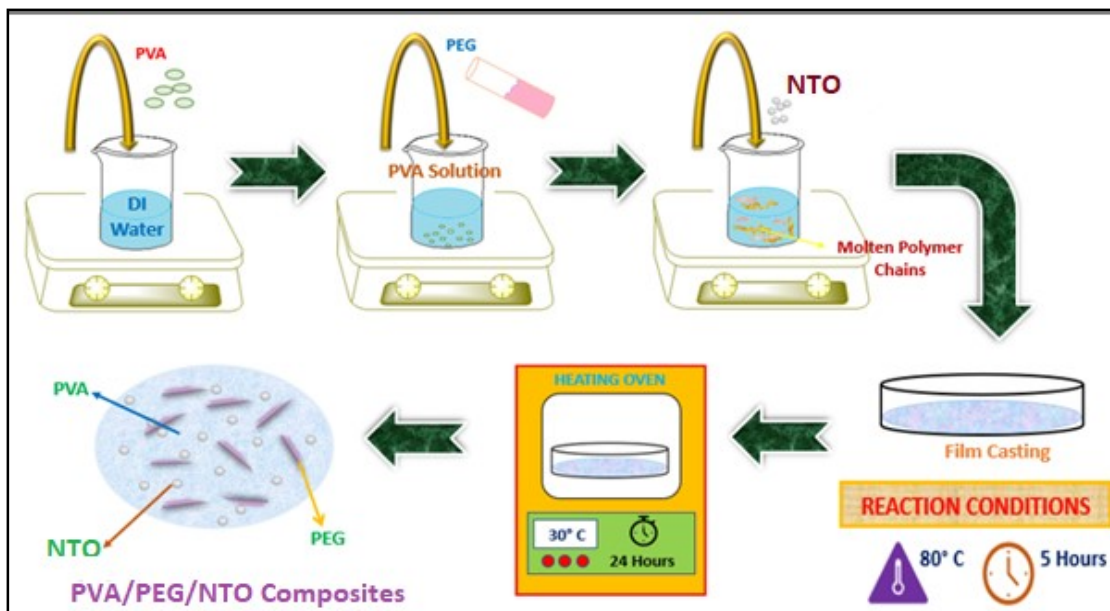


**Figure 2.5: Experimental methodology adopted to obtain form-stable NTO/PEG600/PVA nanocomposites**

### 2.2.6 Development of Fatty Acid incorporated Polyurethane Form-Stable PCMs

PU based form-stable PCM were developed by reacting a polyol (PEG 20,000) and a diisocyanate (polymeric-methylene diphenyl diisocyanate, PMDI). Initially, an appropriate amount of PEG 20,000 was taken in a beaker and subjected to heating at 80 °C till whole PEG flakes were properly melted to yield clear homogenous solution. To the above beaker, capric acid was added in a weight ratio 1:1 and stirred for few minutes. Thereafter, this reaction mixture is transferred to another beaker containing diisocyanate, which is further stirred for 2 minutes at ambient temperature, until the reaction mixture turns pale yellow in colour and then, the resultant

solution was transferred to circular petri-dish and allowed to remain undisturbed to solidify in order to obtain form-stable PCM. The experimental methodology adopted for the preparation of Polyurethane based Form-Stable PCMs is represented in Figure 2.6.

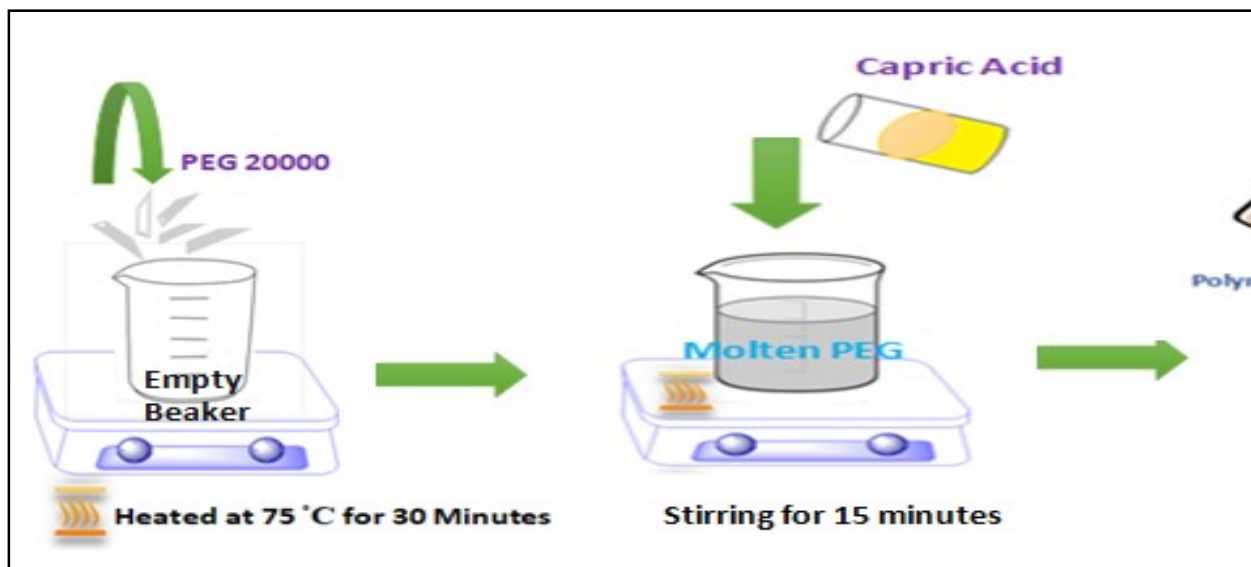


**Figure 2.6:** Experimental methodology adopted for the preparation of Polyurethane based Form-Stable PCMs

## 2.2.7 Characterization of Synthesized Polymer Based Phase Change Materials (PCMs)

### 2.2.7.1 FTIR Analysis

The chemical structure and the inherent functional groups of the developed polymer based PCMs (encapsulated and form-stable) and metal oxide nanoparticles were investigated by Fourier transform infrared spectrometer (Spectrum Two, Perkin Elmer) shown in Figure 2.7. The synthesized PCMs in a small quantity were mixed with KBr to form pellets, and the spectrum was recorded at a resolution of  $4\text{ cm}^{-1}$ , with 128 scans in the range of  $450\text{-}4000\text{ cm}^{-1}$ .

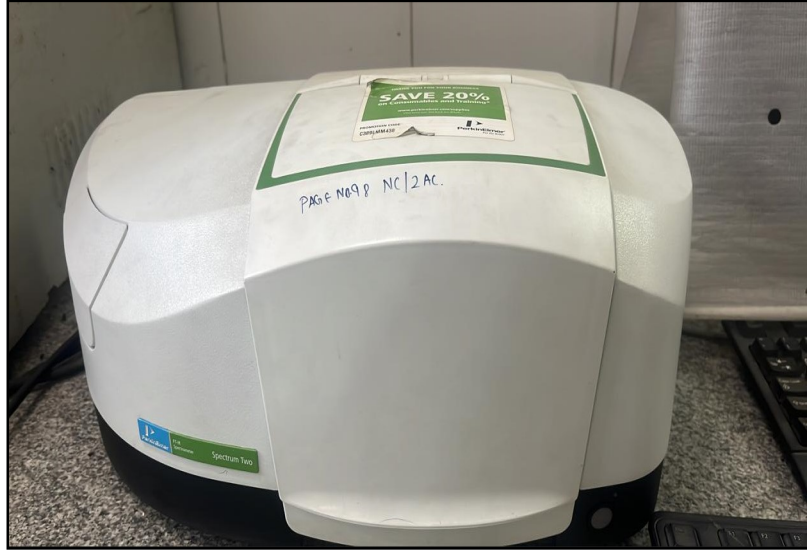


**Figure 2.7: FTIR Spectrophotometer (Spectrum Two, Perkin Elmer)**

### **2.2.7.2 *Differential Scanning Calorimetry Analysis***

Differential scanning calorimetry (DSC 8000, Perkin Elmer) shown in Figure 2.8 was used to evaluate the potential of the prepared PCMs (encapsulated and form-stable) as latent heat energy storage materials, by measuring their important thermal parameters, such as melting point ( $T_m$ ), crystallization point ( $T_c$ ), and the enthalpies associated during both heating ( $\Delta H_m$ ) and cooling ( $\Delta H_c$ ) processes. Three samples of prepared PCMs were analyzed for the determination of their heat storage attributes, along with the encapsulation ability, and each sample was tested thrice, and the average value of obtained DSC results was reported. The analysis was carried out in a temperature sweep between the operating phase change temperature profiles of the respective different PCMs being studied at a standard heating/cooling rate of 10 °C/min under a nitrogen blanket, at a constant flow rate of 40 mL/min.

The accomplishment of the encapsulation process for the production of encapsulated PCMs can be estimated by calculating the encapsulation ratio ( $E_R$ ). Encapsulation Ratio determines the effective encapsulation of a PCM as a core, inside the polymer capsule. The encapsulation ratio



of fatty acid PCM was calculated with the following equation based on the enthalpy values measured from the DSC analysis [83]:

$$E_R(\%) = \frac{\Delta H_{m, \text{ Encapsulated PCMs}}}{\Delta H_{m, \text{ PCMs}}} \times 100 \quad (4)$$

Where,  $\Delta H_{m, \text{ Encapsulated PCMs}}$ , and  $\Delta H_{m, \text{ PCM}}$  are respectively the latent heats of fusion of the encapsulated PCMs and bulk, PCM.



**Figure 2.8: Differential scanning calorimeter (DSC 8000, Perkin Elmer) used to determine phase change characteristics**

### 2.2.7.3 *Thermogravimetric Analysis*

The thermal stability and the weight loss studies were done on the prepared PCMs (encapsulated and form-stable) and metal oxide nanoparticles using a thermal analyzer (TGA 4000, Perkin Elmer) described in Figure 2.9. About 5-6 mg of microcapsules sample was placed in the analyzer's silica crucible and was subjected to a temperature of 30 to 800 °C, at a standard heating rate of 10 °C/min, under nitrogen environment, at a constant flow rate of 20 mL/min. All the samples were run in triplicate and the average value is reported.

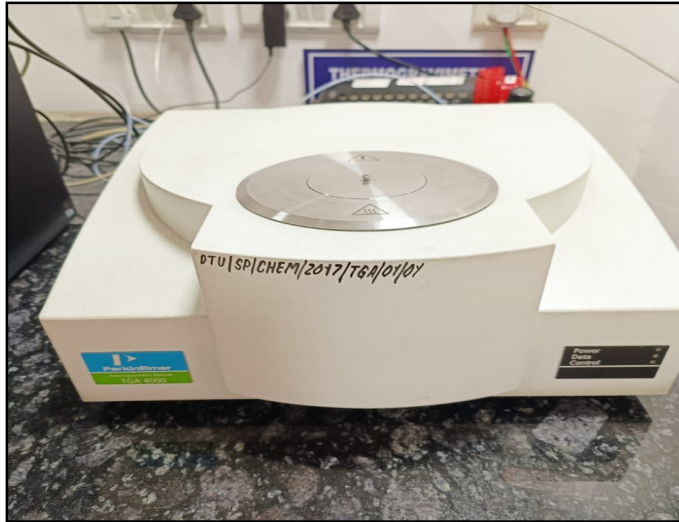


**Figure 2.9: Thermogravimetric Analyzer (Perkin Elmer 4000)**

#### **2.2.7.4 Thermal Energy Storage/Release Ability Test (T-History)**

Thermal Energy Storage Rate Test (T-History) was performed using the experimental set-up depicted in Figure 2.10 for the estimation of the charging and discharging time of the raw PCMs and the developed polymer based PCMs. Each sample is tested three times and the average value was reported. In this method, two temperature-controlled water baths were maintained; first one kept at temperature lower than the phase change temperatures of each studied PCMs (cold-bath) and second bath at temperature higher than the phase change temperatures of each studied PCMs (hot-bath). Both the raw PCMs and the developed polymer based PCMs samples were placed inside cylindrical glass tubing and a K-type thermocouple was placed in the centre of the sample. The tubes were subjected to cold-bath maintained at lower end and after complete temperature saturation; the tubes were quickly transferred to a hot water bath operating at temperatures higher than phase change temperatures to study the heat-storage (charging rate) ability. Thereafter, achieving a constant equilibrating temperature, the tubes were again returned to the cold-bath to study the heat-release (discharging rate) ability. The measurements during this test were

automatically recorded by a data acquisition system with an accuracy of  $\pm 0.2$  °C at a regular time interval of 2 seconds.

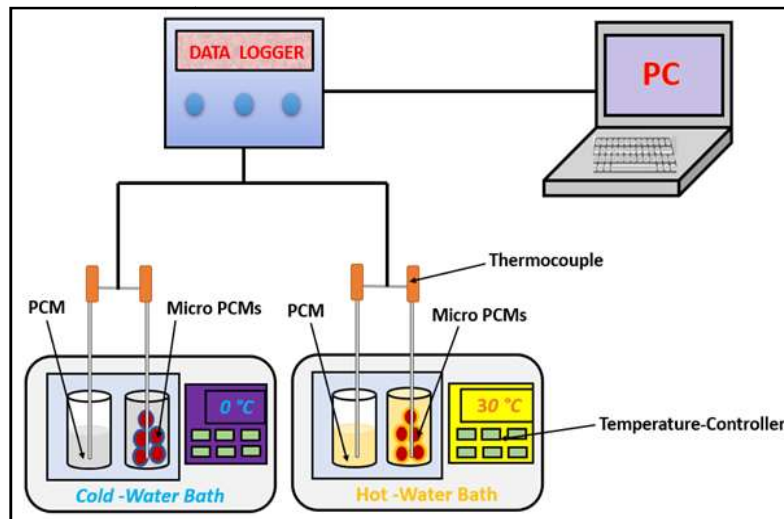


**Figure 2.10: Schematic representation of the experimental set-up for T-History Test**

#### **2.2.7.5 Thermal Reliability Test**

An important property of PCMs was determined to understand how efficiently the prepared PCMs exhibit stability in terms of latent heat energy properties where they were exposed to multiple thermal cycles, followed by DSC analysis to investigate the changes in the thermal properties, post thermal cycling test. The thermal cycling set-up was allowed to operate between 0 and 80 °C. Two different hot and cold sinks were maintained by constant heating one water bath operating at higher temperature (above melting point of PCM) and keeping other water bath operating at lower temperature (below solidification point of PCM) in which occasionally ice cubes were added to maintain the desired temperature. The PCM packed in a closed suitable glass container was subjected to be heated in the heat sink for 15 minutes and once the melting temperature of the sample was achieved, the container was kept into the cold water bath to reach the crystallization temperature of the PCM sample for 15 minutes, afterwards the container was again placed in a hot water bath and thus the cycle was repeated up to 100 thermal cycles.

### **2.2.7.6**      *Field-Emission Scanning Electron Microscopy*

The morphology, surface appearance, and the shape of the prepared encapsulated as well as form-stable PCMs were explored with the help of Field-Emission Scanning Electron Microscopy (FE-SEM)(FEI Quanta 200 FEG SEM, Netherland) represented in Figure 2.11 at an accelerated voltage of 10 kV, by smearing with gold coating and, examined under low-vacuum pressure. Energy Dispersive Spectroscopy was used to determine the purity of the synthesized nanoparticles.



**Figure 2.11: Field-Emission Scanning Electron Microscope**

### **2.2.7.7**      *High-Resolution Transmission Electron Microscopy*

High-Resolution Transmission Electron Microscopy (HR-TEM) (Tecnai™ G2 20) as shown in Figure 2.12 was used to characterize the morphology and microstructure of the synthesized Titanium Dioxide Nanoparticles. The particles were dispersed in ethanol and then the sample was transferred to a copper grid and imaging was carried out.



**Figure 2.12: High-Resolution Transmission Electron Microscope**

#### **2.2.7.8 *Dynamic Light Scattering (DLS)***

The average diameter and the particle size distribution of the synthesized microencapsulated PCMs were estimated by the dynamic light scattering method (Malvern Zetasizer Nano ZS, UK) represented in Figure 2.13. The microcapsules were dispersed in ethanol and homogenized utilizing ultrasonication to prevent aggregation of the suspended particles. The particle size and particle size distribution measurements were recorded by a set of three scans, per observation.



**Figure 2.13: Malvern Zetasizer Nano ZS**

### 2.2.7.9 *XRD Analysis*

The analysis of the structural phases of the prepared titanium dioxide nanoparticles was carried out using Powder X-Ray Diffractometer (Bruker D8 Advance) at a slow-scanning rate under  $2\theta$  range of  $10\text{-}80^\circ$  using fixed Ni-filtered Cu K $\alpha$  radiation ( $\lambda=1.54 \text{ \AA}$ ) as shown in Figure 2.14.



**Figure 2.14: X-Ray Diffractometer**

### 2.2.7.10 *BET Analysis*

Nitrogen adsorption-desorption isotherm at 77 K was carried out using MicrotracBEL (BELSORP, Japan) described in Figure 2.15. The surface area of the synthesized metal oxide nanoparticles was deduced by applying Brunauett–Emmett–Teller (BET) method. Barrett-Joyner-Halenda (BJH) model was used to evaluate the pore size distributions and total pore volume.



**Figure 2.15: Brunauett–Emmett–Teller (BET) Tester (MicrotracBEL)**

### **2.2.7.11 *UV-Visible Analysis***

UV-vis transmittance spectra of the prepared form-stable PCMs were recorded within the wavelength range of 200-800 nm, using a UV-vis spectrophotometer (Agilent Technologies, Carry Series as shown in Figure 2.16, in order to study their resistance toward ultraviolet irradiation.



**Figure 2.16: UV-Vis Spectrophotometer**

### 2.2.7.12 *Flame-Retardancy Characteristics*

The flame-retardant behaviour of the fabricated form-stable PCMs was determined by the measured Limiting Oxygen Index (LOI %) values, using Oxygen Index Apparatus. (Fire Testing Technology, UK) as displayed in Figure 2.17. Minimum 5 specimens of each PCM composition were taken and clamped inside the sample holder. A concentration span of nitrogen gas ( $N_2$ ) was fixed as 99%, whereas oxygen gas ( $O_2$ ) was kept as 17.4%. The gas flow rates of both  $N_2$  and  $O_2$  gases were maintained at 2 bars.



**Figure 2.17: Oxygen Index Apparatus (Fire Testing Technology, UK)**

### 2.2.7.13 *Electrical Conductivity Measurement*

Four-point probe setup shown in Figure 2.18 (SES Instruments Pvt. Ltd., Roorkee) consisting a digital micro voltmeter (DMV-00) and low current source (LCS-02) PID were used to measure the electrical conductivity of the polyaniline based nanoencapsulated PCM at room temperature.





**Figure 2.18: Electrical Resistivity Four point probe setup**

#### **2.2.7.14 Form-Stability Test (Leakage Test)**

For the evaluation of form-stability (for observation of less PCMs leakage), a leakage test was conducted by two different methods as described by several authors [84][85]. A series of films of PVA/PEG blends, with varying weight fractions of PEGs (20-80 wt. %) were prepared by solvent casting method. In the first approach, the fixed amount of samples in their respective concentrations were placed on the filter papers individually and subjected to hot-air oven 70 °C for 2 hours. Following that, they were taken out of the oven and left undisturbed to attain the ambient temperature while transferring the heated samples to fresh filter paper, and then their masses were weighed using electronic balance. The leakage percent was calculated using the equation as follows:

$$L\% = \frac{M_o - M_t}{M_o} \times 100 \quad (5)$$

Where,  $M_o$  is the initial mass of the sample before heating;  $M_t$  is the mass of the sample after oven heating.

Alternative approach used to evaluate the leakage rate was by placing the samples on the Whatman filter paper at centre, within the area of 20 mm diameter, and subjected to heating inside an oven under same heating conditions (70 °C for 2 hours). Afterward, the PEGs traces on the filter paper were observed. The sample with less leakage percentage when heated beyond PEGs phase change temperature was considered as stable PCM. The leakage percent was deduced using the equation as follows:

$$L\% = D - D_0/D_0 \times 100 \quad (6)$$

Where,  $D_0$  is the diameter of the test area i.e. 20 mm;  $D$  is the diameter of the seepage area after the leakage test. The criteria of leakage are shown in the table given below:

**Table 2.2: Leakage Criteria considered for as prepared PEG/PVA Blends**

<b>Criteria of Leakage</b>		
<b>Leakage Percentage (L %)</b>	<b>Phenomenon</b>	<b>Conclusion</b>
$L\% \leq 10$	Negligible or Trace Amounts	Highly Stable
$10 < L\% \leq 30$	Very Little Leakage	Remained Stable
$30 < L\% \leq 50$	Moderate Leakage	Unstable
$L\% > 50$	Severe Leakage	Highly Unstable

**CHAPTER 3**  
**SYNTHESIS OF MICROENCAPSULATED PCMs**

---

**3.1 INTRODUCTION**

The major portion of our principal energy requirements is still derived from classical energy sources like fossil fuels. However, being non-renewable and available in finite quantities, fossil fuels are expected to extinguish in the nearby future. Moreover, due to rising concerns among the researchers for the environmental conservation, continuous scientific efforts are going on to explore renewable sources as raw materials for engineering and daily utility products. Similar progress is evident in the field of energy, where, a wide research is ongoing to replace the petroleum fuels with the environmentally friendly renewable energy sources [3]. One of the latest innovative concepts is to fabricate impressive energy storage devices by utilizing the renewable resources, which could be the fruitful fountains of energy. Thermal energy storage (TES) using latent heat energy storage systems are imperative options for lessening the reliance on fossil fuels and can counter the present energy requirements. The phase change materials (PCMs) have gained recognition in the present generation because of their energy storage density, good chemical stability, and energy storage function via phase transitions at peculiar temperatures [86]. PCMs, as proficient latent heat storage systems, exhibit immense intake or release of latent heat energy during their phase transition. Due to such astonishing features, the PCMs are in high demand in divergent TES operations including air conditioning [87], solar energy utilization [88], thermo-regulating textiles [89,90], thermal energy management in buildings [91] coatings [92] and heat sinks for electronic gadgets [93].

In the past 2-3 decades, there is a rapid interest among the researchers across the globe, in microencapsulated PCMs, that is, PCMs as a core encapsulated (entrapped) inside a polymer entity as shell, owing to their benefits, such as, management of volume changes at the time of phase conversion, increased heat transfer area, boosted heat transfer rate, shielding of the PCMs against outdoor conditions, and enhanced physical strength to the core PCMs. Currently, available approaches for microencapsulation of PCMs are: in-situ polymerization [94], interfacial polymerization [95], emulsion polymerization [96], suspension polymerization [88, 97] and complex coacervation [98] enabling the researchers to select and design microcapsules from an array of polymers such as urea–formaldehyde [99], melamine-formaldehyde [100], polyurea [95] polyurethane [101], polymethylmethacrylate [102], polystyrene [103], divinylbenzene [104] etc.

Lu et al. [105] employed the interfacial polymerization to synthesize butyl stearate microencapsulated polyurethane capsules (PU), with a diameter range of about 10-35  $\mu\text{m}$  and energy storage melting enthalpy of about 81 J/g. Carreira et al. [106] prepared acrylic microcapsules based on octadecane by suspension polymerization method and reported that these paraffin-based microcapsules showed a mean particle size around 12  $\mu\text{m}$  and possess an energy storage density of 175 J/g during the phase change, along with good thermal stability up to 170  $^{\circ}\text{C}$ . Konuklu et al. [107] used complex coacervation method for the microencapsulation of caprylic acid within amino plastic resin–based shells (urea-formaldehyde, melamine–formaldehyde). The formed urea-formaldehyde microcapsules showed good energy storage properties with the phase change enthalpies of melting and crystallization as 93.9 J/g and 106.1 J/g, respectively. Paloma et al. [83] worked on the encapsulation of paraffin and palmitic acid using poly-(styrene-co-ethyl acrylate) (PScEA) shells for solar thermal applications, having

phase change temperatures as 42 °C and 62 °C, respectively. Ma et al. [88] utilized the suspension polymerization technique for the production of microencapsulated n-dodecanol as a core inside an acrylic shell, for textiles applications. Al-Shannaq et al. [108] fabricated microencapsulated PCM capsules based on paraffin encapsulated in PMMA shells via suspension polymerization technique. These microcapsules showed melting and crystallization temperatures and the latent heats as 21.9 °C, 8.0 °C, and 113.4 J/g, 111.9 J/g, respectively, during the phase change.

Literature studies affirm that the encapsulation using the shell materials such as amino plastics (UF, MF resins), sometimes, may become inappropriate due to the leakage of residual formaldehyde, after polymerization, which can pose serious environmental and health problems. From this point of view, encapsulation with a thermoplastic polymer such as polymethylmethacrylate (PMMA) seems to be beneficial due to its following attractive features: (a) easy handling and processability, (b) possess good toughness and hardness resistance, (c) good weathering properties, (d) good chemical resistance, (e) relatively cheap and easily available, and (f) more environment-friendly as compared to formaldehyde plastics. Furthermore, the PCMs derived from the fatty acids are not much explored by the researchers, in past. Most of the encapsulation processes were carried out on paraffin PCMs which are obtained from petrochemical resources, thus are non-renewable and reportedly costlier than the fatty acid PCMs. The fatty acids, as effective PCMs, can give tough competition to paraffins for TES applications. The fatty acids with their linear hydrocarbon chains of varying lengths and terminal carboxylic functional group  $[\text{CH}_3(\text{CH}_2)_n\text{COOH}]$  are derived from the plants and the animal's resources. They exhibit virtuous features as PCMs, like, (a) no phase segregation, (b) congruent melting, (c) non-toxic, (d) abundant in nature, (e) relatively economical than technical grade

paraffins, (f) available in broad melting temperatures, that is, from  $-7$  to  $70$  °C, and (f) possess high latent heat energy density. Caprylic acid (CpA) is a saturated, eight-carbon atom fatty acid, naturally found in the milk of certain mammals and various vegetable oils, is a non-toxic and renewable resource. It has a congruent melting point of  $16$  °C, with no phase segregation behavior, and possesses desirable high latent heat energy storage potential, thus, can be explored for TES applications in fabrics, buildings, food storage, transportation, etc.

As evident from the available literature, most of the research studies conducted in past were on paraffin PCMs, which are non-renewable. Only a limited literature reports about the fatty acid PCMs. Also, no work has been outlined previously on the fabrication of mid-temperature microencapsulated PCMs using fatty acids, having phase change characteristic temperature  $\leq 30$  °C, such as caprylic acid. Moreover, the entrapment of caprylic acid using PMMA polymer shell has not been reported in any previous study. Keeping these research gaps in view, the present study deals with the synthesis of Micro-PCMs capsules comprising of caprylic acid (CpA) as a core, surrounded by PMMA as shell, through a simple suspension-like polymerization technique. These resulted Micro-PCMs were further investigated for their characteristics, including their chemical properties, particle morphology, size distribution, thermal properties, and thermal stability.

## **3.2 RESULTS AND DISCUSSION**

### **3.2.1 Fourier Transform Infrared (FTIR) Spectroscopy**

The FTIR spectra of Caprylic Acid (CpA), Micro-PCMs, and PMMA depicting their chemical properties are presented in Figure 3.1. The pure PCM and the Caprylic Acid peaks at  $2858$   $\text{cm}^{-1}$  and  $1379$   $\text{cm}^{-1}$  respectively belong to C-H stretching and bending modes of the aliphatic chain of fatty acid. The peak at  $1710$   $\text{cm}^{-1}$  and  $1277$   $\text{cm}^{-1}$  related to the stretching vibrations of the

carbonyl group of the acid. The peak at  $724\text{ cm}^{-1}$  corresponds to the C-H rocking vibrations. The spectrum of the Micro-PCMs resembles the attributes of the pure PCM, containing typical vibration mode peaks at  $2856\text{ cm}^{-1}$ ,  $1456\text{ cm}^{-1}$ , and  $723\text{ cm}^{-1}$  respectively, which are found in the aliphatic fatty acid carbon chain and, co-existing along with the vibrations of PMMA polymer. The sharp peak at  $1713\text{ cm}^{-1}$  is due to the carbonyl group and at  $1240\text{ cm}^{-1}$  is due to the C-O stretching of the ester group. The shifting of the peak of the carbonyl group is thought to have resulted from the interaction between the hydrogen atom of the hydroxyl group of the fatty acid and the oxygen atom of the carbonyl group of PMMA. It is clear from the spectrum that the maximum peaks of PCM, Micro PCMs and PMMA overlapped with each other. The spectra of Micro-PCMs showed similar characteristic peaks of both PMMA and fatty acid PCM, giving evidence of the presence of the Caprylic Acid and formation of PMMA shell. Similar findings were reported by several research groups for encapsulation of Caprylic Acid and other PCMs [107, 83, 33].

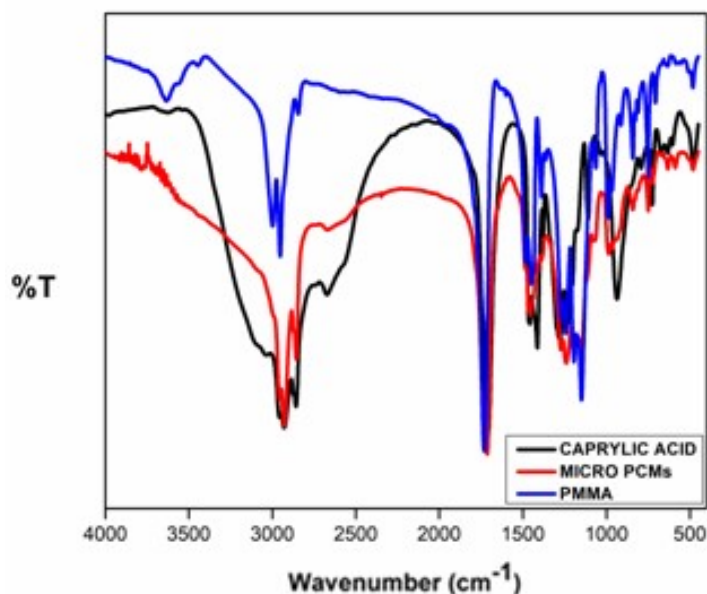


**Figure 3.1: FTIR of Caprylic Acid (CpA), Micro-PCMs and PMMA**

### 3.2.2 Morphology of Micro-PCMs

Particle geometry and size govern many pivotal physical properties of the polymers, namely: solubility in solvents; flowability during the processing stage; chemical reactivity, etc. Microcapsules characteristics like thickness and size of the microcapsules can be rehabilitated by altering the synthesis process or processing parameters, such as by varying the stirring time and rates. In the present study, the Micro-PCMs were produced using a particular synthesis approach i.e., suspension polymerization technique, with the stirring rate of 5000 rpm, for a period of 8 hours leading to the successful completion of the polymerization process. The morphology, shape profiles, and the distribution pattern of the Micro-PCMs, interpreted by the SEM analysis and cross-examined by image J software are as shown in Figure 3.2. The PMMA/Caprylic Acid microcapsules have spherical size configurations, with regular surface appearances. The microcapsules exist in the particle size distribution (PSD) of 2  $\mu\text{m}$  to 10  $\mu\text{m}$ , with an average particle diameter of 4  $\mu\text{m}$ . The shell thickness of the Micro-PCMs was found to be close to 0.26  $\mu\text{m}$ . For the confirmation of the same, an alternative mathematical approach has been applied based on microcapsule average diameter and encapsulation ratio values, attained from DSC results. The microcapsules shell thickness has been calculated by assuming CpA/PMMA microcapsules as a sphere of the diameter of about 4  $\mu\text{m}$ , filled with fatty acid PCM, as depicted in Figure 3.3. Thereby, shell thickness is evaluated from the difference in radii attained from the overall volume of CpA/PMMA microcapsule and the volume of the fatty acid core inside (considering it as a perfect sphere) respectively. However, PMMA shell microcapsules sometimes can form multi-core systems and, in such cases, the mathematical approach does not show the exact reality. The SEM results are in good coordination with the PSD measurements. A few smaller size particles were also seen in the SEM micrograph, which might be the residual emulsifier particles.



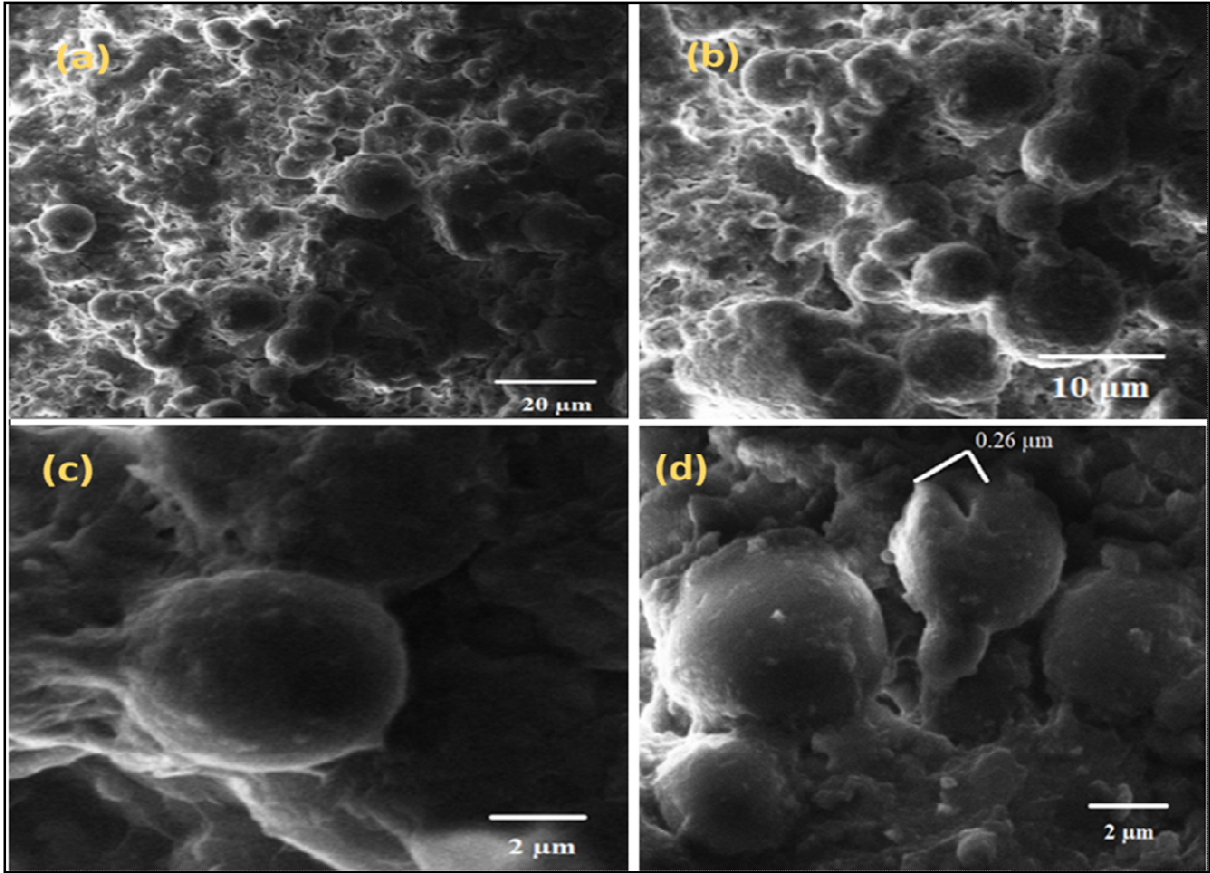


Figure 3.2: SEM micrograph of the synthesized Micro-PCMs A, magnification-5.00 K X B, magnification-10.00 K X C, and D, magnification-20.00 K X

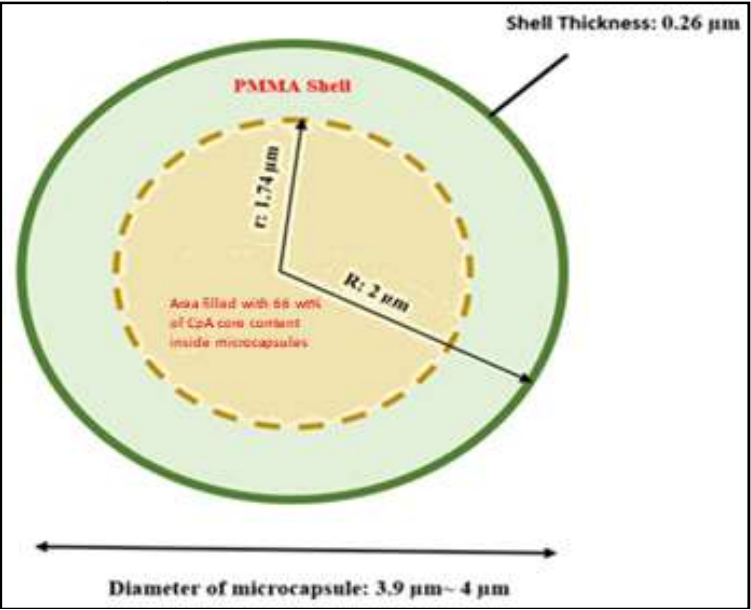
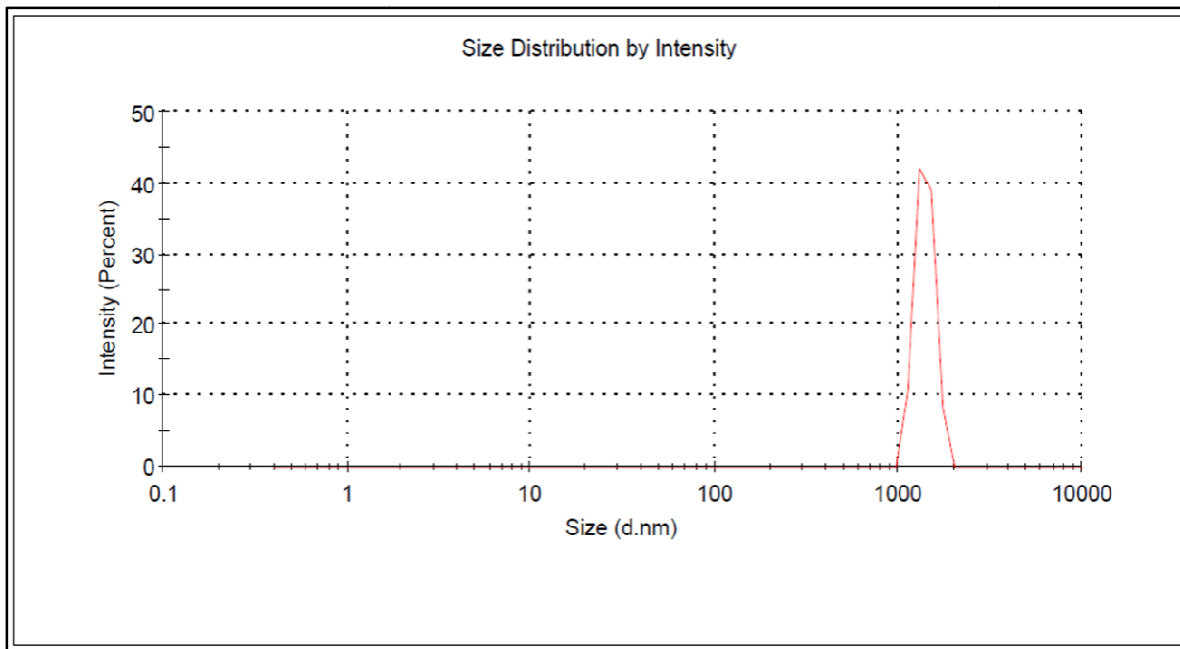


Figure 3.3: Schematic illustration of Caprylic Acid inside PMMA Microcapsule

The Particle Size Distribution (PSD) pattern of the synthesized Micro PCMs is presented in Figure 3.4. The PSD intensity shows that the PMMA/Caprylic Acid microcapsules have narrow size distribution varying from 1.07  $\mu\text{m}$  to 10  $\mu\text{m}$ , with the average particle size of the microcapsules as 3.9  $\mu\text{m}$ . The obtained microcapsules have the Particle Distribution Index (PDI), equal to 0.737.



**Figure 3.4: Particle Size Distribution Analysis of the Micro-PCMs**

### 3.2.3 Thermal Performance of Micro-PCMs

The phase change characteristics of the synthesized fatty acid-based Micro PCMs and Caprylic Acid are evaluated by DSC. The DSC curves representing the phase-change temperatures and the latent heat enthalpy values of the synthesized fatty acid-based Micro-PCMs and raw CpA are shown in Figure 3.5, and their results are summarized in Table 3.1. The DSC curves of both pure PCM and the Micro-PCMs appear to be almost identical, thus, giving evidence of the successful encapsulation of CpA within the PMMA domains. The pure CpA showed the onset of melting and crystallization temperatures at  $16.0 \pm 0.1$   $^{\circ}\text{C}$  and  $10.6 \pm 0.2$   $^{\circ}\text{C}$  respectively. On contrary, the

PMMA/Caprylic Acid microcapsules have revealed decent thermal energy storage ability, with the onset of melting at  $14.3 \pm 0.2$  °C and crystallization at  $9.7 \pm 0.4$  °C respectively. The latent heat of fusion and the latent heat of crystallization of the pure PCM and Micro-PCMs were found to be  $149.4 \pm 1.3$  J/g and  $151.6 \pm 1.4$  J/g and  $98.7 \pm 1.5$  J/g and  $99.0 \pm 1.7$  J/g respectively. The shifting of the phase transition values of the synthesized Micro-PCMs is, probably, the outcome of the encapsulation process. The microencapsulation of the CpA inside the PMMA shell allowed a small increase in the diameter of the tiny polymer particles, which in turn, increased the heat transfer surface area for the PCM, thus, leading to the improved heat transfer rate. Analogous to this, some other research groups also suggested an enhancement in the heat transfer rate, as a result of microencapsulation [21, 32, 33]. The melting and crystallization peaks of the PMMA/CpA microcapsules (Micro PCMs) showed a depression compared to neat PCM (CpA). The calculated encapsulation ratio ( $E_R$ ) of the CA obtained from the measured enthalpies values, using equation 4 was found to be 66 %. The comparison of PCM microcapsules prepared in the current study with few already testified in the literature is reported in Table 3.2. It is apparent from Table 3.2 that, the microcapsules that resulted in the current study exhibit a smaller size and high encapsulation ratio of CpA/PMMA as compared to the PCM microcapsules obtained by different shell and core materials combinations. From the attained results, it is apparent that the prepared Micro-PCMs capsules exhibit good latent heat energy capacity and their storage potential can be utilized in substantial TES applications including thermal buffering in food packaging, thermo-responsive textiles, slurries, indoor temperature control in building structures, etc. [109, 110].

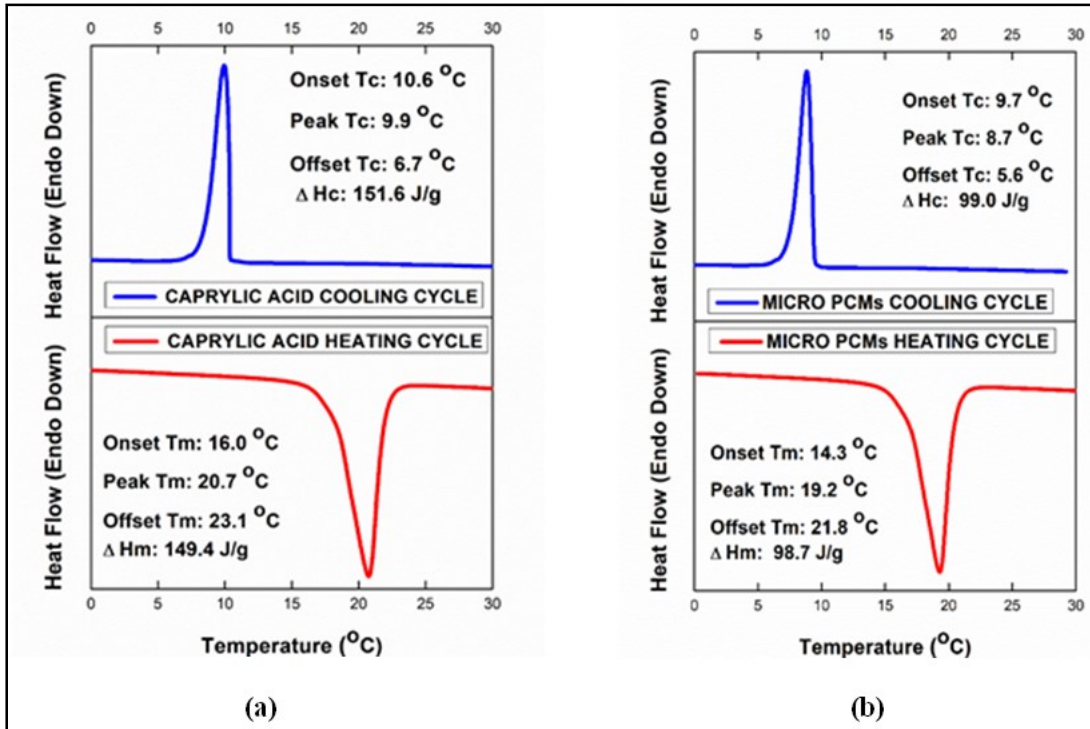


Figure 3.5: DSC Curves for Heating/Cooling Cycles for (a) Pure CpA and (b) Micro PCMs

Table 3.1: DSC Data of Pure PCM and Micro PCMs Representing Their Phase Change Characteristics

Sample	Caprylic Acid (CpA)	PMMA/Caprylic Acid Microcapsules (Micro-PCMs)
Onset $T_m$ ( $^{\circ}\text{C}$ )	$16.0 \pm 0.1$	$14.3 \pm 0.2$
Peak $T_m$ ( $^{\circ}\text{C}$ )	$20.7 \pm 0.1$	$19.2 \pm 0.2$
Offset $T_m$ ( $^{\circ}\text{C}$ )	$23.1 \pm 0.1$	$21.8 \pm 0.3$
Onset $T_c$ ( $^{\circ}\text{C}$ )	$10.6 \pm 0.2$	$9.7 \pm 0.4$
Peak $T_c$ ( $^{\circ}\text{C}$ )	$9.9 \pm 0.3$	$8.7 \pm 0.5$
Offset $T_c$ ( $^{\circ}\text{C}$ )	$6.7 \pm 0.2$	$5.6 \pm 0.6$
$\Delta H_m$ (J/g)	$149.4 \pm 1.3$	$98.7 \pm 1.5$
$\Delta H_c$ (J/g)	$151.6 \pm 1.4$	$99.0 \pm 1.7$
PCM (%)	100	66

**Table 3.2: Comparison of some microencapsulated PCMs from literature and synthesized microencapsulated PCM**

Polymerization Method	Core Material	Shell Materials	Microcapsules Size ( $\mu\text{m}$ )	$\Delta H_m$ (J/g)	Encapsulation Ratio/Core Content (%)	References
Suspension Polymerization	Caprylic Acid	PMMA	3.9	98.7	66	Present Study
UV Curing Dispersion Polymerization	Stearic Acid	PMMA	2-3	92.1	51.8	[111]
Suspension Polymerization	n-Octadecane	TiO <sub>2</sub> Doped PMMA	10-20	153.8	73.2	[112]
Emulsion Polymerization	Capric-Palmitic Acid Eutectic Mixtures	PS	Surface weighted mean diameter: 9.5 $\mu\text{m}$ , Volume weighted mean: 21.2 $\mu\text{m}$	77.3	47.3	[73]
UV initiated Emulsion Polymerization	Paraffin	PMMA	2	101	61.2	[34]
Suspension Polymerization	Paraffin-Butyl Stearate	Acrylate Shell	10-80	63.9-93.9	46-68	[87]
Photocurable Pickering Emulsion Polymerization	n-Octadecane	SiO <sub>2</sub> -PMMA	5-15	122.3	62.5	[33]
Interfacial Polymerization	Paraffin	Polyurea	2.42	92.5	44.5	[95]
Suspension Polymerization	PRS Paraffin wax	P(St-MMA)	380	87.5	43.2	[113]
Suspension Polymerization	PRS Paraffin	P (MMA-co-MA-co-MAA)	244	41.7	93.5	[114]

### 3.2.4 Thermal Stability of Micro-PCMs

The thermal stability and the degradation fashion of the Micro-PCMs are studied by TGA. The TGA curves of the Micro-PCMs are shown in Figure 3.6 and, their respective degradation temperatures are given in Table 3.3. The pure CpA degrades in a single step. The PCM shows 10 % and 50 % weight loss at around 154 °C and 189 °C respectively. The CpA undergoes complete decomposition at 196 °C. Being the small carbon chain fatty acid, CpA has a low

decomposition temperature and thus, experiences a progressive weight loss with the temperature rise. Similar to this, the PMMA shell material also experiences one step degradation pattern, but perceives the 50 % degradation at a much higher temperature of 376 °C, due to the considerably greater molecular weight of the polymer chains. Contrary to this, the PCMs microcapsules exhibited a two-stage degradation profile; the first step is attributed to the degradation of CpA, analogous to the same pattern as that of pure CpA, and the second step corresponds to the degradation of the polymer shell at 393 °C, which is virtually equivalent to that of pure PMMA. The occurrence of the microencapsulation has resulted in a slight increase in the onset of the degradation temperature of the enclosed fatty acid. From the two-step degradation in the case of Micro-PCMs, it is evident that the microencapsulation has led to the improved thermal stability of the PCM encapsulated within, thus, recompensed the better thermal resistance, leakage control, and protection at elevated temperatures.

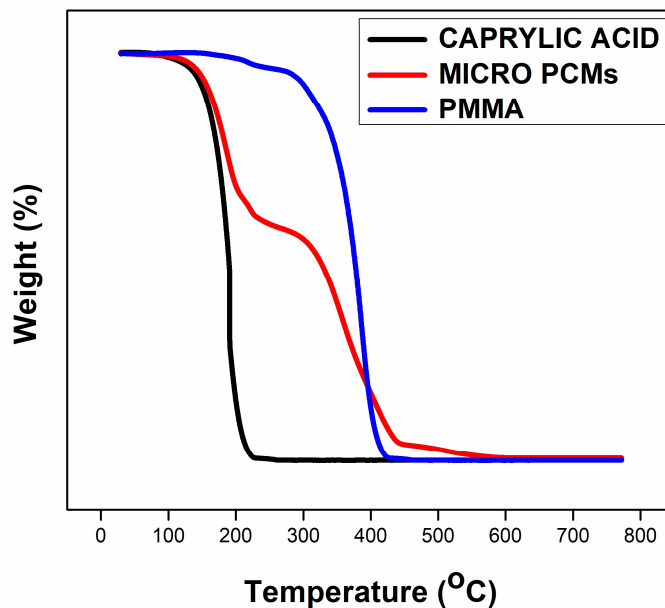


**Figure 3.6: TGA Cures for CpA, Micro-PCMs and PMMA**

**Table 3.3: Thermal Stabilities of CpA, Micro-PCMs and PMMA**

Sample	10% Mass Loss (°C)	50% Mass Loss (°C)	80% Mass Loss (°C)
Caprylic Acid (CpA)	154	189	194
Micro-PCMs	168	325	393
PMMA	311	376	395

### 3.2.5 Thermal Energy Storage/Release Ability of Micro-PCMs

Thermal Energy Storage/Release rates of the Micro-PCMs were determined by monitoring the charging-discharging time of CpA and Micro-PCMs. The melting time was evaluated from the charging cycle of CpA and Micro-PCMs. Similarly, the crystallization time was evaluated from the discharging cycle of CpA and Micro-PCMs. The representative temperature history curves of raw PCM and Micro-PCMs are shown in Figure 3.7. CpA reached its melting temperature (phase change) from 0 °C in 78 seconds whereas, in the case of Micro-PCMs, the time taken was 251 seconds. This difference in the charging time of pure PCM and Micro-PCMs further affirms the successful microencapsulation of CpA. The discharging time for the pure PCM and Micro-PCMs to reach their onset crystallization temperatures were found to be 113 seconds and 254 seconds respectively, which infers the longer latent heat energy release period as compared to the pure PCM.

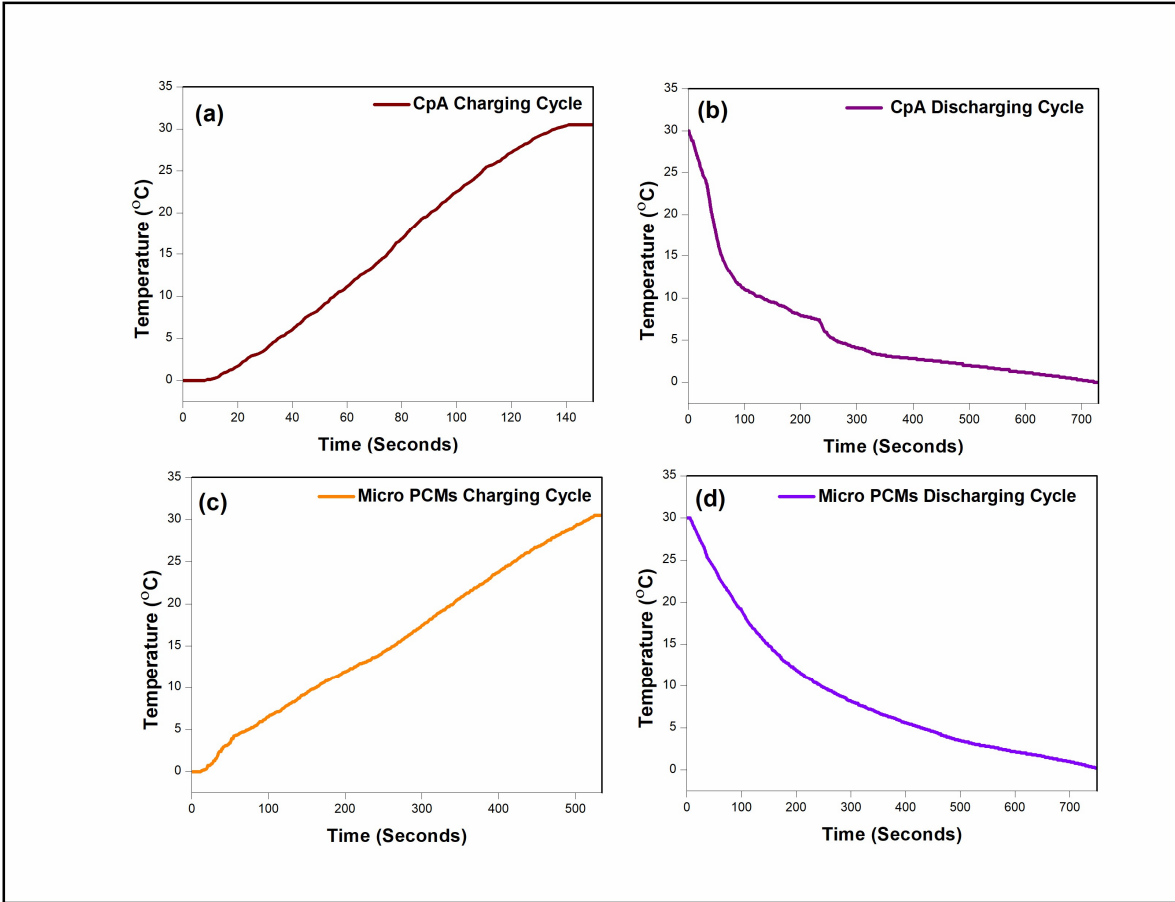


**Figure 3.7: Thermal Energy Storage/Release curves for CpA and Micro-PCMs during charging and discharging cycles (T-History)**

### 3.2.6 Thermal Reliability of Micro-PCMs

Micro-PCMs that are intended to be utilized in the field of thermal energy storage must be capable enough to withstand multiple heat-cool cycles with no or little variation in their energy storage properties. DSC curves and change in thermal characteristics of Micro-PCMs after experiencing various thermal cycles (0, 500, 1000) is shown in Figure 3.8 and Table 3.4 respectively. After 1000 cycles the Micro-PCMs exhibited latent heat enthalpies of melting and crystallization as  $86.6 \pm 2.1$  J/g and  $90 \pm 1.2$  J/g respectively. It is evident from the results obtained that the minor variation in temperature or enthalpy values suggests the good thermal



reliability behaviour of the synthesized Micro-PCMs suitable for utility in thermal energy storage applications.

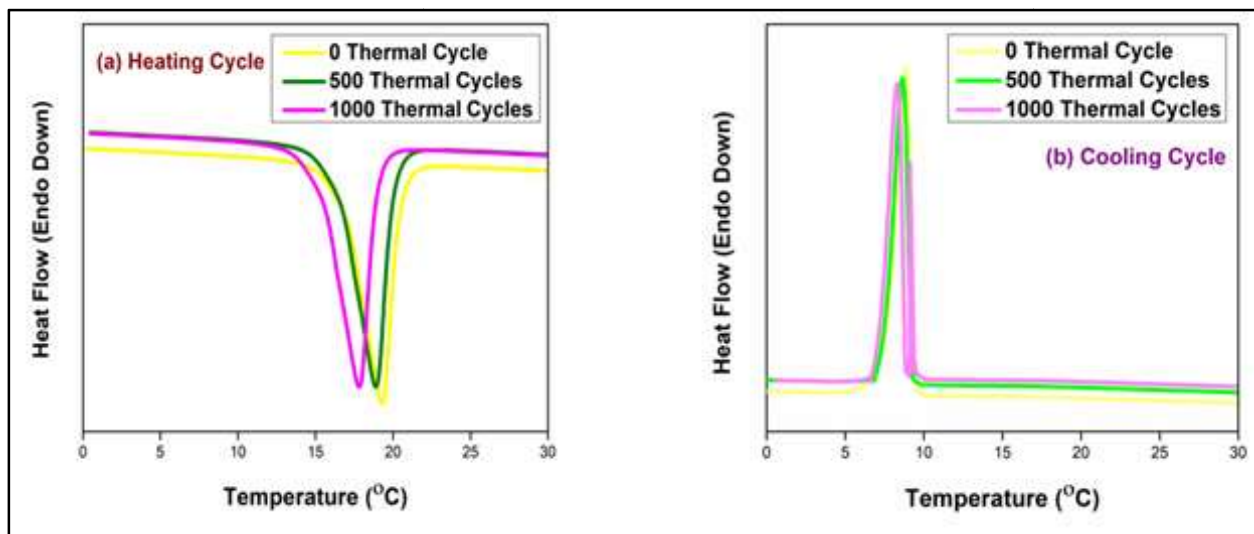


Figure 3.8: Thermal Reliability Curves of Micro-PCMs; (a): Heating Cycle, (b): Cooling Cycle

Table 3.4: Phase change characteristics of Micro-PCMs post thermal cycling exposure

Number of Cycles	Onset $T_m$ ( $^{\circ}\text{C}$ )	Onset $T_c$ ( $^{\circ}\text{C}$ )	$\Delta H_m$ (J/g)	$\Delta H_c$ (J/g)
0	$14.3 \pm 0.2$	$9.7 \pm 0.4$	$98.7 \pm 1.5$	$99.0 \pm 1.7$
500	$13.9 \pm 0.2$	$9.5 \pm 0.3$	$89.4 \pm 1.8$	$93.4 \pm 1.5$
1000	$13.2 \pm 0.3$	$9.1 \pm 0.3$	$86.6 \pm 2.1$	$90 \pm 1.2$

### 3.3 SIGNIFICANT FINDINGS

The Micro-PCMs capsules comprising of caprylic acid as core and surrounded by PMMA, as shell has been synthesized, via simple suspension-like polymerization technique, for the latent heat thermal energy storage (LHTES) applications. FTIR studies have portrayed the successful encapsulation of the fatty acid inside the PMMA. The SEM and the PSD results have confirmed the uniform spherical geometries of the synthesized Micro-PCMs with a mean particle diameter of approximately 4  $\mu\text{m}$ . The TGA analysis has depicted the good thermal stability of the

synthesized PMMA/caprylic acid PCMs, having degradation in a two-step manner. DSC data have proved the eligibility of the prepared Micro-PCMs as LHTES material, with 66 wt. % of PCM core encapsulation, having melting and crystallization temperatures of  $14.3 \pm 0.2$  °C and  $9.7 \pm 0.4$  °C respectively and their corresponding latent heats equal to  $98.7 \pm 1.5$  J/g and  $99.0 \pm 1.7$  J/g. T-History and thermal cycling results indicated good heat storage/release potential and thermal reliability of PMMA/caprylic acid PCM microcapsules. Based on the results obtained in the present study, it has been concluded that the synthesized Micro-PCMs can be successfully employed for thermal energy storage purpose, by incorporating them in the potential areas, like temperature regulating building materials, PCM slurries, thermo-responsive textile fabrics, thermo-responsive functional coatings, etc.

## CHAPTER 4

### SYNTHESIS OF NANOENCAPSULATED PCMs

---

#### 4.1 INTRODUCTION

Phase Change material (PCMs) are the latent heat energy storage material systems that are able to absorb and release the thermal energy in the form of latent heat during phase change process typically including solid-liquid, solid-solid, liquid-gas or solid-gas, etc. at narrow temperature intervals. From view point of practical utilization, most of the PCMs being used worldwide exhibit solid-liquid transformations. Energy storage based on PCMs possess certain merits: (a) storing a large quantity of latent heat per unit volume leads to high energy storage densities (b) phase change at constant temperature leading to uniform latent heat transfer (c) a broad spectrum of PCMs are known with a wide range of operating temperatures which enable to develop products with tunable temperatures as per required application [10]. Many efforts have been made to carry out investigations for PCMs developments for various applications including energy saving building constructions, textiles, cooling systems in air conditioning systems, temperature control in electronics etc. [115-118]

The individual property of PCMs drives and controls the final performance of phase change energy storage. According to the material properties, based on the chemical constitution PCMs can be classified as divided into organic and inorganic. Recent years has witnessed the more use of organic PCMs (mainly paraffins) as compared inorganic PCMs. However, some shortcomings are associated with organic PCMs (especially exhibiting solid-liquid phase transitions) such as low thermal conductivity and leakage during phase transition. The leakage issue is highly undesirable for energy storage system and environment, which limits the further application of

PCMs. In order to solve these problems, the PCM are encapsulated in a capsule to acquire a core-shell configuration leading to formation of “Encapsulated Phase Change Materials (EPCMs)” [4].

The encapsulation provides a space to control the volume changes during the phase change, in addition to protecting the PCMs from the outside environment in their applications. Size of PCM encapsulation may vary from macro- ( $>1000 \mu\text{m}$ ), micro- ( $1-1000 \mu\text{m}$ ) or nano-sized ( $1-1000 \text{nm}$ ). Smaller the container entity size, higher is the surface area to volume ratio of the material, much better than microencapsulated PCMs that facilitate faster thermodynamic process that improves heat transfer and better thermal cycling stability [119]. In recent years, several kinds of nanoencapsulated PCMs synthesized by various chemical routes have been studied.

Fang et al. [120] worked upon cold thermal energy storage applications such as air-conditioning and developed a Latent Functionally Thermal Fluid (LFTF) comprising of nanoencapsulated PCM capsules with n-Tetradecane as core and Polystyrene (PS) made by ultrasonic-assisted miniemulsion polymerization. PS/n-Tetradecane nanocapsules with an average diameter of 132 nm were well distributed in the prepared slurry and formed the main energy storage components. PS nanocapsules possessed the melting and freezing temperatures of  $4.04 \text{ }^\circ\text{C}$  and  $-3.43 \text{ }^\circ\text{C}$  along with their corresponding latent heat enthalpies values of  $98.71 \text{ J/g}$  and  $91.27 \text{ J/g}$ . Fang et al. [121] successfully synthesized Polystyrene (PS)/n-dotriacontane (Dot) Nanoencapsulated Phase Change Material (NEPCM) by ultrasonically initiated miniemulsion polymerization and studied the influence of various factors including ultrasonication parameters such as ultrasonic power output, time and temperature, a ratio of co-emulsifiers used [Sodium dodecyl sulphate (SDS) and Poly-(ethylene glycol) monoethylphenyl ether (OP-10)], Styrene/Dot ratio, etc. on average diameter, rate of polymer conversion, encapsulation efficiency and latent heat capacities of

prepared NEPCM. The obtained results suggested the applied ultrasonic method produced nanocapsules of a mean diameter of 168.2 nm. The prepared NEPCM possessed high latent heat enthalpy of 174.8 J/g. It was reported that the optimum experimental factors to obtain the best PS/Dot PCM nanocapsules were; ultrasonic power output: 60%, shorten reaction time: 35 minutes, reaction temperature: 55 °C, SDS/OP-10 ratio: 1 and Styrene/Dot ratio: 1.

Fang et al. [122] produced nanoencapsulated phase change material slurry for cold energy storage consisting of n-Tetradecanecore based nanocapsules with hybrid shell wall (Polystyrene-Silica, PS-SiO<sub>2</sub>) dispersed in a base fluid. Tetradecane/PS-SiO<sub>2</sub> nanocapsules with an average size of 151.3 nm had a melting enthalpy of 83.38 Kj/kg. Guo et al. [123] obtained nanoencapsulated PCM by encapsulating stearic acid inside PMMA nanocapsules by employing an ultrasonically initiated in-situ polymerization method. Morphological results indicated the formation of nanocapsules spheres having a diameter range of 80-90 nm and DSC data suggested the thermal storage ability of fabricated PMMA/Stearic Acid nanocapsules found to be 155.6 J/g.

Rapid population bloom has resulted in increased fossil fuels consumption which led to threatening global warming by emitting greenhouse gases like CO<sub>2</sub>. The dependency on fossil fuels for generating newer chemicals and products should be reduced and replaced with good alternatives like renewable resources. The finite quantities of fossil reserves motivating the research community to develop bio-based chemicals and products [124]. Most of the encapsulation processes were carried out on paraffin PCMs which are obtained from petrochemical resources, thus are non-renewable and reportedly costlier than the fatty acid PCMs. PCMs derived from the fatty acids are still not much explored by the researcher to the full extent which can be a game changer in the development of the road to sustainable future.

One concealed potential fatty acid is Undecylenic Acid (10-undecenoic acid) (UA) (Melting Point: 23 °C); it is a C11 fatty acid-derivative with a terminal carbon-carbon double bond. It is derived from heating of ricinoleic acid (major fatty acid constituent of castor oil) under vacuum pyrolysis. Undecylenic acid is used in numerous application sectors such as pharmaceutical, cosmetic and perfumery etc. UA is a versatile bio-sourced reactant, bifunctional (terminal double bond and carboxylic acid function) which can be used for example as a key intermediate for the synthesis of Tyromycin A or as for preparation of polyols for the synthesis of bio-based polyurethanes and Nylon -11 [125-128].

Polyaniline is a well known conducting polymers can be synthesized in various known forms depending upon the different oxidation states of polyaniline namely Leucoemeraldine, Emeraldine and Pernigraniline. It is widely used for its unique features including price monomer, facile synthesis, good polymerization yield, high electrical conductivity, good environmental stability, and tunable properties which have received much attention for many potential applications in electrical, electronics, thermoelectric, electrochemical, electromagnetic etc. [129-131].

From the available literature, it has been examined that most of the research studies conducted on the preparation of nanoencapsulated PCMs in past were based on petroleum derived paraffins only. Also, it has been observed that very few available research studies [132-135] which ever carried out so far citing the utilization of polyaniline for the development of PCMs for TES applications have accounted for the synthesis of polyaniline via in-situ polymerization or chemical oxidative polymerization method where the reaction is allowed to occur at low temperature (0-5 °C). Keeping these research gaps in view, the present study aimed to synthesize nanoencapsulated phase change materials (PANI/UA NF PCMs) comprising of an unsaturated

fatty acid renewable material, undecylenic acid (UA), as core latent heat storage material, enshrouded within polyaniline (PANI) nanofibres (NF) obtained by interfacial polymerization technique. These resulted nano-sized PCMs were further investigated for their characteristics, including their chemical properties, morphology, thermal properties and thermal stability.

## 4.2 RESULTS AND DISCUSSION

### 4.2.1 Fourier Transform Infrared (FTIR) Spectroscopy

The FTIR spectra of Undecylenic Acid (UA), Nanoencapsulated PCMs, and PANI describing their chemical characteristics are presented in Figure 4.1. The raw fatty acid PCM [in Figure 4.1 (a)] shows peaks at  $2856\text{ cm}^{-1}$  and  $1413\text{ cm}^{-1}$  respectively related belong to C-H stretching and bending frequencies of the aliphatic chain of fatty acid. The peak at  $1710\text{ cm}^{-1}$  and  $1283\text{ cm}^{-1}$  belong to the stretching vibrations of the carbonyl group of the acid. The band at  $724\text{ cm}^{-1}$  corresponds to the C-H rocking modes. For raw PANI nanofibres as shown in Figure 4.1 (b) the characteristic vibration bands observed at  $1599\text{ cm}^{-1}$ ,  $1493\text{ cm}^{-1}$ ,  $1304\text{ cm}^{-1}$ ,  $1149\text{ cm}^{-1}$  and  $818\text{ cm}^{-1}$  relates to the stretching vibrations of quinoid (Q) and benzenoid (B) rings, C-N vibrational stretching in Q-B-Q and B unites, B-NH<sup>+</sup> = Q stretching vibrations and aromatic C-H out of-plane deformation vibrations of linear PANI backbone, respectively. The characteristic band at  $1149\text{ cm}^{-1}$  is associated with the degree of doping or delocalization of electron. In case of PANI/UA PCMs nanofibres spectrum [in Figure 4.1 (c)] exhibits similar attributes of the pure PCM as well as PANI containing distinctive vibration peaks at  $2930\text{ cm}^{-1}$  and  $2853\text{ cm}^{-1}$  belongs to symmetrical and asymmetrical C-H stretch of fatty acid. Carbonyl stretching (C=O) of fatty acid found to occur at  $1711\text{ cm}^{-1}$ . Also, C=C stretching of the quinoid rings, C=C stretching of the benzenoid rings and C-N vibrational stretching in Q-B-Q and B unites have been observed at  $1568\text{ cm}^{-1}$ ,  $1495\text{ cm}^{-1}$  and  $1305\text{ cm}^{-1}$  respectively. The electronic-like absorption of N=Q=N

associated with the degree of doping or delocalization of electron have been observed at  $1188\text{ cm}^{-1}$ . The spectra of nanoencapsulated PCMs displayed indistinguishable characteristic peaks of both PANI and unsaturated fatty acid PCM, supporting the confirmation of the presence of Undecylenic Acid and formation of PANI nanofibres. Similar findings were reported by other research groups so far [33, 136, 137].

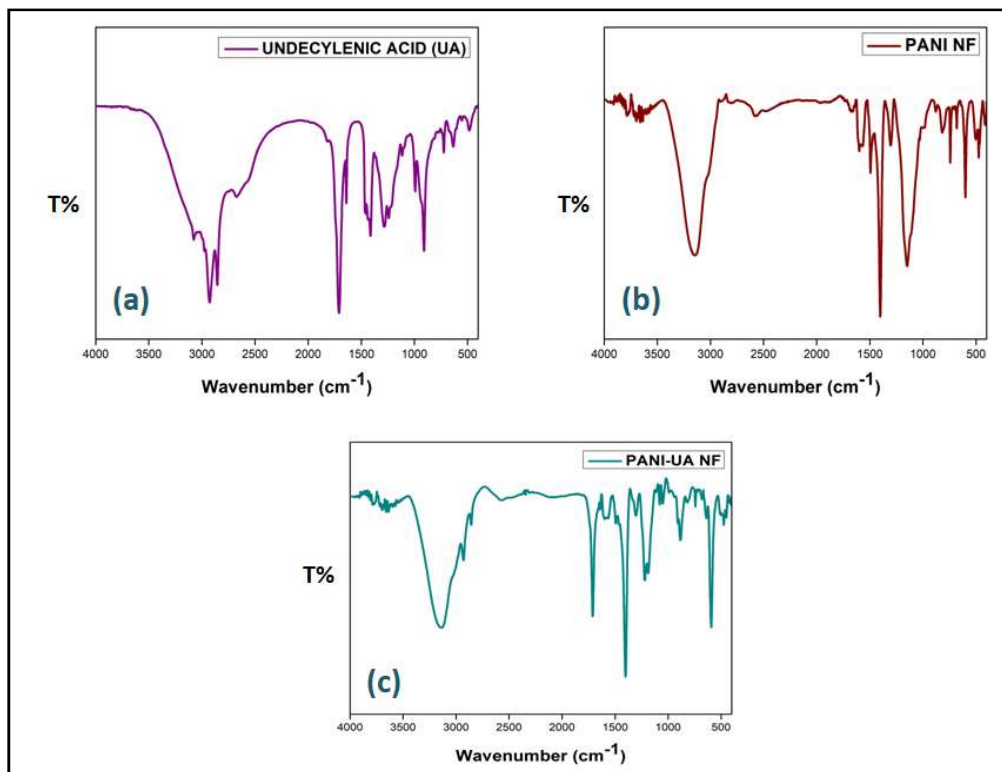


**Figure 4.1: FTIR Spectra of: (a) Undecylenic Acid (UA), (b) PANI NFs and (c) PANI-UA NFs**

#### 4.2.2 Morphology of Nanoencapsulated PCMs

The morphology, shape profiles, and the distribution pattern of the nanoencapsulated PCMs explicated by the HR-TEM analysis and duly verified by image J software are as shown in Figure 4.2. Both raw polyaniline and fatty acid incorporated polyaniline PCMs produced by interfacial polymerization exhibited nanofibrillar morphologies and the nanofibres tend to merge and form interconnected nanofibrous network with narrow diameter distribution. Raw PANI



nanofibres as seen in Figure 4.2 (a-b) showed an average fibrous diameter of 53.1 nm whereas in case of fatty acid filled polyaniline nanofibres showed diameter ranging from 37-78 nm with mean fibre diameter was found to be 56.4 nm. However few polyaniline molecules can also be seen in the form of spherical particles as reported in Figure 4.2 (c-d).

The nanofibres produced in the early stage of polymerization during slow-feeding reactions are subject to secondary growth, which leads to the large agglomerates containing irregularly shaped particles and nanofibres. As the reaction proceed with initiator molecules getting consumed, and polymer chain grows rapidly; the doped emeraldine salt of polyaniline being formed possess hydrophilic nature and can quickly cast away from the interface and diffuses into the water layer. Therefore, in this way, as the nanofibres form, they are continuously withdrawn from the reaction front, thus avoiding secondary growth, and allowing high yield of new nanofibres to grow at this interface. It was observed that diameter of the PANI/UA-NFs seems to be increased as compared to raw PANI, which is attributed to the presence of fatty acid being encapsulated inside nanofibrous structure of polyaniline [138]. The measured electrical conductivity of raw PANI nanofibres as well as that of PANI/UA Nanofibres PCMs was found to be 0.639 S/cm and 0.724 S/cm respectively.

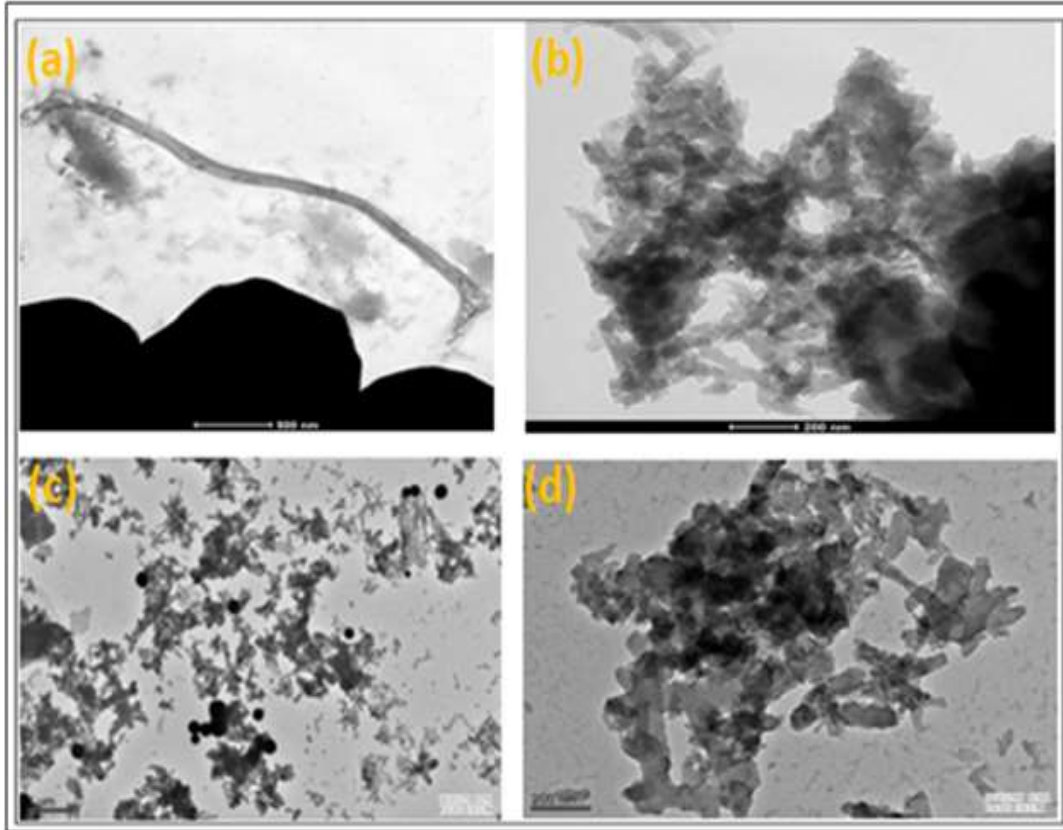


**Figure 4.2: HR-TEM Micrographs of the Synthesized Raw PANI nanofibres: (a) magnification-500 nm; (b) magnification-200 nm; and PANI/UA NF PCMs: (c) magnification-1 $\mu$ m; (d) magnification-200 nm**

### 4.2.3 Thermal Performance of Nanoencapsulated PCMs

The phase change characteristics of the synthesized fatty acid-based nanoencapsulated PCMs and Undecylenic Acid are analyzed by DSC. The DSC curves advocating the phase-change temperatures, and the latent heat enthalpies of the prepared PANI/UA nanofibres PCMs and raw UA are shown in Figure 4.3 and their results are concluded in Table 4.1. The DSC curves of both pure PCM and the nanofibrous PCMs appear to be almost identical, thus, supporting the successful encapsulation of UA within the PANI interstices. The pure UA showed the onset of melting and crystallization temperatures at  $21.5 \pm 0.3$  °C and  $20.8 \pm 0.3$  °C respectively. On contrary, the PANI/UA PCM nanofibres have showed a fair thermal energy storage density, with the onset of melting at  $17.6 \pm 0.2$  °C and crystallization at  $13.5 \pm 0.3$  °C respectively. The latent

heat of fusion and the latent heat of crystallization of the pure fatty acid and nanofibrous PCMs were found to be  $124.39 \pm 2.1$  J/g and  $125 \pm 1.8$  J/g; and  $55.68 \pm 1.4$  J/g and  $56.84 \pm 1.3$  J/g respectively. The shifting of the phase transition temperatures of the synthesized nanoencapsulated PCMs is likelihood, the consequences of the nanoencapsulation event. The encapsulation of the UA inside and along the domains of nano-diameter PANI fibrous entities provided higher heat transfer surface area for the PCM, thus, leading to the improved heat transfer rate as a result of nanoencapsulation. The melting and crystallization peaks of the PANI/UA-NFs showed a depression compared to neat PCM (UA). The calculated encapsulation ratio ( $E_R$ ) of the UA obtained from the measured enthalpies values, using equation 4, was found to be 45%. The comparison of PCM nanofibres prepared in the current study, with few already testified in the literature is reported in Table 4.2. From the attained results, it is apparent that the prepared nanofibrous PCMs exhibit good latent heat energy capacity, and their storage potential can be utilized in substantial TES applications including thermo-responsive textiles, slurries, antistatic/corrosion resistant thermo-regulatory coatings, etc.[139-141]

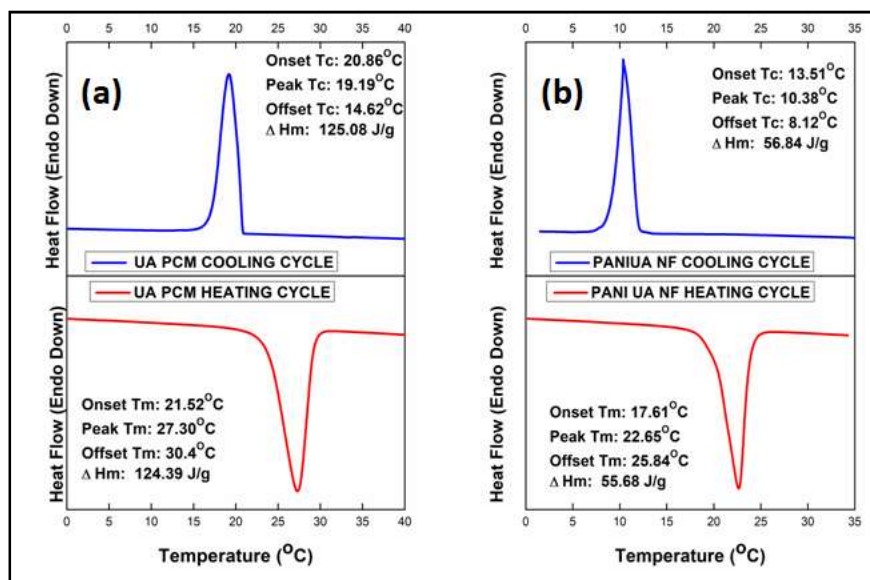


**Figure 4.3: DSC Curves for Heating/Cooling Cycles for (a) Pure UA and (b) PANI/UA-NF PCMs**

**Table 4.1: DSC Data of Pure PCM and Nanoencapsulated PCMs Representing Their Phase Change Characteristics**

Sample	Undecylenic Acid (UA)	PANI/Undecylenic Acid Nanofibres (PANI/UA NFs)
Onset $T_m$ ( $^{\circ}\text{C}$ )	$21.5 \pm 0.3$	$17.6 \pm 0.2$
Peak $T_m$ ( $^{\circ}\text{C}$ )	$27.3 \pm 0.2$	$22.6 \pm 0.3$
Offset $T_m$ ( $^{\circ}\text{C}$ )	$30.4 \pm 0.2$	$25.8 \pm 0.3$
Onset $T_c$ ( $^{\circ}\text{C}$ )	$20.8 \pm 0.3$	$13.5 \pm 0.3$
Peak $T_c$ ( $^{\circ}\text{C}$ )	$19.1 \pm 0.5$	$10.3 \pm 0.4$
Offset $T_c$ ( $^{\circ}\text{C}$ )	$14.6 \pm 0.2$	$8.1 \pm 0.2$
$\Delta H_m$ (J/g)	$124.39 \pm 2.1$	$55.68 \pm 1.4$
$\Delta H_c$ (J/g)	$125 \pm 1.8$	$56.84 \pm 1.3$
PCM (%)	100	45

**Table 4.2: Comparison of some encapsulated PCMs from literature and synthesized nanoencapsulated PCMs**

Core Material	Shell Materials	Size (nm)	$\Delta H_m$ (J/g)	References
Undecylenic Acid	Polyaniline	56.4	55.68	Present Study
Paraffin, M.P. @ $80^{\circ}\text{C}$	Poly-(Styrene-co-Butyl acrylate)	52-112	5-25	[24]
Paraffin, M.P. @ $26^{\circ}\text{C}$	PMMA-SiO <sub>2</sub>	120	71	[142]
Tetradecane	Polystyrene	132	98.7	[120]
Tetradecane	Silica	151.3	83.38	[122]

#### 4.2.4 Thermal Stability of Nanoencapsulated PCMs

The thermal stability and the degradation pattern of the Nanoencapsulated PCMs are studied by TGA. The TGA curves of the PANI/UA-NFs PCMs are shown in Figure 4.4 and, their respective degradation temperatures are given in Table 4.3. The pure UA degrades in a single step. The PCM shows 10 % and 50 % weight loss at around 157.8 °C and 191 °C respectively. The UA undergoes complete decomposition at 198 °C. Due to the compact carbon chain fatty acid chain length, UA has a low decomposition temperature and thus, experiences a progressive weight loss with the temperature rise. Similar to this, the PANI also experiences one step degradation pattern, but perceives the 50 % degradation at a much higher temperature of 370.4 °C, due to the considerably higher molecular weight of the polymer macromolecules. In contrast, the nanoencapsulated PCMs microcapsules underwent a three-stage degradation profile; the first step observed at low temperature is attributed to the vaporization of high volatile compounds, such as remnant organic solvent (toluene) traces or absorbed atmospheric moisture, the second step quite similar to degradation profile corresponds to the degradation of the entrapped fatty acid where 50% thermal degradation occurring around similar temperature range as that of the PCM, and followed by final degradation of conducting macromolecule around 300 °C. This multi-step degradation in the case of nanoencapsulated PCMs supports the success of nanoencapsulation process of unsaturated fatty acid within the used conducting polymer, offering thermal resistance at elevated temperatures.

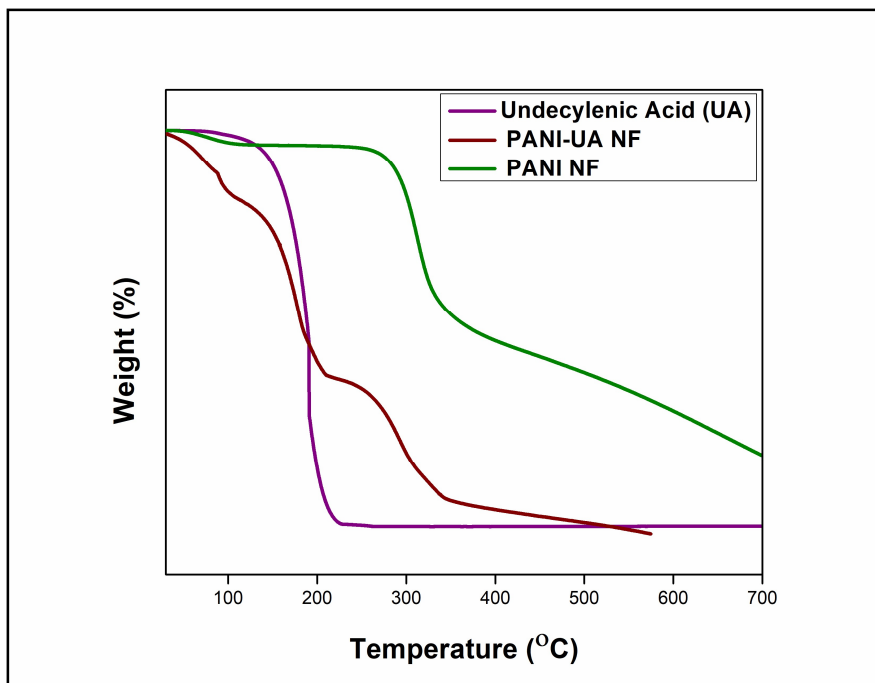


**Figure 4.4: TGA Cures for the UA, Nanoencapsulated PCMs and PANI**

**Table 4.3: Thermal Stabilities of UA, PANI/UA-NFs PCMs and PANI**

Sample	10% Mass Loss (°C)	50% Mass Loss (°C)	80% Mass Loss (°C)
Undecylenic Acid (UA)	157.8	191	198
PANI/UA NFs	90	186	299
PANI	288	370.4	677

#### 4.2.5 Thermal Energy Storage/Release Ability of Nanoencapsulated PCMs

Thermal Energy Storage/Release Ability of the Nanoencapsulated PCMs was evaluated by tracking the charging-discharging rates of UA and PANI/UA-NF PCMs. The melting time was deduced from the charging cycle of UA and Nanoencapsulated PCMs. Similarly, the crystallization time was observed from the discharging cycle of UA and nanofibres PCMs. The distinctive temperature history curves of raw PCM and nanoencapsulated PCMs are shown in Figure 4.5. UA attained its melting temperature (phase change) from 0 °C in 117 seconds

whereas, in the case of nanoencapsulated PCMs, the time consumed was 238 seconds. This difference in the charging time of pure PCM and nanoencapsulated PCMs further attests the successful nanoencapsulation of UA. The discharging time for the pure PCM and nanoencapsulated PCMs to reach their onset crystallization temperatures were found to be 121 seconds and 674 seconds respectively, which, confirms the prolonged latent heat energy release duration against pure PCM.

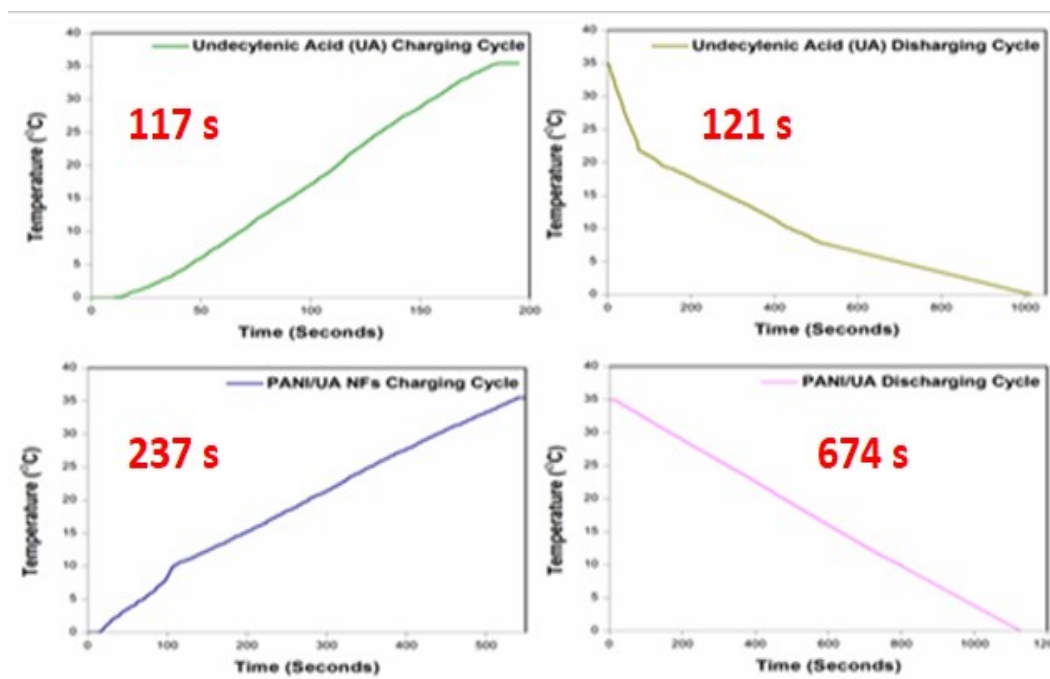


**Figure 4.5: Thermal Energy Storage/Release curves for UA and Nanoencapsulated PCMs during charging and discharging cycles (T-History)**

#### 4.2.6 Thermal reliability of Nanoencapsulated PCMs

Nanoencapsulated PCMs that are used for the purpose of thermal energy storage must be enduring multiple heat-cool cycles with minor deviation in their energy storage properties. DSC plot and changes in latent heat storage characteristics of nanoencapsulated PCMs after facing 100 thermal cycles is shown in Figure 4.6 and Table 4.4 respectively. After 100 cycles the nanoencapsulated PCMs showed latent heat enthalpies of melting and crystallization as  $47.19 \pm$

1.6 J/g and  $49.61 \pm 1.2$  J/g respectively. It is evident from the results obtained that the minor variation in temperature or enthalpy values suggests the good thermal reliability behaviour of the synthesized PCMs suitable for utility in thermal energy storage applications.

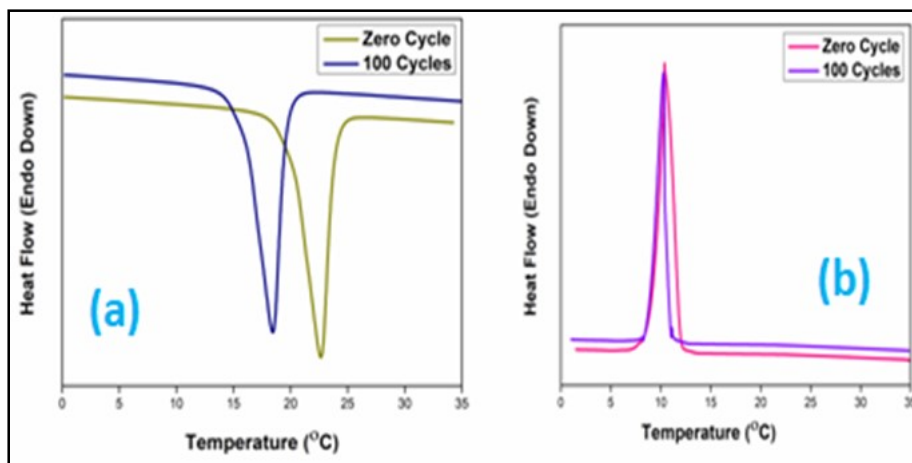


**Figure 4.6: Thermal Reliability Curves of Nanoencapsulated PCMs: (a) Heating Cycle; (b) Cooling Cycle**

**Table 4.4: Phase change characteristics of Nanoencapsulated PCMs post thermal cycling exposure**

Number of Cycles	Onset $T_m$ ( $^{\circ}\text{C}$ )	Onset $T_c$ ( $^{\circ}\text{C}$ )	$\Delta H_m$ (J/g)	$\Delta H_c$ (J/g)
0	$17.6 \pm 0.2$	$13.5 \pm 0.3$	$55.68 \pm 1.4$	$56.84 \pm 1.3$
100	$13.9 \pm 0.4$	$11.1 \pm 0.2$	$47.19 \pm 1.6$	$49.61 \pm 1.2$

### 4.3 SIGNIFICANT FINDINGS

The Nanoencapsulated PCMs consisting of Undecylenic Acid as core and surrounded by nano-scale PANI, as shell have been prepared by interfacial polymerization technique, for the latent heat thermal energy storage (LHTES) applications. FTIR data have depicted the successful encapsulation of the fatty acid inside the PANI nanofibres. HR-TEM results have demonstrated the nanofibrous morphologies of the synthesized nanoencapsulated PCMs with a mean fibre diameter of approximately 56.4 nm. DSC analysis showed that the prepared nanoencapsulated



PCMs exhibited melting and crystallization temperatures of  $17.6 \pm 0.2$  °C and  $13.5 \pm 0.3$  °C respectively and their corresponding latent heats equal to 55.68 J/g and 56.84 J/g. The PCM core content of active PCM inside the PANI nanofibres is approximately 45%. T-History and Thermal reliability test indicated that synthesized PANI based PCM nanofibres exhibited decent thermal cyclic stability. Based on the results obtained in the present study, it has been concluded, that the synthesized Nanoencapsulated PCMs can be successfully employed for thermal energy storage purpose, by incorporating them in the potential areas, like PCM slurries, thermo-responsive textile fabrics, thermo-responsive functional coatings, etc.

**CHAPTER 5**  
**PROPERTY EVALUATION OF SYNTHESIZED TITANIUM DIOXIDE**  
**NANOPARTICLES**

---

## **5.1 INTRODUCTION**

Thermal Energy Storage (TES) systems or technologies based on latent heat thermal energy storage (LHTES) which rely on the utilization of phase change materials (PCMs) have become the center of interest among scientific community for their efficient high-energy storage capacity with little temperature variations. Broad range of materials has been explored and their properties were thoroughly assessed to consider them eligible to act as PCMs, which are further classified into two segments- Inorganic and Organic PCMs [143]. Speaking of the later one, the organic PCMs family including paraffins, fatty acids, polyglycols (PEGs) etc. possesses many positive attributes namely, favourable latent heat density, good thermal and chemical stability, adjustable transition zone, non-toxic, and non-corrosive however, the chemical compounds falling under this category do have certain shortcomings, such as prone to leakage during solid-liquid phase transitions, inadequate heat transfer rate/low thermal conductivity ( $0.1-0.3 \text{ W m}^{-1} \text{ K}^{-1}$ ) flammability etc.[144]

A sensible approach for the enhancement of heat transfer characteristics of PCMs is dispersing the highly conductive micro- or nano-sized particles of thermal fillers or promoters to the PCMs [145]. Till date numerous works have been reported focusing towards the improvement of heat transfer mechanisms in PCMs where various, fillers mainly carbon based materials (graphite powder, expanded graphite, nanotubes, nanoplatelets and graphene) [146-151] or metallic fillers [152-157] have been used.

Nanocomposites containing single-walled carbon nanotubes (SWCNTs) in dosages ranging from 2-10 % and PEG were prepared by impregnation method and studied for the chemical structure, thermal performance and heat transfer enhancement of PEG. The presence of SWCNTs in nanocomposites led to decrease in the supercooling degree as well as exception rise in thermal conductivity was observed when even at low concentration of 4 %, a significantly high 375 % of conductivity enhancement was obtained [158]. In another research work, expanded perlite (EP) was coated with a sucrose solution, followed by carbonation through in-situ by the carbon-bed method in order to obtain EP composites with improved heat transfer efficiency filled with polyethylene glycol. SEM micrographs imply the formation of a highly porous composite structure composed of rough micro-pores could act as a good supporting material for absorbing molten PEG. The prepared PCM undergoes melting and crystallization behaviours at 55.19 and 46.71 °C respectively with corresponding enthalpies found as 134.93 J/g during melting and 129.27 J/g during crystallization, respectively. The thermal conductivity of prepared composites was deduced as  $0.479 \text{ W m}^{-1} \text{ K}^{-1}$  along with good thermal reliability behaviour for 200 thermal cycles [159].

Form-stable PCMs based on Hydrochloric Acid (HCl) modified expanded vermiculite (EVM) and polyethylene glycol (PEG) serving as supporting matrix and a phase change material respectively were prepared while simultaneous addition of graphite to enhance thermal conductivity. The findings indicated that acid modification effectively enhanced the heat storage capacity and thermal conductivity values of the resultant PCM composites [160]. Li et al. [161] incorporated carbon nanotubes (CNTs) during the preparation of the expanded vermiculite (EVM) filled Polyethylene glycol (PEG) form-stable PCM composites. It was observed that the form-stability of the final PCM was governed by EVM pore structure and CNTs surfaces. The

composites possessed better latent heat and heat transfer behaviour with thermal conductivity of  $0.5148 \text{ W m}^{-1} \text{ K}^{-1}$  at 7 wt. % of CNTs. However, the heat storage capacity was inhibited due to pore confinement and EVM surface adsorption of PEG molecules which was more predominant during melting process against crystallization process due to the large specific surface area acting as a heterogeneous nucleation site, thereby supporting numerous nucleation centres for promoting the crystallization of PEG, which contributes to the increased latent heat during the solidification process.

He et al. [162] studied the influence of addition of graphene nanoplatelets (GNPs) in different weight fractions on the latent heat energy storage, thermal conductivity and photo-thermal conversion performance of polyethylene glycol based PCMs for solar energy conversion and storage applications. Halloysite nanotubes (HNT) were infused with PEG400 and PEG600 to yield form-stable HNT/PCM nanohybrids mixture which was melt blended with Low-density polyethylene (LDPE) using twin-screw extruder followed by blown film extrusion to finally obtain flexible nanocomposite films with thermal buffering characteristics at low temperatures cold-chain storage and transportation applications. The produced nanocomposite films bestowed reasonable mechanical properties with phase change transition from  $-17$  to  $26 \text{ }^\circ\text{C}$  with associated latent heat of  $2.3 \text{ J/g}$ . Moreover, the nanocomposite films delayed the warming of frozen and chilled samples for 18 and 20 minutes, respectively, relative to neat LDPE films [163].

For the last decade, there has been a significant increase in research interest in titanium dioxide among many other types of nano-size filler additives with more than 80 % articles published where the number of publications related to  $\text{TiO}_2$  has increased more than 2.5-fold between 2010 and 2020, and  $\text{TiO}_2$  remains one of the most prominent and intensively studied nano-materials, with more than 100 publications per year since 2011, making  $\text{TiO}_2$  the second most studied

nano-scale material after silver and racing up close with other interesting nano-materials including silicon dioxide (SiO<sub>2</sub>), Zinc Oxide (ZnO), carbon nanotubes (CNTs), graphene and reduced graphene oxide etc.[164]

Titanium Dioxide (TiO<sub>2</sub>) is a metal oxide of transition element titanium, existing in three different crystal phases: anatase, rutile and brookite. A well-known n-type semiconductor with wide band-gap energy of 3.0-3.2 eV according to polymorphic crystal structure. It is also commonly used food additive approved as safe (GRAS) by the United States Food and Drug Administration (FDA). This inorganic material possess diverse set of attractive characteristics including chemically inertness, corrosion resistant, excellent photo-catalysis and UV blocking activity, disinfectant, non-toxic, inexpensive etc. [164][165] Therefore, owing to versatile properties, it has been used in various domain applications such as catalytic support, gas sensors, lithium-ion batteries, photo-degradation of biological organisms and organic pollutants, dye-sensitized solar cells, water splitting, anti-bacterial agent, cosmetics etc.[166] It is also widely used as important additive in polymer industry has gathered interest of many experts [167-171].

Particle size of titanium dioxide is critical and influential factor controlling the end properties of the compound and all attention is narrowed down to reduce the particle size thereby optimizing the product properties [172]. Various approaches have been known for the synthesis of nano-titanium dioxide such as sol-gel method, hydrolysis, hydro-thermal method, co-precipitation method, sluggish precipitation, etc. However, sol-gel route is considered as an easy and convenient method for the production of the said metallic oxide of ultra-fine dimension [173].

Sol-gel method is one of the common and the oldest method with origin based on the pioneer experimental works on the synthesis of silica gels by Ebelman and Graham in mid-1800s. Later

on in the 1950s, more progressive studies focused towards the synthesis of ceramics and glass structures using the sol-gel method for the development of many notable mineral oxides such as  $\text{TiO}_2$ ,  $\text{SiO}_2$  and  $\text{ZrO}_2$  came to existence. This method allows good as control over the texture, size and surface properties of the obtained material produced in high quality with large surface areas at low cost. The products can be produced both in powder and thin layers and in porous or dense materials [174]. The process involves development of the colloidal solution (sol phase) being formed after a sequence of hydrolysis reactions and condensation of precursors namely inorganic metal salts or organic metal compounds such as metal alkoxides and subsequent conversion by condensation into continuous liquid phase (gel phase). In general, three steps are involved in the process: (1) hydrolysis, (2) alcohol condensation, and (3) water condensation. With additional drying and heat treatment, the gel becomes a dense glass or ceramic material. Depending on the drying conditions of the wet gel, two types of dry gels are obtained, aerogels and xerogels [175].

### **Advantages of Sol-Gel Method**

- (i) Simplicity of the process.
- (ii) Preparation of high purity products.
- (iii) Low initial investment while having high quality products.
- (iv) Ability of designing and controlling chemical composition and obtaining a homogeneous composition.
- (v) Production of porous and rich materials with organic and polymeric compounds.

In order to sum up with reference to the vast discussions carried out so far related to the development of new PCMs products, with improved performance characteristics, it has been

found that the carbon-based nano-fillers such as graphene, expanded graphite, carbon fibers or carbon nanotubes were used exhaustibly for the improvement of PCMs properties. This study has been representing the assessment of the inherent properties of synthesized titanium dioxide nanoparticles (NTO) produced through sol-gel route in terms of purity, morphological structure and chemical identification and thermal stability etc. Thereafter, these prepared metal oxide nanoparticles will be dispersed in the polymer supporting matrix containing PEG based PCM to obtain thin nanocomposite films developed by solvent casting method. The influence of the addition of these nanoparticles in varying dosage on the thermal, UV and FR characteristics of the PCM composite material will be investigated in the upcoming chapters (6 and 7) of this thesis.

## **5.2 RESULTS AND DISCUSSION**

### **5.2.1 Morphology of Nano-TiO<sub>2</sub> (NTO)**

Figure 5.1 shows HR-TEM images of Nano-TiO<sub>2</sub> (NTO), which revealed that the prepared nanoparticles possess almost spherical geometry and are present in a fair particle size range of 16-40 nm, with the mean particle size found to be 22 nm. Also, the Selected Area Electron Diffraction (SAED) pattern further supports the presence of titanium dioxide nanoparticles having anatase type nature.

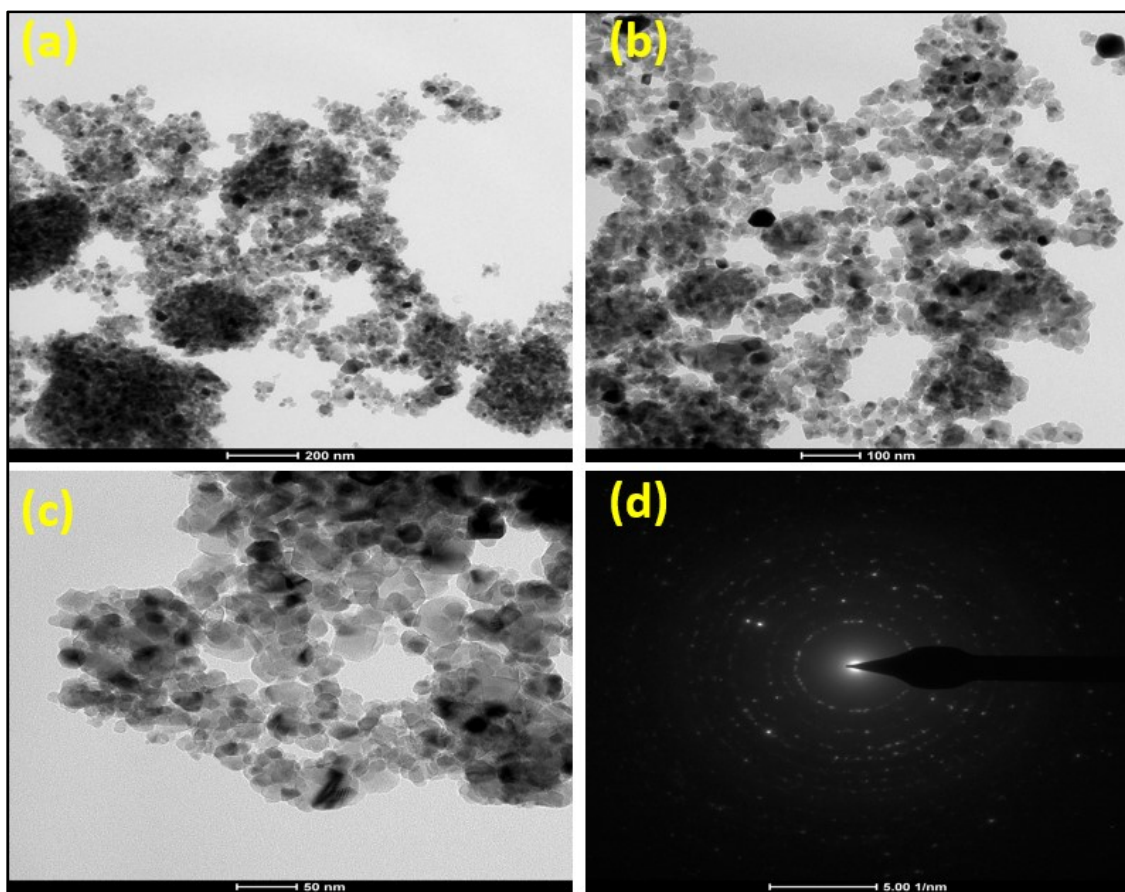


**Figure 5.1: High-Resolution Transmission Electron Microscope (HR-TEM) and Selected Area Electron Diffraction (SAED) images of the synthesized NTO**

### 5.2.2 X-Ray Diffraction (XRD) study of Nano-TiO<sub>2</sub>

The diffraction pattern of prepared NTO using sol-gel method represented in Figure 5.2 shows diffraction peaks at  $2\theta$  values of 25.3, 37.9, 48.1, 54.1, 55.2, 62.8, 69.0, 70.4, and 75.1 corresponding to crystal planes (101), (004), (200), (105), (211), (204), (116), (220) and (107) respectively, indicating the formation of anatase type of titanium nanoparticles in accordance to JCPDS File 21-1272 [176].



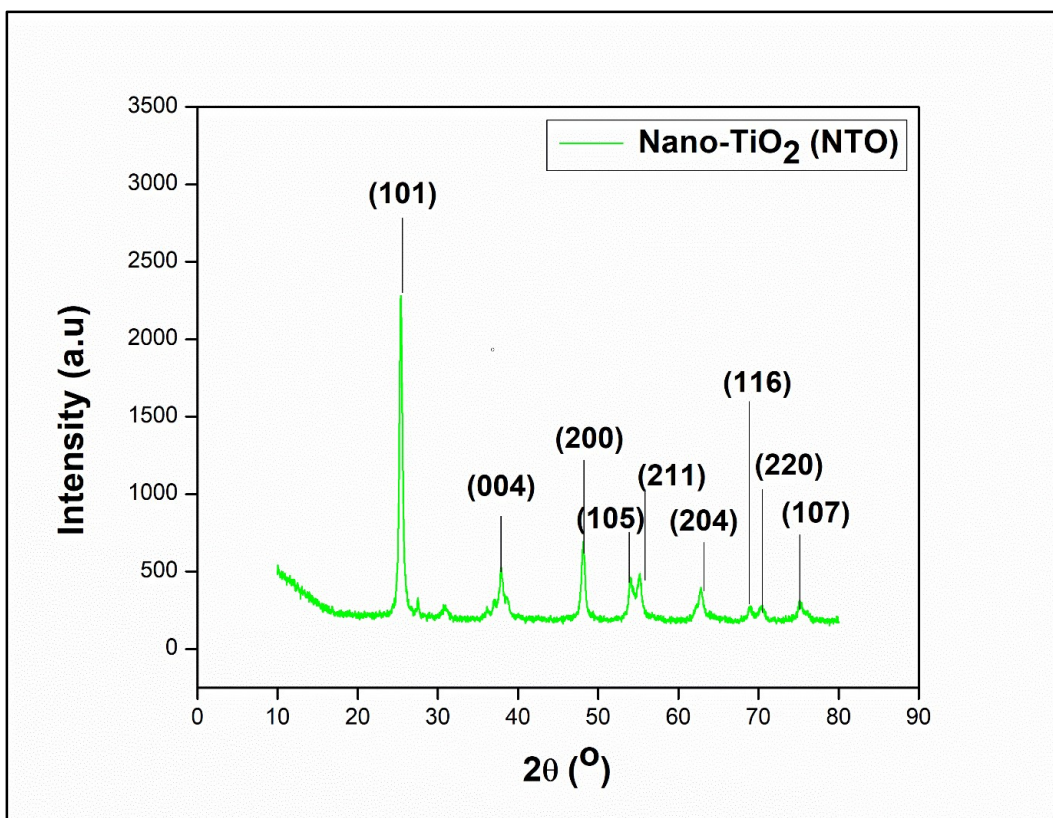


**Figure 5.2: X-Ray Diffraction (XRD) pattern of NTO particles**

### **5.2.3 Fourier Transform Infrared (FTIR) Spectroscopy of Nano-TiO<sub>2</sub> (NTO)**

Figure 5.3 shows the FTIR spectra of Nano-Titanium Dioxide (NTO) synthesized by the sol-gel route observed in the range of 450-4000  $\text{cm}^{-1}$ . The peaks at 3375 and 1623  $\text{cm}^{-1}$  correspond to the stretching and bending vibration of the -OH group because of the absorption of molecular water in the form of moisture, from the atmosphere. Few low-intensity peaks arising at 2896 and 2872  $\text{cm}^{-1}$  indicate the presence of residual organic carbonaceous content of alkoxide precursors. The peaks occurring at 1448 and 664  $\text{cm}^{-1}$  are associated with the stretching vibrations of Ti-O-Ti and Ti-O planes of titanium dioxide nanoparticles, respectively.

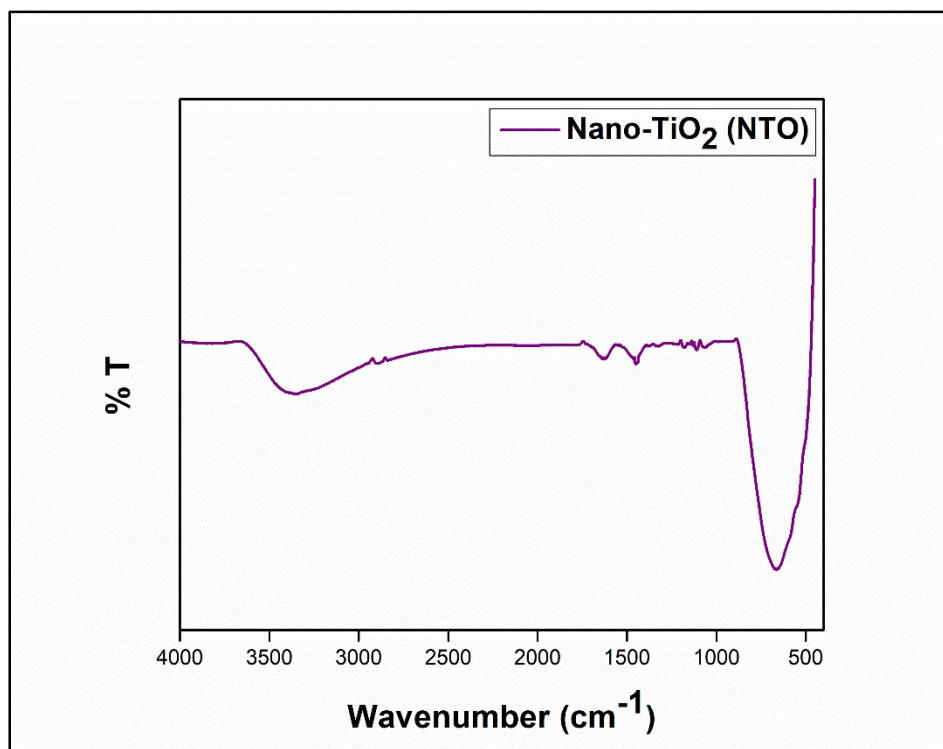


**Figure 5.3: FTIR spectra of Nano-Titanium Dioxide (NTO) derived by sol-gel approach**

#### **5.2.4 Thermal Stability of Nano-TiO<sub>2</sub> (NTO)**

Figure 5.4 shows the thermal stability behaviour of the prepared Nano-TiO<sub>2</sub> characterized by the TGA method carried out up to 800 °C. The titanium dioxide nanoparticles showed an overall weight loss of 17.1 %, when heated to 771.8 °C, thereby indicating the excellent thermal stability of the nanoparticles. The initial weight loss occurring at 130.0 °C is assumed to be the desorption of the water molecules, which were absorbed from the ambient atmosphere over the titanium surface. The second weight loss is observed between 174.6-369.9 °C, which can be considered as the degradation of the remnant carbonaceous impurity (arising from alkoxide moiety) present in trace concentration, along with the titanium dioxide nanoparticles, even after the water washing stage post-synthesis. This is also indicated by EDX analysis as shown in Figure 5.6. The final weight loss is observed at 665.8 °C, which may correspond to the complete burning out of residual organic impurities from the interstices of the synthesized metal oxide nanoparticles.

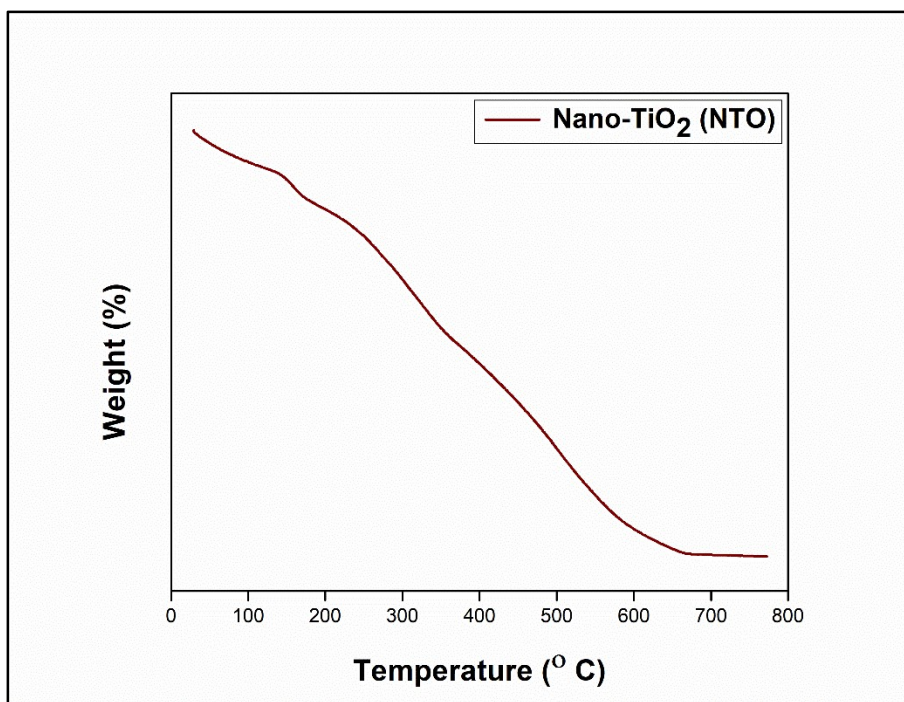


**Figure 5.4: TGA cure of NTO particles**

### 5.2.5 Brunauer-Emmett-Teller (BET) Studies of Nano-TiO<sub>2</sub> (NTO)

The nitrogen adsorption isotherm pattern of the synthesized Nano-TiO<sub>2</sub> (NTO) is shown in Figure 5.5. The characterization of the samples including average surface area, average pore diameter, total pore volume is listed in Table 5.1. The BET measurements confirmed the absence of macropores in the prepared nanoparticles. The nanoparticles exhibited the Type IV isotherm pattern, (BDDT classification) with hysteresis loop of H1 nature inferring the presence of mesoporous structure. BJH (Barrete-Joynere-Halenda) method was utilized to measure the pore-size distribution (inset in Figure 5.5). The BET surface area of the NTO was found to be 53.92 m<sup>2</sup>/g. The pore diameter for NTO was observed as 10.236 nm. The mesoporous total pore volume was calculated and found to be 0.138 cm<sup>3</sup>/g.

**Table 5.1: BET Characteristics of as synthesized NTO particles**

<b>Average Surface Area</b>	<b>53.92 m<sup>2</sup>/g</b>
<b>Total Pore Volume</b>	<b>0.138 cm<sup>3</sup>/g</b>
<b>Mean Pore Diameter</b>	<b>10.236 nm</b>

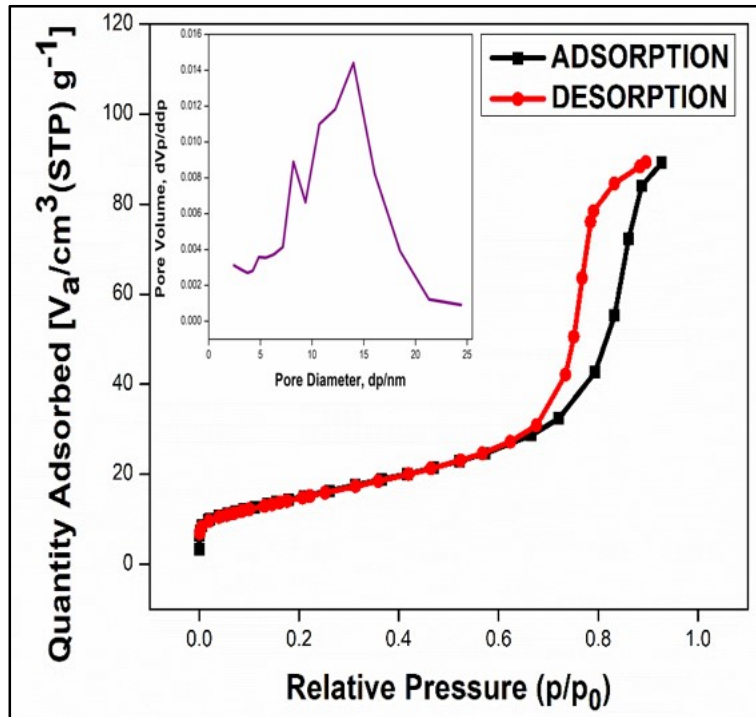


**Figure 5.5: Nitrogen adsorption isotherm of prepared titanium dioxide nanoparticles with pore volume distribution (inset)**

### 5.2.6 Energy -Dispersive X-ray (EDX) Spectra of Nano-TiO<sub>2</sub> (NTO)

Energy Dispersive X-ray (EDX) spectra of the prepared Nano-TiO<sub>2</sub> (NTO), as shown in Figure 5.6 indicates the peaks for Ti element and oxygen which suggests the chemical constituents of Ti and O present in the sample. Apart from the little traces of C, no trace of any other undesirable impurities has been observed in the spectrum.

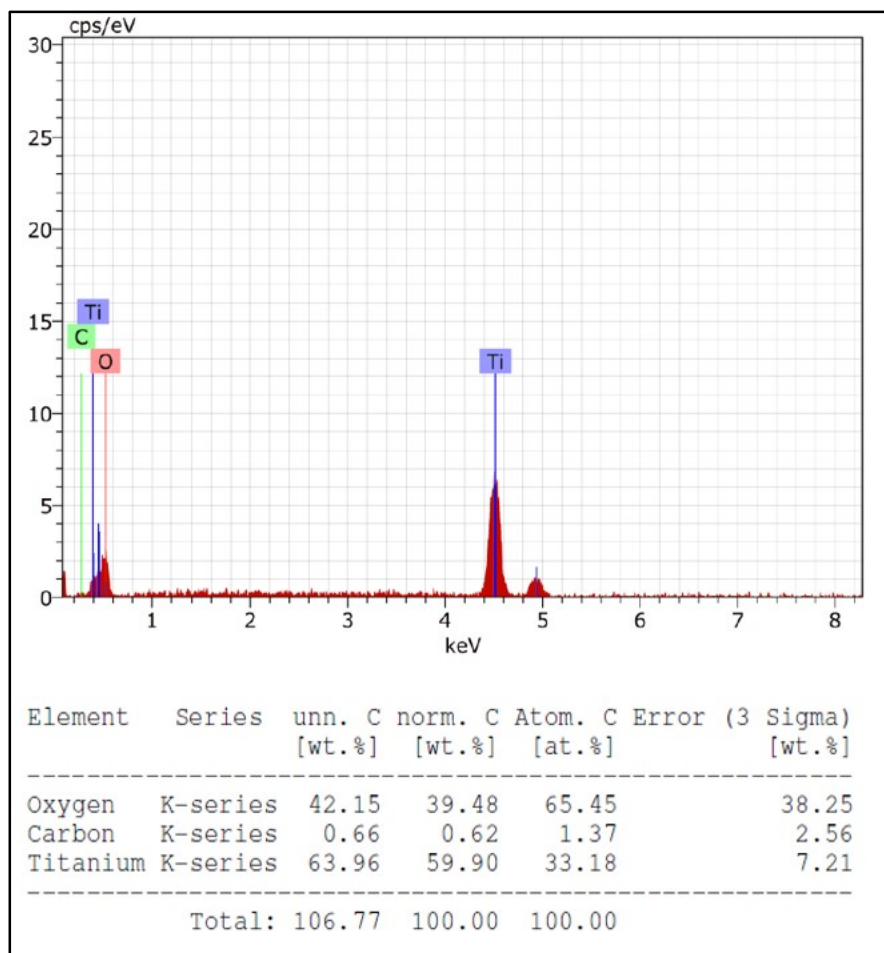


**Figure 5.6: EDX Spectra of synthesized NTO particles**

### 5.3 SIGNIFICANT FINDINGS

HR-TEM images of Nano-TiO<sub>2</sub> (NTO), revealed that the prepared nanoparticles possess almost spherical geometry and are present in a fair particle size range of 16-40 nm, with the mean particle size found to be 22 nm. The diffraction pattern of the prepared NTO shows diffraction peaks at  $2\theta$  values of 25.3, 37.9, 48.1, 54.1, 55.2, 62.8, 69.0, 70.4, and 75.1 corresponding to crystal planes (101), (004), (200), (105), (211), (204), (116), (220) and (107) respectively, indicating the formation of anatase type of titanium nanoparticles. FTIR spectra of Nano-Titanium Dioxide (NTO) inferred that the recorded vibrational bands are concordant and

associated with the titanium dioxide in nature. The BET surface area of the NTO was found to be 53.92 m<sup>2</sup>/g. The nanoparticles exhibited the Type IV isotherm pattern, (BDDT classification) with hysteresis loop of H1 nature, inferring the presence of mesoporous structure. EDX results indicate the peaks for Ti element and oxygen which suggests the chemical constituents of Ti and O present in the sample.

## CHAPTER 6

### FABRICATION OF PEG1500 BASED FORM-STABLE PCMs

---

#### 6.1 INTRODUCTION

To sustain day-to-day life, a variety of basic commodities products/goods are the vital obligations that include fresh food items, medicinal products, electrical or electronic goods, etc. A crucial factor that can strongly affect the quality or deteriorate the inherent product properties is the temperature variations during storage, transportation, and distribution chain until the commodities/goods are delivered to the end-user [177]. Many efforts and huge monetary value of manufacturers and logistic providers come into play to maintain the required temperature and preserve the product's temperature but an undesirable spike in product temperature leads to premature failure of many temperature sensitive goods. One handsome approach in the direction to limit the undesirable temperature surge and ensure the quality of the goods is the incorporation of Phase Change Materials (PCMs) within the base packaging materials to control the temperature within acceptable limits [178].

Phase change materials (PCMs) are well known for temperature control and thermal energy storage in the form of latent heat energy. These materials absorb and release a good amount of latent heat energy during the phase change, within a narrow temperature range [179]. Potential applications for PCMs employment include energy storage building structures, thermo-regulating textiles, solar energy storage, photovoltaics, thermal buffering in food or pharmaceutical etc. [180-182]. A wide range of PCMs which undergo solid-liquid phase change during operation namely, salt hydrates, paraffins, sugar alcohols, polyethylene glycol, fatty acids, and their ester derivatives have been explored in the past decades for thermal energy storage application [183].

However, these solid-liquid PCMs possess some drawbacks such as large volume change during phase transitions, leakage issues, requires containment during thermal energy storage, low thermal stability (except inorganic PCMs salt hydrates), etc.

To resolve the handling and working issues of solid-liquid PCMs, Shape-Stabilized PCMs or Form-Stable PCMs technology has been introduced into the market. Form-Stable PCMs are the combination of active energy storage PCMs and a supporting matrix of inorganic or organic nature. Working methodology of the form-stable PCMs can be understood in a manner as in when the temperature reaches the phase change temperature of the in-housed PCM, the active latent heat energy storage component (PCMs) undergoes melting accompanied by a change of physical state from solid to liquid while the supporting matrix forming the form-stable PCMs can remain in solid state [184].

Much research has been done focusing on the development of variety of Form-Stable PCMs by employing different supporting matrices such as High-Density Polyethylene (HDPE) [185-187], Low-Density Polyethylene (LDPE) [188], Linear-Low Density Polyethylene (LLDPE) [189], Ethylene-Vinyl Acetate (EVA) [190], Polypropylene (PP) [191], Polyacrylonitrile (PAN) [192], Polyvinyl Alcohol (PVA) [193], Styrene Polymers [194], Polyamide (PoA) [195], Polyurethane (PU) [196], Cellulose Acetate [197] etc.

Cao et al. [198] fabricated Wood Plastic Composites (WPCs) based form stable PCMs by mixing Dodecanol filled Melamine-Formaldehyde (MF) Microcapsules with wood flour/HDPE supporting matrix. Prepared WPCs exhibited phase change around 22.2-28.7 °C with associated enthalpies of fusion and crystallization as 20.3 J/g and 31.6 J/g respectively. The presence of MF microcapsules in the HDPE matrix of WPCs caused a decrease in the tensile and flexural



strength of WPCs, on contrary; the PCM microcapsules boosted the impact strength and surface hardness of the final product. Fang et al. [199] studied the effect of the addition of Expanded Graphite (EG) into the form-stable PCMs composed of Stearyl Alcohol (SAL) as working PCMs and HDPE. It was found that the added EG turns out to be very effective in limiting the leakage of SAL during phase change, by acting as a co-matrix along with HDPE and, highly efficient in promoting the thermal conductivity of the final article, as only the 3 wt. % EG dosage inside the HDPE matrix rose its thermal conductivity to  $0.6698 \text{ W m}^{-1} \text{ K}^{-1}$  from  $0.1966 \text{ W m}^{-1} \text{ K}^{-1}$ . Fang et al. [200] prepared form-stable PCMs containing Palmitic Acid (PA) active PCM and HDPE supporting matrix filled with Graphene Nanoplatelets (GNP). It was found that the presence of GNP at 4 wt. % led to 2.5-fold increase in the thermal conductivity as compared to unfilled HDPE matrix and showed phase change temperature around  $62 \text{ }^\circ\text{C}$  and latent heat enthalpy of  $155.8 \text{ J/g}$ . Alkan et al. [201] have chosen Polyvinyl Alcohol (PVA) to hold inorganic salt hydrates such as sodium sulphate decahydrate ( $\text{Na}_2\text{SO}_4 \cdot 10\text{H}_2\text{O}$ ) and calcium chloride hexahydrate ( $\text{CaCl}_2 \cdot 6\text{H}_2\text{O}$ ) inside the interstices of hydrophilic polymer, to be used for passive thermal energy storage systems. Tang et al. [202] prepared Form-Stable Composite PCM made by incorporating Hexadecanol inside dye linked Polyurethane (Dye-PU). Dye-PU is well effective in visible light absorption and its subsequent conversion to thermal energy. Also, the composite PCM exhibited high latent heat enthalpy of  $229.5 \text{ J/g}$ .

Among solid-liquid PCMs, Polyethylene Glycols (PEGs) have gathered the attention of a lots of researchers active in the field of thermal energy storage, and are proved to be potential latent heat energy storage components, due to certain attributes such as availability in a series of molecular weights with diverse melting temperatures ranging from  $4.2$  to  $68.7 \text{ }^\circ\text{C}$ , tunable high latent heat enthalpy depending upon molecular weights, moderate chemical and thermal stability,

congruent melting behaviour, no phase separation, biodegradable in nature, low vapor pressure, non-corrosive, non-toxic, etc. However, PEGs suffer from some shortcomings being leak-prone, have low thermal conductivity, low flammability and slight supercooling [203,204].

In the study, the form-stable PCMs nanocomposite films with thermal buffering ability have been made by using PEG 1500 as an active latent heat energy storage component and Polyvinyl Alcohol (PVA) as a supporting matrix to control the leakage and accommodate large volume change of PEG1500 during phase change, which is duly filled with Titanium Dioxide Nanoparticles (NTO). The influence of the incorporation of titanium dioxide nanoparticles on the thermal energy storage characteristics, thermal stability, flammability, and UV-blocking characteristics of PVA/PEG1500 PCM films have been studied in detail.

## **6.2 RESULTS AND DISCUSSION**

### **6.2.1 Form-Stability of PEG1500/PVA Blends**

The form-stable characteristics of the PEG1500/PVA blends have been examined based on their leakage rate (in %). Figure 6.1 depicts the leakage stability of the hydrophilic polymer blend compositions. The experiment results obtained indicate that the leakage rates varied linearly with increasing PEG content, added to the PVA matrix. The blend composition up to 40 wt. % PEG exhibited a negligible trace of PEG on the filter paper surface. The two highest blend concentrations of 70 wt. % and 80 wt. % showed maximum leakage rate, thus, indicating the poor form-stability characteristics of PEG1500/PVA blends derived from these weight fractions. It has been found out that, the optimum and maximum concentration with decent form-stability behaviour that can be achieved successfully in above-prepared blend compositions turns out to be 60 wt.% of PEG 1500 and is thus, labeled as form-stable PCM. Further, all the nanocomposites reinforced with titanium dioxide nanoparticles are prepared using this particular

optimized form-stable PCM composition and their intrinsic properties are evaluated thoroughly, for thermal energy storage applications.

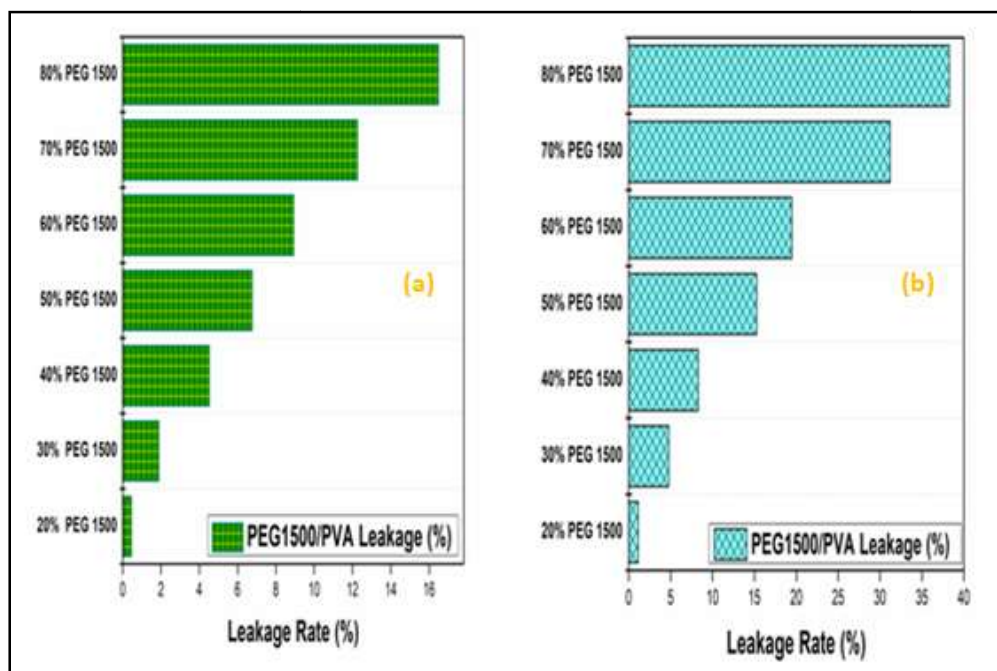


**Figure 6.1: Leakage rates observed for various prepared blend compositions based on (a) measuring the mass loss percentage on weight basis; (b) measuring the diameter of seepage area**

### 6.2.2 Fourier Transform Infrared (FTIR) Spectroscopy of PEG1500/PVA Blends and NTO/PEG1500/PVA Form-Stable PCMs Nanocomposites

FTIR spectrum of pure PVA is represented in Figure 6.2 (a). The most peculiar band of -OH stretching inferring the inherent feature of alcohol has been found at  $3425\text{ cm}^{-1}$ . Also, the peaks arising respectively at  $3238$  and  $1341\text{ cm}^{-1}$  corresponds to the stretching and bending modes of H-OH and mixed -CH and -OH interactions associated with alcohols. The peaks observed at  $2948\text{ cm}^{-1}$  and  $2881\text{ cm}^{-1}$  are related to asymmetric stretching of  $-\text{CH}_2$  groups and C-H stretching vibration modes. It has been observed that the peaks found at  $1718$  and  $1534\text{ cm}^{-1}$  are associated with the stretching vibrations of the carbonyl group, which hypothesizes the presence of residual acetate groups, at the manufacturing stage of PVA, involving the hydrolysis of the polyvinyl

acetate precursor. The peak recorded at  $1405\text{ cm}^{-1}$  represents the bending vibrations of  $-\text{CH}_2$  or  $-\text{CH}_3$  groups. The characteristic peak at  $1131\text{ cm}^{-1}$  has been regarded as crystallization sensitive peak of PVA and it indicates the extent (degree) of crystallinity possessed by the hydrophilic polymer. The peak observed at  $927\text{ cm}^{-1}$  gives evidence about the syndiotactic structure and is attributed to  $-\text{CH}_2$  rocking vibrational modes. The vibrational modes which represent the C-C stretching and  $-\text{OH}$  out of plane bending were observed at peaks  $853$  and  $634\text{ cm}^{-1}$  respectively. In case of raw PEG 1500 [Figure 6.2 (b)], the peaks observed at  $3427$  and  $1633\text{ cm}^{-1}$  have been attributed to the vibrational modes of the  $-\text{OH}$  functional group. The C-H stretching band of PEG 1500 has been noted at  $2887\text{ cm}^{-1}$ . The peak found at  $1115\text{ cm}^{-1}$  is assigned to the C-O stretching mode of ether moiety. The peaks observed at  $964$  and  $843\text{ cm}^{-1}$  correspond to the crystal peak of PEG and C-C-O stretching vibrations.

The FTIR spectrum of PVA blends with different PEG concentrations, as illustrated in Figure 6.2 (c), exhibited nearly identical absorption bands, within the scanned wavelength range, therefore, confining the retention of the primary functional groups of both individual hydrophilic polymers, within the newly formed blend compositions. Though, there is an observable moderate shift in both band positions, as well as, the relative intensities of the stretching vibrations of the hydroxyl group in the resultant blends. This is accredited to the formation of H-bonds between PVA and PEG, at various PEG ratios. Other primary peaks observed in all the blend compositions (20-80 wt.%) are found ranging between  $2892\text{-}2896\text{ cm}^{-1}$ ,  $1710\text{-}1712\text{ cm}^{-1}$ ,  $1413\text{-}1423\text{ cm}^{-1}$ ,  $1088\text{-}1090\text{ cm}^{-1}$ ,  $961\text{-}964\text{ cm}^{-1}$ ,  $840\text{-}843\text{ cm}^{-1}$ , thus, correspond respectively to C-H, C=O (residual acetate groups of PVA),  $-\text{CH}_2$ , C-O-C, C-H (PEG), C-C-O (PEG) stretching and bending vibrational modes. These findings are concordant with the already reported literature [205].

Figure 6.2 (d) depicts the FTIR spectrum of NTO/PVA/PEG1500 (60 wt. %) nanocomposite films, with varying nanoparticles loadings. The films showed indistinguishable peaks recorded for the particular blend composition, as also observed earlier in this study. However, the minor peak shifting of -OH bands has been observed, which occurred due to the H-bonding formation between the hydroxy group present in the blend, and the oxygen groups of titanium dioxide nanoparticles. Also, the shifting in the peak intensity of -OH groups in the nanocomposite films with the increasing dosage of NTO has been observed, which might be due to the agglomeration of metal oxide particles, leading to the weakening in H-bond interactions [205].

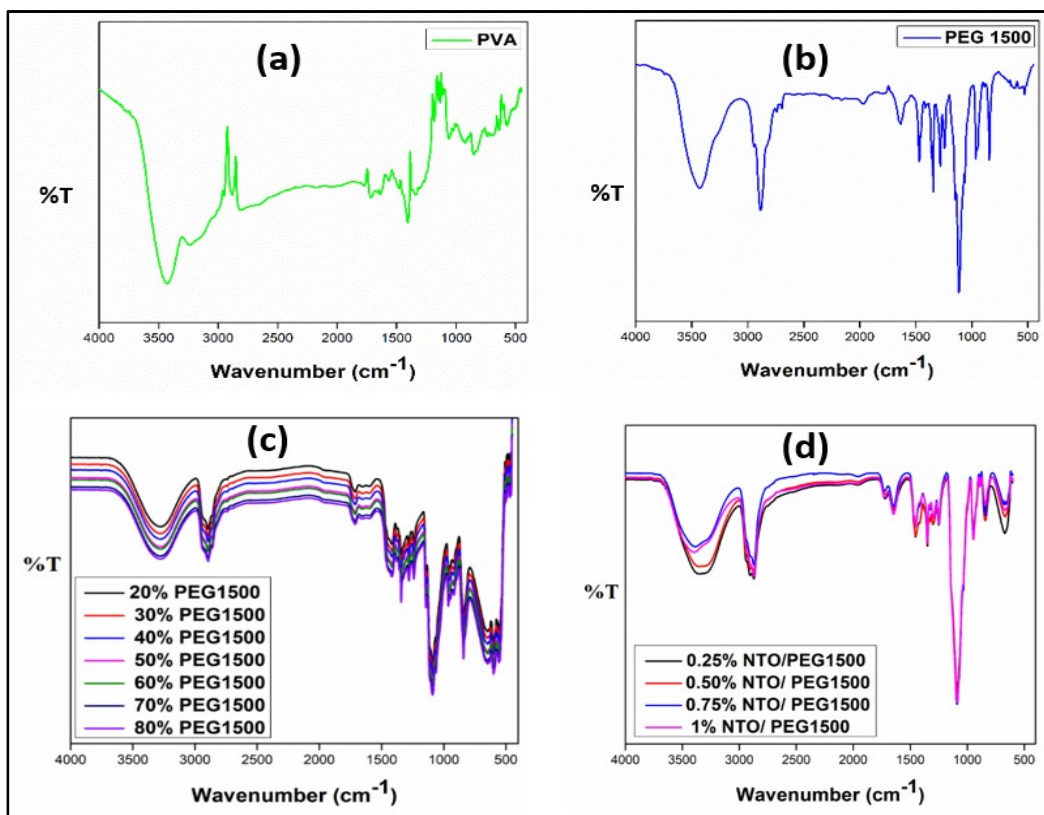


**Figure 6.2: FTIR spectra for (a) PVA; (b) PVA; (c) PEG1500/PVA blends with different PEG concentrations; (d) NTO/PEG1500/PVA nanocomposites at different NTO loadings**

### **6.2.3 Phase Change Characteristics of PEG1500/PVA Blends and NTO/PEG1500/PVA Form-Stable PCM Nanocomposites**

Differential Scanning Calorimetry (DSC) has been utilized for the evaluation of the phase change behaviour of all the blend compositions (with 20-80 wt. % of PEG1500) and the NTO filled-60 wt. % PEG1500/PVA nanocomposites. Figure 6.3 (a) and Table 6.1 (a & b) portray the melting and crystallization temperatures of PEG1500 and its corresponding blend compositions. Pure PEG used as the main latent heat storage PCM showed onset melting and crystallization temperatures at 38.13 °C and 34.18 °C, respectively. The enthalpies accompanying the phase change were estimated as 150.75 and 151.25 J/g, respectively. In case of blend compositions, it was found that the melting temperatures, and their associated enthalpies increases in a progressive manner, due to an increase in active PEG PCM concentrations, in the molecular domains of the PVA supporting matrix. The optimized blend composition of 60 wt. % PEG1500/PVA undergoes melting and crystallization transitions at 36.14 °C and 31.02 °C, respectively. Also, it exhibited peak melting and crystallization temperatures at 48.27 °C, with the latent heat of fusion of 60.65 J/g, and 22.56 °C, with the corresponding latent heat of crystallization 62.08 J/g, respectively.

The influence on the thermal energy storage parameters after the incorporation of metal oxide nanoparticles to the optimized blend composition (PEG~ 60 wt.%) can be seen significantly from the obtained thermal performance data, demonstrated by the DSC analysis. The phase change curves representing the phase-change temperatures, and the latent heat enthalpy values for the varied loading of synthesized nanoparticles in the NTO/PEG1500/PVA nanocomposites are shown in Figure 6.3 (b) and their results are summarized in Table 6.2 (a & b). The obtained results suggest that the addition of titanium dioxide nanoparticles has led to enhanced heat

transfer rates, which, tend to escalate with increasing order of NTO loading, owing to the high thermal conductivity of the metal oxide nanoparticles. This also accounts for the surge in the latent heat enthalpies of the nanocomposites against the gradual increase in the concentration of nanoparticles, in the form-stable PCM nanocomposites, as depicted in Figure 6.4 (a). For the maximum NTO concentration of 1%, the onset melting and crystallization temperatures are reported as 29.69 °C and 34.13 °C, respectively. The peak melting and crystallization temperatures have been recorded at 43.88 °C and 26.85 °C, along with corresponding estimated enthalpies of 73.02 J/g and 70.23 J/g, respectively.

An important concerning aspect associated with PEG PCMs, about their possible utilization as an effective latent heat thermal energy storage system, is the supercooling phenomenon. Typically, the degree of supercooling of a PCM is derived by calculating the difference between the peak melting and crystallization temperatures of the working PCM. It is desirable for a PCM used for varying TES application, to possess a narrow supercooling degree as possible. Figure 6.4 (b) represents the variation in the degree of supercooling of the nanocomposite films subjected to different loading of NTO in the form-stable PCMs. It has been estimated that increasing the NTO amount in form-stable composites, can remarkably refine the supercooling degree to a slightly better extent. This control in supercooling phenomenon arises due to the foremost action of titanium dioxide nanoparticles, by acting as a potent nucleating agent during the heat-cool cycle of PEG-based form-stable nanocomposites, resulting in an improved solidification rate of the PEG macromolecules, during cooling process. The comparison of the form-stable PCM prepared in the current study with few existing counterparts, testified in the literature is reported in Table 6.3. Therefore, the resulted form-stable nanocomposites displayed very good latent heat energy potential and can be applied for suitable thermal buffering applications.

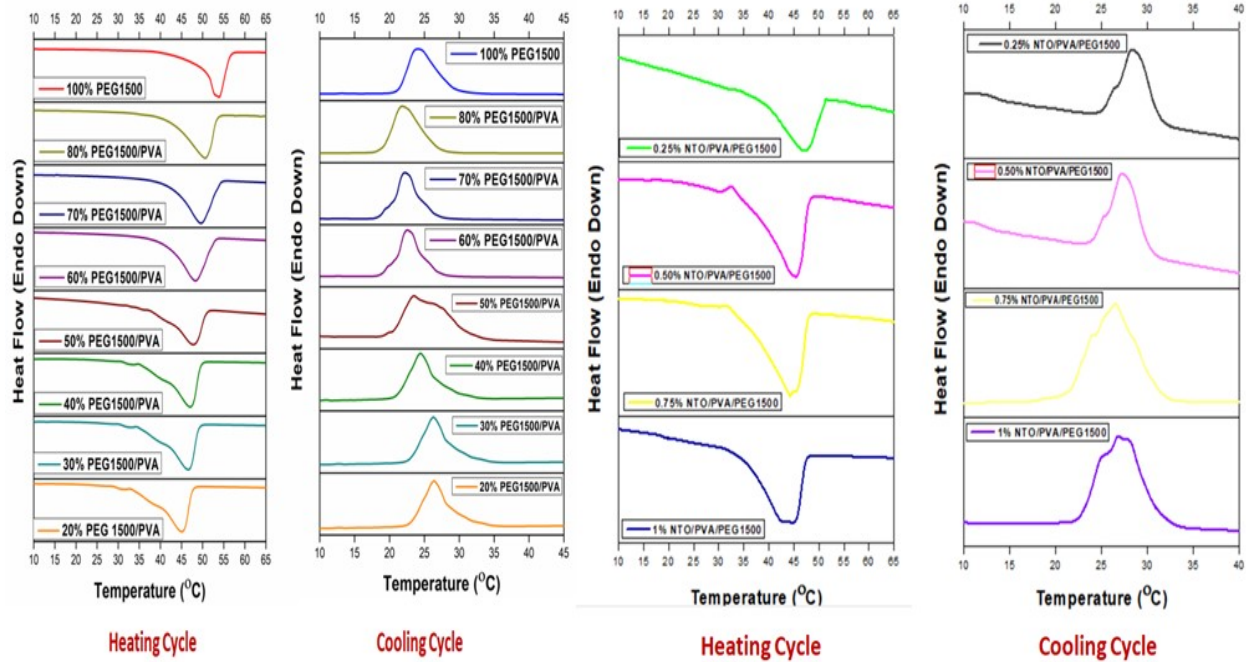


**Figure 6.3: Phase change characteristics for (a) PEG1500 and its associated blends; (b) form-stable PCMs**

**Table 6.1: DSC Data of Pure PCM and PEG Blends Representing Their Phase Change Characteristics**

(a)

Samples	Onset Melting Temperature, $T_{Mo}$ (°C)	Peak Melting Temperature, $T_{Mp}$ (°C)	Offset Melting Temperature, $T_{Mc}$ (°C)	Latent Heat of Fusion, $\Delta H_m$ (J/g)
PEG1500	38.13	53.89	58.18	150.75
20% PEG1500/PVA	28.59	45.08	49.21	8.81
30% PEG1500/PVA	30.19	46.61	50.78	19.36
40% PEG1500/PVA	30.62	47.10	51.23	30.57
50% PEG1500/PVA	32.07	47.78	52.20	57.56
60% PEG1500/PVA	36.14	48.27	54.15	60.65
70% PEG1500/PVA	37.66	49.65	55.15	81.45
80% PEG1500/PVA	37.88	50.63	55.38	131.32



(b)

Samples	Onset Crystallization Temperature, $T_{Co}$ (°C)	Peak Crystallization Temperature, $T_{Cp}$ (°C)	Offset Crystallization Temperature, $T_{Ce}$ (°C)	Latent Heat of Crystallization, $\Delta H_f$ (J/g)
PEG1500	34.18	24.09	20.2	151.25
20% PEG1500/PVA	36.48	26.39	19.98	10.68
30% PEG1500/PVA	36.45	26.28	20.13	17.29
40% PEG1500/PVA	35.04	24.42	18.2	33.38
50% PEG1500/PVA	34.61	23.51	18.27	60.37
60% PEG1500/PVA	31.02	22.56	17.59	62.08
70% PEG1500/PVA	30.29	22.18	17.46	85.49
80% PEG1500/PVA	29.14	21.82	17.17	139.44

**Table 6.2: DSC Data of NTO/PEG1500/PVA form-stable PCMs Representing Their Phase Change Characteristics**

(a)

Samples	Onset Melting Temperature, $T_{Mo}$ (°C)	Peak Melting Temperature, $T_{Mp}$ (°C)	Offset Melting Temperature, $T_{Me}$ (°C)	Latent Heat of Fusion, $\Delta H_m$ (J/g)
0.25% NTO/PEG1500/PVA	33.48	47.27	51.3	65.59
0.50% NTO/PEG1500/PVA	32.49	45.24	49.43	68.43
0.75% NTO/PEG1500/PVA	31.48	44.25	48.8	71.70
1% NTO/PEG1500/PVA	29.69	43.88	48.52	73.02

(b)

Samples	Onset Crystallization Temperature, $T_{Co}$ (°C)	Peak Crystallization Temperature, $T_{Cp}$ (°C)	Offset Crystallization Temperature, $T_{Ce}$ (°C)	Latent Heat of Crystallization, $\Delta H_f$ (J/g)
0.25% NTO/PEG1500/PVA	32.74	28.34	24.05	63.97
0.50% NTO/PEG1500/PVA	32.98	27.32	23.13	66.12
0.75% NTO/PEG1500/PVA	33.65	26.53	20.47	69.82
1% NTO/PEG1500/PVA	34.13	26.85	21.29	70.23

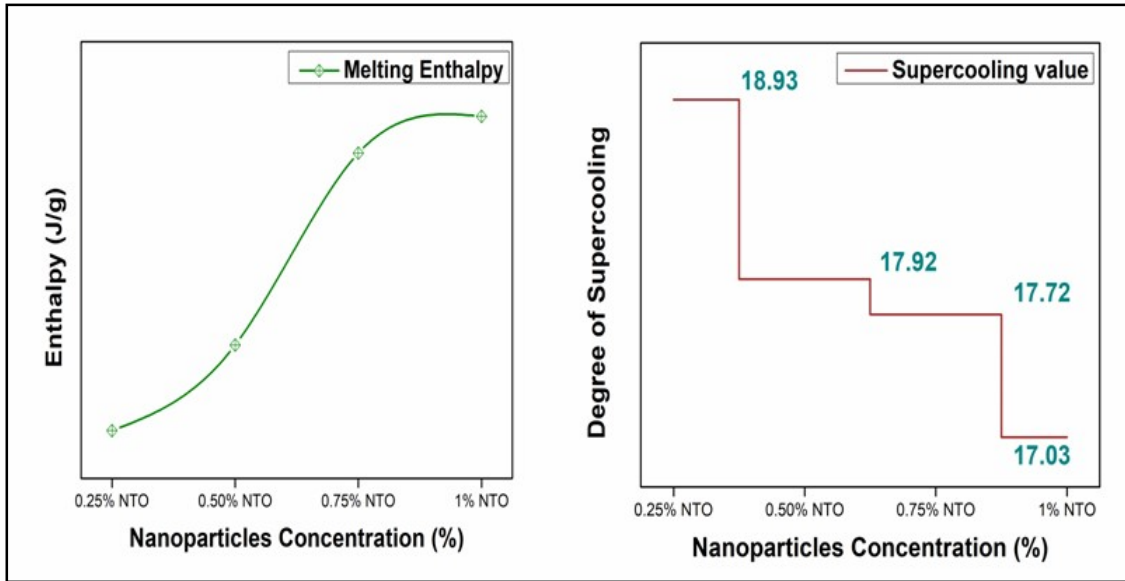


**Figure 6.4: Effect of Nanoparticles concentrations on (a) Latent Heat Enthalpy of Fusion; (b) Degree of Supercooling**

**Table 6.3: Comparison of some form-stable PCMs from literature and prepared form-stable PCMs**

Core PCM	Matrix	Additive	$\Delta H_m$ (J/g)	References
PEG	PVA	Titanium Dioxide Nanoparticles	73.02	Present Study
PEG	Graphitic Carbon Nitride	-	45.8	[206]
Dodecanol Microcapsules	HDPE	Wood Flour	31.6	[198]
Paraffin Microcapsules	PVC	Wood Flour	15.92	[207]
n-Octadecane	PVC	Titanium Dioxide Nanoparticles	9.22	[76]
Paraffin Microcapsules	HDPE	Wood Flour	42.8	[187]

#### **6.2.4 Thermal stability of PVA/PEG1500 blends and NTO/PEG1500/PVA nanocomposites**

From a practical viewpoint, the thermal stability is a significant property to evaluate the polymer products, especially the thin plastic films. In commercial approach, generally, the temperature ( $T_{50}$ ) corresponding to a weight loss equivalent to 50 %, is considered as an important parameter to access the thermal stability performance. Sometimes in many industrial applications from thermo-mechanical stability aspect, the 50 % weight loss is regarded as the initial failure of the material during service life, even before reaching the maximum degradation. Figure 6.5 (a) represents the thermal stability characteristics of pure PVA, PEG1500, and PVA/PEG1500 blend compositions with varying PEG1500 content. The pure PVA showed  $T_{50}$  and  $T_{80}$  at 326.2 °C and 366.6 °C, respectively whereas in the case of working PCM 50 % and 80 % degradation have been observed to be occurring at 416.1 °C and 427.9 °C, respectively, which signifies the high thermal stability of the active PCM, even more than that of the supporting matrix. This is due to the more crystalline nature of PEG compared to PVA, which arises because of more compact and linear chain structure of PEG macromolecule, which leads to an effective packing of the crystal lattice structure, in the crystalline region of the polymer. On the other hand, in PVA, the pendant hydroxyl groups (-OH) attached to PVAs main backbone chain creates hindrance in the chain folding arrangement and disturbs the effective crystal packing phenomenon of the macromolecule chains, that enables the PVA to exhibit amorphous nature, and thus, a little less thermally stable, compared to PEG blend compositions, with varying PEG contents (20-80 wt. %). It was found that the thermal stability behaviour of the PVA/PEG blends tends to improve, with increase in PEG concentration within the PVA matrix, owing to the high crystalline nature of polyethylene glycol. Therefore, it strongly can be considered as a highly advantageous

approach for the incorporation of polymeric PCM into the PVA matrix, wherein the active PCM acts as dual roles including working as an efficient latent heat storage component, as well as, for enhancing the overall thermal stability, at elevated temperatures, in all blend compositions. The addition of 60 wt. % PEG to a vinyl polymer resulting in PEG1500/PVA blend improves and shifts the  $T_{50}$  of the PVA matrix to 354.8 °C and finally undergoes degradation at 410.6 °C.

The thermal stability of metal oxide filled nanocomposite films, (NTO/PEG1500/PVA) comprising of 60 wt. % PEG loading, with varying concentrations of titanium dioxide nanoparticles (NTO: 0.25-1 %) is shown in Figure 6.5 (b). It has been observed that the addition of prepared nanoparticles to the fabricated 60 wt. % PEG1500/PVA film, in increasing order dosage, has resulted in the enhancement of thermal stability of the nanocomposite films. This is attributed to the high thermally stable nature of nano-sized inorganic metal oxide filler particles. It is believed that the presence of NTO particles embedded inside the PEG1500/PVA blend boosts the thermal stability of the nanocomposites films by restricting the bond dissociation or the mobility of polymer chains due to the crowding of nanoparticles across the macromolecular network of blended polymers, at elevated temperatures.

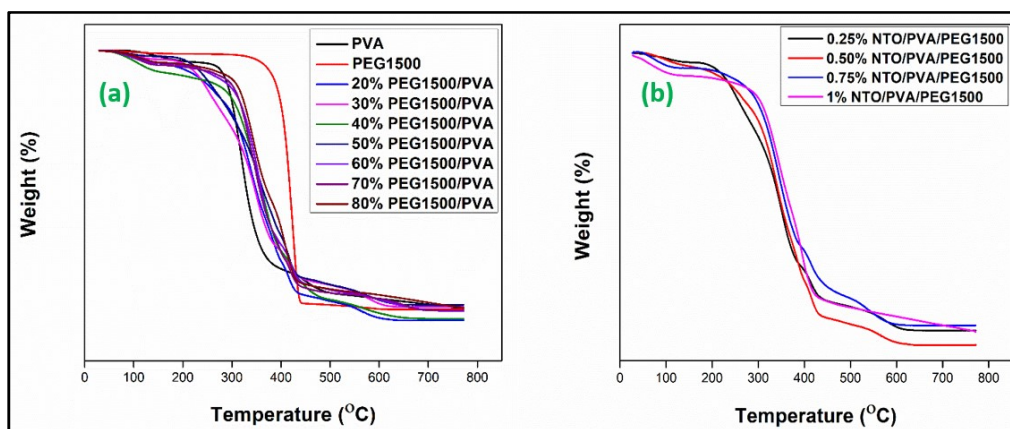


**Figure 6.5: TGA Cures for (a) PEG1500/PVA blends with different PEG concentrations; (b) NTO/PEG1500/PVA nanocomposites at different NTO loadings**

**Table 6.4: Thermal Stabilities of (a) PEG1500/PVA blends with different PEG concentrations; (b) NTO/PEG1500/PVA nanocomposites at different NTO loading**

(a)

Samples	50% Weight Loss Temperature, $T_{50}$ (°C)	80% Weight Loss Temperature, $T_{80}$ (°C)
PVA	326.2	366.6
PEG 1500	416.1	427.9
20% PEG 1500/PVA	340.3	393.6
30% PEG 1500/PVA	342.4	402.5
40% PEG 1500/PVA	351.0	405.1
50% PEG 1500/PVA	353.9	405.6
60% PEG 1500/PVA	354.8	410.6
70% PEG 1500/PVA	355.1	413.7
80% PEG 1500/PVA	364.6	414.6

(b)

Samples	50% Weight Loss Temperature, $T_{50}$ (°C)	80% Weight Loss Temperature, $T_{80}$ (°C)
0.25% NTO/PVA/PEG 1500	355.8	412.2
0.50% NTO/PVA/PEG 1500	358.4	416.3
0.75% NTO/PVA/PEG 1500	360.6	422.4
1% NTO/PVA/PEG 1500	362.1	425.6

### 6.2.5 Thermal energy storage performance of NTO/PEG1500/PVA form-stable nanocomposites

The thermal energy storage capability of the 1% NTO/PEG1500/PVA nanocomposite form-stable PCM was determined by observing the charging-discharging times of the form-stable PCM relative to pure PEG. The melting and crystallization time were evaluated from the charging and discharging cycles of PEG and composite PCM. The representative temperature history curves of raw PCM and form-stable PCM nanocomposite are shown in Figure 6.6. It has been observed that the PEG1500 reached its phase change temperature ( $T_{mo}$ : 38.13 °C) from 10 °C in 481 seconds whereas, in the case of form-stable PCMs, the time taken to hit its onset

melting temperature ( $T_{mo}$ : 29.69 °C) was 472 seconds. Similarly, the discharging time for the pure PCM and metal oxide filled PCM nanocomposite were found as 519 and 747 seconds, respectively. The obtained results can be interpreted in such a manner that the introduction of titanium dioxide nanoparticles metal oxide nanoparticles to the form-stable PCM end product fastens the heat transfer mechanism within the composite structure, owing to their high thermal conductivity and large specific surface area. Secondly, in the case of nanocomposite films, the PCM content is only 60 wt. % against the 100 wt. % fraction of pure PEG PCM. Therefore, the presence of active ingredient components in lesser amounts tends to undergo phase transitions much faster, at shorter temperature profiles than that of the bulk material. Furthermore, since both samples were heated and cooled under the same temperature profile, as the water baths were thermo-stated constantly between 10-60 °C, it can be observed that the nanocomposite material took more time to attain this temperature limit during crystallization process as compared to raw PEG, which indicates the presence of polymer macromolecules in the neighborhood of PEG molecules; giving evidence of successful fabrication of form-stable PCM. Thus, the insulating nature of the plastic supporting matrix along with the crowding of nanoparticles within the composite material hinders the mobility of PEG molecules at the time of crystallization period should be accounted for the delay in achieving the equilibrium temperature.

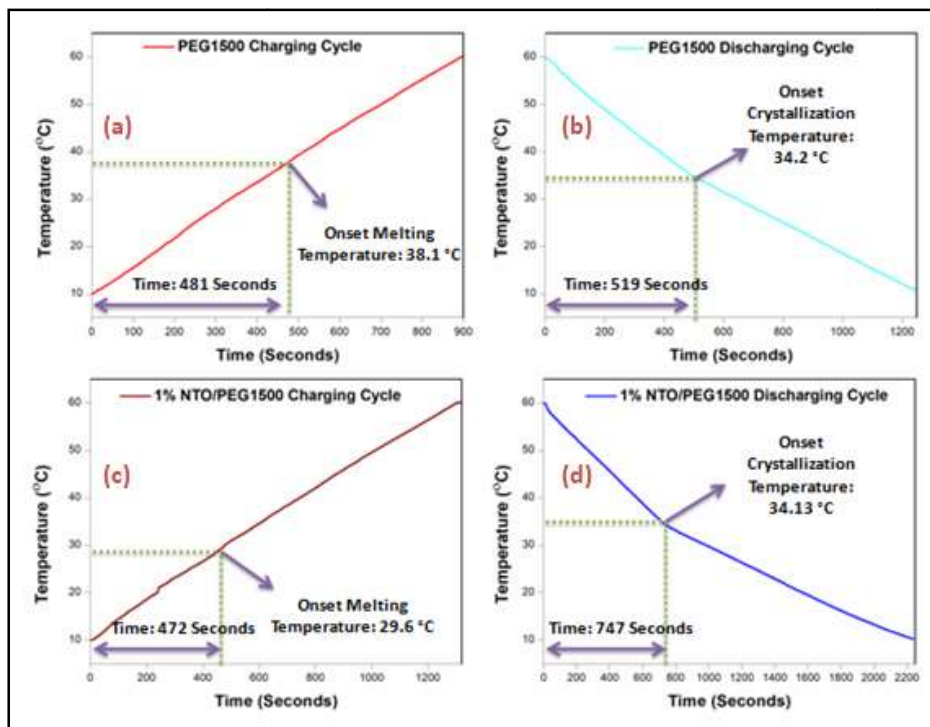


**Figure 6.6: Thermal Energy Storage curves for bulk PEG 1500 and Form-Stable PCM (T-History)**

### **6.2.6 Thermal reliability performance of NTO/PEG1500/PVA form-stable nanocomposites**

DSC curves and changes in thermal characteristics of form-stable PCM after exposure to 100 thermal cycles are represented in Figure 6.7 and Table 6.5 respectively. After 100 cycles, the metal oxide-filled PEG nanocomposite PCM exhibited latent heat enthalpies of melting and crystallization as 66.38 J/g and 63.14 J/g respectively. It is clear from the results obtained that the little variation in temperature or enthalpy values suggests the decent thermal reliability behaviour of the prepared form-stable PCMs, and these are much suitable for utility in the thermal energy storage applications.

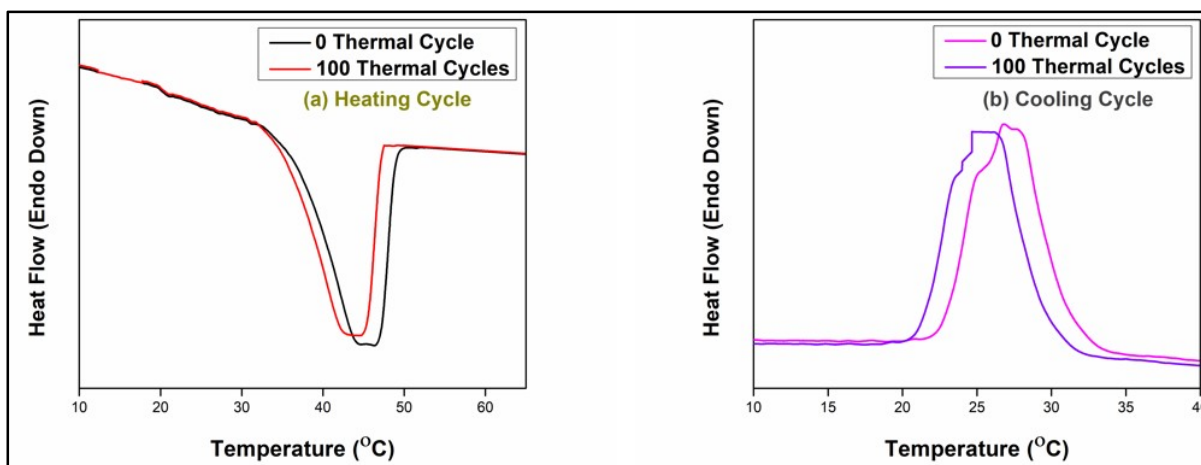


**Figure 6.7: Thermal Reliability Curves of form-stable PCMs: (a) Heating Cycle; (b) Cooling Cycle**

**Table 6.5: Phase change characteristics of 1% NTO/PEG1500/PVA Nanocomposite PCM post thermal cycling exposure**

Number of Cycles	Onset $T_m$ (°C)	Onset $T_c$ (°C)	$\Delta H_m$ (J/g)	$\Delta H_c$ (J/g)
0	29.69	34.13	73.02	70.23
100	31.9	32.63	66.38	63.14

### 6.2.7 Structural characterization of NTO/PEG1500/PVA form-stable PCMs

FE-SEM photographs of 1% NTO/60 wt. % PEG1500/PVA shown in Figure 6.8 (a-d) provide an insight into the resulting microstructures of the prepared form-stable nanocomposites. From these obtained figures, it can be inferred that the PEG crystals of uneven shape and size can be seen randomly distributed and held together, throughout within the surface of the supporting matrix. This affirms the role of polymers such as PVA as an effective supporting matrix and could be considered as a potential matrix material component for fabrication of form-stable PCMs. Although, it seems difficult to observe the individual filler particles dispersion in the examined nanocomposite film due to the small size of fine nanoparticles, however, a few aggregates of NTO (represented in yellow circles) can be found present over the macromolecular



structural networks of the resultant hydrophilic matrix blend composition. Therefore, the existence of the nano-sized metal oxide particles in the nanocomposites eventually contributed toward the enhancement in the heat-transfer rates, thermal resistance, flame-retardant, and UV protection characteristics of the successfully fabricated final product.

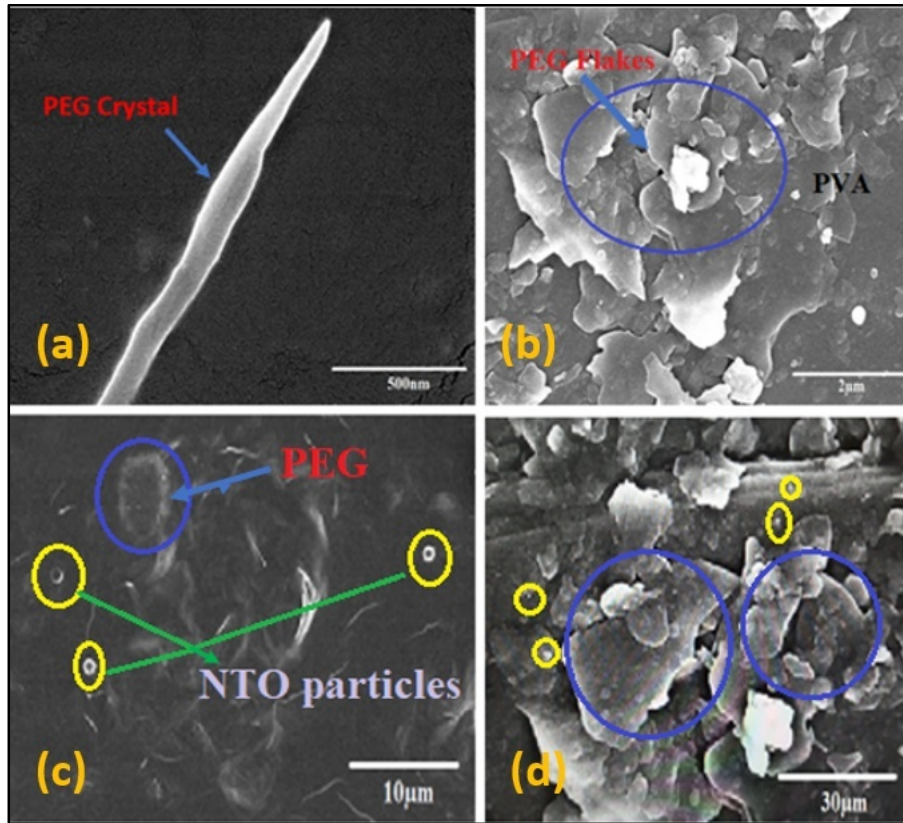


**Figure 6.8: FE-SEM Micrographs of the prepared Form-Stable PCMs (a) magnification-7.6 mm X 70.0K X (b) magnification-7.6 mm X 25.0K X (c)magnification-7.6 mm X 5.0K X and (d) magnification-7.6 mm X 1.50K X**

### 6.2.8 UV-blocking characteristics of NTO/PEG1500/PVA form-stable PCMs

It is now a well-known fact governing the ultraviolet rays (UV) incident on earth's surface and the adverse issues associated with them prolong unsafe exposure, which is considered critical both to human's safety and efficient materials performance. UV radiation is generally sub-categorized as: (i) UV-A ( $\lambda=315-380$  nm), (ii) UV-B ( $\lambda=280-315$  nm) and (iii) UV-C ( $\lambda=100-280$  nm), respectively. The sunlight elapses across the earth's atmosphere, most of the UV-B and UV-C get absorbed by the ozone layer, oxygen, carbon dioxide, water vapor, etc. However, unfortunately, the natural climatic ambiance is unable to filter out UV-A much significantly. Prolong UV irradiation has not been ever fruitful to human health. UV-A exposure causes intense aging, by diminishing the immunological response of skin cells. In addition, erythema and skin cancer are the harmful effects associated with unsafe exposure to UV-B [76]. These fabricated nanocomposites, depending upon the requirement, may be intended to serve outdoor applications. Also, it is well-known fact that the titanium dioxide profoundly absorbs the UV rays, owing to its semiconducting properties, which are well supported and elaborated by the electronic band theory of solids. Keeping all these points in mind, the titanium dioxide nanoparticles (NTO) have been added to the optimized blend composition films to impart UV-blocking features to the end product. Figure 6.9 shows the UV-vis transmittance spectra describing the UV protection characteristics of the NTO filled polymer nanocomposites. It is evident from the obtained results, that a progressive significant reduction in UV transmittance percentage (%) in the UV-A region has been observed in the metal oxide reinforced nanocomposites, with the gradual increase in the NTO concentrations (0.25-1 %). It is accounted in general, that there is a sort of ion transfer mechanism between the (PVA-PEG) polymer blend and NTO particles. Also, it is assumed, for titanium dioxide, or its derived products, such as,

nanocomposites filled with titanium dioxide nanoparticles, the UV-blocking properties of such materials are governed by the absorption and reflection of UV rays, because of its high refractive index [208,164]. Hence, these findings signify the key role of the dispersed titanium dioxide nanoparticles in the produced nanocomposites, bestowing them with excellent UV-resistant nature.

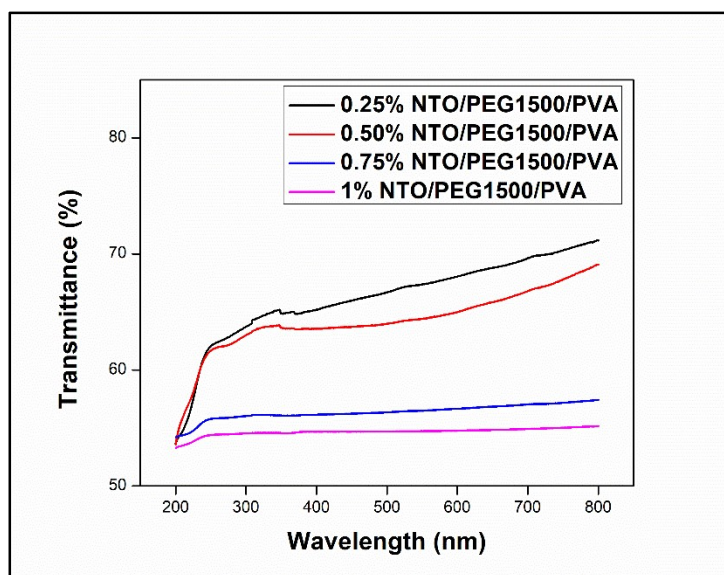


**Figure 6.9: UV-vis transmittance spectra of NTO/PEG1500/PVA with varying loading of titanium dioxide nanoparticles**

### 6.2.9 Flammability Characteristics of NTO/PEG1500/PVA PCMs Nanocomposite Films

Limiting Oxygen Index (LOI) is a widely performed qualitative test method to access the flame retardant (FR) behaviour of the polymers. It is expressed in number percentage (%). The significance of the LOI value obtained during the performance of the test provides the information about the minimum concentration of oxygen (in a mixture of oxygen and nitrogen) required to support continuous combustion of the polymer. There exists an inverse relationship between the LOI and flammability nature. Table 6.6 represents the LOI values of 60 wt. % PEG1500/PVA blend and their metal oxide-filled nanocomposites, with varying NTO dosage.

Pure PVA has LOI value of 22.7 %. After blending 60 wt. % PEG1500 into the PVA matrix has led to a sudden decline in LOI value of the blend composition to 19.8%. It is possibly due to the colossal molecular size difference between the macromolecules used for the blend preparation. In comparison to the PVA molecular chain size, having molecular weight; M.W.: 14000, the PEG 1500 can be considered to be acting as a low molecular weight plasticizer molecule, with respect to the vinyl polymer, which offers more flexibility to the resultant blend thus, led to the reduction in LOI value in the examined blend composition. However, the incorporation of the metal oxide nanoparticles to the above-formed blend is significant for their flame retardancy characteristics, as they tend to minimize the production of toxic burning products, by allowing the formation of the protective shield layer against the flame as compared to the production of low molecular weight fragments or by forming complex products as found with other conventional FR additives such as antimony, phosphorous, or halogenated compounds, etc. It has been observed that, the introduction of titanium nanoparticles has led to a jump in the LOI value of the NTO/PEG1500/PVA nanocomposites, and it further increases linearly with the increasing NTO weight fraction in the final products. This is credited to the basic flame retardant working mechanism of metal oxides nanoparticles, as the Titanium Dioxide is often considered as an inert mineral FR agent, which follows the physical pathway mechanism for flame retardancy action. Because of the high specific surface area of the NTO particles, they tend to fill more and more localized spaces between the macromolecular chains, and, such effective crowding of nanoparticles restricts the chain mobility at elevated temperature, and thus, demands more thermal energy for bond dissociation. During the burning process, uniformly distributed NTO particles inside the nanocomposites are supposed to accumulate over the surface of the composite sample, forming a barrier layer. This newly formed inert protective thermal layer,

reduces the heat transfer to the remaining unexposed surface layer of the composite material, and hinders the passage of burning combustible gases and cut-off the oxygen supply, along with suppressing the smoke generation during combustion [209-211].

**Table 6.6: Flammability characteristics of NTO/PEG1500/PVA form-stable PCMs**

Samples	LOI Value (%)
PVA	22.7 ± 0.2
PVA/PEG 1500	19.8 ± 0.3
0.25% NTO/PEG1500	20.3 ± 0.2
0.50% NTO/PEG1500	21.2 ± 0.3
0.75% NTO/PEG1500	21.8 ± 0.4
1% NTO/PEG1500	22.4 ± 0.3

### 6.3 SIGNIFICANT FINDINGS

A series of form-stable PCM nanocomposites have been prepared successfully, comprising of PEG based phase change material confined inside PVA supporting matrix reinforced with Titanium Dioxide Nanoparticles. FTIR studies have provided the information about the chemical composition of nanocomposites. The FE-SEM images inferred that the mixing of both hydrophilic polymers has resulted into the formation of immiscible blend. Also, the crystal of PEG and NTO particles can be well distributed within the PVA domains, in the microphotograph. The TGA analysis has portrayed the good thermal stability of the prepared form-stable PCMs, which tends to increase with increasing NTO loading. DSC analysis has shown the potential of the prepared form-stable PCMs as efficient thermal energy storage component. Besides this, the latent heat capacities of the nanocomposite PCMs progresses linearly with increased loading of the metal oxide nanoparticles. The PEG-based form-stable PCMs exhibited a valuable thermal cycling stability post 100-thermal cycle exposure. In UV-vis transmittance spectra, the NTO particles prove effective in decreasing the UV transmittance rates, even though the nanocomposite films, by absorbing/scattering the large amount of part of

solar radiation. Furthermore, the incorporation of NTO contributed toward the significant improvement in the flame-retardancy of the form-stable PCMs. Insight of the results obtained in the present study, the fabricated form-stable PCMs can play a vital role in the field of thermal energy storage applications, wherein, their thermal buffering capacity can be utilized in different sectors such as packaging, building, transportation and logistic support etc.

## CHAPTER 7

### DEVELOPMENT OF PEG600 BASED FORM-STABLE PCMs

---

#### 7.1 INTRODUCTION

The progress in science and technology, population growth, and drastic transitions in the economy are the major factors that led to energy crises across the planet. This energy crisis and depletion of the petroleum resources have contributed to the exorbitant exploitation of non-renewable resources of energy, to accomplish the daily needs of the society [212]. Thermal energy storage (TES) method employing Phase Change Materials (PCMs), have gained recognition among researchers owing to their extensive set of attributes, including high latent energy storage/release enthalpy, narrow temperature variations, minor or no volume change during phase change, etc.[213]

Two distinguish ways for the classifications of PCMs are based upon (i) chemical nature-inorganic and organic PCMs; (ii) state of phase change-solid-solid, solid-liquid, and liquid-gas. The former two types of phase transitions are mainly utilized in TES applications and the liquid-gas phase transition is not suitable for practical use due to undesirable associated large volume changes accompanying the transition [8]. Among organic and solid-liquid PCMs, Polyethylene Glycol (PEG) has become a potential PCM candidate for TES components, over the last decade. PEGs composed of dimethyl ether chains bearing hydroxyl functionality (-OH) at the terminal end. The presence of both hydrophilic and hydrophobic moieties in the main chain backbone allows them to be dually miscible with aqueous and organic compounds. PEGs are commercially available in many grades based on their molecular weights (i.e.; 300 to 20,000), with corresponding diverse phase change temperatures. Both melting temperatures and heat storage

enthalpies of PEGs increase with increasing molecular weights [214]. Versatile characteristic features of this macromolecular nature of PCM have been represented in Figure 7.1.

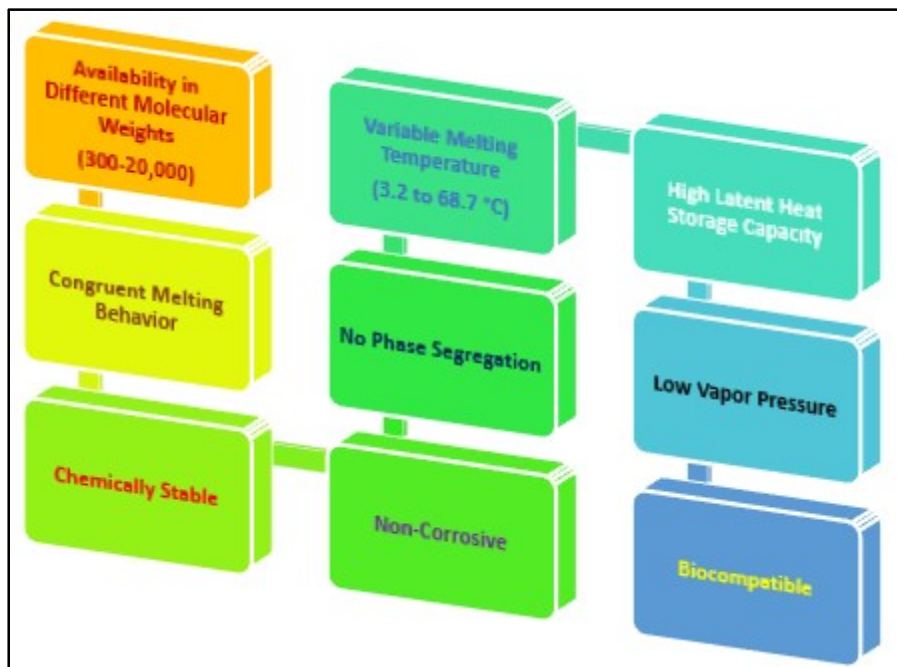


**Figure 7.1: Features of PEGs**

Nonetheless, PEGs as PCMs carry a few associated shortcomings such as moderate supercooling tendency, low thermal conductivity and leakage, while undergoing a solid-liquid phase change transition during the operation [158]. To resolve the impediment of leakage, the judicious approach is to enclose the PCM within the supporting matrix, which is, either inorganic or organic nature, and bestows structural integrity and controls the seepage of PCM, thus, yielding a material system, classified as Shape-Stable PCMs, or Form-Stable PCMs; both terms are often used interchangeably. Many investigations on the preparation of form-stable PCMs through the confinement of PEG inside a series of inorganic or organic supporting materials have been carried out widely including silica [215, 216], expanded graphite [217], active carbon [218], graphene [219], titanium dioxide [220], hydroxyapatite [221], cellulose acetate [222], etc., as the



supporting material. Also, the complications in the supercooling phenomenon and heat transfer rates related to PEGs can be sorted out by incorporating some additives or fillers into the final compositions of PCM products.

In the previous chapter a series of form-stable PCM nanocomposites have been prepared successfully, comprising of PEG1500 based phase change material confined inside PVA supporting matrix reinforced with Titanium Dioxide Nanoparticles. Prior to the nanoparticles addition, PVA thin films with different PCM concentrations (20-80%) for different operating temperatures (30-40 °C) for thermal energy storage applications have successfully prepared and evaluated, and the optimum PEG concentration in the developed series of form-stable PCMs was reportedly found to be 60% based upon leakage stability test. DSC analysis had shown the potential of the prepared form-stable PCMs as efficient thermal energy storage component in view of the fact that the latent heat capacities of the nanocomposite PCMs progresses linearly with increased loading of the metal oxide nanoparticles.

Subsequently, contemplating the available literature on performance of PCMs for TES applications, it has been observed that, the active PCM content inside form-stable PCMs composites should be a minimum of 50 wt. %, within the supporting material. Keeping all the aforesaid in mind, and after circumspection of technical requirements, the current study can be regarded as an extension work with a motive to focus on the development of packaging material by simple solvent-casting method, with thermal buffering properties for low temperature applications (-10-15 °C). Previously, for such kind of low-temperature applications, mostly the PCMs used earlier was of either inorganic nature (salt hydrates) or petroleum based paraffins but PEGs has not been explored. Therefore, the objective of this study is to fabricate the form-stable PCMs nanocomposite films by implementing PEG 600 as a core working PCM, blended with the

Polyvinyl Alcohol (PVA) as a supporting matrix, in a proportional ratio (1:1), along with reinforcing metal oxide nanoparticles (NTO). The effect of the addition of the nanoparticles in varying dosages on heat storage potential, thermal stability, flame retardancy and UV-resistance properties of the resultant form-stable has been extensively examined.

## **7.2 RESULTS AND DISCUSSION**

### **7.2.1 Form-Stability of (50:50) PEG600/PVA Blend Composition**

The behaviour of form-stability for the studied PEG600/PVA blend composition has been deduced according to leakage percentage (%) criteria. The obtained data inferred that the blended film composition of 50 wt. % of PEG 600, present inside the domains of hydrophilic polymer supporting matrix, exhibits leakage percentage of 17.43 %. It duly lies within the permissible limits of leakage control, according to criteria for leakage stability, as described in Table 2.3 and can be designated as form-stable PCM. Therefore, all samples of form-stable PCMs consisting varying dosage of synthesized nanoparticles have been developed, based on currently studied blend composition constituting PEG based form-stable PCM.

### **7.2.2 Fourier transform infrared (FTIR) spectroscopy of NTO/PEG600/PVA PCMs composites**

The raw PVA powder yields to FTIR spectrum as depicted in Figure 7.2 (a). The distant vibration peak related to -OH stretching indicating the fundamental characteristic of an alcohol compound was observed at  $3426\text{ cm}^{-1}$ . The band observed at  $2950\text{ cm}^{-1}$  and  $2883\text{ cm}^{-1}$  correspond to asymmetric stretching of -CH<sub>2</sub> groups and C-H stretching peaks. The vibrations mode found at  $1408\text{ cm}^{-1}$  corresponds to the bending of -CH<sub>2</sub> groups. The vibration peak attributed to -CH<sub>2</sub> rocking was observed at  $925\text{ cm}^{-1}$ . The peaks found at  $854$  and  $635\text{ cm}^{-1}$  corresponds to

stretching of C-C bonds and out of plane -OH bending vibrations. Talking about the PCM (PEG 600) in Figure 7.2 (b), peak recorded at  $3312\text{ cm}^{-1}$  account for stretching of -OH groups. The band recorded at  $2901\text{ cm}^{-1}$  relates to C-H stretching modes. The sharp vibration band noted at  $1090\text{ cm}^{-1}$  correlates to stretching vibrations of C-O groups of ether functionality. The C-C-O stretching vibration band is found at  $842\text{ cm}^{-1}$ . Figure 7.2 (c) illustrates the spectrum of (50:50) PVA:PCM composition which displayed almost the similar absorption bands within the scanned region, hence, such results provide assertiveness, that the intrinsic functional groups of both hydrophilic polymers are ably preserved within blended formulation.

Figure 7.2 (d) illustrates the FTIR spectra of phase change composites with different nanoparticles dosage. It can be seen that the films represent identical peaks observed for the prepared PVA/PEG blend composition. Although, minute shift in peak positions of -OH vibration bands have been observed, which arises due to the emergence of H-bonding interactions between the hydroxyl groups of blended composition and the oxygen atom of metal oxide nanoparticles. Besides, the rearrangements in the peak intensity of -OH groups in the formed composites along rising concentrations of NTO has been noted, owing to possible aggregation of filler nanoparticles, causing reduction in H-bond interaction. These findings are analogous to the already reported studies [205, 223].

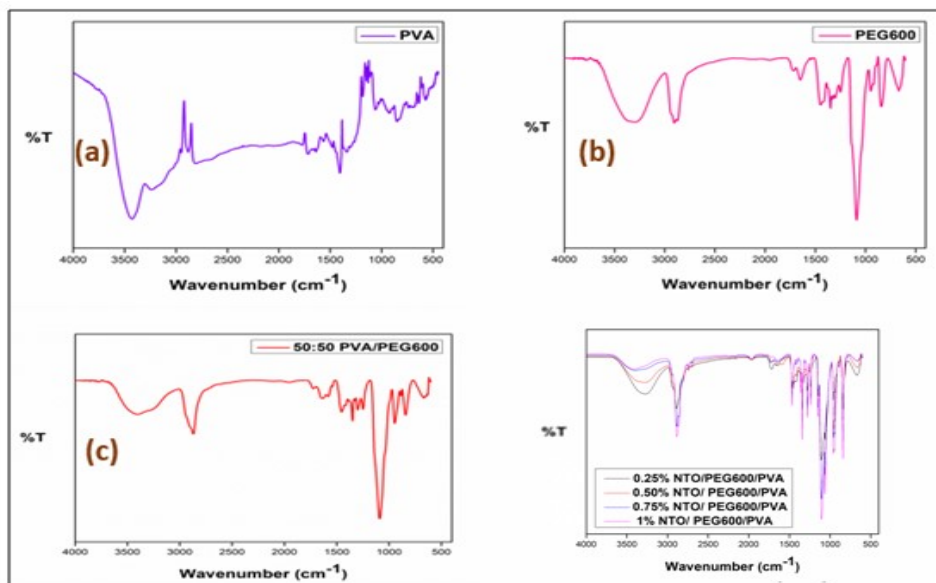


**Figure 7.2: FTIR spectra for (a) PVA; (b) PEG600; (c) PEG600/PVA Blend (50 wt. % PCM) concentration and (d) NTO/PVA/PEG600 composites with varying NTO concentrations**

### **7.2.3 Thermal Energy Storage Characteristics of NTO/PEG600/PVA Phase Change Composites**

DSC analysis was employed for the determination of the latent heat storage attributes of the NTO filled-50 wt. % PEG600/PVA composites. Figure 7.3 (a and b) and Table 7.1 (a and b) depicts the melting and crystallization temperatures of raw PEG600 and derived PEG600 composites. PEG600 acting as working PCM undergoes onset melting and crystallization transitions at 13.3 °C and 12.4 °C, respectively. The latent heats associated with the transformation of phases were calculated as 36.15 and 41.7 J/g, respectively. Talking about 50 wt. % PEG600/PVA composition, it was observed that the phase change transitions occurred at 6.2 °C (melting) and 10.5 °C (crystallization), respectively. Furthermore, the peak melting and crystallization temperatures were observed at 14.4 °C and 2.4 °C, with respective heat capacities of 13.35 J/g and 14.95 J/g. The influence of the incorporation of sol-gel derived nanoparticles on the phase change attributes of the PCM containing polymer thin film is studied further. It was

apparent that the presence of metal oxide nanoparticles aids in enhancing the heat transfer rates, which varied linearly with nanoparticles concentrations, owing to high thermal conductivity of metal oxide nanoparticles against the insulating nature of polymeric materials. In addition to this, there may be a combined effect of PCM being enclosed within macromolecular domains of PVA, and simultaneously surrounded by the metal oxide nanoparticles, could cause the retardation of free mobility of the PEG chains, at the time of phase transitions (melting process). This can subsequently more hampered with the further crowding of the nanoparticles, at higher concentrations within the supporting polymer matrix, requiring more heat energy for compensating the encountered restrictions in fluidity of PCM, at the time of phase change. This further supports the reason of hike in the phase change enthalpy values of the developed PCMs as a function of the nanoparticles loadings within developed composites as depicted in Figure 7.4. The nanocomposite PCM film with 1% NTO concentration exhibited onset melting and crystallization temperatures at  $-9.9\text{ }^{\circ}\text{C}$  and  $13.5\text{ }^{\circ}\text{C}$ , respectively, as well as, peak melting and crystallization transitions occurring at  $8.7\text{ }^{\circ}\text{C}$  and  $3.6\text{ }^{\circ}\text{C}$ , with associated heat enthalpies of  $25.57\text{ J/g}$  and  $22.22\text{ J/g}$ , respectively. The comparison of the form-stable PCM prepared in the current study with few existing counterparts, testified in the literature is reported in Table 7.2. Consequently, the virtue of the obtained results indicates that the developed phase change composites possess efficient latent heat storage potential, suitable for thermal regulatory property.

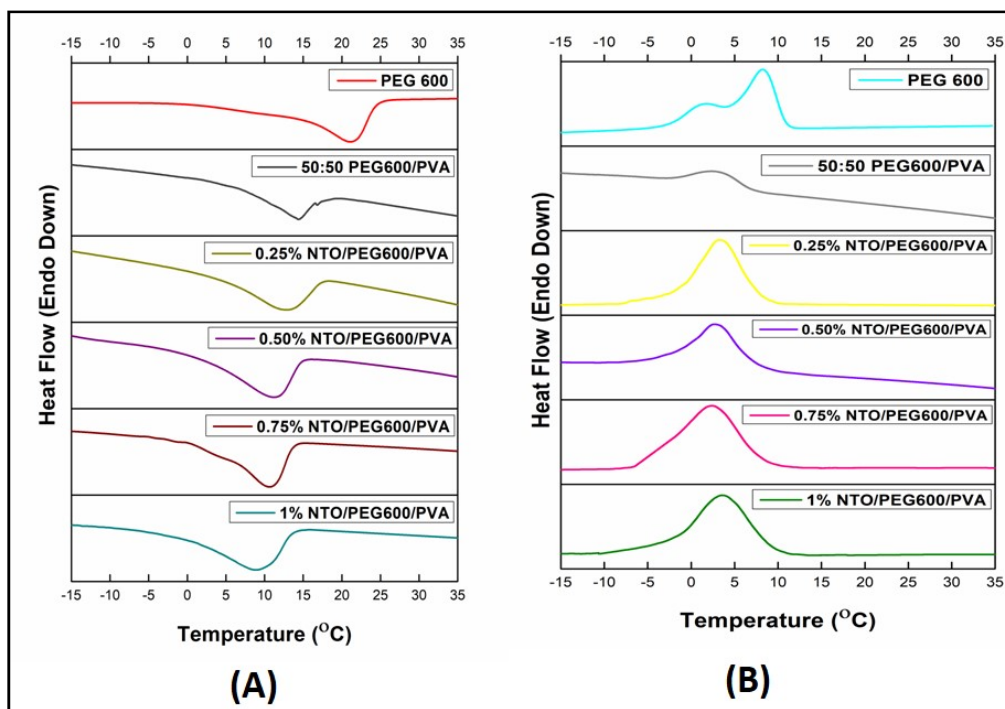


Figure 7.3: Phase change properties of PEG 600 and metal oxide filled composites (a) Heating Cycle and (b) Cooling Cycle

Table 7.1: DSC Data of NTO/PEG600/PVA form-stable PCMs

(a)

Samples	Onset Melting Temperature, $T_{Mo}$ (°C)	Peak Melting Temperature, $T_{Mn}$ (°C)	Offset Melting Temperature, $T_{Me}$ (°C)	Latent Heat of Fusion, $\Delta H_m$ (J/g)
PEG600	13.3	21.1	26.5	36.15
50% PEG600/PVA	6.2	14.4	19.8	13.35
0.25% NTO/PEG600/PVA	2.6	12.9	18.4	15.76
0.50% NTO/PEG600/PVA	0.2	11.2	16.1	18.58
0.75% NTO/PEG600/PVA	-5.2	10.6	15.1	22.84
1% NTO/PEG600/PVA	-9.9	8.7	14.9	25.57

(b)

Samples	Onset Crystallization Temperature, $T_{Co}$ (°C)	Peak Crystallization Temperature, $T_{Cp}$ (°C)	Offset Crystallization Temperature, $T_{Ce}$ (°C)	Latent Heat of Crystallization, $\Delta H_f$ (J/g)
PEG600	12.4	8.2	-3.9	41.7
50% PEG600/PVA	10.5	2.4	-2.9	14.95
0.25% NTO/PEG600/PVA	11.4	3.2	-7.8	16.21
0.50% NTO/PEG600/PVA	11.8	2.7	-8.6	17.76
0.75% NTO/PEG600/PVA	12.6	2.3	-8.9	20.31
1% NTO/PEG600/PVA	13.5	3.6	-10.5	22.22

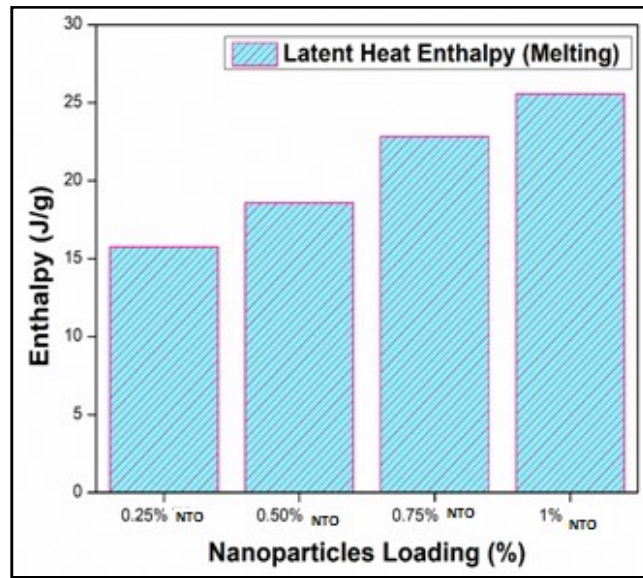


**Figure 7.4: Effect on Latent Heat Enthalpy of Fusion of PEG600 based form-stable PCMs as a function of nanoparticles loading**

**Table 7.2: Comparison of some form-stable PCMs from literature and prepared form-stable PCMs**

Core PCM	Matrix	Additive	$\Delta H_m$ (J/g)	References
PEG	PVA	Titanium Dioxide Nanoparticles	25.57	Present Study
Dodecanol Microcapsules	HDPE	Wood Flour	31.6	[198]
Paraffin Microcapsules	PVC	Wood Flour	15.92	[207]
n-Octadecane	PVC	Titanium Dioxide Nanoparticles	9.22	[76]

#### 7.2.4 Thermal stability of NTO/PEG600/PVA nanocomposites

Figure 7.5 (a) depicts the thermal stability characteristics of the supporting matrix, PEG600, and PVA/PEG600 blend respectively. The raw PVA had shown  $T_{50}$  and  $T_{80}$  respectively at 326.2 °C and 366.6 °C, on contrary active PCM (PEG600), 50 % and 80 % degradation have been seen at 400.6 °C and 416.7 °C, respectively. The incorporation of 50 wt.% PEG to a supporting matrix polymer leading to PEG600/PVA composition of this study, improves the  $T_{50}$  of the PVA matrix to 331.3 °C and at last undergoes degrades at 390.2 °C.

The resistance against thermal degradation of the reinforced composite films with different concentrations of titanium dioxide nanoparticles (0.25-1 wt. %) is represented in Figure 7.5 (b). It has been observed that the incorporation of metal oxide filler, in increasing order, within film samples has ensured the improved thermal resistance of the composite films, owing to high thermal resistant nature of inorganic nanoparticles. It can be understood by viewing in a manner that the random distribution (crowding) of NTO particles in the nanocomposite film limits the molecular movement of polymer chains of both hydrophilic macromolecules at elevated temperatures.



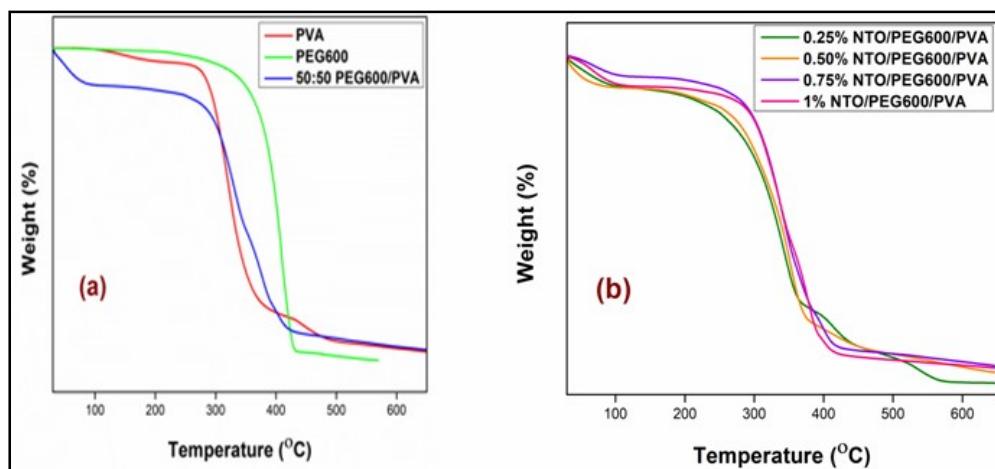


**Figure 7.5: TGA Cures for (a) PEG600, PVA, PVA with 50 wt. % PEG concentration; (b) NTO/PEG600/PVA composites at different NTO concentrations**

**Table 7.3: Thermal Stabilities of NTO/PEG600/PVA nanocomposites**

Samples	50% Weight Loss Temperature, $T_{50}$ (°C)
PVA	326.2
PEG 600	400.6
50% PEG 600/PVA	331.3
0.25% NTO/PEG600/PVA	336.8
0.50% NTO/PEG600/PVA	338.4
0.75% NTO/PEG600/PVA	341.6
1% NTO/PEG600/PVA	342.7

### 7.2.5 Thermal reliability performance of NTO/PEG600/PVA form-stable nanocomposites

DSC data and variations in thermal characteristics of the PCM composites (1% NTO/PEG600/PVA) following 100 thermal cycles are depicted in Figure 7.6 and Table 7.4 respectively. After experiencing the thermal cycles, the NTO reinforced PEG filled nanocomposite film, displayed the latent heat energy storage potential values of 16.88 J/g and 13.09 J/g respectively. It is asserted based upon the data that the minimum changes in the phase change parameters advocates for the satisfactory thermal reliability characteristics of the fabricated PCMs and thus the material can be utilized judiciously in the area of thermal energy storage.

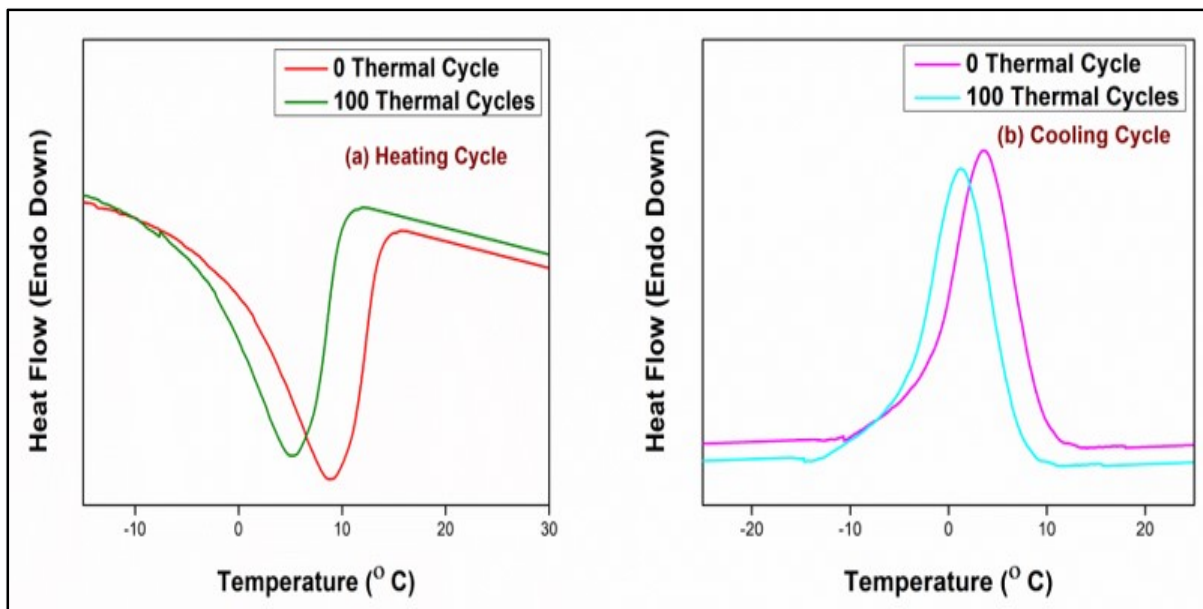


**Figure 7.6: Data for Thermal Reliability of form-stable PCMs; (a) Heating Cycle; (b) Cooling Cycle**

**Table 7.4: Phase change property of 1% NTO/PEG600/PVA PCMs post thermal cycling experience**

Number of Cycles	Peak $T_m$ ( $^{\circ}\text{C}$ )	Peak $T_c$ ( $^{\circ}\text{C}$ )	$\Delta H_m$ (J/g)	$\Delta H_c$ (J/g)
0	8.7	3.6	25.57	22.22
100	5.1	1.2	16.88	13.09

### 7.2.6 Structural characterization of NTO/PEG600/PVA form-stable PCMs

FE-SEM micrograph of 1% NTO/PEG600/PVA shown in Figure 7.7 depicts the resulting microstructures of the prepared composites. These obtained images suggest that the PEG PCM is loosely distributed across the macromolecular network of the hydrophilic matrix (PVA). Also, it was observed that, some of the PEG molecules got melted, during the viewing of the sample, due to the heat energy associated with high energy electronic beam, produced by electron gun, at the time of interaction with the specimen, but it still appears to remain intact inside the supporting matrix, which, further highlight the effective utilization of polymers such as PVA, as an interesting candidate for the role supporting matrix during fabrication of form-stable PCMs. Yet,

it is unfortunate and cumbersome task to notice discrete nano-range particulate filler at the time of sample investigation because of nano-scopic dimensions of the metal oxide nanoparticles. Some metal oxide particles can be viewed, having approximate particle size in the range of few microns, existing as aggregates, due to the clubbing up some titanium dioxide nanoparticles, and thoroughly distributed, across the macromolecular structural networks of the fabricated composites. It is assumed that the presence of the nano-size filler has led to faster heat-transfer mechanism, thermal stability, flame-retardant and UV resistance to UV irradiation of the resultant composite material.

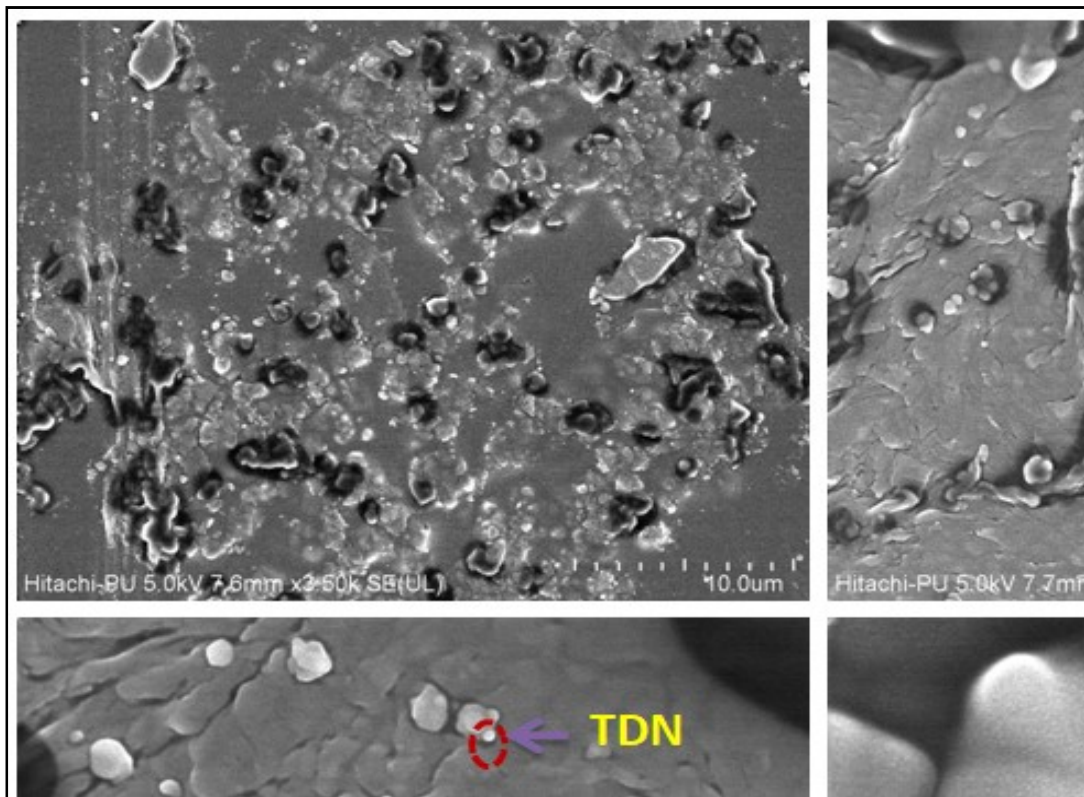


**Figure 7.7: FE-SEM Micrograph of the prepared PCMs at magnification-7.6 mm X 3.50K X**

### **7.2.7 UV-resistance characteristics of NTO/PEG600/PVA Phase Change Composites**

It has been stated in many studies, that, the titanium dioxide, being of semiconducting in nature, remarkably absorbs the ultraviolet irradiation, which is concordantly supported by the electronic band theory of the solids. The synthesized NTO particles, incorporated to the films impart UV-obstructing functionality to polymer thin film. These form-stable PCMs may be utilized for the outdoor applications, as per the requirements. Figure 7.8 illustrates the UV–vis transmittance spectra elaborating the resistance towards ultraviolet rays of the NTO filled polymer composites. From the attained results, it is inferred that an escalating decrement in the percentage (%) of ultraviolet transmittance can be noted in nanocomposites, with the increasing order of NTO dosage. It might be due to the occurrence of ion transfer mechanism between the polymers and NTO particles. Moreover, it has also been reported for titanium dioxide, or its associated products, such as titanium dioxide filled composite films, the UV-resistance properties are controlled by the absorption and reflection of UV rays owing to its high refractive index [208,164]. Therefore, these results assert the significant contribution of dispersed titanium dioxide nanoparticles in the produced composites, thus offering them significant UV-resistant features.

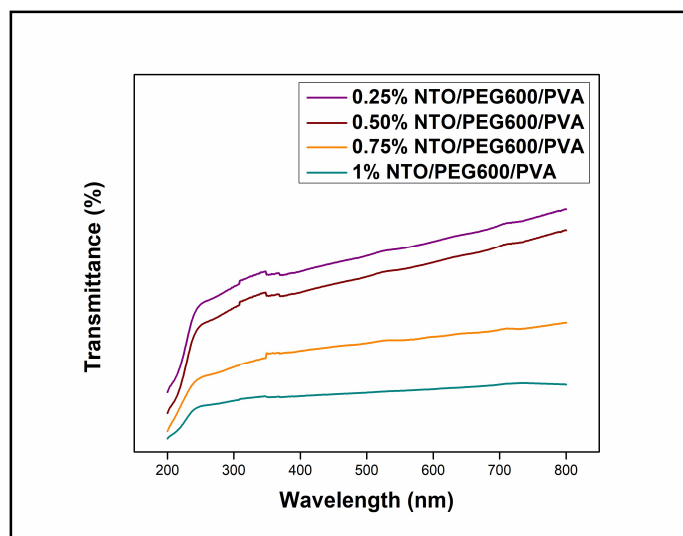


**Figure 7.8: UV-vis transmittance spectra of NTO/PEG600/PVA with varying loading of titanium dioxide nanoparticles**

### **7.2.8 Flammability Characteristics of NTO/PEG600/PVA Phase Change Nanocomposite Films**

Limiting Oxygen Index (LOI) is extensively known test method to evaluate the flame retardant (FR) characteristics of the polymeric materials. Figure 7.9 represents the LOI values of (50:50) PEG600/PVA composition, and corresponding nanoparticles containing composites, having different TDN loadings. Raw supporting polymer matrix exhibited LOI value of 22.5 %. On subsequent addition of PEG600 into the PVA matrix, sudden drop in LOI value has been observed and reached at 19.2 %. It can be assumed because of the difference in size of the studied hydrophilic polymers (PVA and PEG). The supporting matrix material, PVA macromolecule has molecular weight; M.W.: 14000 (as supplied by the manufacturer), on contrary, the PEG600 can be regarded as a low molecular weight plasticizer in contrast to matrix polymer, which confers improved segmental mobility and ductility to the resultant composition, hereby a decline in LOI value was observed. Although, the introduction of metal oxide nanoparticles to the above solvent casted PEG600/PVA films, turns out to be crucial while

imparting flame retardant characteristics, as they improve LOI value of the form-stable PCMs, and it tends to vary in regular manner as a function of NTO dosage. At the time of burning, the distributed titanium dioxide nanoparticles inside the composites tends to gather and surround the burning polymer sample surface forming a protective guard (Char Layer). The presence of such layer acts as a thermal shield and aids in mitigating the spread of flame (heat) to the interior level of fabricated PCMs, which further prevents the flow of burning combustible gases, and slashing down the supply of atmospheric oxygen with repressing the smoke generation in the course of combustion process [209, 210].

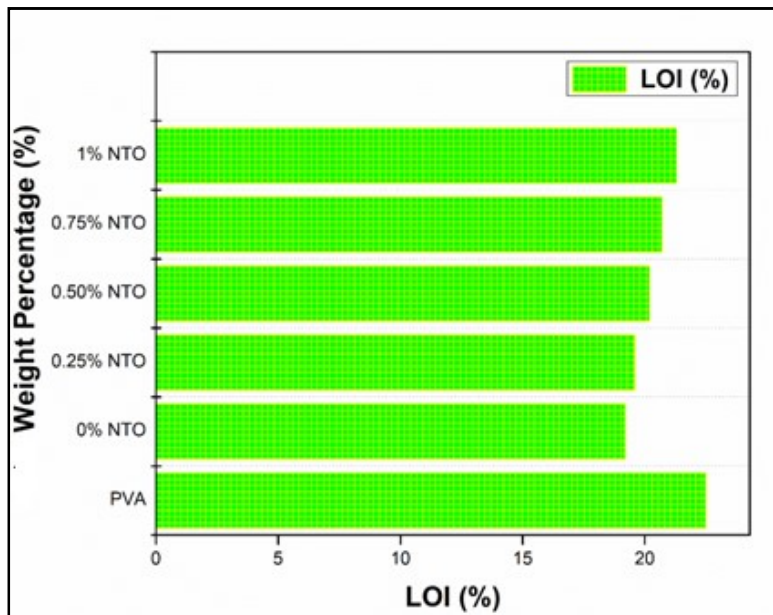


**Figure 7.9: Flammability characteristics of NTO/PEG600/PVA nanocomposite PCMs**

### 7.3 SIGNIFICANT FINDINGS

Phase Change Composites have been developed successfully constituting PEG600 PCM, caged within PVA strengthened with nanoparticles of titanium dioxide. FTIR studies have depicted their information, regarding their chemical composition. The FE-SEM micrographs affirm the mixing of both hydrophilic polymers, as indicated in the morphology. Also, the PCM and metal oxide particles can be seen well confined within the PVA domains. The TGA analysis has suggested that the thermal stability of the prepared PCMs is good and it increases with increase in the loading of nanoparticles. The DSC analysis has portrayed the scope of the fabricated PCM composites as effective thermal energy storage module. Also, the latent heat capacity of the PCM composites varies linearly with increasing order of NTO loadings. The PEG-based composites have shown good thermal cycling stability, after 100-thermal cycle exposure. In UV-vis transmittance spectra, the NTO particles are found to be efficient in suppressing the UV transmittance rates through prepared films, by absorbing/scattering the large amount of the UV radiation. In addition, the introduction of metal oxide nanoparticles, has offered a notable contribution in the enhancement of flame-retardant properties of the resultant PCM composites. The findings observed in the current study advocates the utilization of the fabricated phase change composites for low-temperature temperature regulatory applications.

## CHAPTER 8

### DEVELOPMENT OF PU BASED PCMs (PUPCMs)

---

#### 8.1 INTRODUCTION

Energy can be regarded as one of the indispensable requirements in the modern life for the adequate survival of humans. Rapid population bloom and technological advancements have caused skyrocketing energy demands [224]. Present-day technologists and policy law-makers are desperately searching in the direction of alternative and renewable energy sources due to brisk depletion of fossil fuel resources that further encouraging the maximum utilization of abundantly available solar energy which is however intermittent in nature [225]. Consequently, it has become vital to develop materials and systems processes for harvesting and storage of thermal energy. One of the promising sustainable means for thermal energy storage is the exploration of latent heat thermal energy storage (LTHES) systems based on phase-change materials (PCMs) has gathered attention in recent times [226].

Organic PCMs can be categorized into two segments: Paraffins and Non-Paraffins. Among non-paraffins group, an interest has been raised to one member of this group known as “Fatty Acids”, owing to several points of merit including favorable high latent heat storage density, congruent melting behaviour, good long-term thermal stability, no or negligible supercooling degree, non-toxic nature and biocompatibility, high surface tension that allows their impregnation into a host material, readily available in nature as they are extracted from vegetable and animal oils ensuring uninterrupted regulated supply despite the shortage or fluctuation in price of fuel. They are found be extensively useful in the cosmetic industry, food industry, building construction etc. [227-230]. The individual properties of fatty acid PCM is governed by the length of carbon chain



atoms, longer the chain length, higher would be the melting temperature and latent heat density [231]. In addition, their operating phase change temperature can be customized according to the end requirement by formation of eutectic mixtures through blending of two or more fatty acids in different mass ratios and hence they could be resourceful in thermal management for wide application in the field of textiles, constructions, packaging, electronic devices etc.[232].

Fatty acid group of organic PCMs category comprises of several known compounds with different melting temperatures such as Capric Acid (CA) with melting temperature falls within human thermal comfort temperature range, Myristic Acid (MA) undergoes phase transitions around 52-54 °C, Palmitic Acid (PA) with melting temperature of 61-64 °C suitable for domestic solar water heating [233]. However, being possessing a solid-liquid phase change behaviour, this family of PCMs they suffer from leakage during phase change at operating temperatures; therefore it is crucial to contain the working latent heat storage material inside a supporting matrix (can be either of inorganic nature or organic nature) to overcome leakage problem and ensure smooth controlled performance of the PCM.

Different studies have been done for the confinement of the fatty acid inside various host materials in form of encapsulated or form-stable PCMs [234-236]. Implementation of Polymers as a supporting material for development of new PCMs products seems to be beneficial approach, owing to positive attributes of the said material such as low density, high specific tensile strength and impact strength, corrosion resistant, ease of processability etc.

Among the reported methods, the literature also describes the preparation of form-stable PCMs from Polyurethanes (PU). In general, polyurethanes macromolecular chains are composed of soft segments based on polyester or polyether polyols and covalently bonded with hard segments based diisocyanates leading to formation of urethane functional groups with three-dimensional

cross-linked structures [237-240]. Alkan et al. [241] synthesized different series of Polyurethanes based PCMs composed of different molecular weights of PEGs (1000, 6000, 10,000) as soft-segment and different types of diisocyanates- Hexamethylene Diisocyanates (HDI), Isophorone Diisocyanates (IPDI) and Toluene Diisocyanates (TDI) as hard-segments. The obtained PCMs showed melting transitions ranging between 19-60 °C with associated enthalpy of fusion of 179 kJ/kg. Thermoplastic polyurethane phase change materials were made through two-step condensation reaction of polyethylene glycol (6000), 4, 4-diphenylmethane diisocyanates and terephthalic acid bis-(2-hydroxy-1-hydroxymethyl-ethyl) ester) and later on evaluated for their thermal energy storage characteristics. DSC analysis confirmed the phase change temperature varying through 22.4-48.4 °C with corresponding melting and cooling heat enthalpies of 153.5 J/g and 143.9 J/g, respectively. TGA data suggested initial decomposition and maximum decomposition temperatures of resultant phase change material were found to be 323 °C and 451 °C, respectively [242].

Sistla et al. [243] put efforts to mitigate the phase segregation issue of inorganic hydrates salts- Anhydrous Sodium Sulphate ( $\text{Na}_2\text{SO}_4$ ) and Magnesium Sulphate Heptahydrate ( $\text{MgSO}_4 \cdot 7\text{H}_2\text{O}$ ) by utilizing open cell polyurethane foam sheets as heterogeneous support of thickness 0.01m, with the density of  $32 \text{ kg m}^{-3}$ . It was observed that the porous structures of PU foams existed as reactive nucleation sites for crystal growth leading to availability of heterogeneous surface that was efficient in providing improved nucleation characteristics for the independent droplet of aqueous salt solution. PCM trapped inside the pores and subsequently controlled the phase segregation phenomenon in the fabricated composite structures. A series of comb-polyurethane PCMs consisting PEG as side chains had been produced by reacting diethanolamine-modified methoxypolyethylene glycol (DMPEG) with different diisocyanates- 1,6-Hexamethylene

Diisocyanate (HDI), 4,4-Diphenylmethane Diisocyanate, 2,4-Toluene Diisocyanate (TDI) and Isophorone Diisocyanate (IPDI) in the presence of 1,4-butanediol (BDO) as chain extender. It was found that prepared PCMs derived from IPDI or HDI based hard segment along with methoxypolyethylene glycol (MPEG) having molecular weight of 5000 based soft segment showed favourable phase change attributes. The latent heat enthalpies and phase transition temperatures of synthesized comb-shape urethane polymers PCMs found to decrease as a function of decreasing weight fraction of MPEG [244].

Harlé Thibault et al. [245] synthesized set of PCMs based on linear polyurethanes involving reaction of different molecular weights of PEG (1000, 1500, 2000) with Hexamethylene Diisocyanate (HDI) at varying NCO ratio as well as cross-linked polyurethanes PCMs by reacting the same polyols and diisocyanates in the presence of glycerol as cross-linker. The researchers studied the influence of PEG molecular size, stoichiometry and the cross-linker content on the thermal properties, hardness, solubility behaviour etc. of the developed PCMs. The fabricated polyurethanes exhibited wide phase change temperature range of 22-50 °C accompanied by latent heat of fusion ranges between 79 J/g and 108 J/g and possessed high thermal stability. Furthermore, thermal conductivity of PCM was found to be 0.231 W K<sup>-1</sup> m<sup>-1</sup>. Their hardness, improved by cross-linkage, was between 30 and 39 on Shore D scale; this property allows grain size reduction into a fine powder. Tian et al. [246] prepared and evaluated the performance of form-stable PCMs comprising of n-octadecane and paraffin wax as latent heat storage component having different weight fractions-10 %, 20 %, 25 %, 30 % duly supported by polyurethane matrix. The obtained composites were found to be suitable for solar energy and building saving materials. Zhou et al. [247] successfully synthesized polyurethane PCMs by relying on the reaction between polyethylene glycol, polycarbonatediol and polyaryl

polymethylene diisocyanate, where the finally derived material possessed latent heat energy greater than 110 J/g and phase change temperature are in the range of 15-75 °C.

In summary it has been observed that the earlier work reported in the literature employing polyurethanes as supporting matrix were focused on exploration of technical grade paraffins as latent heat energy storage material are again the fruit seed of non-renewable resources and not much economical also. Thus, this creates a necessity for searching alternative thermal energy harvesting material. Furthermore, not much work has been outlined earlier on the development of fatty acid PCMs in combination with a stable polyurethane matrix. Keeping these research gaps in view, the present study deals with the synthesis of polyurethane based PCMs (PUPCMs), while incorporating capric acid (CA) as an active working latent heat energy storage entity confined within the macromolecular domains of polyurethane made through the polycondensation reaction between PEG20000 as soft-segment and polymeric MDI as diisocyanate as hard segment. The obtained product was further investigated for its characteristics, including chemical properties, morphology, thermal properties, and thermal stability.

## **8.2 RESULTS AND DISCUSSION**

### **8.2.1 Fourier Transform Infrared (FTIR) Spectroscopy of Polyurethane Based PCMs (PUPCMs)**

FTIR spectra of capric acid (CA), raw polyurethane and polyurethane based PCM (PUPCM) are shown in Figure 8.1. The fatty acid PCM exhibit vibrations at  $2930\text{ cm}^{-1}$  and  $2851\text{ cm}^{-1}$  respectively corresponding to symmetrical and asymmetrical stretching vibrations of carbon chain of fatty acid. The vibration modes related to C=O and C-O stretching were observed at  $1708\text{ cm}^{-1}$  and  $1200\text{ cm}^{-1}$  respectively. The peak at  $724\text{ cm}^{-1}$  corresponds to the C-H rocking

vibrations. The pure polyurethane exhibits N-H stretching vibration band at  $3330\text{ cm}^{-1}$ . The formation of urethane group can say to occur on account of the peaks observed at  $1710\text{ cm}^{-1}$  and  $1540\text{ cm}^{-1}$  relates to C=O stretching and N-H bending present in urethane linkages. Vibrations due to C-N stretching were found at  $1510\text{ cm}^{-1}$  and  $1230\text{ cm}^{-1}$ . The band appearing at  $1090\text{ cm}^{-1}$  is due to C-O-C stretching vibration of ether moiety contributing from PEG. In case of PU PCMs notable characteristics peaks have been recorded at  $3340\text{ cm}^{-1}$ ,  $2960\text{ cm}^{-1}$ ,  $2920\text{ cm}^{-1}$ ,  $2860\text{ cm}^{-1}$ ,  $1710\text{ cm}^{-1}$ ,  $1541\text{ cm}^{-1}$ ,  $1510\text{ cm}^{-1}$ ,  $1232\text{ cm}^{-1}$  corresponding to N-H stretching arising from final PU, aliphatic symmetrical and asymmetrical stretching vibrations of  $-\text{CH}_2$  groups coinciding for both fatty acid and PU chains, carbonyl functionality and N-H bending from urethane group and C-N vibration mode of the resultant polymer. It is clear from the spectrum that the maximum characteristic bands of PCM, raw PU and PUPCM overlapped with each other. The spectra of PUPCMs showed equivalent characteristic peaks of both PU and fatty acid PCM, giving evidence of the presence of the Capric Acid and formation of PU supporting matrix leading to the development of PU based PCMs.

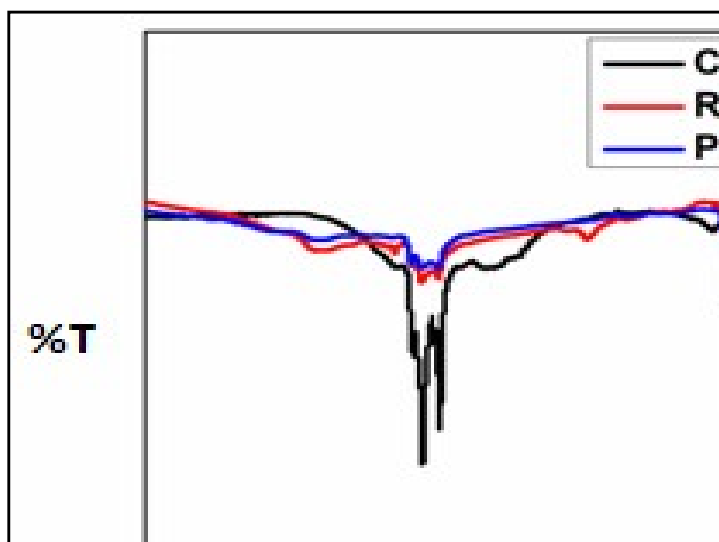


**Figure 8.1: FTIR of Capric Acid (CA), Raw PU and PUPCMs**

## 8.2.2 Thermal Energy Storage Characteristics of Polyurethane Based PCMs (PUPCMs)

The phase change characteristics of the Capric Acid and developed PU based PCMs are determined by DSC analysis. The DSC curves indicating the phase-change temperatures and the latent heat density values of the prepared fatty acid filled polyurethanes and the raw CA is shown in Figure 8.2, and their results are summarized in Table 8.1. The DSC curves of both pure PCM and the PUPCMs seem to be alike supporting the presence of CA inside the domains of formed polyurethane macromolecular network. The pure CA exhibited the onset of melting and crystallization temperatures at  $31.9 \pm 0.2$  °C and  $28.9 \pm 0.3$  °C respectively. On the other hand, the PUPCMs possessed reasonable thermal energy storage characteristics, with the onset of melting at  $28.8 \pm 0.4$  °C and crystallization at  $26.1 \pm 0.2$  °C respectively. The latent heat of fusion and the latent heat of crystallization of the pure PCM and PUPCMs were deduced as  $122.02 \pm 1.3$  J/g and  $124.76 \pm 1.6$  J/g and  $30.7 \pm 1.2$  J/g and  $31.9 \pm 1.5$  J/g respectively.

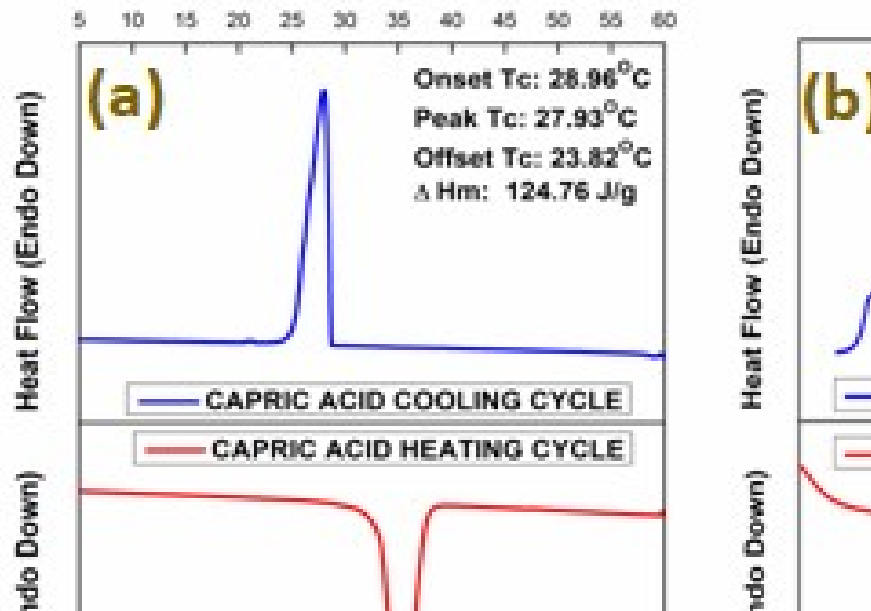


Figure 8.2: DSC Curves for Heating/Cooling Cycles for; (a) Pure CA and (b) PUPCMs

**Table 8.1: DSC Data of Pure PCM and PUPCMs Representing Their Phase Change Characteristics**

Sample	Capric Acid (CA)	PUPCMs
Onset T <sub>m</sub> (°C)	31.9 ± 0.2	28.8 ± 0.4
Peak T <sub>m</sub> (°C)	35.4 ± 0.3	32.7 ± 0.3
Offset T <sub>m</sub> (°C)	38.4 ± 0.2	35.9 ± 0.3
Onset T <sub>c</sub> (°C)	28.9 ± 0.3	26.1 ± 0.2
Peak T <sub>c</sub> (°C)	27.9 ± 0.3	25.5 ± 0.2
Offset T <sub>c</sub> (°C)	23.8 ± 0.2	24.0 ± 0.2
ΔH <sub>m</sub> (J/g)	122.02 ± 1.3	30.7 ± 1.2
ΔH <sub>c</sub> (J/g)	124.76 ± 1.6	31.9 ± 1.5

### 8.2.3 Thermal stability of Polyurethane Based PCMs (PUPCMs)

The thermal stability and the degradation behaviour of the PUPCMs are evaluated by TGA. The TGA curves of the pure CA, PU and CA filled PU are shown in Figure 8.3, and their respective degradation temperatures are given in Table 8.2. The pure CA degrades in a single step. The PCM shows 10 % and 50 % weight loss at 161.1 °C and 193 °C respectively. The fatty acid PCM finally decomposes at 201.2 °C as the temperature proceeds, owing to small size of carboxylic acid terminated fatty acid chain. Similar to this, the neat PU material also possessed one step degradation pattern, but undergoes the 50 % degradation at a much higher temperature around 407.3 °C, due to the cross-linked network polymer chains. Contrary to this, the prepared PUPCMs showed a two-step degradation profile; the first step is attributed to the degradation of CA similar to the pattern as that of pure CA and the second step corresponds to the degradation of the polymer at 441.5 °C. The entrapment of fatty acid within thermoset polymer matrix has resulted in increase in the T<sub>50</sub> and T<sub>80</sub> temperatures of the enclosed fatty acid PUPCMs.

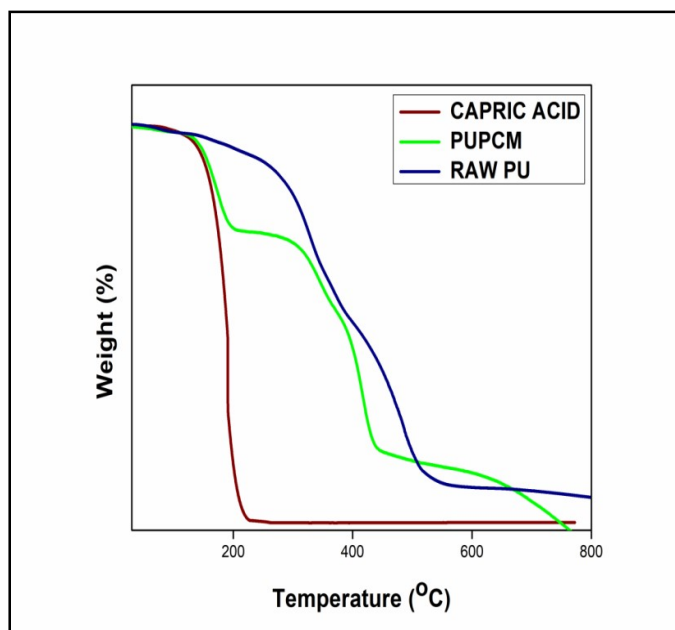


**Figure 8.3: TGA Cures for Capric Acid (CA), PUPCMs and Raw PU**

**Table 8.2: Thermal Stabilities of Capric Acid (CA), PUPCMs and PU**

Sample	10% Mass Loss (°C)	50% Mass Loss (°C)	80% Mass Loss (°C)
Capric Acid (CA)	161.1	193	201.2
PUPCMs	164.3	389.4	441.5
PU	258.2	407.3	497.5

#### **8.2.4 Structural characterization of Polyurethane Based PCMs (PUPCMs)**

The morphological information regarding the prepared PUPCMs has been depicted in Figure 8.4 (a-f). These obtained SEM images (a-c) suggest that the raw PU possessed rough and uneven surface texture resembling a marshy island like hard land mass structure which represents the formation of brittle and thermoset nature of polyurethane polymer. The morphology of fatty acid PCM filled polyurethanes illustrated by Figure 8.4 (d-f). It can be clearly observed that the drastic change in the microstructures of the obtained PU based PCMs where incorporation of



fatty acid in the structural domains of PU have led to conversion in the topographical appearance of the developed PCM, resulting in fine, smooth and uniform surface texture. The capric acid molecules can be seen uniformly distributed across the structural framework of the polyurethane supporting matrix. Also, it can be observed that the capric acid grains (molecules) seems to be thoroughly wetted and completely covered by the layers of polyurethane resin as an out-turn of successful confinement of the fatty acid PCM inside the polymer matrix.

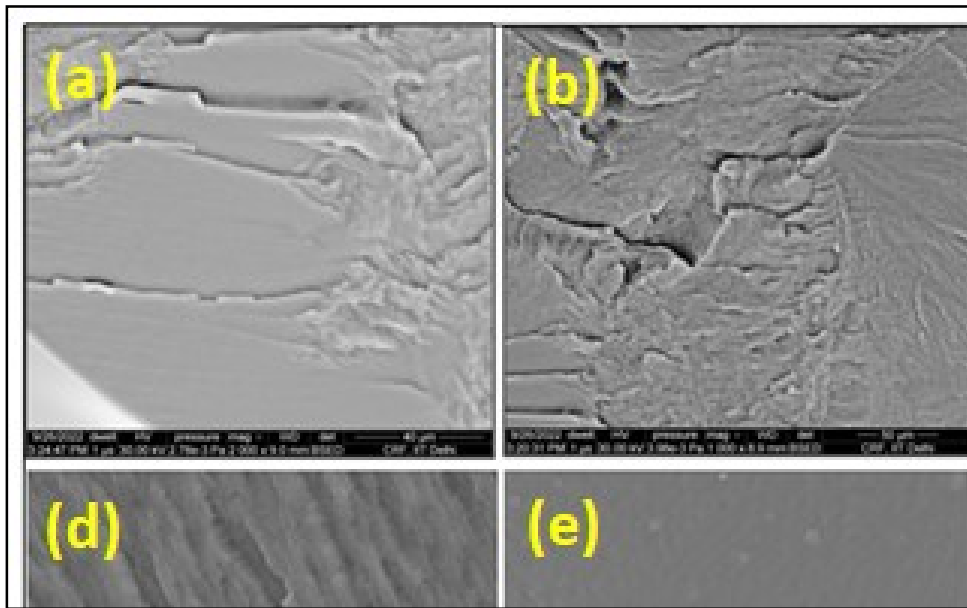


**Figure 8.4: SEM Micrographs of the Synthesized: (1) Raw PU- (a) magnification-2000 X ;(b) magnification-1000 X; (c) magnification-500 X and (2) PUPCMs-(d) magnification-2000 X ;(e) magnification-1000 X; (f) magnification-500 X**

### 8.2.5 Thermal reliability performance of Polyurethane Based PCMs (PUPCMs)

In order to be successful explored as latent heat storage material, the fabricated product must be sound enough to endure multiple heat-cool cycles with less deviation in their energy storage properties post cycling period. DSC data and change in thermal characteristics of PUPCMs following 100 thermal cycles are depicted in Figure 8.5 and Table 8.3 respectively. After experiencing the thermal cycles, the fabricated PUPCMs still effectively able to harness the

latent heat energy storage densities of 21.44 J/g and 22.63 J/g respectively. It can be deduced according to the obtained data that the little changes in the phase change properties have been recorded that, accounts for the acceptable thermal reliability characteristics of the fabricated PCMs, and thus the material can be employed in the area of thermal energy storage.

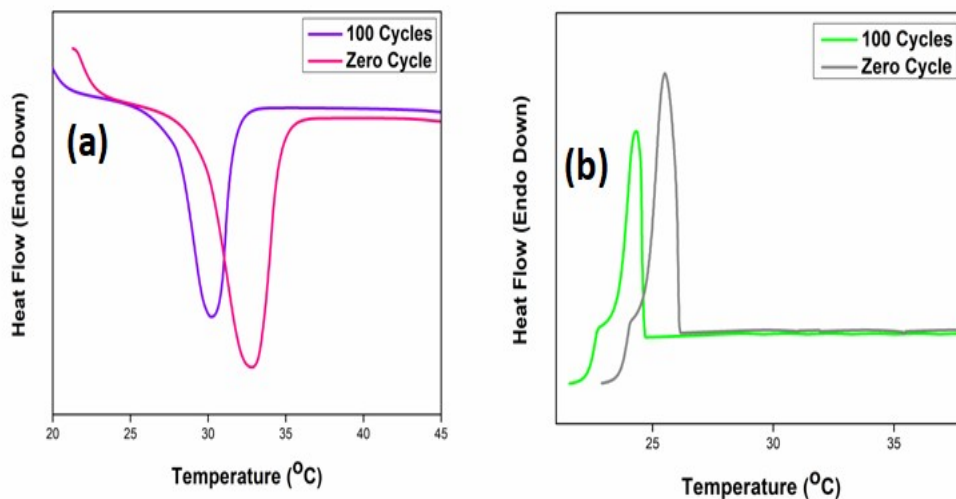


**Figure 8.5: Data for Thermal Reliability of PUPCMs: (a) Heating Cycle; (b) Cooling Cycle**

**Table 8.3: Phase change property of PUPCMs post thermal cycling experience**

Number of Cycles	Onset T <sub>m</sub> (°C)	Onset T <sub>c</sub> (°C)	ΔH <sub>m</sub> (J/g)	ΔH <sub>c</sub> (J/g)
0	28.8	26.1	30.78	31.96
100	25.7	24.7	21.44	22.63

### 8.3 SIGNIFICANT FINDINGS

A new PCM has been successfully developed comprising of PU matrix based phase change material incorporating capric acid as latent heat storage component. FTIR studies have provided the information about the chemical composition of nanocomposites. PU-Capric Acid based PCM exhibited melting and crystallization transitions at 28.8 °C and 26.1 °C, with the latent heat of

fusion of 30.7 J/g, and latent heat of crystallization of 31.9 J/g, respectively. PUPCMs also found to possess decent thermal cycling stability post 100-thermal cycle exposure. SEM images inferred that the mixing of fatty acid have a profound influence in viewpoint of morphology to the PU resin. The addition of fatty acid led to smoothness of surface roughness along with fair distribution of capric acid particles in the polymer matrix.

## CHAPTER 9

### CONCLUSIONS AND FUTURE PROSPECTS

---

#### 9.1 CONCLUSIONS

Phase Change Materials (PCMs) derived from renewable resources shall be effective in reducing the reliance on the latent heat storage materials generated through fossil fuels while potentially acting as an environment friendly energy solution help in making a “cleaner” and “greener” ecosystem as well as boosting the concept of sustainable development. From viewpoint of sustainable development, the present study deals with the development of PCMs based on renewable resources (such as fatty acids) which are abundantly available, non-toxic in nature and are less expensive than technical grade paraffins. Polymeric material can be utilized in an effective manner in order to anchor the performance of PCMs, which can further lead to development of new class of phase change materials for TES applications. They can turn out to be beneficial in critical applications wherein being lightweight, leak-proof, corrosion-resistance and ease of processability is required.

Production of encapsulated PCMs based on thermoplastic polymers such as PMMA would be beneficial as it is including easy to synthesize in high yields at low cost by employing simple polymerization methods (bulk, suspension, or emulsion), can be recyclable post-consumer use and can be used for the production of further new articles. Most importantly it is compatible with other variety of host polymers (polyvinyl chloride, polyesters, acrylics, polar elastomers) which in turn, can lead to the manufacturing of products with diverse properties, for a wide range of applications, such as, textile fabrics, packaging films, composites, etc. Also, it seems to be interesting in case of form-stable PCMs being produced from the polymers of synthetic origin

however, the hydrophilic nature of the both components PVA and PEG can be beneficial play in minimizing and addressing the plastic pollution crises, as they tend to show biodegradability characteristics to some extent which is well supported and proven by many past research works, carried all across the globe. Hence, use of such polymer matrix and PCM can aid in mitigating the post-consumer plastic waste litter menace.

PCM microcapsules consisting of caprylic acid as core and surrounded by PMMA, as shell has been synthesized using suspension polymerization technique. SEM and PSD results suggested the formation of the uniform spherical microcapsules with average particle diameter of approximately 4  $\mu\text{m}$ . TGA analysis indicated that the encapsulation of caprylic acid by polymer shell has slightly improved the initial degradation of the entrapped fatty acid and offered thermal protection at elevated temperatures. DSC data showed that Micro-PCMs with 66 wt. % of PCM core content possessed melting and crystallization temperatures of  $14.3 \pm 0.2$  °C and  $9.7 \pm 0.4$  °C respectively and their corresponding latent heats equal to  $98.7 \pm 1.5$  J/g and  $99.0 \pm 1.7$  J/g. T-History test indicated that charging and discharging times associated with the microencapsulated PCMs are observed as 251 and 254 seconds respectively.

Nanoencapsulated PCMs comprising of undecylenic acid as active PCM and surrounded by nano-scale PANI fibres have been prepared by interfacial polymerization technique. HR-TEM results have demonstrated that the as prepared PCMs existed in nanofibrous morphologies a mean fibre diameter of approximately 56.4 nm. DSC analysis showed that the prepared nanoencapsulated PCMs with active core content of 45 wt. % exhibited phase change temperature around  $17.6 \pm 0.2$  °C with corresponding latent heat of fusion measured as 55.68 J/g. Moreover, the synthesized PCMs nanofibres have been observed to exhibit thermo-regulatory

and electrical conductivity dual behaviour where the measured electrical conductivity of PANI/UA Nanofibres PCMs was found to be 0.724 S/cm.

Form-stable PCMs containing PEG1500 and PEG600 as working PCMs supported by PVA matrix have been prepared by solvent casting method and later on consequently incorporated with titanium dioxide nanoparticles in order to provide positive contributed toward the enhancement in phase change characteristics, UV resistance behavior and flame-retardant property of the fabricated PCM composites. The latent heat capacities of both PEG1500 and PEG600 based form-stable PCMs found to vary linearly with increasing concentration of metal oxide nanoparticles. It has been estimated that while increasing the nanoparticles concentration in form-stable composites, can also refine the supercooling degree and thermal stability of the prepared PCMs to better extent. The presence of the nanoparticles in PCM filled films has proved to be effective in successfully reducing the UV transmittance across the films. The metal oxide nanoparticles also enhance the flame-retardant behavior of the form-stable PCMs.

Further efforts have been put to prepare PU based PCMs composed of PU supporting matrix filled with capric acid as latent heat storage component. PU-Capric Acid based PCMs undergoes melting and crystallization transitions at 28.8 °C and 26.1 °C, with associated latent heat enthalpies of 30.7 J/g and 31.9 J/g, respectively. PUPCMs also exhibited decent thermal stability up to 441.5 °C. The fabricated PUPCMs withstand 100-thermal cycles and showed latent heat energy storage densities of 21.44 J/g and 22.63 J/g respectively at their melting and crystallization temperatures. Morphological data inferred that the incorporation of fatty acid to PU domains resulted in drastic impact on the surface morphology of the produced PCMs.

## 9.2 FUTURE ROSPECTS OF WORK

From the attained results, it is apparent that the prepared polymer supported PCMs (encapsulated or form-stable form) can exhibit good latent heat energy capacity, and their storage potential can be utilized in substantial TES applications with thermal buffering properties which can undergo phase transition around room temperature concerning human thermal comfort zone for applications including thermal buffering in food packaging, thermo-responsive textiles, slurries, indoor temperature control in building structures and helpful in limiting the undesirable temperature surge while ensuring the quality of the basic commodities products/goods (including fresh food items, medicinal products, electrical or electronic goods, etc.) during storage, transportation, and logistics distribution chain until the commodities/goods are delivered to the end-user. Efforts must be made in the direction to optimize the properties of organic PCMs (fatty acids or any other suitably fit compound) so that they can give stiff competition to other PCM counterpart such as salt hydrates and paraffins. This may be achievable by several approaches either focusing on development of new eutectic organic mixtures, enhancement of thermal conductivity or improving the flammability characteristics by incorporation of high thermal conductive and heat resistant additives derived either from synthetic route or extracted from readily available nature resources.

## REFERENCES

---

1. Dheep, G. R.; Sreekumar, A. Influence of nano-materials on properties of latent heat solar thermal energy storage materials – A review. *Energy Convers. Manag.* 2014, 83, 133-148.
2. Zhou, D.; Zhao, C.Y.; Tian, Y. Review on thermal energy storage with phase change materials (PCMs) in building applications. *Appl. Energy* 2012, 92, 593-605.
3. Kant, K.; Shukla, A.; Sharma, A. Advancement in phase change materials for thermal energy storage applications. *Sol. Energy Mater. Sol. Cells* 2017, 172, 82-92.
4. Liu, C.; Rao, Z.; Zhao, J.; Huo, Y.; Li, Y. Review on nanoencapsulated phase change materials: Preparation, characterization and heat transfer enhancement. *Nano Energy* 2015, 13, 814-826.
5. Sharma, R. K.; Ganesan, P.; Tyagi, V.V.; Metselaar, H.S.C.; Sandaran, S.C. Developments in organic solid–liquid phase change materials and their applications in thermal energy storage. *Energy Convers. Manag.* 2015, 95, 193-228.
6. Sharma, A.; Tyagi, V.V.; Chen, C. R.; Buddhi, D. Review on thermal energy storage with phase change materials and applications. *Renew. Sustain. Energy Rev.* 2009, 13, 318-345.
7. Fallahi, A.; Guldentops, G.; Tao, M.; Granados-focil, S.; Dessel, S. Van. Review on solid-solid phase change materials for thermal energy storage: Molecular structure and thermal properties. *Appl. Therm. Eng.* 2017, 127, 1427-1441.
8. Pielichowska, K.; Pielichowski, K. Phase change materials for thermal energy storage. *Prog. Mater. Sci.* 2014, 65, 67-123.



9. Veerakumar, C.; Sreekumar, A. Phase change material based cold thermal energy storage: Materials, techniques and applications – A review. *Int. J. Refrig.*2016, 67, 271-289.
10. Mohamed, S. A.; Al-sulaiman, F. A.; Ibrahim, N.I.; Zahir, H.; Al-ahmed, A.; Saidur, R.; Yılbaş, B.S.; Sahin, A.Z. A review on current status and challenges of inorganic phase change materials for thermal energy storage systems. *Renew. Sustain. Energy Rev.*2017, 70, 1072-1089.
11. Mondal, S. Phase change materials for smart textiles-An overview. *Appl. Therm. Eng.*2008, 28, 1536-1550.
12. Oró, E.; Gracia, A. De; Castell, A.; Farid, M. M.; Cabeza, L.F. Review on phase change materials (PCMs) for cold thermal energy storage applications. *Appl. Energy* 2012, 99, 513-533.
13. Liu, M.; Saman, W.; Bruno, F. Review on storage materials and thermal performance enhancement techniques for high temperature phase change thermal storage system. *Renew. Sustain. Energy Rev.*2012, 16, 2118-2132.
14. Su, W.; Darkwa, J.; Kokogiannakis, G. Review of solid–liquid phase change materials and their encapsulation technologies. *Renew. Sustain. Energy Rev.*2015, 48, 373-391.
15. Sharma, S. D.; Sagara, K. Latent Heat Storage Materials and Systems: A Review. *Int. J. Green Energy*, 2005, 2 (1), 1-56.
16. Chandel, S.S.; Agarwal, T. Review of current state of research on energy storage, toxicity, health hazards and commercialization of phase changing materials. *Renew. Sustain. Energy Rev.*2017, 67, 581-596.

17. Edsjø, S.; Petter, B. Phase change materials and products for building applications: A state-of-the-art review and future research opportunities. *Energy Build.* 2015, 94, 150-176.
18. Sarier, N.; Onder, E. Organic phase change materials and their textile applications: An overview. *Thermochim. Acta* 2012, 540, 7-60.
19. Kenisarin, M. M. Thermo-physical properties of some organic phase change materials for latent heat storage-A review. *Sol. Energy* 2014, 107, 553-575.
20. Alam, T. E.; Dhau, J.S.; Goswami, D.Y.; Stefanakos, E. Macroencapsulation and characterization of phase change materials for latent heat thermal energy storage systems. *Appl. Energy* 2015, 154, 92-101.
21. Alva, G.; Lin, Y.; Liu, L.; Fang, G. Synthesis, characterization and applications of microencapsulated phase change materials in thermal energy storage: A review. *Energy Build.* 2017, 144, 276-294.
22. Karthikeyan, M.; Ramachandran, T. Review of thermal energy storage of micro and nanoencapsulated phase change materials. *Mater. Res. Inno.* 2014, 18, 541-554.
23. Zhang, G.H.; Bon, S.A.F.; Zhao, C.Y. Synthesis, characterization and thermal properties of novel nanoencapsulated phase change materials for thermal energy storage. *Sol. Energy* 2012, 86, 1149-1154.
24. Fuensanta, M.; Paiphansiri, U.; Romero-sánchez, M. D.; Guillem, C.; López-buendía, Á. M.; Landfester, K. Thermal properties of a novel nanoencapsulated phase change material for thermal energy storage. *Thermochim. Acta* 2013, 565, 95-101.
25. Giro-paloma, J.; Martínez, M.; Cabeza, L.F.; Fernández, A.I. Types, methods, techniques, and applications for microencapsulated phase change materials (MPCM): A review. *Renew. Sustain. Energy Rev.* 2016, 53, 1059-1075.

26. Salaün, F.; Devaux, E.; Bourbigot, S.; Rumeau, P. Thermoregulating response of cotton fabric containing microencapsulated phase change materials. *Thermochim. Acta* 2010, 506, 82-93.
27. Zhang, Y.; Wang, S.; Rao, Z.; Xie, J. Experiment on heat storage characteristic of microencapsulated phase change material slurry. *Sol. Energy Mater. Sol. Cells* 2011, 95, 2726-2733.
28. Giro-paloma, J.; Alkan, C.; Chimenos, J.M.; Fernández, A.I. Comparison of Microencapsulated Phase Change Materials Prepared at Laboratory Containing the Same Core and Different Shell Material. *Appl. Sci.* 2017, 7(7), 723, 1-9.
29. Liang, C.; Lingling, X.; Hongbo, S.; Zhibin, Z. Microencapsulation of butyl stearate as a phase change material by interfacial polycondensation in a polyurea system. *Energy Convers. Manag.* 2009, 50, 723-729.
30. Sánchez, P.; Sánchez-Fernandez, M.V.; Romero, A.; Rodríguez, J.F.; Sánchez-Silva, L. Development of thermo-regulating textiles using paraffin wax microcapsules. *Thermochim. Acta* 2010, 498, 16-21.
31. Qiu, X.; Lu, L.; Wang, J.; Tang, G.; Song, G. Preparation and characterization of microencapsulated n-octadecane as phase change material with different n-butyl methacrylate-based copolymer shells. *Sol. Energy Mater. Sol. Cells* 2014, 128, 102-111.
32. Alkan, C.; Sari, A.; Karaipekli, A. Preparation, thermal properties and thermal reliability of microencapsulated n-eicosane as novel phase change material for thermal energy storage. *Energy Convers. Manag.* 2011, 52, 687-692.

33. Wang, H.; Zhao, L.; Chen, L.; Song, G.; Tang, G. Facile and low energy consumption synthesis of microencapsulated phase change materials with hybrid shell for thermal energy storage. *J. Phys. Chem. Solids* 2017, 111, 207-213.
34. Ma, S.; Song, G.; Li, W.; Fan, P.; Tang, G. UV irradiation-initiated MMA polymerization to prepare microcapsules containing phase change paraffin. *Sol. Energy Mater. Sol. Cells* 2010, 94, 1643-1647.
35. Santos, M.G.; Bozza, F.T.; Thomazini, M.; Favaro-Trindade, C.S. Microencapsulation of xylitol by double emulsion followed by complex coacervation. *Food Chem.* 2015, 171, 32-39.
36. Hawlader, M.N.A.; Uddin, M.S.; Mya, M. Microencapsulated PCM thermal-energy storage system. *Appl. Energy* 2003, 74, 195-202.
37. O'zonur, Y.; Mazman, M.; Paksoy, H. O.; Evliya, H. Microencapsulation of coco fatty acid mixture for thermal energy storage with phase change material. *Int. J. Energy Res.* 2006, 30, 741-749.
38. Zhang, Q.; Zhao, Y.; Feng, J. Systematic investigation on shape stability of high-efficiency SEBS/paraffin form-stable phase change materials. *Sol. Energy Mater. Sol. Cells* 2013, 118, 54-60.
39. Wang, Y.; Wang, S.; Wang, J.; Yang, R. Preparation, stability and mechanical property of shape-stabilized phase change materials. *Energy Build.* 2014, 77, 11-16.
40. Mhike, W.; Focke, W.W.; Mofokeng, J.P.; Luyt, A.S. Thermally conductive phase-change materials for energy storage based on low-density polyethylene, soft Fischer-Tropsch wax and graphite. *Thermochim. Acta* 2012, 527, 75-82.

41. Iqbal, K.; Sun, D. Development of thermo-regulating polypropylene fibre containing microencapsulated phase change materials. *Renew. Energy* 2014,71, 473-479.
42. Cai, Y.; Gao, C.; Zhang, T.; Zhang, Z.; Wei, Q.; Du, J.; Hu, Y.; Song, L. Influences of expanded graphite on structural morphology and thermal performance of composite phase change materials consisting of fatty acid eutectics and electrospun PA6 nanofibrous mats. *Renew. Energy* 2013, 57, 163-170.
43. Cai, Y.; Ke, H.; Dong, J.; Wei, Q.; Lin, J.; Zhao, Y.; Song, L. Effects of nano-SiO<sub>2</sub> on morphology, thermal energy storage, thermal stability, and combustion properties of electrospun lauric acid/PET ultrafine composite fibers as form-stable phase change materials. *Appl. Energy* 2011, 88, 2106-2112.
44. Chen, W.; Weng, W. Ultrafine lauric–myristic acid eutectic/poly-(meta-phenylene isophthalamide) form-stable phase change fibers for thermal energy storage by electrospinning. *Appl. Energy* 2016, 173, 168-176.
45. Nejman, A.; Cies'lak, M. The impact of the heating/cooling rate on the thermoregulating properties of textile materials modified with PCM microcapsules. *Appl. Therm. Eng.* 2017, 127, 212-223.
46. Ramakrishnan, S.; Sanjayan, J.; Wang, X.; Alam, M.; Wilson, J. A novel paraffin/expanded perlite composite phase change material for prevention of PCM leakage in cementitious composites. *Appl. Energy* 2015, 157, 85-94.
47. Zhang, H.; Feng, X.; Cui, H.Z.; Chen, D.Z.; Ouyang, X.; Xu, S.Z.; Wang, J.X.; Huang, Y.T.; Zuo, J.D.; Tang, J.N. A novel phase-change cement composite for thermal energy storage: Fabrication, thermal and mechanical properties. *Appl. Energy* 2016,170, 130-139.

48. Borreguero, A.M.; Garrido, I.; Valverde, J.L.; Rodríguez, J.F.; Carmona, M. Development of smart gypsum composites by incorporating thermoregulating microcapsules. *Energy Build.* 2014, 76, 631-639.
49. Zhang, H.; Xu, Q.; Zhao, Z.; Zhang, J.; Sun, Y.; Sun, L.; Fen, X.; F.; Sawada, Y. Preparation and thermal performance of gypsum boards incorporated with microencapsulated phase change materials for thermal regulation. *Sol. Energy Mater. Sol. Cells* 2012, 102, 93-102.
50. Ji, R.; Zou, Z.; Liu, L.; Wei, S.; Qu, S. Development and energy evaluation of phase change material composite for building energy-saving. *Int. J. Energy Res.* 2019, 43 (14), 8674-8683.
51. Tan, S.; Yu, S.; Xu, G.; Zhang, Y. Preparation and properties studies of paraffin/high density polyethylene composites and phase-change coatings. *Prog. Organic Coatings* 2013, 76, 1761-1764.
52. Jeong, S.G.; Chang, S.J.; Wi, S.; Kang, Y.; Kim, S. Development and performance evaluation of heat storage paint with MPCM for applying roof materials as basic research. *Energy Build.* 2016, 112, 62-68.
53. Chen, P.; Zhang, P. Preparation and characterization of nano-sized phase change emulsions as thermal energy storage and transport media. *Appl. Energy* 2017, 190, 868-879.
54. Zhang, G.H.; Zhao, C.Y. Thermal property investigation of aqueous suspensions of microencapsulated phase change material and carbon nanotubes as a novel heat transfer fluid. *Renew. Energy* 2013, 60, 433-438.

55. Jia, Y.; Zhu, C.; Fang, G. Performance optimization of a photovoltaic/thermal collector using microencapsulated phase change slurry. *Int. J. Energy Res.* 2019, 44 (3), 1812-1827.
56. Huo, J.H.; Peng, Z.G.; Yang, S.S. Novel cement slurry containing microencapsulated phase change materials: Characterization, application and mechanism analysis. *Int. J. Energy Res.* 2020, 44 (6), 4235-4248.
57. Gao, G.; Zhang, T.; Guo, C.; Jiao, S.; Rao, S. Photo-thermal conversion and heat storage characteristics of multi-walled carbon nanotubes dispersed magnetic phase change microcapsules slurry. *Int. J. Energy Res.* 2020, 44 (8), 6873-6884.
58. Lou, L.; He, Z.; Li, Y.; Li, Y.; Zhou, Y.; Lin, C.; Yang, Z.; Fan, J.; Zhang, K.; Yang, W. Multifunctional silicone rubber/paraffin@PbWO<sub>4</sub> phase-change composites for thermoregulation and gamma radiation shielding. *Int. J. Energy Res.* 2020, 44 (9), 7674-7686.
59. Huang, Z.; Luo, Z.; Gao, X.; Fang, X.; Fang, Y.; Zhang, Z. Preparation and thermal property analysis of Wood's alloy/expanded graphite composite as highly conductive form-stable phase change material for electronic thermal management. *Appl. Therm. Eng.* 2017, 122, 322-329.
60. Masiá, R.P.; Rubio, A L.; Lagarón, J.M. Development of zein-based heat-management structures for smart food packaging. *Food Hydrocolloids* 2013, 30, 182-191.
61. Sandoval, W.C.; Fabra, M.J.; Rubio, A.L.; Lagarón, J.M. Electrospun Heat Management Polymeric Materials of Interest in Food Refrigeration and Packaging. *J. Appl. Polym. Sci.* 2014, 131 (16), 1-11.

62. Xu, X.; Zhang, X.; Liu, S. Experimental study on cold storage box with nanocomposite phase change material and vacuum insulation panel. *Int. J. Energy Res.* 2018, 42 (14), 4429-4438.
63. Su, W.; Zhou, T.; Li, Y.; Lv, Y. Development of microencapsulated phase change material with poly (methyl methacrylate) shell for thermal energy storage. *Energy Procedia* 2019, 158, 4483-4488.
64. Ma, Y.; Chu, X.; Tang, G.; Yao, Y. Synthesis and thermal properties of acrylate-based polymer shell microcapsules with binary core as phase change materials. *Mater. Lett.* 2013, 91, 133-135.
65. Fang, Y.; Kuang, S.; Gao, X.; Zhang, Z. Preparation and characterization of novel nanoencapsulated phase change materials. *Energy Convers. Manag.* 2008, 49, 3704-3707.
66. Zhang, T.; Wang, Y.; Shi, H.; Yang, W. Fabrication and performances of new kind microencapsulated phase change material based on stearic acid core and polycarbonate shell. *Energy Convers. Manag.* 2012, 64, 1-7.
67. Lashgari, S.; Arabi, H.; Mahdavian, A.R.; Ambrogi, V. Thermal and morphological studies on novel PCM microcapsules containing n-hexadecane as the core in a flexible shell. *Appl. Energy* 2017, 190, 612-622.
68. Srinivasaraonaik, B.; Singh, L.P.; Tyagi, I.; Rawat, A.; Sinha, S. Microencapsulation of a eutectic PCM using in situ polymerization technique for thermal energy storage. *Int. J. Energy Res.* 2020, 44 (5), 3854-3864.



69. Konuklu, Y.; Erzin, F. Preparation of pentadecane/poly-(melamine-urea-formaldehyde) microcapsules for thermal energy storage applications. *Int. J. Energy Res.* 2019, 43 (12), 6322-6326.
70. Li, C.; Yu, H.; Song, Y.; Liang, H.; Yan, X. Preparation and characterization of PMMA/TiO<sub>2</sub> hybrid shell microencapsulated PCMs for thermal energy storage. *Energy* 2018, 167, 1031-1039.
71. Qiu, X.; Song, G.; Chu, X.; Li, X.; Tang, G. Microencapsulated n-alkane with p-(n-butyl methacrylate-co-methacrylic acid) shell as phase change materials for thermal energy storage. *Sol. Energy* 2013, 91, 212-220.
72. Yang, Y.; Ye, X.; Luo, J.; Song, G.; Liu, Y.; Tang, G. Polymethyl methacrylate based phase change microencapsulation for solar energy storage with silicon nitride. *Sol. Energy* 2015, 115, 289-296.
73. Döğüşcü, D.K.; Altıntaş, A.; Sari, A.; Alkan, C. Polystyrene microcapsules with palmitic-capric acid eutectic mixture as building thermal energy storage materials. *Energy Build.* 2017, 150, 376-382.
74. Cao, F.; Yang, B. Supercooling suppression of microencapsulated phase change materials by optimizing shell composition and structure. *Appl. Energy* 2014, 113, 1512-1518.
75. Fang, Y.; Kang, H.; Wang, W.; Liu, H.; Gao, X. Study on polyethylene glycol/epoxy resin composite as a form-stable phase change material. *Energy Convers. Manag.* 2010, 51, 2757-2761.
76. Zhang, H.; Zou, Y.; Sun, Y.; Sun, L.; Xu, F.; Zhang, J. A novel thermal-insulating film incorporating microencapsulated phase-change materials for temperature regulation and nano-TiO<sub>2</sub> for UV-blocking. *Sol. Energy Mater. Sol. Cells* 2015, 137, 210-218.

77. Yoo, S.; Kandare, E.; Shanks, R.; Al-maadeed, M.A.; Khatibi, A.A. Thermo-physical properties of multifunctional glass fibre reinforced polymer composites incorporating phase change materials. *Thermochim. Acta* 2016, 642, 25-31.
78. Shi, H.; Li, J.; Jin, Y.; Yin, Y.; Zhang, X. Preparation and properties of poly(vinyl alcohol)-g-octadecanol copolymers based solid–solid phase change materials. *Mater. Chem. Phys.* 2011, 131, 108-112.
79. Mu, M.; Basheer, P.A.M.; Sha, W.; Bai, Y.; McNally, T. Shape stabilized phase change materials based on a high melt viscosity HDPE and paraffin waxes. *Appl. Energy* 2016, 162, 68-82.
80. Sobolciak, P.; Abdelrazeq, H.; Ouederni, M.; Karkri, M.; Al-maadeed, M.A.; Krupa, I. The stabilizing effect of expanded graphite on the artificial aging of shape stabilized phase change materials. *Polym. Testing* 2015, 46, 65-71.
81. Giro-paloma, J.; Rayón, E.; Roa, J. J.; Martínez, M.; Fernández, A.I. Effect of the filler on the nano-mechanical properties of polypropylene in contact with paraffinic phase change material. *Eur. Polym. J.* 2015, 63, 29-36.
82. Janigová, I.; Boh, B.; Sumiga, B.; Krupa, I.; Nógellová, Z.; Špitalsky, Z.; Kleinová, A.; Karkri, M.; Almaadeed, M.A. Phase change materials based on high-density polyethylene filled with microencapsulated paraffin wax. *Energy Convers. Manag.* 2014, 87, 400-409.
83. Giro-Paloma, J.; Konuklu, Y.; Fernández, A.I. Preparation and exhaustive characterization of paraffin or palmitic acid microcapsules as novel phase change material. *Sol. Energy* 2015, 112, 300-309.
84. Jiesheng, L.; Yuanyuan, Y.; Xiang, H. Research on the preparation and properties of lauric acid/expanded perlite phase change materials. *Energy Build.* 2016, 110, 108-111

85. Zhang, L.; Yang, W.; Jiang, Z.; He, F.; Zhang, K.; Fan, J.; Wu, J. Graphene oxide modified microencapsulated phase change materials with high encapsulation capacity and enhanced leakage-prevention performance. *Appl. Energy* 2017, 197, 354-363.
86. Jacob, R.; Bruno F. Review on shell materials used in the encapsulation of phase change materials for high temperature thermal energy storage. *Renew. Sustain. Energy Rev.* 2015, 48, 79-87.
87. Ma Y.; Sun, S.; Li, J.; Tang, G. Preparation and thermal reliabilities of microencapsulated phase change materials with binary cores and acrylate-based polymer shells. *Thermochim. Acta* 2014, 588, 38-46.
88. Ma, Y.; Zong, J.; Li, W. et al. Synthesis and characterization of thermal energy storage microencapsulated n-dodecanol with acrylic polymer shell. *Energy* 2015, 87, 86-94.
89. Ke, H.; Wei, Q. Use of MWNTs-COOH to improve thermal energy storage and release rates of capric–palmitic–stearic acid ternary eutectic/polyacrylonitrile form-stable phase change composite fibrous membranes. *Polym. Eng. Sci.* 2019, 59, E403- E411.
90. Golestaneh, S.I.; Mosallanejad, A.; Karimi, G.; Khorram, M.; Khashi, M. Fabrication and characterization of phase change material composite fibers with wide phase-transition temperature range by co-electrospinning method. *Appl. Energy* 2016, 182, 409-417.
91. Bastani, A.; Haghghat, F.; Kozinski, J. Designing building envelope with PCM wallboards: design tool development. *Renew. Sustain. Energy Rev.* 2014, 31, 554-562.
92. Zhu, K.; Li, X. Su, J.; Li, H.; Zhao, Y.; Yuan, X. Improvement of anti-icing properties of low surface energy coatings by introducing phase-change microcapsules. *Polym. Eng. Sci.* 2017, 1, E1-E7.

93. Zhang, L.; Zhu, J.; Zhou, W.; Wang, J.; Wang Y. Characterization of polymethyl methacrylate/polyethylene glycol/aluminum nitride composite as form-stable phase change material prepared by in situ polymerization method. *Thermochim. Acta* 2011, 524, 128-134.
94. Wan, X.; Guo, B.; Xu, J. A facile hydrothermal preparation for phase change materials microcapsules with a pliable self-recovering shell and study on its thermal energy storage properties. *Powder Technol.* 2017, 312, 144-151.
95. Zhan, S.; Chen, S.; Chen, L.; Hou, W. Preparation and characterization of polyurea microencapsulated phase change material by interfacial polycondensation method. *Powder Technol.* 2016, 292, 217-222.
96. Wang, Y.; Zhang, Y.; Xia, T.; Zhao, W.; Yang, W. Effects of fabricated technology on particle size distribution and thermal properties of stearic-eicosanoic acid/polymethylmethacrylate nanocapsules. *Sol. Energy Mater. Sol. Cells* 2014, 120, 481-490.
97. Huang, M.; Luo, Y.; Zhong, Y.; Xiao, M.; Hu, J. Preparation and characterization of microencapsulated phase change materials with binary cores and poly (allyl methacrylate) (PALMA) shells used for thermo-regulated fibers. *Thermochim. Acta* 2017, 655, 262-268.
98. Deveci, S.S.; Basal, G. Preparation of PCM microcapsules by complex coacervation of silk fibroin and chitosan. *Colloid Polym. Sci.* 2009, 287, 1455-1467.
99. Jin, Z.; Wang, Y.; Liu, J.; Yang, Z. Synthesis and properties of paraffin capsules as phase change materials. *Polymer (Guildf)* 2008, 49, 2903-2910.

100. Trivedi, G.V.N.; Parameshwaran, R. Cryogenic conditioning of microencapsulated phase change material for thermal energy storage. *Sci. Rep.* 2020, 10, (18353), 1-11.
101. Pielichowska, K.; Nowak, M.; Szatkowski, P.; Macherzynska, B. The influence of chain extender on properties of polyurethanebased phase change materials modified with graphene. *Appl. Energy* 2016, 162, 1024-1033.
102. Wang, H.; Luo, J.; Yang, Y.; Zhao, L.; Song, G.; Tang, G. Fabrication and characterization of microcapsulated phase change materials with an additional function of thermo-chromic performance. *Sol. Energy* 2016, 139, 591-598.
103. Sari, A.; Biçer, A.; Alkan, C. Poly-(styrene-co-maleic anhydride)-graft-fatty acids as novel solid–solid PCMs for thermal energy storage. *Polym. Eng. Sci.* 2019, 59, E337-E347.
104. Ma, Y.; Chu, X.; Li, W.; Tang, G. Preparation and characterization of poly-(methyl methacrylate-co-divinylbenzene) microcapsules containing phase change temperature adjustable binary core materials. *Sol. Energy* 2012, 86, 2056-2066.
105. Lu, S.; Shen, T.; Xing, J. et al. Preparation and characterization of cross-linked polyurethane shell microencapsulated phase change materials by interfacial polymerization. *Mater. Lett.* 2018, 211, 36-39.
106. Carreira, A.S.; Teixeira, R.F.A.; Beirao, A.; Vaz, V. R., Figueiredo, M.M.; Gil MH. Preparation of acrylic based microcapsules using different reaction conditions for thermoregulating textiles production. *Eur. Polym. J.* 2017, 93, 33-43.

107. Konuklu, Y.; Unal, M.; Paksoy, H.O. Microencapsulation of caprylic acid with different wall materials as phase change material for thermal energy storage. *Sol. Energy Mater. Sol. Cells*. 2014, 120, 536-542.
108. Al-Shannaq, R.; Farid, M.; Al-Muhtaseb, S.; Kurdi, J. Emulsion stability and cross-linking of PMMA microcapsules containing phase change materials. *Sol. Energy Mater. Sol. Cells* 2015, 132, 311-318.
109. Ünal, M.; Konuklu, Y.; Paksoy, H. Thermal buffering effect of a packaging design with microencapsulated phase change material. *Int. J. Energy Res.* 2019, 43, 1-11.
110. Zhang, G.H.; Zhao, C.Y. Synthesis and characterization of a narrow size distribution nano phase change material emulsion for thermal energy storage. *Sol. Energy* 2017, 147, 406-413.
111. Wang, Y.; Xia, T.D.; Feng, H.X.; Zhang, H. Stearic acid/ polymethylmethacrylate composite as form-stable phase change materials for latent heat thermal energy storage. *Renew. Energy* 2011, 36, 1814-1820.
112. Zhao, J.; Yang, Y.; Li, Y.; et al. Microencapsulated phase change materials with TiO<sub>2</sub>-doped PMMA shell for thermal energy storage and UV-shielding. *Sol. Energy Mater. Sol. Cells* 2017, 168, 62-68.
113. Sánchez-Silva, L.; Rodríguez, J.; Romero, A.; Borreguero, A.; Carmona, M.; Sánchez, P. Microencapsulation of PCMs with a styrene-methylmethacrylate copolymer shell by suspension-like polymerization. *Chem. Eng. J.* 2010, 157, 216-222.
114. Sanchez-Silva, L.; Savalas, J.T.; Sundberg, D.; Sanchez, P.; Rodriguez, J. Synthesis and characterization of paraffin wax microcapsules with acrylic-based polymer shells. *Ind. Eng. Chem. Res.* 2010, 49, 12204-12211.

115. Mukram, T.A.; Daniel, J. Building bricks with PCM inserts for Passive cooling applications. *IOP Conf. Ser.: Earth Environ. Sci.*2020, 573, 1-7.
116. Skurkyte-Papieviene, V.; Abraitiene, A.; Sankauskaite, A.; Rubeziene, V.; Baltusnikaite Guzaitiene, J. Enhancement of the Thermal Performance of the Paraffin Based Microcapsules Intended for Textile Applications. *Polymers* 2021, 13, 1-16.
117. Kuta, M; Matuszewska, D.; Wójcik, T.M. Reasonableness of phase change materials use for air conditioning-a short review. *Energy Fuels* 2016, 14, 1-16.
118. Righetti, G.; Zilio, C.; Doretto, L.; Longo, G.A.; Mancin, S. On the design of Phase Change Materials based thermal management systems for electronics cooling. *Appl. Therm. Eng.*2021, 196 (117276), 1-10.
119. Shchukina, E.M.; Graham, M.; Zheng, Z.; Shchukin, D. G. Nanoencapsulation of phase change materials for advanced thermal energy storage systems. *Chem. Soc. Rev.*2018, 47, 4156-4175.
120. Fang, Y.; Yu, H.; Wan, W.; Gao, X.; Zhang, Z. Preparation and thermal performance of polystyrene/n-tetradecane composite nanoencapsulated cold energy storage phase change materials. *Energy Convers. Manag.* 2013, 76, 430-436.
121. Fang, Y.; Liu, X.; Liang, X.; Liu, H.; Gao, X.; Zhang, Z. Ultrasonic synthesis and characterization of polystyrene/n-dotriacontane composite nanoencapsulated phase change material for thermal energy storage. *Appl. Energy* 2014, 132, 551-556.
122. Fu, W.; Liang, X.; Xie, H.; Wang, S.; Gao, X.; Zhang, Z.; Fang, Y. Thermo-physical properties of n-tetradecane@polystyrene-silica composite nanoencapsulated phase change material slurry for cold energy storage. *Energy Build.* 2017, 136, 26-32.

123. Wang, G.; Xu, W.; Hou, Q.; Guo, S. A simple sonochemical method for fabricating poly-(methyl methacrylate)/stearic acid phase change energy storage nanocapsules. *Ultras. Sonochem.* 2015, 27, 403-407.
124. Somiseti, V.; Allauddin, S.; Narayan, R.; Raju, K.V.S.N. Flexible, hard, and tough bio-based polyurethane thermosets from renewable materials: glycerol and 10-undecenoic acid *J. Coat. Technol. Res.* 2018, 15, 210-218.
125. Valverde, C.; Lligadas, G.; Ronda, J.C.; Galià, M.; Cádiz, V. Hydroxyl functionalized renewable polyesters derived from 10-undecenoic acid: Polymer structure and post polymerization modification. *Eur. Poly. J.* 2018, 105, 68-78.
126. Bigot, S.; Daghrir, M.; Mhanna, A.; Boni, G.; Pourchet, S.; Lecamp, L.; Plasseraud, L. Undecylenic acid: A tunable bio-based synthon for materials applications *Euro. Poly. J.* 2016, 74, 26-37.
127. Pang, C.; Zhang, J.; Wu, G.; Wang, Y.; Gao, H.; Ma, J. Renewable polyesters derived from 10-undecenoic acid and vanillic acid with versatile properties. *Polym. Chem.* 2014, 5, 2843-2853.
128. Somiseti, V.; Allauddin, S.; Narayan, R.; Raju, K.V.S.N. Multifunctional polyurethane coatings derived from phosphated cardanol and undecylenic acid based polyols. *Prog. Org. Coatings* 2019, 134, 91-102.
129. Kaur, R.; Duhan, M. Nano-Structured Polyaniline as a Potential Adsorbent for Methylene Blue Dye Removal from Effluent. *J. Compos. Sci.* 2021, 5 (7), 1-11.
130. Jamil, S.; Ahmad, Z.; Ali, M.; Khan, S.R.; Ali, S.; Hammami, M.A.; Haroon, M.; Saleh, T.A.; Janjua, M.R.S.A. Synthesis and characterization of polyaniline/nickel oxide composites for fuel additive and dyes reduction. *Chem. Phy. Lett.* 2021, 776, 138713.



131. Khandelwala, V.; Sahooa, S.K.; Kumar, A.; Manik, G. Electrically conductive green composites based on epoxidized linseed oil and polyaniline: An insight into electrical, thermal and mechanical properties. *Composites Part B* 2018, 136, 149-157.
132. Zeng, J.L.; Zhu, F.R.; Yu, S.B.; Xiao, Z.L.; Yan, W.P.; Zheng, S.H.; Zhang, L.; Sun, L.X.; Cao, Z. Myristic acid/polyaniline composites as form stable phase change materials for thermal energy storage. *Sol. Energy Mater. Sol. Cells* 2013, 114, 136-140.
133. Ju, C.; Wang, Y.; He, D.; Gao, Q.; Gao, L.; Fu, M. Synthesis and Infrared Property of Polyaniline/ Phase-Change Nanocapsule Composite. *J. Nano Sci. Nanotech.* 2011, 11, 9665-9670.
134. Halvae, M.; Didehban, K.; Goodarzi, V.; Ghaffari, M.; Ehsani, M.; Saeb, M.R. Comparison of pristine and polyaniline-grafted MWCNTs as conductive sensor elements for phase change materials: Thermal conductivity trend analysis. *J. Appl. Polym. Sci.* 2017, 134, (45389) 1-10.
135. Mathew George, M.; Pandey, A.K.; Rahima, N.A.; Tyagi, V.V.; Shahabuddin S.; Saidur, R. A novel polyaniline (PANI)/paraffin wax nano composite phase change material: Superior transition heat storage capacity, thermal conductivity and thermal reliability. *Sol. Energy* 2020, 204, 448-458.
136. Patra, B.N.; Majhi, D. Removal of Anionic Dyes from Water by Potash Alum Doped Polyaniline: Investigation of Kinetics and Thermodynamic Parameters of Adsorption. *J. Phys. Chem. B* 2015, 119, 8154-8164.
137. Bhaumik, M.; McCrindle, R.I.; Maity, A.; Agarwal, S.; Gupta, V.K. Polyaniline nanofibers as highly effective re-usable adsorbent for removal of reactive black 5 from aqueous solutions. *J. Col. Inter. Sci.* 2016, 466, 442-451.

138. Huang, J.; Kaner, R.B. Nanofiber Formation in the Chemical Polymerization of Aniline: A Mechanistic Study. *Angewandte Chemie* 2004, 43 (43), 5817-5821.
139. Jaworski, M. Mathematical model of heat transfer in PCM incorporated fabrics subjected to different thermal loads. 2019, 150, 506-511.
140. Borri, E.; Hua, N.; Sciacovelli, A.; Wu, D.; Ding, Y.; Li, Y.; Brancato, V.; Zhang, Y.; Frazzica, A.; Li, W. Phase Change Slurries for Cooling and Storage: An Overview of Research Trends and Gaps. *Energies* 2022, 15 (687), 1-17.
141. Zhu, X.; Sheng, X.; Jun Li, J.; Chen, Y. Thermal comfort and energy saving of novel heat-storage coatings with microencapsulated PCM and their application. *Energy Build.* 2021, 251 (11349), 1-11.
142. Shi, J.; Wua, X.; Fua, X.; Sun, R. Synthesis and thermal properties of a novel nanoencapsulated phase change material with PMMA and SiO<sub>2</sub> as hybrid shell materials. *Thermochim. Acta* 2015, 617, 90-94.
143. Kibria, M.A.; Anisur, M.R.; Mahfuz, M.H.; Saidur, R.; Metselaar, I.H.S.C. A review on thermo-physical properties of nanoparticles dispersed phase change materials. *Energy Convers. Manag.* 2015, 95, 69-89.
144. Wu, C.H.; Pu, N.W.; Liao, C.W.; Wu, B.R.; Liu, Y.H.; Ger, M.D. High-electrical-resistivity thermally-conductive phase change materials prepared by adding nanographitic fillers into paraffin. *Microelect. Eng.* 2015, 138, 91-96.
145. Karaipekli, A.; Biçer, Ahmet Sari, A.; Tyagi, V.V. Thermal characteristics of expanded perlite/paraffin composite phase change material with enhanced thermal conductivity using carbon nanotubes. *Energy Convers. Manag.* 2017, 134, 373-381.
146. Reddy, P.B.; Gunasekar, C.; Mhaske, A.S.; Krishna, N.V. Enhancement of

- thermal conductivity of PCM using filler graphite powder materials. *IOP Conf. Ser.: Mater. Sci. Eng.* 2018, 402, 1-10.
147. Zhang, Y.; Li, W.; Huang, J.; Cao, M.; Du, G. Expanded Graphite/Paraffin/Silicone Rubber as High Temperature Form-stabilized Phase Change Materials for Thermal Energy Storage and Thermal Interface Materials. *Materials* 2020, 13 (894) 1-14.
148. Wang, Z.; Huang, G.; Jia, Z.; Gao, Q.; Li, Y.; Gu, Z. Eutectic Fatty Acids Phase Change Materials Improved with Expanded Graphite. *Materials* 2022, 15 (6856), 1-15.
149. Li, M.; Guo, Q.; Nutt, S. Carbon nanotube/paraffin/montmorillonite composite phase change material for thermal energy storage. *Sol. Energy* 2017, 146, 1-7.
150. Choi, D.H. Lee, J.; Hong, H.; Kang, Y.T. Thermal conductivity and heat transfer performance enhancement of phase change materials (PCM) containing carbon additives for heat storage application. *Int. J. Refrig.* 2014, 42, 112-120.
151. Fan, L.W.; Fang, X.; Wang, X.; Zeng, Y.; Xiao, Y.Q.; Yu, Z.T.; Xu, X.; Hu, Y.C.; Cen, K.F. Effects of various carbon nano-fillers on the thermal conductivity and energy storage properties of paraffin-based nanocomposite phase change materials. *Appl. Energy* 2013, 110, 163-172.
152. Zeng, J.L.; Cao, Z.; Yang, D. W.; Sun, L. X.; Zhang, L. Thermal conductivity enhancement of Ag nanowires on an organic phase change material. *J. Therm. Anal. Calorim.* 2010, 101, 385-389.
153. Xu, S.; Zhang, X.; Huang, Z.; Liu, Y.; Fang, M.; Wu, X.; Min, X. Thermal conductivity enhanced polyethylene glycol/expanded perlite shape-stabilized composite phase change materials with Cu powder for thermal energy storage. *Mater. Res. Express*

- 2018, 5, 1-10.
154. Şahan, N.; Paksoy, H.O. Thermal enhancement of paraffin as a phase change material with nano-magnetite. *Sol. Energy Mater. Sol. Cells* 2014, 126, 56-61.
155. Tang, B.; Wu, C.; Qiu, M.; Zhang, X.; Zhang, S. PEG/SiO<sub>2</sub>-Al<sub>2</sub>O<sub>3</sub> hybrid form-stable phase change materials with enhanced thermal conductivity. *Mater. Chem. Phys.* 2014, 144, 162-167.
156. Cai, Y.; Hou, X.; Wang, W.; Liu, M.; Zhang, J.; Qiao, H.; Huang, F.; Wei, Q. Effects of SiO<sub>2</sub> nanoparticles on structure and property of form-stable phase change materials made of cellulose acetate phase inversion membrane absorbed with capric-myristic-stearic acid ternary eutectic mixture. *Thermochim. Acta* 2017, 653, 49-58.
157. Wang, W.; Yang, X.; Fang, Y.; Ding, J.; Yan, J. Enhanced thermal conductivity and thermal performance of form-stable composite phase change materials by using  $\beta$ -Aluminum nitride. *Appl. Energy* 2009, 86, 1196-1200.
158. Qian, T.; Li, J.; Feng, W.; Nian, H. Single-walled carbon nanotube for shape stabilization and enhanced phase change heat transfer of polyethylene glycol phase change material. *Energy Convers. Manag.* 2017, 143, 96-108.
159. Zhang, X.; Wen, R.; Tang, C.; Wu, B.; Huang, Z.; Min, X.; Huang, Y.; Liu, Y.; Fang, M.; Wu, X. Thermal conductivity enhancement of polyethylene glycol/expanded perlite with carbon layer for heat storage application. *Energy Build.* 2016, 130, 113-121.
160. Song, S.; Li, J.; Yang, Z.; Wan, C. Enhancement of Thermo-Physical Properties of Expanded Vermiculite-Based Organic Composite Phase Change Materials for Improving the Thermal Energy Storage Efficiency. *ACS Omega* 2021, 6, 3891-3899.
161. Deng, Y.; He, M.; Li, J.; Yang, Z. Polyethylene Glycol-Carbon

- Nanotubes/Expanded Vermiculite Form-Stable Composite Phase Change Materials: Simultaneously Enhanced Latent Heat and Heat Transfer. *Polymers* 2018, 10 (889), 1-15.
162. He, L.; Wang, H.; Zhu, H.; Gu, Y.; Li, X.; Mao, X. Thermal Properties of PEG/Graphene Nanoplatelets (GNPs) Composite Phase Change Materials with Enhanced Thermal Conductivity and Photo-Thermal Performance. *Appl. Sci.* 2018, 8 (2613), 1-14.
163. Tas, C.E.; Unal, H. Thermally buffering polyethylene/halloysite/phase change material nanocomposite packaging films for cold storage of foods. *J. Food Eng.* 2021, 292 (110351), 1-8.
164. Rashid, M.M.; Simoncic, B.; Tomsic, B. Recent advances in TiO<sub>2</sub>-functionalized textile surfaces. *Surf. Interfaces* 2021, 22, 100890.
165. Zamanian, M.; Sadrnia, H.; Khojastehpour, M.; Hosseini, F.; Thibault, J. Effect of TiO<sub>2</sub> Nanoparticles on Barrier and Mechanical Properties of PVA Films. *J. Membrane Sci. Res.* 2021, 7, 67-73.
166. Wang, L.; Yuan, Z.; Egerton, T.A. Comparison of nano-particulate TiO<sub>2</sub> prepared from titanium tetrachloride and titanium tetraisopropoxide. *Mater Chem. Phys.* 2012, 133, 304-310.
167. Goñi-Ciaurriz, L.; Senosiain-Nicolay, M.; Vélaz, I. Aging Studies on Food Packaging Films Containing  $\beta$ -Cyclodextrin-Grafted TiO<sub>2</sub> Nanoparticles. *Int. J. Mol. Sci.* 2021, 22, (2257) 1-13.
168. Li, K.; Peng, J.; Zhang, M.; Heng, J.; Li, D.; Mu, C. Comparative study of the effects of anatase and rutile titanium dioxide nanoparticles on the structure and properties of waterborne polyurethane. *Coll. Surf. A: Physicochem. Eng. Aspects* 2015, 470, 92-99.
169. Vidakis, N.; Petousis, M.; Maniadi, A.; Papadakis, V.; Manousaki, A. MEX 3D

- Printed HDPE/TiO<sub>2</sub> Nanocomposites Physical and Mechanical Properties Investigation. *J. Compos. Sci.* 2022, 6 (209) 1-16.
170. Chueangchayaphan, W.; Luangchuang, P.; Chueangchayaphan, N. High Performance of Titanium Dioxide Reinforced Acrylonitrile Butadiene Rubber Composites. *Polymers* 2022, 14 (5267) 1-12.
171. Yu, L.; Skov, A.L. Silicone rubbers for dielectric elastomers with improved dielectric and mechanical properties as a result of substituting silica with titanium dioxide. *Int. J. Smart Nano Mater.* 2015, 6 (4), 268-289.
172. Li, B.; Wang, X.; Yan, M.; Li, L. Preparation and characterization of nano-TiO<sub>2</sub> powder. *Mater. Chem. Phys.* 2002, 78, 184-188.
173. Liu, Z. Wang, R.; Kan, F.; Jiang, F. Synthesis and Characterization of TiO<sub>2</sub> Nanoparticles. *Asian J. Chem.* 2014, 26, 655-659.
174. Bokov, D.; Jalil, A.T. Chupradit, S.; Suksatan, W.; Ansari, M.J.; Shewael, I.H.; Valiev, G.H.; and Ehsan Kianfar, E. Nano-material by Sol-Gel Method: Synthesis and Application. *Adv. Mater. Sci. Eng.* 2021, 21, 1-21.
175. Navas, D.; Fuentes, S.; Castro-Alvarez, A.; Chavez-Angel, E. Review on Sol-Gel Synthesis of Perovskite and Oxide Nano-materials. *Gels* 2021, 7 (275) 1-19.
176. Phromma, S.; Wutikhun, T.; Kasamechonchung, P.; Eksangsri, T.; Sapcharoenkun, C. Effect of calcination temperature on photocatalytic activity of synthesized TiO<sub>2</sub> nanoparticles via wet ball milling sol-gel method. *Appl. Sci.* 2020, 10, 1-13.
177. Jiang, F.; Wang, X.; Wu, D. Design and synthesis of magnetic microcapsules based on n-eicosane core and Fe<sub>3</sub>O<sub>4</sub>/SiO<sub>2</sub> hybrid shell for dual-functional phase change

- materials. 2014, *Appl. Energy* 134, 456-468.
178. Melone, L.; Altomare, L.; Cigada, A.; De Nardo, L. Phase change material cellulosic composites for the cold storage of perishable products: From material preparation to computational evaluation. *Appl. Energy* 2012, 89, 339-346.
179. Konuklu, Y.; Paksoy, H. Polystyrene-based caprylic acid microencapsulation for thermal energy storage. *Sol. Energy Mater. Sol. Cells*. 2017, 159, 235-242.
180. Nejman, A.; Cieslak, M.; Gajdzick, B.; Grabowska, B.G.; Karaszewska, A. Methods of PCM microcapsules application and the thermal properties of modified knitted fabric. *Thermochim. Acta* 2014, 589, 158-163.
181. Mofijur, M., Mahlia, T.M.I.; Arridina Susan Silitonga, A.S.; Ong, H.C; Silakhori, M.; Hasan, M.H.; Putra, N.; Rahman, S.M.A. Phase Change Materials (PCM) for Solar Energy Usages and Storage: An Overview. *Energies* 2019, 12 (3167), 1-20.
182. Bao, J.; Tu, H.; Li, J.; Li, Y.; Yu, S.; Gao, J.; Lei, K.; Zhang, F.; Li, J. Applications of phase change materials in smart drug delivery for cancer treatment. 2022 *Front. Bioeng. Biotechnol.* 10, 1-11.
183. Su, D.; Jia, Y.; Alva, G; Tang, F.; Fang, G. Preparation and thermal properties of n-octadecane/stearic acid eutectic mixtures with hexagonal boron nitride as phase change materials for thermal energy storage. *Energy Build.* 2016, 131, 35-41.
184. Feng, L.; Zheng, J.; Yang, H.; Guo, Y.; Li, W.; Li, X. Preparation and characterization of polyethylene glycol/active carbon composites as shape-stabilized phase change materials. *Sol. Energy Mater. Sol. Cells* 2011, 95, 644-650.

185. Nawaz, K.; Freeman, T.B.; Rafael M. Rodriguez, R.M.; Boetcher, S.K.S. Moisture affinity of HDPE/phase-change material composites for thermal energy storage applications. *RSC Adv.* 2021, 11, 30569-30573.
186. Xu, L.; Wang, J.; Yang, R. A new flame retardancy strategy for shape stabilized phase change materials by surface coating. *Sol. Energy Mater. Sol. Cells.* 2017, 170, 87-94.
187. Jamekhorshid, A.; Sadrameli, S.M.; Barzin, R.; Farid, M.M. Composite of wood-plastic and micro-encapsulated phase change material (MEPCM) used for thermal energy storage. *Appl. Therm. Eng.* 2017, 112, 82-88.
188. Premnath, D.; Vamsi, V. B.; Tomar, M.; Freezing characteristics in finned LDPE spherical capsule. *J. Phys.: Conf. Ser.* 2021, 2054, 1-9.
189. Sobolciak, P.; Karkri, M.; Al-Maadeed, M.A.; Krupa, I. Thermal characterization of phase change materials based on linear low-density polyethylene, paraffin wax and expanded graphite. *Renew. Energy* 2016, 88, 372-382.
190. Tian, B.; Yang, W.; Luo, L.; Wang, J.; Zhang, K.; Fan, J.; Wu, J.; Xing, T. Synergistic enhancement of thermal conductivity for expanded graphite and carbon fiber in paraffin/EVA form-stable phase change materials. *Sol. Energy* 2016, 127, 48-55.
191. Li, L.; Wang, G.; Guo, C. Influence of intumescent flame retardant on thermal and flame retardancy of eutectic mixed paraffin/polypropylene form-stable phase change materials. *Appl. Energy* 2016, 162, 428-434.
192. Mu, S.; Guo, J.; Yu, Y.; An, Q.; Zhang, S.; Wang, D.; Chen, S.; Huang, X.; Li, S. Synthesis and thermal properties of cross-linked poly-(acrylonitrile-co-



- itaconate)/polyethylene glycol as novel form-stable change material. *Energy Convers. Manag.* 2016, 110, 176-183.
193. Bonadies, I.; Renzi, A.I.; Cocca, M.; Avella, M.; Carfagna, C.; Persico, P. Heat Storage and Dimensional Stability of Poly-(vinyl alcohol) Based Foams Containing Microencapsulated Phase Change Materials. *Ind. Eng. Chem. Res.* 2015, 54(38), 9342-9350.
194. Chen, P.; Gao, X.; Wang, Y.; Xu, T.; Fang, Y.; Zhang, Z. Metal foam embedded in SEBS/paraffin/HDPE form-stable PCMs for thermal energy storage. *Sol. Energy Mater. Sol. Cells* 2016, 149, 60-65.
195. Babapoor, A.; Karimi, G.; Khorram, M. Fabrication and characterization of nanofiber-nanoparticle-composites with phase change materials by electrospinning. *Appl. Therm. Eng.* 2016, 99, 1225-1235.
196. Zhou, Y.; Sheng, D.; Liu, X.; Lin, C.; Ji, F.; Dong, L. Synthesis and properties of cross-linking halloysite nanotubes/polyurethane- based solid-solid phase change materials. *Sol. Energy Mater. Sol. Cells* 2018, 174, 84-93.
197. Sundararajan, S.; Samui, A.B.; Kulkarni, P.S. Shape-stabilized poly-(ethylene glycol) (PEG)-cellulose acetate blend preparation with superior PEG loading via microwave-assisted blending. *Sol. Energy* 2017, 144, 32-39.
198. Guo, X.; Cao, J.; Peng, Y.; Liu, R. Incorporation of microencapsulated dodecanol into wood flour/high-density polyethylene composite as a phase change material for thermal energy storage. *JMADE.* 2016, 89, 1325-1334.

199. Tang, Y.; Lin, Y.; Jia, Y.; Fang, G. Improved thermal properties of stearyl alcohol/high density polyethylene/expanded graphite composite phase change materials for building thermal energy storage. *Energy Build.* 2017, 153, 41-49.
200. Tang, Y.; Jia, Y.; Alva, G.; Huang, X.; Fang, G. Synthesis, characterization and properties of palmitic acid/high density polyethylene/graphene nanoplatelets composites as form-stable phase change materials. *Sol. Energy Mater. Sol. Cells* 2016, 155, 421-429.
201. Alkan, C.; Kahraman, D.; Gottschalk, A.; Ramamoorthi, U.; Alt, Ö.; Daml, Y.; Çetin, A. Polyvinyl alcohol-salt hydrate mixtures as passive thermal energy storage systems. *Energy Procedia* 2016, 91 1012-1017.
202. Tang, B.; Wang, L.; Xu, Y.; Xiu, J.; Zhang, S. Hexadecanol/phase change polyurethane composite as form-stable phase change material for thermal energy storage. *Sol. Energy Mater. Sol. Cells* 2016, 144, 1-6.
203. Tian, F.; Zhang, S.; Zhai, M.; Sui, J.; Lan, X.; Gao, J. Thermal properties of nano-sized polyethylene glycol confined in silica gels for latent heat storage. *Thermochim. Acta* 2017, 655, 211-218.
204. Wang, Y.; Liang, D.; Liu, F.; Zhang, W.; Di, X.; Wang, C. A polyethylene glycol/hydroxyapatite composite phase change material for thermal energy storage. *Appl. Therm. Eng.* 2017, 113, 1475-1482.
205. Falqi, F.H.; Bin-Dahman, O.A.; Hussain, M.; Al-Harthi, M.A. Preparation of miscible PVA/PEG blends and effect of graphene concentration on thermal, crystallization, morphological, and mechanical properties of PVA/PEG (10 wt.%) blend. *Int. J. Polym. Sci.* 2018, 1-10.

206. Feng, L.; Song, P.; Yan, S.; Wang, H.; Wang, J. The shape-stabilized phase change materials composed of polyethylene glycol and graphitic carbon nitride matrices. *Thermochim. Acta* 2015, 612, 19-24.
207. Jin, X.; Li, J.; Xue, P.; Jia, M. Preparation and characterization of PVC-based form-stable phase change materials. *Sol. Energy Mater. Sol. Cells* 2014, 130, 435-441.
208. Alsaad, A.; Al Dairy, A.R.; Ahmad, A.; Qattan, I.A.; Al Fawares, S.; Al-Bataineh, Q. Synthesis and characterization of polymeric (PMMA-PVA) hybrid thin films doped with TiO<sub>2</sub> nanoparticles using dip-coating technique. *Crystals* 2021, 11, 1-21.
209. Suhailath, K.; Ramesan, M.T.; Naufal, B.; Periyat, P.; Jasna, V.C.; Jayakrishnan, P. Synthesis, characterisation and flame, thermal and electrical properties of poly-(n-butyl methacrylate)/titanium dioxide nanocomposites. *Polym. Bull.* 2017, 74, 671-688.
210. Afzal, A.; Usama, M.; Abdul Rashid, I.; Khalid, Z.; Mohsin, M.; Shakir, M.F.; Tariq, A. Effect of MgOH/TiO<sub>2</sub> on flame retardancy and mechanical behavior of composite. *Mater. Res. Express.* 2019, 6, 1-7.
211. Jiao, C.; Chen, X. Synergistic Effects of Titanium Dioxide with Layered Double Hydroxides in EVA/LDH Composites. *Polym. Eng. Sci.* 2011, 51, 2166-2170.
212. Zhang, X.; Huang, Z.; Ma, B.; Wen, R.; Min, X.; Huang, Y.; Yin, Z.; Liu, Y.; Fang, M.; Wu, X. Preparation and performance of novel form-stable composite phase change materials based on polyethylene glycol/White Carbon Black assisted by super-ultrasound-assisted. *Thermochim. Acta* 2016, 638, 35-43.
213. Zahir, M.H.; Mohamed, S.A.; Saidur, R.; Al-Sulaiman, F.A. Supercooling of phase-change materials and the techniques used to mitigate the phenomenon. *Appl. Energy* 2019, 240, 793-817.

214. Mishra, D.K.; Bhowmik, S.; Pandey, K.M. Polyethylene Glycol Based Form Stable Composite Phase Change Material: A Review. *J. Phys.: Conf. Ser.* 2020 (1455) 1-5.
215. Chen, X.; Tang, Z.; Chang, Y.; Gao, H.; Cheng, P.; Tao, Z.; Lv, J. Toward Tailoring Chemistry of Silica-Based Phase Change Materials for Thermal Energy Storage. *iScience* 2020, 23 (10), 1-31.
216. Nguyen, G. T. Polyethylene glycol/fumed silica composites as shape-stabilized phase change materials with effective thermal energy storage. *RSC Adv.* 2023, 13, 7621-7631.
217. Zhang, D.; Chen, M.; Wu, S.; Liu, Q.; Wan, J. Preparation of expanded graphite/polyethylene glycol composite phase change material for thermoregulation of asphalt binder. *Constr. Build. Mater.* 2018, 169, 513-521.
218. Atinafu, D.G.; Yun, B.Y.; Wi, S.; Kang, Y.; Kim, S. A comparative analysis of bio-char, activated carbon, expanded graphite, and multi-walled carbon nanotubes with respect to PCM loading and energy-storage capacities. *Environ. Res.* 2021, 195 (110853), 1-9.
219. Qi, G.Q.; Yang, J.; Bao, R.Y.; Liu, Z.Y.; Yang, W.; Xie, B.H.; Yang, M.B. Enhanced comprehensive performance of polyethylene glycol based phase change material with hybrid graphene nano-materials for thermal energy storage. *Carbon* 2015, 88, 196-205.
220. Deng, Y.; Li, J.; Nian, H.; Li, Y.; Yin, X. Design and preparation of shape-stabilized composite phase change material with high thermal reliability via

- encapsulating polyethylene glycol into flower-like TiO<sub>2</sub> nanostructure for thermal energy storage. *Appl. Therm. Eng.* 2017, 114, 328-336.
221. Wang, Y.; Li, J.; Miao, W.; Su, Y.; He, X.; Strnadel, B. Preparation and characterizations of hydroxyapatite microcapsule phase change materials for potential building materials. *Constr. Build. Mater.* 2021, 297 (123576) 1-8.
222. Cai, Y.; Liu, M.; Song, X.; Zhang, J.; Wei, Q.; Zhang, L. A form-stable phase change material made with a cellulose acetate nanofibrous mat from bicomponent electrospinning and incorporated capric–myristic–stearic acid ternary eutectic mixture for thermal energy storage/retrieval. *RSC Adv.* 2015, 5, 84245-84251.
223. Shehata, A.M.; Akil, D.S. Structural and optical properties of TiO<sub>2</sub> nanoparticles/PVA for different composites thin films. *Int. J. Nanoelectronics and Mater.* 2016, 9, 17-36.
224. Prasanna, P.; Ramkumar, R.; Sunilkumar, K.; Rajasekar, R. Experimental study on a binary mixture ratio of fatty acid-based PCM integrated to PV panel for thermal regulation on a hot and cold month. *Int. J. Sustain. Energy* 2020, 40 (3), 218-234.
225. Kant, K.; Shukla, A.; Sharma, A. Ternary mixture of fatty acids as phase change materials for thermal energy storage applications. *Energy Rep.* 2016, 2, 274-279.
226. Chen, K.; Liu, R.; Zou, C.; Shao, Q.; Lan, Y.; Cai, X.; Zhai, L. Linear polyurethane ionomers as solid–solid phase change materials for thermal energy storage. *Sol. Energy Mater. Sol. Cells* 2014, 130, 466-473.
227. Sari, A.; Alkan, C.; Altıntaş, A. Preparation, characterization and latent heat thermal energy storage properties of micro-nanoencapsulated fatty acids by polystyrene shell. *Appl. Therm. Eng.* 2014, 73, 1158-1166.

228. Liu, S.; Xin, S.; Jiang, S. Study of Capric–Palmitic Acid/Clay Minerals as Form-Stable Composite Phase-Change Materials for Thermal Energy Storage. *ACS Omega* 2021, 6, 24650-24662.
229. Gallart-Sirvent, P.; Martin, M.; Villorbina, G.; Balcells, M.; Sole, A.; Barrenche, C.; Cabeza, L.F.; Canela-Garayoa, R. Fatty acid eutectic mixtures and derivatives from non-edible animal fat as phase change materials. *RSC Adv.* 2017, 7, 24133-24139.
230. Wang, R.; Ren, M.; Gao, X.; Qin, L. Preparation and properties of fatty acids based thermal energy storage aggregate concrete. *Constr. Build. Mater.* 2018, 165, 1-10.
231. Yusuf, A.; Putri, R.A.; Rahman, A.; Anggraini, Y.; Kurnia, D.; Wonorahardjo, S.; Sutjahja, I.M. Time-Controlling the Latent Heat Release of Fatty Acids using Static Electric Field. *J. Energy Storage* 2021, 33 (102045) 1-8.
232. Xie, N.; Niu, J.; Gao, X.; Fang, Y.; Zhang, Z. Fabrication and characterization of electrospun fatty acid form-stable phase change materials in the presence of copper nanoparticles. *Int. J. Energy Res.* 2020, 44 (11), 8567-8577.
233. Jebasingh, B.E. Preparation of organic based ternary eutectic fatty acid mixture as phase change material (PCM), optimizing their thermal properties by enriched solar treated exfoliated graphite for energy storage. *Mater. Today: Proceedings* 2016, 3, 1592-1598.
234. Zhou, D.; Xiao, S.; Xiao, X. Preparation and Thermal Performance of Fatty Acid Binary Eutectic Mixture/Expanded Graphite Composites as Form-Stable Phase Change Materials for Thermal Energy Storage. *ACS Omega* 2023, 8, 8596-8604.
235. Liu, P.; Gu, X.; Zhang, Z.; Rao, J.; Shi, J.; Wang, B.; Bian, L. Capric Acid Hybridizing Fly Ash and Carbon Nanotubes as a Novel Shape-Stabilized Phase Change

Material for Thermal Energy Storage. *ACS Omega* 2019, 4, 14962-1496.

236. Wen, R.; Zhang, X.; Huang, Z.; Fang, M.; Liu, Y.; Wu, X.; Min, X.; Gao, W.; Huang, S. Preparation and thermal properties of fatty acid/diatomite form-stable composite phase change material for thermal energy storage. *Sol. Energy Mater. Sol. Cells* 2018, 178, 273-279.
237. Du, X.; Wang, H.; Wu, Y.; Du, Z.; Cheng, X. Solid–solid phase-change materials based on hyperbranched polyurethane for thermal energy storage. *J. Appl. Polym. Sci.* 2017, 134 (26) 1-8.
238. Tariq, A.; Shakir, M.F.; Afzal, A.; Rashid, I.A.; Iqbal, M.A.; Rauf, A. Fabrication and characterization of the blend of Polyurethane (PU) and Phase Change Materials (PCM) for energy storage and release. *IOP SciNotes* 2020, 1 (024803), 1-6.
239. Aftab, W.; Mahmood, A.; Guo, W.; Yousaf, M.; Tabassum, H.; Huang, X.; Liang, Z.; Cao, A.; Zou, R. Polyurethane-Based Flexible and Conductive Phase Change Composites for Energy Conversion and Storage. *Energy Storage Mater.* 2019, 20, 401-409.
240. Pielichowska, K.; Bieda, J.; Szatkowski, P. Polyurethane/graphite nano-platelet composites for thermal energy storage. *Renew. Energy* 2016, 91, 456-465.
241. Alkan, C.; Gunther, E.; Hiebler, S.; Ensari, O.F.; Kahraman, D. Polyurethanes as solid–solid phase change materials for thermal energy storage. *Sol. Energy* 2012, 86, 1761-1769.
242. Xi, P.; Zhao, F.; Fu, P.; Wang, X.; Cheng, B. Synthesis, characterization, and thermal energy storage properties of a novel thermoplastic polyurethane phase change material. *Mater. Lett.* 2014, 121, 15-18.

243. Purohit, B.K.; Sistla, V.S. Crystallization of inorganic salt hydrates in polymeric foam for thermal energy storage application. *J. Energy Storage* 2017, 12, 196-201.
244. Xiaosheng, D.; Haibo, W.; Zongliang, D.; Xu, C. Synthesis and thermal properties of novel solid-solid phase change materials with comb-polyurethane block copolymer structure for thermal energy storage. *Thermochim. Acta* 2017, 651, 58-64.
245. Thibault, H.; Nguyen, G.T.M; Ledesert, B.; Mélinge, Y.; Hebert, R.L. Cross-linked polyurethane as solid-solid phase change material for low temperature thermal energy storage. *Thermochim. Acta* 2020, 685, 178191.
246. Chen, K.; Yu, X.; Tian, C.; Wang, J. Preparation and characterization of form-stable paraffin/polyurethane composites as phase change materials for thermal energy storage. *Energy Convers. Manag.* 2014, 77, 13-21.
247. Kong, W.; Yang, Y.; Zhou, C.; Lei, J. Novel thermosetting phase change materials with polycarbonatediol based curing agent as supporting skeleton for thermal energy storage, *Energy Build.* 2017, 146, 12-18.



## RESEARCH PUBLICATIONS

---

### PUBLICATIONS IN INTERNATIONAL JOURNALS

- **Surya Tanwar**, Raminder Kaur\*, “Development and Investigation of Microencapsulated Caprylic Acid-Based Phase Change Materials for Thermal Energy Storage Applications” **International Journal of Energy Research (SCIE indexed)**, **45 (2021) 17302–17314**, Wiley (**Impact Factor: 5.16**).
- **Surya Tanwar**, Raminder Kaur\*, “Fabrication and Investigation on Influence of Metal Oxide Nanoparticles on Thermal, Flammability and UV Characteristics of Polyethylene Glycol Based Phase Change Materials” **Journal of Energy Storage (SCIE indexed)**, **54 (2022) 1-15**, Elsevier (**Impact Factor: 9.4**).
- **Surya Tanwar**, Raminder Kaur\*, Pooja Singh, Gunjan Varshney and Sarla Yadav, “Assessment of Bio-Based Polyurethanes: Perspective on Applications and Bio-Degradation” **Macromol (CAS/Sci Finder) 2(3) (2022)**, **284-314**, MDPI.
- **Surya Tanwar**, Raminder Kaur\*, “Studies on the Effect of Addition of Titanium Dioxide Nanoparticles on the Properties of PEG Based Phase Change Composite Materials” **Journal of Energy Storage**, Elsevier (**under review**).
- **Surya Tanwar**, Raminder Kaur\*, “Nanoencapsulated Undecylenic Acid Based Phase Change Materials: A Renewable Route Towards Thermal Energy Storage Applications”, **Energy**, Elsevier (**under review**).
- **Surya Tanwar**, Raminder Kaur\*, “Role of Polymers in Anchoring the Performance of Phase Change Materials for Thermal Energy Storage Applications: An Overview” **Energy for Sustainable Development**, Elsevier (**under review**).

- **Surya Tanwar** and Raminder Kaur\* “Preparation & Characterization of Polyurethane Based Phase Change Materials for Thermal Energy Storage Applications” **European Polymer Journal** (under review).

#### **PUBLICATIONS IN CONFERENCE PROCEEDINGS**

- **Surya Tanwar**, Raminder Kaur, “Development & Investigation of PVA/PEG blends-based Phase Change Materials for Thermal Energy Storage Applications”, **International Online Conference on Materials Science and Technology (ICMT 2021)** organized by Mahatma Gandhi University, Kottayam, Kerala, India (12<sup>th</sup> -14<sup>th</sup> December, 2021).
- **Surya Tanwar**, Raminder Kaur, “Preparation & Characterization of Microencapsulated PCMs for TES Applications”, **International Conference on Advanced Materials 2019: (ICAM2019)** organized by Jamia Millia Islamia, Delhi, India (6<sup>th</sup>-7<sup>th</sup> March, 2019).
- **Surya Tanwar**, Raminder Kaur, “Synthesis & Characterization of Polymer Microencapsulated Fatty Acid as PCMs for TES Applications: A Renewable Approach”, **International Conference on Polymer Science & Technology: SPSI-MACRO 2018** organized by IISER Pune, Maharashtra, India (19<sup>th</sup> -22<sup>th</sup> December 2018).

## CURRICULUM VITAE

---

### SURYA TANWAR

e-mail id: surya3tanwar@gmail.com



#### ACADEMIC QUALIFICATIONS:

S.No.	Degree	Division	University /Institute	Year
1.	M.Sc. (Polymer Science)	I (74%)	Central Institute of Petrochemicals Engineering and Technology, Ahmedabad	2016
2.	B.Sc. (H) (Polymer Science)	I (74%)	Delhi University	2014
3.	Intermediate (12th)	I (72%)	C.B.S.E.	2011
4.	High school (10th)	I (82%)	C.B.S.E.	2009

#### WORK EXPERIENCE:

S.No.	Organization	Designation	Duration
1.	J.J. Plastalloy Pvt. Ltd.	Technical Marketing Executive	July-October 2016
2.	Nahata Plastics	Intern	October-November 2015
3.	Pluss Polymers	Intern	May-July 2013

#### NATIONAL LEVEL EXAMS QUALIFIED:

Qualified GATE 2019 in Engineering Sciences (XE).

#### **PROJECTS UNDERTAKEN:**

[1] Carried out Master's Project Work on Dissertation Title:-Fabrication & Study of Mechanical Properties of Randomly-Oriented Short Glass/Bagasse/Coir Fibers Reinforced Unsaturated Polyester Based Hybrid Composites.

[2] Worked in an Innovation Project of the University of Delhi with Title:-Agro-Waste Management: From Waste to Wealth (BCAS-202).

[3] Worked in an Innovation Project of the University of Delhi with Title:-Determine the Specification of Some Heavy Metals from E-Wastes & their Impact on Ground Water (BCAS-105).

#### **TECHNICAL EXPERTISE**

- **Laboratory Exposure:** Polymer Synthesis, Plastic Blends & Composites Fabrication, Latex & Rubber Compounding, PU Foam Synthesis, Adhesive Synthesis & Formulation, Paint Synthesis & Formulation.
- **Processing Exposure:** Extrusion (SSE, TSE), Hand-Injection Molding, Blown-Film Extrusion, Compression Molding and Two-Roll Mill.
- **Advanced Characterization & Analysis Exposure:** DSC (Perkin Elmer, DSC 8000), TGA (Perkin Elmer, TGA 4000), Zetasizer (Malvern, Nano), FTIR Spectrophotometer (Perkin Elmer, Spectrum Two), Cone Calorimeter (Jupiter Electronics), L.O.I (Fire Testing Technology), UV-Vis Spectrophotometer (Agilent Technologies, Cary Series), Four Probe Set-up: Electrical Resistivity Meter (SES Instruments, DFP-RM-200), Fluorescence Microscopy (Motic, BA410E).

**RESEARCH INTERESTS:**

Phase Change Materials (PCMs), Polymer Blends & Composites, Polymer Foams, Biopolymers, Flame-Retardancy (FR).

**PROFESSIONAL SOCIETY MEMBERSHIPS:**

- Asian Polymer Association (Life Member), No. L526.
- Society for Polymer Science, India (Life Member), No. L580.

**PERSONAL DETAILS:**

**Name:** Surya Tanwar

**Father's Name:** Sh. Ashok Tanwar

**Date of Birth:** 21-09-1992

**Nationality:** Indian

**Marital Status:** Unmarried